Elucidation of Group B Streptococcus hemolytic pigment and hyaluronidase during infection

Blair Armistead

A dissertation

submitted in partial fulfillment of the

requirements for the degree of

Doctor of Philosophy

University of Washington

2020

Reading Committee:

Lakshmi Rajagopal, Chair

Jairam Lingappa

Chetan Seshadri

Program Authorized to Offer Degree:

Pathobiology

University of Washington

Abstract

Elucidation of Group B Streptococcus hemolytic pigment and hyaluronidase during infection

Blair E. Armistead

Chair of the Supervisory Committee:
Lakshmi Rajagopal, Ph.D.
Department of Pediatrics
Department of Global Health

Group B Streptococci (GBS) are β-hemolytic, Gram-positive bacteria that colonize the lower genital tract of approximately 18% of women worldwide as asymptomatic components of the gastrointestinal and/or vaginal flora. If established in other host niches, however, GBS are highly pathogenic. During pregnancy, ascending GBS infection from the vagina to the intrauterine space is associated with preterm birth, stillbirth, and fetal injury. In addition, vertical transmission of GBS during birth results in life-threatening neonatal infections, including pneumonia, sepsis, and meningitis. Notably, invasive GBS infections in non-pregnant adults are on the rise. Novel strategies to prevent GBS colonization and disease are an urgent global health priority and require a better understanding of the complex interactions between GBS virulence factors and host

defenses. This dissertation summarizes efforts to uncover fundamental insights into two GBS virulence factors during infection, namely the surface-associated hemolytic pigment toxin and the extracellular enzyme hyaluronidase.

Over 100 years ago, GBS isolates of human origin were first described as β-hemolytic, which was invariantly linked to orange/red pigmentation. In the century that followed, research uncovered the importance of hemolysis to GBS colonization and disease. Non-hemolytic/non-pigmented strains were shown to be deficient vaginal colonizers and less able to disseminate into vulnerable host niches in *in vivo* models. Moreover, hyper-hemolytic/hyper-pigmented strains were isolated from people with invasive infections and shown to more readily breach host barriers *in vitro* and *in vivo*. Despite the strong genetic and phenotypic link between hemolysis and pigment, these factors were thought to be independent. In 2013, the GBS hemolysin and pigment were shown to be one and the same, initiating a paradigm shift in understanding this virulence factor.

The GBS hemolytic pigment, also known as granadaene, is a cell-surface-associated ornithine rhamnolipid consisting of a 12-alkene chain and is dissimilar to many other commonly studied Gram-positive pore-forming toxins, which are proteinaceous in nature. Here, we describe the genetic elements sufficient for granadaene production using a heterologous bacterial host (*Lactococcus lactis*) and trace the evolutionary origins of this toxin before the divergence of Gram-positive bacteria. In addition, we show that GBS release granadaene in membrane vesicles (MVs), which are cytotoxic to host immune cells and promote GBS infection in neonatal mice. Using organic chemical synthesis for the generation of granadaene analogs, we demonstrate the importance of the polyene chain length and terminal head groups to hemolytic activity. And lastly, we identify a non-toxic analog that, unlike granadaene, is well tolerated by cells of the adaptive

immune system and confers protection against infection with hyper-hemolytic GBS. Collectively, the studies on the GBS hemolytic pigment presented in this dissertation provide novel biosynthetic, evolutionary, structural, and functional insight into this crucial GBS virulence factor and offer proof-of-concept for a targeted vaccine approach to attenuate its activity during infection.

Next, we explore the role of another key virulence factor, hyaluronidase, in promoting GBS dissemination during pregnancy using a non-human primate model. Hyaluronidase, or HylB, has endoglycosidase activity, which is correlated to GBS's invasive potential. Using a pregnant non-human primate model, we show that a non-pigmented/non-hemolytic GBS strain invaded the amniotic cavity and induced fetal injury and preterm labor in a HylB-dependent manner. Despite increased recruitment of neutrophils at the maternal-fetal interface, HylB dampened ROS production and neutrophil-mediated killing of GBS. Our studies show how this unique bacterial enzyme enables GBS to circumvent host defenses, leading to the rapid induction of infection of the amniotic cavity and preterm labor.

Together, the work presented in this dissertation elucidates novel mechanisms of host-GBS interactions through the study of two key virulence factors, the hemolytic pigment and hyaluronidase. The findings here offer basic insights that may alleviate challenges associated with the development of improved therapeutic strategies against GBS.

TABLE OF CONTENTS

LIST OF FIGURES

LIST OF TABLES

ACKNOWLEDGEMENTS

I want to thank my advisor, Dr. Lakshmi Rajagopal, who approaches scientific problems intelligently, perseveres through challenges to find the truth, and above all, is an advocate for her students. I am forever grateful for her mentorship and unwavering support throughout my graduate studies. I am a better scientist and a better person because of her.

Second, I want to thank my family. I am so lucky that my mom, Julie, and my dad, Will, instilled in me the value of education and always encouraged me to be myself. I would be nowhere without their love and support, along with that of my brother, Chas, and my sister-in-law, Katie. I am incredibly thankful for my wonderful partner, Emily Evanson, who encouraged me to keep my head up during the most challenging moments, and who celebrated my achievements loudly.

Third, I want to acknowledge my brilliant colleagues and friends in the Pathobiology Program: Chris Whidbey, Jay Vornhagen, Justine Levan, and Taylor Stepien. They were fundamental to my success in the program, and I am so honored to call them friends.

And finally, I want to thank my teachers in the West Virginia public schools, especially Eric Kincaid, who pushed me to be the best student I could be.

DEDICATION

I dedicate this work to my grandfather, Albert John Rosenwald, who taught me the joy of scientific curiosity.

Chapter 1. INTRODUCTION

This chapter was adapted from the following article:

Armistead, B., Oler, E., Adams Waldorf, K., Rajagopal, L. (2019). The double life of Group B Streptococcus: Asymptomatic colonizer and potent pathogen. *Journal of Molecular Biology*, doi: 10.1016/j.jmb.2019.01.035.

1.1 EPIDEMIOLOGY OF GROUP B STREPTOCOCCUS COLONIZATION AND DISEASE

Group B Streptococcus (GBS or *Streptococcus agalactiae*) is a leading cause of neonatal infectious morbidity and mortality globally. GBS is a β-hemolytic, Gram-positive coccus that asymptomatically colonizes the lower genital and gastrointestinal tracts but is an invasive pathogen in other host niches. Fetuses and neonates are especially susceptible to GBS infections, which most commonly include sepsis, pneumonia, meningitis, and encephalopathy (Fig. 1.1)[1]. Maternal colonization with GBS is associated with stillbirth and preterm birth, and thus the sequelae of prematurity in the neonate (e.g. bronchopulmonary dysplasia)[2,3]. Rarely, GBS causes maternal sepsis[4]. Notably, in recent years, the incidence of invasive GBS disease including bloodstream, skin, soft tissue, and joint infections has increased in non-pregnant adults, particularly among the elderly and persons with comorbidities[5-8].

In newborns, the timing of GBS bacteremia or sepsis may be early-onset (within the first week), which is thought be associated with either an *in utero* infection or exposure during vaginal delivery. Alternatively, late-onset GBS disease presents after the first week, but within the first three months. To date, the only clinical intervention to prevent early-onset disease in neonates is the administration of intravenous antibiotics to pregnant women during birth, known as intrapartum antibiotic prophylaxis (IAP). Of note, these measures have had little effect on the incidence of late-onset disease, as exposure likely occurs postnatally[9]. Although clinical trials in pregnant and non-pregnant adults have shown promise[10,11], no FDA approved vaccine exists to date to prevent GBS disease.

As a colonizing microbe, GBS is detected in the gastrointestinal and genital tracts of approximately 18% of pregnant women globally; rates of colonization range from 1 in 3 pregnant women in the Caribbean to 1 in 6 women in Southern and Eastern Asia[12]. Interestingly, only a small proportion of people colonized with GBS experience invasive disease, suggesting that host-specific factors potentially play a role in determining an individual's susceptibility to invasive disease. The

most comprehensive systematic review and meta-analysis to date estimated the pooled incidence of neonatal morbidity and mortality to be 0.49 per 1000 worldwide, which includes GBS-associated preterm birth, stillbirth, and neonatal GBS infection[13]. Low- and middle-income countries experience increased rates of invasive GBS disease in neonates, and this is correlated with the lack of availability of IAP[14,15]. In countries that have adopted screening protocols for maternal colonization and IAP, the burden of early-onset GBS disease has diminished dramatically; when data was first collected in the U.S. in 1997, the rate was 0.7 per 1,000 and in 2016 was 0.22 per 1,000 newborns[15,16]. However, IAP appears to have little to no effect on the rate of late-onset disease in newborns or preterm birth and stillbirth, which are estimated to collectively affect 97,000 to 4 million pregnancies per year[1-3,13,14]. Additionally, the widespread use of IAP has increased concern over antibiotic resistance in GBS; in regions in which IAP is commonly implemented, macrolide resistance occurs in approximately 15-32% of GBS isolates[17]. As such, the design of novel strategies for the prevention and treatment of GBS colonization and invasive disease is an urgent global health priority.

1.2 AN INTRODUCTION TO GBS FACTORS DISCUSSED IN THIS DISSERTATION

Through the study of the complex interactions between GBS and host, the development of improved therapeutics against GBS becomes more within reach. GBS encode hundreds of virulence factors, and research has revealed many mechanisms by which GBS deploy these factors to overcome host defenses in the transition from asymptomatic colonizer to invasive pathogen. This dissertation aims to build on this body of knowledge by offering novel insights into two of the most critical virulence factors encoded by GBS: the hemolytic pigment (also known as granadaene) and hyaluronidase. The following subsections are intended as background to what was known about these virulence factors at the onset of this dissertation research.

1.2.1 *Hemolytic pigment, granadaene*

Hemolytic activity in GBS is due to the cell surface-associated[18] ornithine rhamnolipid pigment known as granadaene [19], which is produced by the gene products of the *cyl* operon [20,21]. Several genes within the *cyl* operon have homology to those involved in fatty acid biosynthesis, and the *cylE* gene, which encodes an N-acyl transferase, is necessary for pigment production[19-21]. Transcription of *cyl* genes is negatively regulated by the CovR/S two-component system (TCS), so loss of function in this TCS results in a hyper-hemolytic/hyper-pigmented phenotype in GBS[22]. The hemolytic pigment contains a polyene chain consisting of 12 double-bonds [19,23], and serves both as a potent cytotoxin [19,24] and an antioxidant with reactive oxygen species (ROS)-quenching properties [25]. In a murine model of vaginal colonization, GBS lacking the hemolytic pigment were deficient vaginal colonizers compared to WT GBS and were associated with amplified neutrophil response in the vagina [26]. However, GBS over-expressing the hemolytic pigment were more readily cleared from the murine vagina [27,28], likely due to an inflammatory response resulting in an infiltration of neutrophils [27] and/or mast cell degranulation [28]. The finely tuned expression of the hemolytic pigment in the lower genital tract, therefore, is essential to GBS survival; GBS must achieve an optimum level of pigment production to resist ROS but also avoid inflammation and subsequent clearance.

In addition to modulating vaginal colonization, the hemolytic pigment permits GBS dissemination to host niches outside the vagina and facilitates tissue damage. In a murine model of vaginal colonization, non-hemolytic GBS were less likely to disseminate or cause fetal injury [29], suggesting the hemolytic pigment plays a role in GBS's ability to breach the placental barrier. Indeed, hyper-hemolytic GBS strains lacking CovR were found to more readily invade amniotic epithelial cells, cause amniotic epithelial cell barrier disruption, and penetrate the human placenta compared to WT GBS and non-hemolytic GBS also lacking CovR (GBSΔ*covR*Δ*cylE*) [19]. Furthermore, hyper-hemolytic GBS with CovR/S mutations were isolated from women in preterm labor [19], suggesting that some GBS

isolates have evolved the ability to constitutively over express the hemolytic pigment and that these are associated with human disease. In a non-human primate (NHP) study of GBS infection during pregnancy, GBS lacking CovR invaded the amniotic cavity more efficiently than non-hemolytic GBS, resulting in uterine contractions and inflammation indicative of preterm labor [30]. Notably, even though hyper-hemolytic GBS caused an infiltration of neutrophils to the chorioamniotic (placental) membranes of NHP and the subsequent release of neutrophils extracellular traps (NETS), hyper-hemolytic GBS were able to resist killing by NETs [30]. Other inflammatory cascades initiated by the pigment during pregnancy, such as the NLRP3 inflammasome, can likewise result in fetal injury and preterm birth [24].

Neonates, particularly those born prematurely, are especially susceptible to the toxic effects of the hemolytic pigment. Many infants acquire early onset GBS by aspirating infected vaginal or amniotic fluid, resulting in colonization of the lung. Higher expression of the hemolytic pigment correlates to greater cytotoxicity of the very cells that constitute the mucosal barrier of the lung: alveolar epithelial cells [31] and capillary endothelial cells [32]. Additionally, mutant GBS strains lacking the *cylE* gene are less capable of adhering to, invading, and initiating inflammatory cascades in lung epithelial cells [33]. Once GBS breach the lung's barrier, they deploy several virulence other factors (such as adhesins and invasins) to disseminate to peripheral organs, resulting in septicemia and neurotropism. At the blood-brain barrier, the hemolytic pigment facilitates bacterial penetration into the brain and promotes acute inflammatory responses in microvascular endothelial cells, thus contributing to the severity of GBS meningitis [34,35].

While recent advances have greatly improved understanding of this virulence factor, several unknowns remain, including its evolutionary origins, the chemical components important for hemolytic and cytolytic activity, and how GBS release it during infections. The work in this dissertation addresses these and other remaining questions, including how a novel vaccine targeting the hemolytic pigment may reduce GBS pathogenicity.

1.2.2 *Hyaluronidase*

The GBS hyaluronidase, also known as HylB, is an endoglycosidase that cleaves glycosaminoglycan chains, such as hyaluronic acid (HA) into disaccharides [36]. HylB activity has long been demonstrated to correlate to GBS's invasive potential. In a 1978 study, increased expression of HylB was observed in GBS strains isolated from infected neonates [37,38]. Similarly, in 1989, the highly virulent GBS clonal type now known as CC17 was shown to have increased expression of hyaluronidase compared to strains less often associated with invasive disease in neonates [38-40]. Even in a GBS strain that lacks the potent hemolytic pigment toxin, over-expression of HylB confers hypervirulence [41].

GBS mutants lacking HylB induce more pro-inflammatory cytokines *in vitro* and *in vivo* [42], and a mechanism of HylB-mediated immune suppression was elucidated in a recent study by Kolar, et al [43]. HylB's substrate, HA, is present in almost all human tissues and is important for stability and structure of the ECM as well as immune surveillance [44,45]. Upon sterile or microbial-induced tissue injury, HA is degraded into multimeric fragments by ROS or host hyaluronidases, which act as damage-associated molecular patterns (DAMPs) that bind to pattern recognition receptors such as TLRs on innate immune cells to initiate a pro-inflammatory response. The HA dimers generated by GBS HylB inhibit TLR2 and TLR4 inflammatory pathways by blocking the direct binding of stimulatory HA fragments and other pathogen-associated molecular patterns (PAMPs) to TLR2 and TLR4 [43]. Using a non-pregnant mouse model of vaginal inoculation, Kolar, et al. established that the immune-suppressing properties of HylB facilitate vaginal colonization of GBS [43]. In pregnant mice, wild-type GBS caused increased ascending infection into the uterus, decreased uterine inflammation, and higher rates of fetal demise compared to HylB-deficient mice [46], indicating suppression of inflammatory responses in the uterus also facilitates GBS-associated fetal injury.

The work in this dissertation illuminates how GBS use HylB to overcome immune defenses at the placenta, invade the amniotic cavity and fetus and cause preterm labor in a model relevant to human pregnancy.

1.3 HOST FACTORS THAT MEDIATE GBS DISEASE

Although some host defenses are effective at clearing GBS, others are permissive to or exploited by GBS, allowing these bacteria to gain a foothold in invasive niches. The following subsections provide background and context to host responses to GBS that are discussed in the chapters of this dissertation.

1.3.1 *Humoral and cellular immunity*

The generation of antibodies specific to GBS surface components, such as the capsular polysaccharide (CPS), plays an important role in GBS's state as an asymptomatic colonizer or invasive pathogen. Clinical studies have suggested a correlation between naturally acquired maternal CPS-specific antibodies and asymptomatic vaginal carriage and/or clearance [47,48], and maternal titers of CPS-specific antibodies >1 μg/mL at birth were associated with a 70% reduction in the risk of early onset disease in newborns [49]. Given the CPS-dependent antibody protection observed in these studies, the CPS is a frequent target for GBS vaccine candidates, and several multivalent CPS conjugate vaccines have shown promising safety and immunogenicity outcomes in phase I and II clinical trials [50-56]. However, the diversity of GBS CPS types and CPS switching are significant challenges to the development of broadly efficacious GBS vaccines targeting the CPS [57,58]. Additional studies have suggested the generation of antibodies specific to other GBS surface components, such as the Sip protein [59], serine rich repeat protein (Ssr1) [60], C5a peptidase (ScpB) [61,62], alpha-like proteins[63], and pilus[64], confers protection against GBS infection. In addition, work in this dissertation (shown in

Chapter 3) demonstrates for the first time that antibodies generated against the surface-associated hemolytic lipid (granadaene) can diminish GBS infection. Although some reports have indicated a role for CD4+ T cells in GBS clearance[65,66], more research on the cellular immune response to GBS infection is warranted.

1.3.2 *Immunity at the maternal-fetal interface*

The placenta is an organ of maternal and fetal origin that nourishes and protects the fetus from maternal immune rejection and invasive pathogens. GBS is one of few bacterial pathogens capable of infecting the placenta, making it a potential site of perinatal acquisition of GBS[67]. Several recent studies examining the immunological dynamics of the placenta during GBS infection have revealed that GBS disrupt tolerogenic functions of the placenta, which subsequently influences GBS invasion of the amniotic cavity, GBS-associated fetal injury, and preterm labor. For instance, when in contact with GBS, placental macrophages secrete release pro-inflammatory mediators and extracellular traps containing matrix metalloproteases, which may promote the degradation of the placental barrier and permit intra-amniontic infection or premature rupture of membranes[68-70]. Similarly, GBS infection at the maternal-fetal interface results in the recruitment of neutrophils to the placental membranes, causing placental inflammation and the release of neutrophil extracellular traps[71,72]. While neutrophil and macrophage responses may promote the clearance of GBS[71], certain strains have evolved strategies to evade these cells' antimicrobial activity[72], and inflammation at the maternal-fetal interface is associated with fetal injury[73]. Novel data regarding this phenomenon are presented in Chapter 5 of this dissertation.

1.4 DISSERTATION SUMMARY

Overall, GBS remains a significant etiological agent of neonatal and maternal morbidity and mortality worldwide[1-3,13,14], and rates of invasive infections in non-pregnant adults are increasing[5-8].

Improved, rationally designed strategies to prevent invasive GBS disease are a pressing global health need. To accomplish this, a greater understanding of the complex interplay between GBS factors and host defenses is essential. The work presented in this dissertation aims to add fundamental insights into two critical GBS virulence factors, the hemolytic pigment (granadaene) and hyaluronidase. Chapter 2 explores the biosynthetic and evolutionary foundations of granadaene through heterologous expression and phyletic analysis of the *cyl* genes. In Chapter 3, synthetic analogs of granadaene are utilized to identify chemical moieties important to hemolytic activity and to generate a granadaene-targeted vaccine that diminishes GBS infection. Chapter 4 shows that GBS deploy granadaene in membrane vesicles (MVs), which exacerbate GBS infection in neonatal hosts. Chapter 5 explores the role of GBS hyaluronidase in evading neutrophils to promote preterm birth and microbial invasion of the amniotic cavity during pregnancy in a non-human primate model. Finally, in Chapter 6, I provide a summary of my findings, conclusions, and thoughts on how this work may contribute to strategies aimed at reducing the burden of invasive GBS disease.

1.5 FIGURES

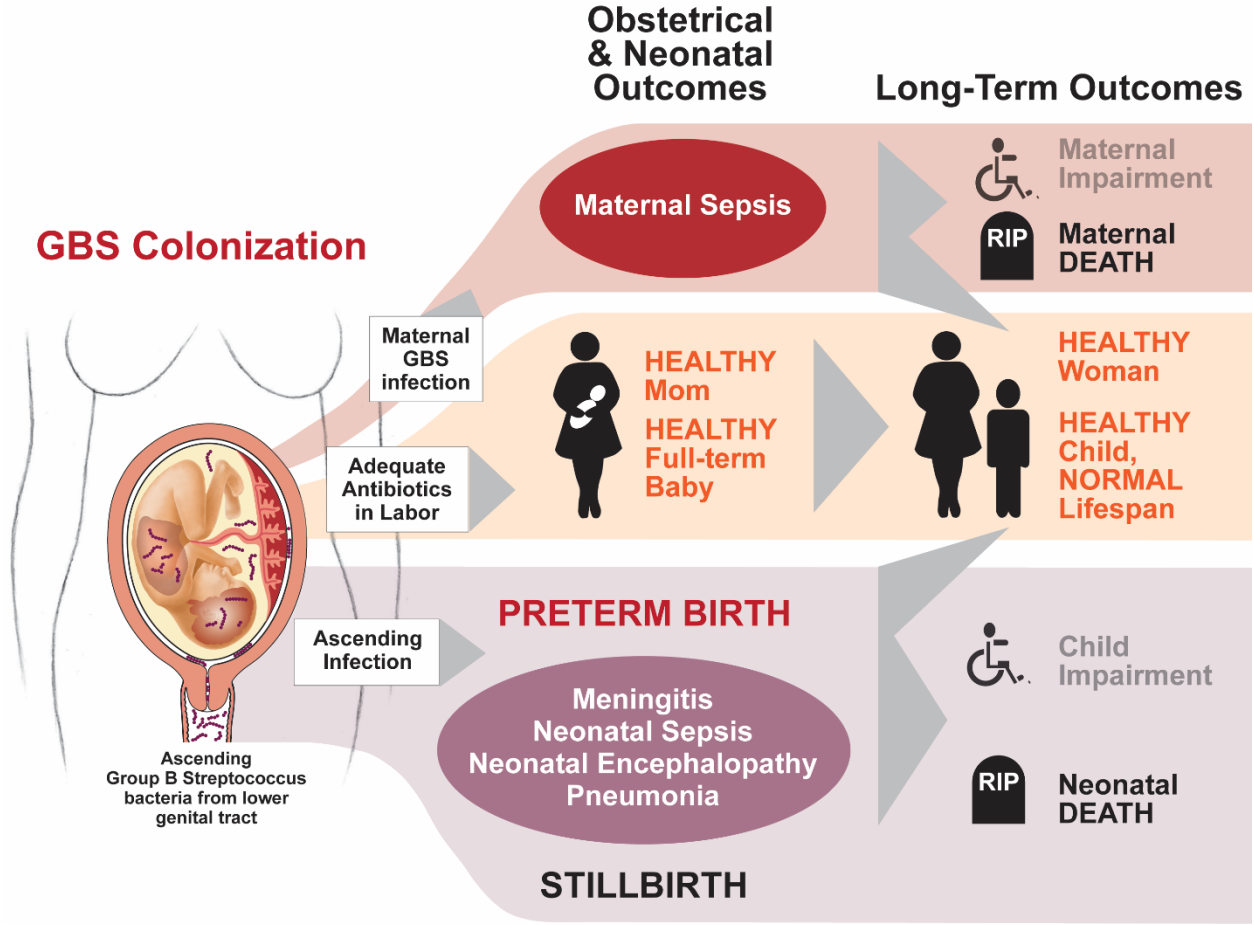

Figure 1.1. Clinical pathways in maternal Group B Streptococcus (GBS) colonization.

GBS is associated with several perinatal outcomes. In the case of adequate antibiotic prophylaxis, most mothers and babies are healthy with normal lifespan. Virulent ascending GBS is associated with significant morbidity and mortality, some of which is not preventable with intrapartum prophylaxis. With adequate treatment of ascending infection, normal and healthy outcomes may be achieved. Figure adapted from Lawn, et al, 2017 [74].

Chapter 2. THE *CYL* GENES REVEAL THE BIOSYNTHETIC AND EVOLUTIONARY ORIGINS OF THE GBS HEMOLYTIC LIPID, GRANADAENE

This chapter is from the following article:

Armistead, B., Whidbey, C., Iyer, L.M., Herrero-Foncubierta, P., Quach, P., Haidour, A., Aravind, L., Cuerva, J.M., Jaspan, H.B., Rajagopal, L. (2019). The *cyl* genes reveal the biosynthetic and evolutionary origins of the Group B Streptococcus hemolytic lipid, Granadaene. *Frontiers in Microbiology*. doi: 10.3389/fmicb.2019.03123.

2.1 ABSTRACT

Group B Streptococcus (GBS) is a β-hemolytic, Gram-positive bacterium that commonly colonizes the female lower genital tract and is associated with fetal injury, preterm birth, spontaneous abortion, and neonatal infections. A major factor promoting GBS virulence is the β-hemolysin/cytolysin, which is cytotoxic to several host cells. We recently showed that the ornithine rhamnolipid pigment, granadaene, produced by the gene products of the *cyl* operon, is hemolytic. Here, we demonstrate that heterologous expression of the GBS *cyl* operon conferred hemolysis, pigmentation, and cytotoxicity to *Lactococcus lactis*, a model non-hemolytic Gram-positive bacterium. Similarly, pigment purified from *L. lactis* is hemolytic, cytolytic, and identical in structure to granadaene extracted from GBS, indicating the *cyl* operon is sufficient for granadaene production in a heterologous host. Using a systematic survey of phyletic patterns and contextual associations of the *cyl* genes, we identify homologues of the *cyl* operon in physiologically diverse Gram-positive bacteria and propose undescribed functions of *cyl* gene products. Together, these findings bring greater understanding to the biosynthesis and evolutionary foundations of a key GBS virulence factor and suggest that such potentially toxic lipids may be encoded by other bacteria.

2.2 INTRODUCTION

Hemolytic activity is a key determinant of colonization and pathogenesis in Group B Streptococcus (GBS)[24,27,31,33,34,72,75], a Gram-positive bacterium that resides in the lower genital and/or gastrointestinal tract of approximately 18% of women and is a major cause of preterm birth and severe neonatal infections [2,12,13,76]. Nearly 100 years ago, GBS isolates of human origin were first described as β-hemolytic [77,78], which was invariantly linked to a pigmented phenotype [21,31,79]. Recently, the GBS hemolysin and pigment were shown to be one and the same [75], initiating a shift in understanding this virulence factor. The GBS hemolytic pigment, also known as granadaene [23], is a cell surface-associated

[18] ornithine rhamnolipid consisting of a 12-alkene chain and is unrelated to other commonly studied Gram-positive pore-forming toxins, such as lysteriolysin O [80] or alpha toxin [81], which are proteinaceous in nature. Many gaps remain in our understanding of granadaene, including the specifics of its biosynthesis in bacterial cells and reasons why GBS may have evolved to produce this potent toxin. Such insights would improve our understanding of this critical GBS virulence factor as well that of other similar, potentially toxic microbial lipids.

The *cyl* operon (*cylX-K*) is necessary for hemolytic pigment production in GBS [20,21,75,79]. We have previously postulated that enzymes encoded in the *cyl* operon use acetyl-CoA, malonyl Co-A, ornithine, and rhamnose as the building blocks for pigment biosynthesis in GBS [75]. Here, for the first time, we show that heterologous expression of the GBS *cyl* operon is sufficient to confer the production of functional granadaene in *Lactotoccus lactis*, a generally recognized as safe (GRAS) Gram-positive bacterial strain [82]. Phyletic analysis revealed previously undescribed functional categories of *cyl* gene products, indicated that the *cyl* operon genes are present in a diverse range of Gram-positive bacteria, and suggested that pigment biosynthesis evolved in free-living bacteria, likely as a photoprotectant or as a defense mechanism against competing organisms. Collectively, these findings provide biosynthetic and evolutionary insight into a critical GBS virulence factor.

2.3 Results and Discussion

2.3.1 *Heterologous expression of the GBS cyl operon in Lactococcus lactis confers hemolysis, pigmentation, and cytotoxicity.*

Our recent studies [24,72,75,83] have revealed that the hemolytic pigment encoded by the GBS *cyl* operon genes is cytotoxic to many eukaryotic cells. Given that GBS colonizes the human host with other commensal microbes, we wondered whether horizontal gene transfer of this operon would enable production of the hemolytic lipid pigment to non-hemolytic bacteria. To test this hypothesis, we expressed the *cyl* operon genes in a model Gram-positive bacterium, *Lactococcus lactis*. First, we

cloned the 12-gene *cyl* operon (i.e. genes *cylX*-*cylK*) into a complementation vector pDC123 [84] to generate the p*cylX*-*K* plasmid. Then, we complemented a non-hemolytic/non-pigmented GBS strain lacking the entire *cyl* operon (GBSΔ*cylX*-*K* [75]) with the p*cylX*-*K* plasmid and confirmed that the plasmid restored hemolysis and pigmentation as observed on blood agar and Granada media (Supplementary Fig. 2.1). Next, we transformed the p*cylX*-*K* plasmid into *L. lactis* to generate *L. lactis* p*cylX*-*K*. As a control, *L. lactis* was transformed with the empty plasmid vector (*L. lactis* pEmpty). Like hemolytic GBS, β-hemolysis and pigmentation were observed with *L. lactis* p*cylX*-*K* and not *L. lactis* pEmpty (Fig. 2.2a, b). Consistent with previous observations with GBS [75], plasmids encoding only *cylE* (p*cylE*) or *cylABE* (p*cylABE*) were insufficient to confer hemolysis and pigmentation to *L. lactis* (Fig. 2.1c, d). Also, the recombinant p*cylX*-*K* plasmid did not confer hemolysis to *E. coli* (Supplementary Fig. 2.2), which we predict is due to the abundance of rare codons present in the *cyl* operon (Supplementary Table 2.1). Together, these results indicate that expression of the *cyl* operon is necessary and sufficient for hemolysis and pigmentation in GBS and even in *L. lactis*.

We next tested if the *cyl* operon expression by *L. lactis* conferred neutrophil cytotoxicity. In GBS, expression of the *cyl* operon is transcriptionally repressed by the CovR/S two-component system, and the absence of the repressor CovR results in increased expression of the hemolytic pigment, granadaene [22,35,85]. GBS strains lacking a functional CovR (Δ*covR*) cause significantly greater cytotoxicity in neutrophils compared to wildtype (WT) GBS and isogenic non-pigmented/non-hemolytic mutants due to enhanced production of granadaene [22,72,85,86] (Fig. 2.1 a,b). Furthermore, GBS strains lacking CovR have been identified and isolated from women in preterm labor [75] and from patients with other GBS infectious morbidities [87-91]. We hypothesized that *L. lactis* p*cylX*-*K*, which lacks transcriptional repressors specific to the *cyl* operon, would induce neutrophil cytotoxicity similar to GBSΔ*covR*. To test this, we exposed primary human neutrophils to *L. lactis* p*cylX*-*K* at a multiplicity of infection (MOI) of 10 or 100 and measured cytotoxicity by lactate dehydrogenase (LDH) release in cell supernatants as described [72,75,83]. WT GBS or hyper-hemolytic/pigmented GBSΔ*covR* were also

included for comparison. As controls, we exposed neutrophils to *L. lactis* pEmpty, non-pigmented/non-hemolytic GBSΔ*cylE*, and non-pigmented/non-hemolytic GBSΔ*covR*Δ*cylE*. The results, shown in Fig. 1e, demonstrate that the cell death caused by *L. lactis* p*cylX-K* was similar to that caused by the hyper-hemolytic strain GBSΔ*covR*. Importantly, cytotoxicity in cells exposed to *L. lactis* p*cylX-K* was greater than those exposed to *L. lactis* pEmpty. These results demonstrate that expression of the *cyl* operon in *L. lactis* is sufficient to confer neutrophil cytotoxicity like hyper-hemolytic/hyper-pigmented GBS.

2.3.2 *Pigment isolated from L. lactis pcylX-K is identical to granadaene from GBS.*

We next tested if pigment produced by *L. lactis* p*cylX-K* was similar in structure to the GBS pigment, granadaene. Accordingly, we extracted and purified pigment from *L. lactis* p*cylX-K* using methods described with GBS [23,24,72,75,83] (see Materials and Methods). As a control, we performed the same extraction and purification procedure on *L. lactis* pEmpty. In mass spectrometry studies, pigment purified from *L. lactis* p*cylX-K* demonstrated an M+ H ion at *m/z* 677.3795 (Fig. 2.2a). This exact mass is associated with an ion formula of $C_{39}H_{53}N_2O_8$ (expected mass of 677.3796), which is identical to that of granadaene from GBS, as described [23,75]. As expected, no peaks corresponding to the mass of granadaene were observed in the extract from control *L. lactis* pEmpty. To gain further insight into the structure of pigment produced by *L. lactis* p*cylX-K*, we performed ^{1}H NMR studies (Fig. 2.2b). These analyses revealed a signal corresponding to a polyene structure (7.20 – 5.5 ppm), as well as signals corresponding to an ornithine (4.32, 2.77, 1.80, 1.59, and 1.64 ppm) and a rhamnose (4.63, 3.52, 3.43, 3.39, 3.16, 1.09 ppm), which are identical to those described for natural granadaene [23,75]. The ornithine and rhamnose were also confirmed to be present in *L. lactis* p*cylX-K* pigment extract by 1D TOCSY (total correlation spectroscopy). Notably, none of these structures were present in the NMR analysis of *L. lactis* pEmpty extract. Together, these results demonstrate that the nominal formula and the structure of pigment produced by *L. lactis* p*cylX-K* are indistinguishable from those previously assigned to granadaene (Fig. 2.2b) [23,75].

To confirm that pigment purified from *L. lactis* p*cylX-K* possessed hemolytic and cytolytic activity analogous to granadaene, we performed a hemolytic titer assay using the *L. lactis* p*cylX-K* pigment extract [31,75]. The results shown in Fig. 2.2c indicate that purified pigment from *L. lactis* p*cylX-K* possessed hemolytic activity similar to that of granadaene [75]. Moreover, the EC_{50} (the effective concentration at which 50% of human red blood cells are lysed) of *L. lactis* p*cylX-K* pigment (0.128 µM, 95% CI: 0.108, 0.153) was no different than that of granadaene (0.127 µM, 95% CI: 0.100, 0.162).

Finally, we sought to determine if *L. lactis pcylX-K* pigment is cytolytic to host cells like granadaene. Purified granadaene was previously reported to be cytolytic to host cells such as neutrophils [72]. Human neutrophils isolated from fresh adult blood were treated with *L. lactis* p*cylX-K* pigment (0.5 µM) or equivalent amount of control extract from *L. lactis* pEmpty for 4 hours, as described [72], and cytotoxicity was measured by LDH release in cell supernatants. As observed previously with granadaene, *L. lactis* p*cylX-K* pigment caused significantly greater cell death than non-hemolytic control extracts (Fig. 2.2d) [72]. Together, these data indicate that purified pigment from *L. lactis* p*cylX-K* possesses hemolytic and cytolytic activity that are no different than granadaene. Furthermore, our findings confirm that the *cyl* operon encode proteins sufficient for production of this ornithine rhamnolipid in a heterologous Gram-positive bacterium.

2.3.3 *Phyletic analysis suggests the cyl operon evolved prior to the diversification of Gram-positive bacteria.*

Our heterologous expression experiments suggest a possible advantage for lateral transfer of *cyl* genes between various bacteria. To understand the evolutionary origins of the ornithine rhamnolipid pigment, we conducted a systematic survey of the phyletic patterns and contextual associations of the *cyl* genes. We found that *cyl* genes are present in diverse Gram-positive phyla such as Firmicutes and Actinobacteria as well as the *Thermosporothrix* genus in the *Chloroflexi* phylum. A phylogenetic tree using the *cylE* acyl transferase gene, which is universally present in *cyl* operons, showed that the

Actinobacterial and Firmicute proteins group within their respective bacterial clades, whereas the *Thermosporothrix cylE* groups outside the two principal clades (Fig. 2.3a, Supplementary Fig. 2.3). The *Thermosporothrix* operons seem to contain elements of both the Actinobacterial and Firmicute types of operon, supporting that it has retained features of an ancestral version (Fig. 2.3a, Supplementary Fig. 2.3). The presence of *cyl* operons in diverse Firmicutes (spore formers and non-spore formers) and Actinobacteria, and a largely vertical inheritance of the Firmicute and Actinobacterial versions, indicates that the pigment biosynthesis genes evolved prior to the diversification of Gram-positive bacteria.

We identified five functional groups of genes in homologous *cyl* operons (Table 2.1): 1) those involved in lipid biosynthesis, 2) ornithine biosynthesis, 3) acyl-lipid transfer to the ornithine, 4) sugar biosynthesis and transfer, and 5) pigment export. Of these, our data indicate a vertically inherited orthologous core of seven genes comprising of *cylA*, *cylG*, *acpC*, *cylZ*, *cylE*, *cylF* and *cylH*. This likely comprises the most ancient core of the operon. Further, non-orthologous but biochemically functionally equivalent versions of four genes are observed, which encode the following: 1) CylK (*Streptococcus, Lactococcus, Leuconostoc*) and ACP synthase (actinobacteria, *Clostridium* and *Paenisporosarcina* species); 2) CylJ (Streptococci, certain Lactococci and *Clostridium* species) and one or two distinct glycosyltransferases (various Firmicutes, Actinobacteria and Chloroflexi) involved in sugar conjugation; 3) CylD (Streptococci, *Leuconostoc* and *Lactococci*) and ACP-S-malonyltransferase (in various Firmicutes, Chloroflexi and Actinobacteria); and 4) at least three distinct versions of ABC-transporter permease subunits have been alternatively recruited for pigment transport (Fig. 2.3b, Table 2.1). Of note, the non-orthologous displacements are supported by change in operon position of the genes (Supplementary Fig. 2.4). Taken together, this suggests a core of approximately eleven genes in an ancient operon prior to the divergence of Actinobacteria and Firmicutes, which encoded proteins belonging to one of the five functional groups involved in pigment synthesis (Table 2.1).

We observe that some *cyl* genes are exclusive to specific bacterial lineages, suggesting that they were acquired post-divergence. For instance, genes encoding CylJ and CylD are likely to have displaced those encoding the ancestral glycosyltransferase and ACP-S-malonyltransferase, respectively, in certain Streptococci (Fig. 2.3b). These also include rhamnose biosynthesis genes, which are only seen in Firmicutes and Chloroflexi, as well as ornithine cyclodeaminase (OCD), PLP-dependent aminotransferases, acyl coA ligase and various redox enzymes, which are only found in actinobacteria and partly in Chloroflexi. We predict that these genes evolved to increase the availability of the building blocks for pigment biosynthesis or add diversity to the functional groups on the pigment. For example, the presence of two glycosyltransferases in various Bacillus species in the *cyl* operons (Fig. 2.3a, Supplementary Fig. 2.3) could imply that these species possess a more complex sugar modification than rhamnose, and this warrants further study. In short, while there is little evidence to suggest extensive lateral transfer of *cyl* genes, our data indicate that individual genes were likely lost or displaced by non-orthologous genes across various species.

2.3.4 *The evolution of CylE and CylF conferred critical functions in granadaene biosynthesis to the cyl operon.*

One of the previously unresolved questions was the role of the lipoate-dependent aminomethyltransferase (CylF), as this is a universally conserved gene encoded by *cyl* operons. We predict that this is involved in ornithine biosynthesis. We infer this based on the presence of OCD-encoding genes in some Actinobacterial *cyl* operons (Fig. 2.3b, Table 2.1), which suggests in these organisms and, perhaps more generally in all organisms with the pigment, ornithine is synthesized by combining proline with ammonia. This provides a role for the aminomethylase CylF as this enzyme splits amino acids such as glycine to give rise to ammonia [92]. Given the need for ammonia in the ornithine synthesis by the OCD enzyme, we predict that CylF generates ammonia in the local milieu of the pigment biosynthesis complex, which is then used by OCD to make ornithine. Of the five basic

components of the *cyl* operon, the fatty acid biosynthesis genes often appear together in other contexts. However, the accretion of the acetyltransferase CylE and CylF in an ancient bacterium were perhaps the key events in the fixation of the *cyl* genes for pigment biosynthesis.

Given the phyletic patterns, we hypothesize that the ancient *cyl* operon evolved in free-living bacteria, where we conceive two possible biological roles that might not be mutually exclusive. First, the ornithine rhamnolipid might be involved in photoprotection, as with many microbial pigments [93-96]. Second, it might have evolved as a general defense/predation mechanism against competing organisms in which the pigment disrupts their cell membrane. The latter is supported by the hemolytic and cytolytic activity of the granadaene pigment in GBS [24,72,75] and *cyl*-expressing *L. lactis* (Fig. 2.1, Fig. 2.2). The presence of an identical or similar hemolytic pigment in a range of Gram-positive bacteria with *cyl* genes [97,98], as well as our heterologous expression experiments, suggest that granadaene can potentially function across a physiologically diverse group of organisms if they likely possess a Gram-positive-type cell wall structure. In fact, a recent study correlated pigmentation with hemolysis and *cyl* gene expression in *Acidipropionibacterium* species that have roles in cheese production and food preservation [98]. Accordingly, the hemolytic and cytotoxic properties of other pigmented, *cyl* operon-containing microbes found in soil environments or utilized for industrial application warrant further examination.

These findings broaden our understanding of the biosynthesis and evolutionary history of granadaene in GBS, along with that of other homologous microbial lipid pigments. Although our phyletic analyses do not establish horizontal gene transfer of the entire *cyl* operon, our heterologous gene expression studies indicate that this remains a formal possibility, particularly in Gram-positive bacteria. Because GBS cohabitates the human lower genital and gastrointestinal tract with other commensal bacteria, the possibility of lateral transfer of the *cyl* operon to otherwise avirulent bacteria in the human niche should be explored further.

2.4 MATERIALS AND METHODS

2.4.1 *Ethics statement*

Written informed consent for donation of human blood was obtained from patients, per the Principles in the WMA Declaration of Helsinki and Dept. of Health and Human Services Belmont Report. The study was approved by the Seattle Children's Research Institute Institutional Review Board (protocol #11117). Children under the age of 18 were not recruited for donation of human blood.

2.4.2 *Bacterial strains*

The GBS strain A909 was used in all studies. A909 is a clinical isolate obtained from an infected human neonate and is classified as serotype Ia [99]. The Δ*cylE*, Δ*covR*, and Δ*covR*Δ*cylE* mutants were derived from A909 as described [35,85]. Cultures of GBS were grown in tryptic soy broth (TSB; Difco Laboratories) at 37 ºC in 5% CO2, and cultures of Escherichia coli MC1016 were grown in lysogeny broth (LB; Difco Laboratires) at 37 ºC. Cultures of Lactococcus lactis were grown in TSB at 30 ºC in 5% CO2. Culture growth for all bacterial strains was measured at 600nm, and bacterial strains were washed twice in PBS before being used in experiments. Photographs of bacterial strains on blood agar (Remel) or Granada medium (Hardy Diagnostics) were captured with an SLR camera (EOS Rebel XSi 12.2MP; Cannon) with an 18–55 mm zoom lens and processed using Photoshop CC (Adobe).

2.4.3 *Heterologous expression of the cyl operon in Lactococcus lactis*

The *cyl* operon was amplified using high fidelity PCR and primer pairs cyl1, cyl2, and cyl3 (IDT, see Supplementary Table 2.2) to obtain three overlapping DNA fragments. The PCR fragments were ligated to a PCR fragment representing the vector pDC123 ([84], referred to in the main text and hereafter as pEmpty) using Gibson Assembly. The recombinant plasmid, which contained a chloramphenicol resistance gene, was electroporated into Escherichia coli MC1061 and then isolated by midiprep (Qiagen). After the presence of the *cyl* operon within the recombinant plasmid was

confirmed by PCR amplification, the recombinant plasmid was transformed into electrocompetent Lactococcus lactis. Upon the addition of the recombinant or empty plasmid, L. lactis was grown in the presence of 5 μg/mL chloramphenicol (Sigma-Aldrich).

2.4.4 *Isolation and purification of pigment from GBS and L. lactis*

Pigment was isolated from wildtype GBS and *L. lactis* p*cylX-K* as described, with minor modifications [23,24,72,75,83]. Wildtype GBS A909 or *L. lactis* p*cylX-K* were grown in 500 mL Granada medium [100], and the bacterial pellet was washed twice with HPLC-grade water and twice with DMSO. Then, the pellet was resuspended in DMSO + 0.1% trifluoroacetic acid (TFA; Sigma-Aldrich) to extract the pigment. Extractions with DMSO + 0.1% TFA continued until no pigmentation was observed in the bacterial pellet. The pigment extract was pooled and precipitated overnight with NH_4OH (Scientific Products). The precipitated pellet was washed twice with HPLC-grade water, and twice with DMSO. Pigment was then extracted using DMSO + 0.1% TFA as above, pooled, and then column-purified using high pressure liquid chromatography (HPLC, Shimadzu 10A system) with a Vydac 214TP C4 column (solvent: DMSO + 0.1% TFA, flow rate: 1 mL/min; detection: 489 nm). Fractions were collected between 10.5 min and 17.5 min of each run (when detection level was > 100,000 μV, see Supplementary Fig. 2.5). Purified fractions were pooled, precipitated with NH_4OH (Scientific Products), washed three times with HPLC-grade water and then twice with DMSO, and lyophilized to dryness. Lyophilized pigment toxin was stored at -80ºC and working pigment toxin solutions were dissolved in DMSO + 0.1% TFA + 20% starch (DTS), as described [75]. The purification and isolation procedure was also performed on corresponding GBS A909Δ*cylE* (non-pigmented/non-hemolytic isogenic mutant of wildtype A909) and *L. lactis* pEmpty (transformed with empty vector, non-pigmented/non-hemolytic) as described above. Extract from A909Δ*cylE* and *L. lactis* pEmpty were used as controls for pigment in all experiments, along with the DTS solvent. For NMR analysis, purified pigment from *L. lactis* p*cylX-K* or control extract from *L. lactis* pEmpty were resuspended in

DMSO + 0.1% TFA. ^{1}H, ^{13}C, ^{1}H-COSY NMR experiments were performed at 298K on a Varian 600 MHz NMR Spectrometer. Residual DMSO-d_5 was used to calibrate chemical shifts. High resolution mass spectra (HRMS) of samples dilute in DMSO + 0.1% TFA were recorded on a mass spectrometer using via ESI.

2.4.5 *Hemolytic assays*

Lyophilized pigment toxin or control extracts were dissolved in DTS to a final concentration of 200 µM and were incubated overnight at room temperature and protected from light before use. To perform the hemolytic titer, twofold serial dilutions of purified pigment in DTS from A909 WT or *L. lactis* p*cylX-K* were performed in PBS in a final volume of 100 µL. Twofold serial dilutions of control extracts (from GBSΔ*cylE* or *L. lactis* pEmpty) in DTS were also performed in PBS as controls. The samples were incubated with 100 µL of EDTA-treated human red blood cells (0.5% in PBS) in 96-well plates for 1 hour at 37 ºC. Then, the 96-well plate was centrifuged for 4 minutes at 300 x *g* to pellet the unlysed red blood cells, and supernatants were transferred to a replica 96-well plate. Hemoglobin release was measured by recording the absorbance at 420 nm of the supernatants (Spectramax i3x Plate Reader, Molecular Devices), and percent hemolysis was determined relative to red blood cells treated with positive control Triton X-100 (0.1%, Sigma-Aldrich) and negative control PBS only.

2.4.6 *Isolation of neutrophils from adult human blood*

As described [72], 5-15 mL of human adult blood was collected from independent healthy human adults into EDTA tubes (BD Bioscience). Immediately following collection, neutrophils were isolated using a MACSxpress neutrophil isolation kit, per the manufacturer's instructions (Miltenyi Biotec). Cells were then pelleted, and any residual red blood cells (RBC) were removed by re-suspending the cell pellet in RBC lysis solution (0.15nM NH_4Cl, 1mM $NaHCO_3$) for 15 minutes at room temperature.

Following RBC lysis, cells were washed with Roswell Park Memorial Institute 1640 tissue culture medium containing L-glutamine (Corning; hereafter referred to as RPMI-G). Neutrophil purity in the prepared cell suspension was assessed by examining the proportion of cells positive for the neutrophil cell markers CD15 (PerCP/Cy5.5, clone HI98, BD Biosciences) and CD16 (FITC, clone 3G8, BD Biosciences) by flow cytometry. Briefly, approximately 1 x 10^6 cells from the neutrophil purification preparation or 1 x 10^6 cells from whole blood (following two RBC lysis steps, as described above) were incubated with Fc receptor block (1:200, BD Biosciences) for 15 minutes at room temperature. Then, immunofluorescent antibodies were added to the cells at concentrations recommended by the manufacturer (1:10, CD15-PerCP/Cy5.5; 1:200, CD16-FITC), and cells incubated for 30 minutes at room temperature. Stained cells were washed twice in FACS (fluorescence-activated cell sorting) buffer (1mM EDTA, 25mM HEPES, 1% BSA (w/v) in PBS) and were analyzed immediately on an LSR II flow cytometer (BD Biosciences). Single-stained flurochrome-reactive AbC beads (Thermo Fisher) and unstained cells were used for compensation. Data were analyzed using FlowJo v. 10.1 (FlowJo, LLC).

2.4.7 *Testing bacterial strains and pigment extracts for neutrophil cytotoxicity*

Neutrophils were isolated as described above and were seeded in a U-bottom 96-well plate at approximately 4 x 10^5 cells/mL in 90 µL RPMI-G. *L. lactis* p*cylX-K* and *L. lactis* pEmpty were grown to mid-exponential growth phase (OD_{600} = 0.3), washed twice in sterile PBS, and added to neutrophils at a multiplicity of infection (MOI) of 10 and 100. MOIs were confirmed by dilution plating. Additionally, pigment in DTS from *L. lactis* pcylX-K or WT GBS was added to neutrophils at a final concentration of 0.5 µM. As positive and negative controls for all assays, neutrophils were incubated in 0.1% Triton X-100 (Sigma Aldrich) or sterile PBS, respectively. After incubating for 4 hours at 37ºC, cells were analyzed for cytotoxicity by the presence of cytoplasmic lactate dehydrogenase (LDH) in cell supernatants using the colorimetric LDH kit (Clontech), per the manufacturer's instructions.

Percent cytotoxicity was calculated by normalizing to PBS-treated cells (0% cell death) and Triton X-100-treated cells (100% cell death), as described [24,72,75].

2.4.8 *Phyletic analysis*

Phyletic pattern searches were done using the PSI-BLAST program [101] against a locally constructed compressed non-redundant database (NR50) of the National Center for Biotechnology Information (NCBI). Multiple sequence alignments were built using the Kalign program [102]. Contextual information from prokaryotic gene neighborhoods was retrieved by a Perl custom script that extracts the upstream and downstream genes of the query gene. Phylogenetic analysis was conducted using an approximately-maximum-likelihood method implemented in the FastTree 2.1 program under default parameters [103] (http://www.microbesonline.org/fasttree/). Network analysis was performed using the R language with the igraph package [104].

2.4.9 *Statistical analysis*

A value of $p < 0.05$ was considered significant. Nonlinear regression analysis was used to interpolate EC_{50} concentrations. In LDH release assays, an unpaired t test or one-way ANOVA with Tukey's posttest was employed as appropriate to analyze differences between treatment groups, unless otherwise noted. GraphPad Prism (version 7.03) was used to compute all statistical tests.

2.5 ACKNOWLEDGEMENTS

2.5.1 *Conflict of interest*

The authors declare that the research was conducted in the absence of any commercial or financial relationships that could be construed as a potential conflict of interest.

2.5.2 *Author contributions*

B.A., C.W., L.M.I., L.A., J.M.C., and L.R. designed the experiments. B.A., C.W., L.M.I., P.H.F., P.Q., and A.H. performed the experiments. B.A., C.W., L.M.I., L.A., J.M.C., and L.R. analyzed the results, and B.A., L.M.I., L.A., H.B.J., and L.R. wrote the manuscript.

2.5.3 *Funding*

This work was supported by funding from the National Institutes of Health grants R01AI112619, R01AI33976, R01AI00989, and R21AI125907 to L.R. The NIH training grant T32AI07509 (PI: Lee Ann Campbell) supported C.W. L.M.I. and L.A. were supported by intramural funds from NLM, NIH. The content is solely the responsibility of the authors and does not necessarily represent the official views of the National Institutes of Health. The funders had no role in study design, data collection and interpretation, or the decision to submit the work for publication.

2.5.4 *Other*

Special thanks to Connie Hughes for administrative support.

2.6 FIGURES AND TABLES

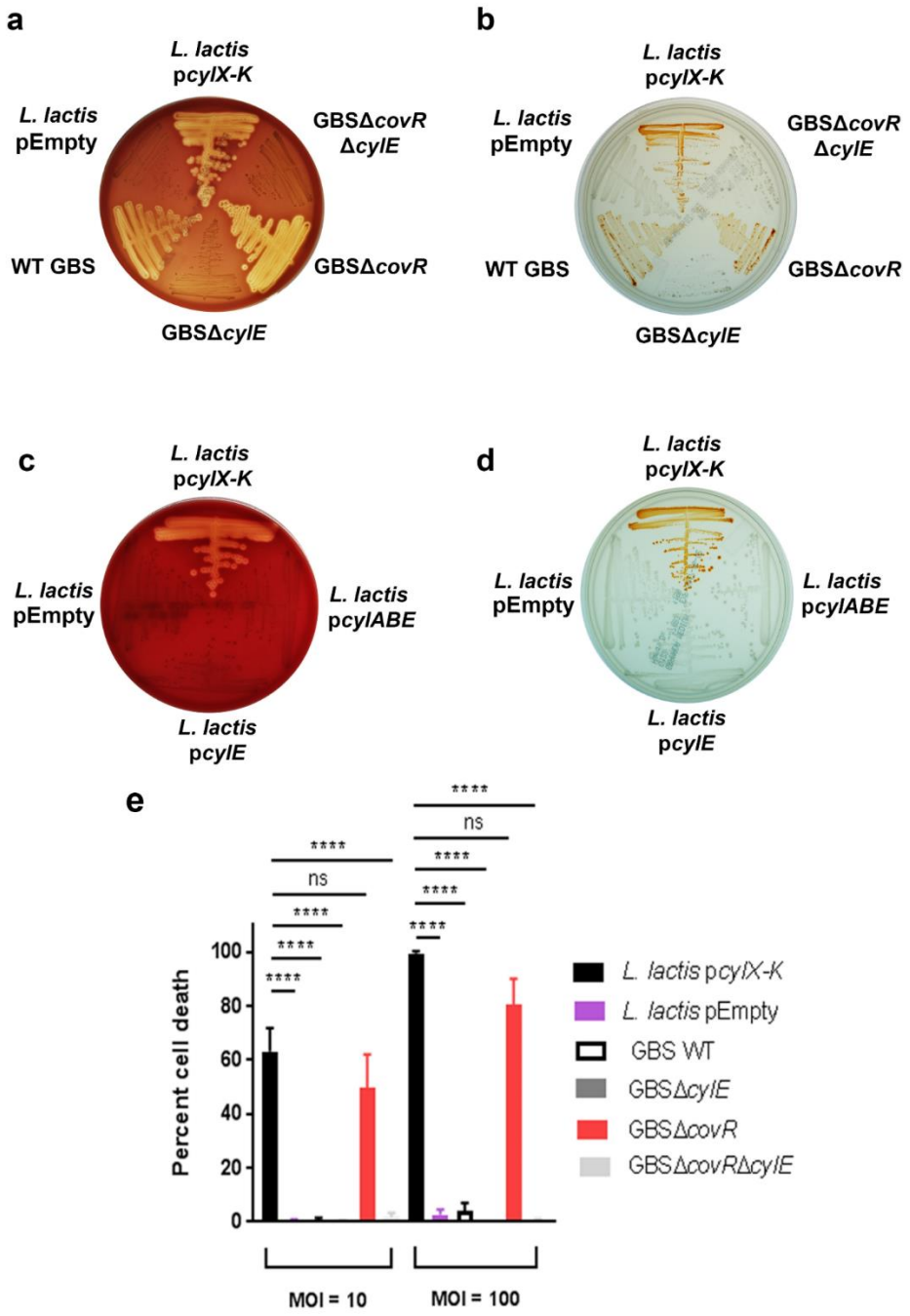

Figure 2.1. Heterologous expression of the *cyl* operon in *L. lactis* resulted in hemolysis and pigmentation.

Complementation of *L. lactis* with pcylX-K, but not empty plasmid vector, pEmpty, conferred hemolysis (**a**) and pigmentation (**b**) similar to that observed for hemolytic GBS, including strains that

lack the transcriptional repressor of the *cyl* operon, CovR (GBSΔ*covR*). Of note, GBS strains lacking CylE (i.e. GBSΔ*cylE*, GBSΔ*covR*Δ*cylE*) are neither hemolytic nor pigmented. Complementation of *L. lactis* with *cylE* alone or *cylA, cylB,* and *cylE* did not confer hemolysis (**c**) or pigmentation (**d**) to *L. lactis*. (**e**) *L. lactis* p*cylX-K, L. lactis* pEmpty, GBS WT, GBSΔ*cylE*, GBSΔ*covR*, or GBSΔ*covR*Δ*cylE* were incubated with human neutrophils for 4 hours at an MOI of 10 and 100, and neutrophil death was measured by LDH release into cell supernatants relative to Triton X-100 and PBS-only controls. Mean and standard error from three independent experiments performed in triplicate are shown. One-way ANOVA with Tukey's post-test was performed. **** indicates $p < 0.0001$, and ns indicates not significant, or $p \geq 0.05$.

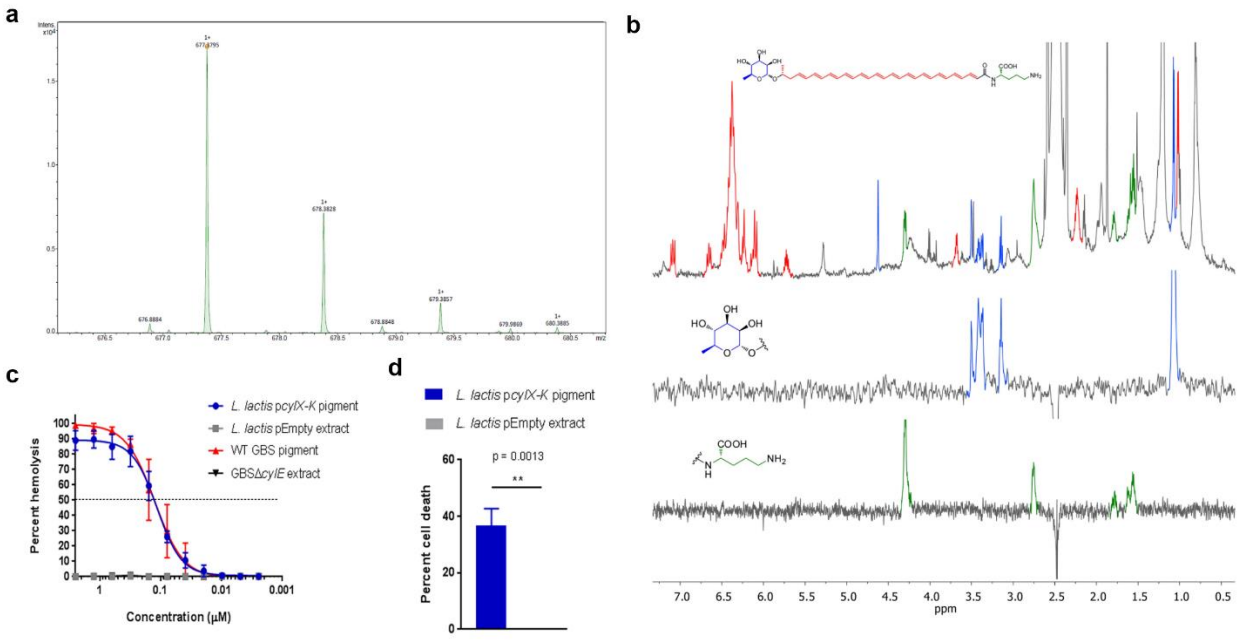

Figure 2.2. Pigment extracted and purified from *L. lactis* p*cylX-K* is identical to granadaene extracted from WT GBS.

(**a**) High resolution mass spectrometry was performed on pigment extracted from *L. lactis* p*cylX-K* and demonstrated an M+ H ion at *m/z* 677.3795, which is associated with an ion formula of $C_{39}H_{53}N_2O_8$ (expected mass of 677.3796). (**b**) ^{1}H NMR analyses on *L. lactis* p*cylX-K* pigment revealed a signal corresponding to a polyene structure (7.20 – 5.5 ppm), as well as signals corresponding to an ornithine (4.32, 2.77, 1.80, 1.59, and 1.64 ppm) and a rhamnose (4.63, 3.52, 3.43, 3.39, 3.16, 1.09 ppm). (**c**) HPLC-purified pigment from *L. lactis* p*cylX-K* or WT GBS in DMSO + trifluoroacetic acid + starch (DTS) was added to human erythrocytes in twofold serial dilutions starting from 2.5 to 0.0024 μM for 1 hour. As controls, equivalent amounts of extracts from *L. lactis* pEmpty and from non-pigmented/hemolytic GBSΔ*cylE* were tested. Mean and standard error from three independent experiments performed in triplicate are shown. The EC_{50} for *L. lactis* p*cylX-K* pigment (0.128 μM, 95% CI: 0.108, 0.153) is no different than that of WT GBS pigment/granadaene (0.127 μM, 95% CI: 0.100, 0.162). (**d**) Primary human neutrophils were incubated with 0.5 μM purified pigment from *L. lactis* p*cylX-K* for 4 hours at 37°C. As a control, neutrophils were treated with an equivalent amount of *L.*

lactis pEmpty extract. Neutrophil death was measured by LDH release into cell supernatants relative to Triton X-100 and PBS-only controls. Mean and standard error from three independent experiments performed in triplicate are shown. An unpaired t test was performed, and $p = 0.0013$.

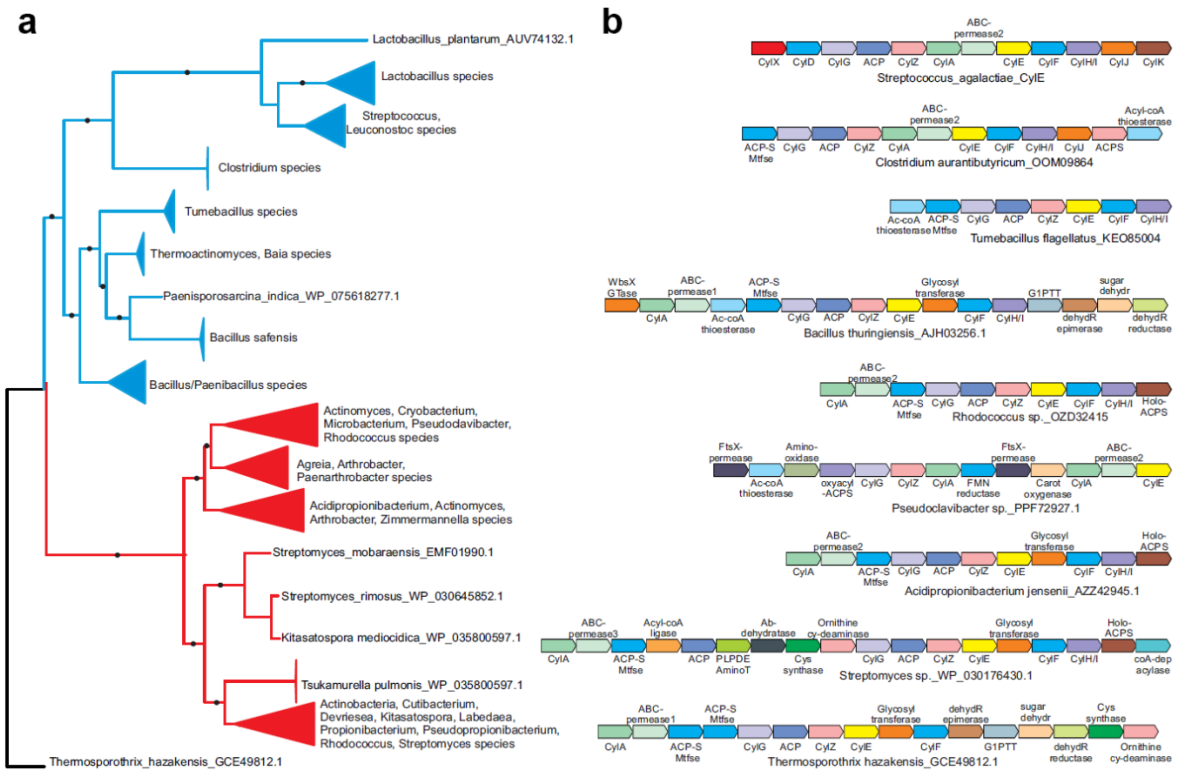

Figure 2.3. Phyletic analysis suggests the *cyl* operon evolved prior to the diversification of Gram-positive bacteria.

(**a**) A phylogenetic tree of the CylE protein is shown. Clades with strong bootstrap support were collapsed into filled triangles for convenience (see Supplementary Fig. 3 for full tree). Firmicute and Actinobacterial branches are colored blue and red respectively. (**b**) Representative *cyl* operons derived from the phylogenetic tree in (**a**) are shown. Genes are shown as boxed arrows, with the arrow head pointing to the 3' gene. Operons are labeled using the accession number of the *cylE* gene in the operon. Proteins are denoted using their species names followed by their Genbank accession number or gene names.

Table 2.1. Genes in *cyl* operons encode proteins that fall into one of five functional categories. Although orthologs of all genes present in the GBS *cyl* operon are not present in other *cyl* operons, non-orthologous, functionally equivalent proteins are encoded. A biosynthetic pathway for GBS pigment was previously proposed [75]. Briefly, CylX-generated malonyl-CoA units are linked to the acyl carrier protein (ACP) by CylD. The fatty-acid like pathway is initiated through the action of CylI, which joins the malonyl-CoA to an initial fatty acid-ACP complex. The fatty acid intermediate is reduced by CylG and CylZ, creating an alkene. CylI then utilizes the alkene as a substrate and adds another keto group, which is reduced further, resulting in another alkene on the unsaturated fatty acid chain. The elongation/reduction cycle repeats until the polyene chain contains twelve alkenes. Meanwhile, CylF cleaves amino acids such as glycine to generate ammonia, which can then be utilized by ornithine cyclodeaminase (OCD) or another functionally similar enzyme to generate ornithine. CylE replaces ACP with ornithine in the full-length polyene chain, and CylJ links the terminal glycosyl group to the polyene chain in the final step of pigment biosynthesis. The pigment is then transported to the bacterial cell surface via the CylA/B ABC transporter.

Functional category	**Gene product in GBS *cyl* operon**	**Putative function (reference)**	**Orthologs conserved in all *cyl* operons?**	**Non-orthologous, functionally equivalent gene products in other *cyl* operons**
Lipid biosynthesis	CylX	Generates malonyl-CoA units [75]	Yes	
	CylK	Phosphopantetheinyl transferase, involved in ACP synthesis [75]	No	ACP synthase
	ACP	Acyl carrier protein [20]	Yes	
	CylD	Conjugates ACP to malonyl-CoA units [20]	No	ACP-s-malonyltransferase
	CylH/I	Forms initial fatty acid-ACP complex and	Yes	

		adds new keto groups to elongate unsaturated fatty acid chain [21,75]		
	CylG	Reduces keto group added by CylH/I to hydroxyl [20,75]	Yes	
	CylZ	Further reduces keto group to alkene [75]	Yes	
Ornithine biosynthesis	CylF	Generates ammonia for ornithine biosynthesis (this study)	Yes	
Acetyltransferase	CylE	Replaces ornithine with ACP group on unsaturated fatty acid [75]	Yes	
Sugar biosynthesis and conjugation	CylJ	Attaches glycosyl group to unsaturated fatty acid [105]	No	glycosyltransferase, WbsX glucosyltransferase
Pigment export	CylA	Transport of pigment to cell surface; ATP binding domain [20,106]	Yes	
	CylB (ABC permease 2)	Transport of pigment to cell surface; transmembrane domain [20,106]	No	ABC permease1, ABC permease3

Chapter 3. LIPID ANALOGS REVEAL FEATURES CRITICAL FOR HEMOLYSIS AND DIMINISH GRANADAENE-MEDIATED GROUP B STREPTOCOCCUS INFECTION

This chapter is from the following article:

Armistead, B., Herrero-Foncubierta, P., Coleman, M., Quach, P., Whidbey, C., Justica, J., Tapia, Casares, R., Millan, A., R., Haidour, A., Rodriguez Granger, J., Santana-Ufret, V., Vornhagen, J., Merillat, S., Adams Waldorf, K., Cuerva, J.M., Rajagopal, L. (2020). Lipid analogs reveal features critical for hemolysis and diminish granadaene mediated Group B Streptococcus infection. *Nature Communications*, doi: 10.1038/s41467-020-15282-0.

3.1 ABSTRACT

Although certain microbial lipids are toxins, the structural features important for cytotoxicity remain unknown. Increased functional understanding is essential for developing therapeutics against toxic microbial lipids. Group B Streptococci (GBS) are bacteria associated with preterm births, stillbirths, and severe infections in neonates and adults. GBS produce a pigmented, cytotoxic lipid, known as granadaene. Despite its importance to all manifestations of GBS disease, studies towards understanding granadaene's toxic activity are hindered by its instability and insolubility in purified form. Here, we report the synthesis and screening of lipid derivatives inspired by granadaene, which reveal features central to toxin function, namely the polyene chain length. Furthermore, we show that vaccination with a non-toxic synthetic analog confers the production of antibodies that inhibit granadaene-mediated hemolysis *ex vivo* and diminish GBS infection *in vivo*. This work provides unique structural and functional insight into granadaene and a strategy to mitigate GBS infection, which will be relevant to other toxic lipids encoded by human pathogens.

3.2 INTRODUCTION

Microbial lipids with hemolytic or cytotoxic activity have been reported from several human bacterial pathogens, including mycolactone from *Mycobacterium ulcerans*[107,108], rhamnolipids from *Pseudomonas aeruginosa*[109,110], commendamide from *Bacteroides spp.*[111], and the pigmented ornithine rhamnopolyene (granadaene) from Group B Streptococcus (GBS)[24,75]. However, structure-activity studies demonstrating the features important for cytotoxicity are lacking, hindering the development of therapies or vaccines targeting these compounds. GBS is a β-hemolytic Gram-positive bacterium frequently associated with preterm birth and severe neonatal infections[3,13,112]. Although clinical trials involving maternal vaccination of a trivalent capsular polysaccharide based CRM197 conjugate was shown to provide serotype-specific antibody[10] and a six-valent vaccine is being explored[11], no FDA approved vaccine exists to date for GBS prevention. In recent years, the incidence of invasive GBS

disease including bloodstream, skin, soft tissue, and joint infections has increased in non-pregnant adults, particularly among the elderly and persons with comorbidities[5-7]. These trends, along with concerns regarding the emergence of antibiotic resistant GBS strains, has increased the urgency of novel preventive and curative treatments[113,114].

Granadaene produced by GBS confers pigmentation[23] and hemolytic activity[24,75] and is a major contributor to all manifestations of GBS disease, making it an attractive therapeutic target. Hemolytic and hyper-hemolytic GBS strains have been isolated from patients with GBS infections, including women in preterm labor and adults with invasive infections[8,75,88-90]. Furthermore, non-hemolytic GBS strains are typically virulence-attenuated, and hyper-hemolytic GBS strains exhibit increased virulence in various models of infection, including sepsis, meningitis, and preterm birth[29,34,72,75,89]. In addition, we showed that purified granadaene isolated from GBS is hemolytic and cytotoxic to innate immune cells, including mast cells, macrophages, and neutrophils[24,72,75,83]. Despite these advances, the structural features responsible for hemolysis and cytotoxicity are unknown.

A major barrier for elucidating the functions of GBS ornithine rhamnopolyene is its limited solubility and instability in its purified form, which is typical for compounds containing long polyene chains[115]. Here, we use chemical synthesis to overcome these challenges associated with studying polyenic compounds. Through the synthesis of analogs of granadaene, we demonstrate how the polyene chain length and polar head groups influence hemolytic activity. Further, we identify a non-toxic analog which, unlike granadaene, is tolerated by cells of the adaptive immune system and diminished granadaene-mediated GBS infection when incorporated into a vaccine formulation. Together, these data advance our chemical, molecular, and biological understanding of a key GBS virulence factor whose mechanism has eluded us thus far. Moreover, our findings provide proof-of-concept for a promising therapeutic strategy to mitigate the effects of this lipid toxin during infection.

3.3 RESULTS

3.3.1 *Polyene chain length is critical for hemolysis*

To understand components necessary for granadaene-mediated hemolysis and cytolysis, we identified target compounds for synthesis that contained chemical features analogous to those in granadaene (Fig. 1a) and were sufficiently soluble and stable *in vitro*. We focused on three relevant moieties: the polyene chain, the terminal amino acid, and the rhamnose. The chemical structure of each target compound that was synthesized is listed in Table 3.1. The synthetic compounds were designed to contain a varying number of alkene bonds, ranging from one to nine, denoted in the compound names by "P" and then the number of alkenes in the polyene chain (e.g. P9). The rhamnose group found in granadaene (Fig. 3.1a) was replaced with hydrophobic tert-Butyldimethylsilyl (TBS) protecting group (denoted by "p") in some target compounds, namely pP7X, pP7, pP9, and pP1, to ensure reasonable solubility of these derivatives during the synthetic sequence and subsequent biological tests. One compound, R-P4, was sufficiently stable, which enabled us to include a terminal rhamnose moiety without compromising solubility. In other compounds, such as P7 and P9, a hydroxyl group was included to test the effect of a hydrophilic head group. Because the L-ornithine residue at the terminus of granadaene was previously observed to lactamize in several synthetic reaction conditions[116], which could confound interpretation of the biological assays, it was replaced with a simpler L-alanine residue in all synthetic compounds except pP7X, which contained a carboxyl group instead; this compound was synthesized to test the effect of the terminal amino acid on hemolytic activity. Each of the target compounds was fully characterized (Materials and Methods and Supplementary Materials) and analyzed by mass spectrometry and ^{1}H and ^{13}C NMR (see Supplementary Materials).

To examine if analogs had hemolytic activity, we first examined their ability to lyse red blood cells on red blood agar plates and then quantitatively examined them for lysis of red blood cells using methods described[75]. While pP1, R-P4, and P7 showed no hemolytic activity (Supplementary Fig. 3.1),

hemolysis was observed in pP7X, pP7, pP9, and P9 (Fig. 3.1b-e), which indicates that the length of the polyene chain facilitates hemolysis. In addition, these results suggest that the protecting group is important for the activity of compounds with shorter polyene chains. Except for P9, no statistically significant difference in hemolysis was observed between compounds resuspended in DTS versus DMSO, indicating that starch, which is used to stabilize purified granadaene solutions[75], may be important to stabilize longer polyene chains that are unprotected. Of note, no hemolysis was observed in red blood cells treated with DTS or DMSO alone (Supplementary Fig. 3.1). Collectively, these findings emphasize the importance of the length of the polyene chain to GBS hemolysis (Fig. 3.2), thus, for the first time, providing insight into the chemical features key to granadaene activity.

3.3.2 *Granadaene is cytotoxic to CD4+ T cells and B cells*

In addition to lysis of red blood cells, we have described the cytotoxic activity of granadaene to various innate immune cells, including mast cells, neutrophils, and macrophages[24,72,75,83]. To date, the effect of granadaene on adaptive immune cells has not been described but is critical to determine for vaccine strategies. Furthermore, antibodies specific to this toxin have not been identified. As a few studies have reported that GBS can activate CD4+ T cells[65,66], we explored the effect of granadaene on adaptive immune cells.

First, primary CD4+ T cells or B cells isolated from the blood of healthy adult humans were incubated with GBS that were either hyper-hemolytic (NCTC10/84, serotype V) or non-hemolytic (NCTC10/84Δ*cylE*; the non-hemolytic strain lacks the *cylE* gene, which is necessary for granadaene production[21]) at a multiplicity of infection (MOI) of 10 for 1 hour. We noted that the hyper-hemolytic strains induced cell death at a significantly greater rate compared to cells treated with non-hemolytic GBS (Fig. 3.3a). These findings indicate that adaptive immune cells are susceptible to death by hyper-hemolytic GBS strains. Of note, only minimal cytotoxicity (<10%) was observed with modestly hemolytic GBS strains (A909, serotype Ia; and COH1, serotype III), similar to our previous

observations with innate immune cells[24,72,83]. Next, to explore the mechanism and kinetics of cell death, we measured propidium iodide (PI) uptake and Annexin V (AV) staining in both cell types at 0 minutes, 15 minutes, and 30 minutes following incubation with hyper-hemolytic GBS at an MOI of 10 using flow cytometry. Briefly, PI is a membrane impermeable fluorescent stain that binds nucleic acid, indicating cell membrane damage. Fluorescently-labeled AV marks phosphatidylserine, which is present on the surface of cell membranes during apoptosis or is exposed as a result of membrane rupture[117]. We found that at 0 minutes, most cells were negative for both PI and AV, but after just 15 minutes of incubation, a proportion of each cell type were positive for PI and AV, and by 30 minutes, more cells became positive for both PI and AV (Fig. 3.3b). The rapid phenotypic shift of PI-/AV- to PI+/AV+ suggests that CD4+ T cells and B cells underwent a lytic form of cell death, rather than apoptosis[118]. Notably, cells remained PI-/AV- after 30 minutes of treatment with non-hemolytic GBS (Supplementary Fig. 3.3). When CD4+ T cells were imaged using scanning electron microscopy (SEM) after exposure to hyper-hemolytic GBS, non-hemolytic GBS, or PBS, striking changes in cell surface morphology were observed in cells treated with hyper-hemolytic GBS, but not with cells exposed to non-hemolytic GBS or saline controls (PBS) (Fig. 3.3c).

To determine if granadaene alone was sufficient for induction of these cytolytic effects, the above assays were performed with purified granadaene (0.5 μM), equivalent amount of extract from non-hemolytic GBS (GBSΔ*cylE* extract), or solvent (DTS) alone. Similar to our observations with live bacteria, significantly greater cell death was observed when CD4+ T cells and B cells were exposed to granadaene compared to the controls (GBSΔ*cylE* extract or DTS) (Fig. 3.3d), and these cells also rapidly switched to PI+/AV+ (Fig. 3.3e) while the vast majority of controls remained PI-/AV- (Supplementary Fig. 3.2). Further, SEM revealed that CD4+ T cells treated with granadaene exhibited morphological changes on the cell surface unlike cells treated with GBSΔ*cylE* extract or DTS (Fig.

3.3f). Together, these findings demonstrate that granadaene and hyper-hemolytic GBS strains are cytotoxic to cells of the adaptive immune system.

3.3.3 *Synthetic analog R-P4 is not toxic to T cells and B cells*

Our results above indicate that granadaene is likely to be a poor candidate for incorporation into a vaccine for prevention of GBS infection. We reasoned that a non-toxic synthetic analog of the GBS ornithine rhamnopolyene may be better suited in a vaccine formulation. Because R-P4 was non-hemolytic and contains structural components most like granadaene of all the synthesized analogs (i.e. terminal rhamnose, polyene chain, and terminal amino acid), we tested its cytotoxicity to CD4+ T cells and B cells. We found that primary human CD4+ T cells or B cells exposed to R-P4 (20 μM) for 1 hour showed minimal cell death (Fig. 3.4a). Next, we determined whether CD4+ T cells and B cells could respond to activation stimuli in the presence of R-P4. To this end, primary human CD4+ T cells were stimulated with PMA and αCD3ε, and primary human B cells were stimulated with αCD40 and IL-4. Cells were then treated with PBS, R-P4 (20 μM), or purified granadaene (5 μM). After 48 hours, cells were stained for the canonical activation marker CD69[119], resuspended in DAPI as a viability stain, and analyzed by flow cytometry (see gating strategy in Supplementary Fig. 3.3). Compared to unstimulated controls treated with PBS, stimulated CD4+ T cells and B cells exposed to R-P4 up-regulated CD69 (Fig. 3.4b, c). Furthermore, CD69 expression in stimulated cells exposed to R-P4 was no different than stimulated cells exposed to PBS (Fig. 4b, c). Of note, less than 10% of cells treated with granadaene were viable (DAPI-) (Supplementary Fig. 3.3), so this group was excluded from the CD69 analysis in both cell types. However, the proportion of DAPI- cells was no different among other treatment groups in either cell type (Supplementary Fig. 3.3). Collectively, these results indicate that CD4+ T cells and B cells survive and respond to activating stimuli when exposed to R-P4.

3.3.4 *Vaccination with R-P4 analog diminished GBS infection*

Next, we hypothesized that vaccination with R-P4 may generate an immune response that counteracts the effects of granadaene during systemic GBS infection. Given that hyper-hemolytic GBS cause lethal infection in adult mice[35], we used the adult systemic model of GBS infection to test if R-P4 could diminish infection with a hyper-hemolytic strain. To this end, mice were immunized (I.P.) with an emulsion of R-P4 (10 μM in PBS) and Freund's adjuvant (see Materials and Methods) and boosted 14 days later with the same dose. On day 21 after initial vaccination, mice were euthanized for plasma collection or were challenged (I.P.) with the hyper-hemolytic GBS strain NCTC10/84 (Fig. 3.5a). As controls, mice were injected with adjuvant alone on the same vaccination schedule.

Immunoblots revealed that plasma from mice vaccinated with R-P4 contained more IgG bound to purified granadaene compared to adjuvant-only controls (Fig. 3.5b). Furthermore, plasma from analog-vaccinated mice inhibited granadaene-mediated hemolysis in contrast to plasma from adjuvant-only controls (Fig. 3.5c, n = 10/group). The amount of granadaene-bound IgG detected in plasma significantly correlated with inhibition of granadaene hemolysis (Supplementary Fig. 3.4), suggesting that granadaene-reactive IgG partially neutralizes toxin function. At 24 hours post-bacterial challenge mice were euthanized, and GBS CFU were enumerated in the spleen, lung, brain, and blood. Significantly fewer CFU were recovered from the tissues and blood of analog-vaccinated mice compared to adjuvant-only control mice (n = 24/group) (Fig. 3.5d), indicating that immunization with R-P4 limited bacterial dissemination. Together, these data demonstrate for the first time that vaccination with a non-toxic granadaene analog generates granadaene-specific antibodies with neutralizing properties and protects against infection with hyper-hemolytic GBS.

3.4 DISCUSSION

Microbial lipids produced by several human pathogens, including mycolactone from *Mycobacterium ulcerans*[107,108], rhamnolipids from *Pseudomonas aeruginosa*[109,110], commendamide from *Bacteroides spp.*[111], and granadaene from GBS[24,75], contribute to pathogenesis by killing host cells. Yet structure-function studies demonstrating the underpinnings of cytotoxicity in such compounds are lacking, and no strategies exist to attenuate toxin activity during infection. Here, we use chemical synthesis to understand the characteristics important for hemolytic activity in the ornithine rhamnopolyene produced by GBS. Furthermore, we provide proof-of-concept for a vaccine that mitigates the effect of this lipid toxin during infection.

Our studies indicate that the polyene chain length is a key factor in the ability of granadaene to lyse red blood cells. We show that lipids with one or four alkenes (pP1 and R-P4) are not hemolytic despite having a terminal amino acid and protecting group (Supplementary Fig. 3.1). Similarly, polyenes containing seven double bonds were non-hemolytic (P7) unless the terminal polar group was replaced with a hydrophobic group such as TBS (pP7X, pP7). In contrast, lipids with nine alkenes (P9, pP9) were hemolytic, with or without the TBS protecting group (Fig. 3.1). Interestingly, a much greater concentration of each hemolytic analog was required for activity (62.5 to 250 μM, Fig. 3.1) compared to that previously observed for granadaene (0.1 to 1 μM)[75]. We predict that this may be due to the length of the polyene chains; the predicted length of granadaene (> 32 Å) is longer when compared to the length of each analog (< 24 Å, Table 3.1). Our data suggest that granadaene's hydrophobic polyene moiety can span the thickness of the target cell's plasma membrane (30-40 Å)[24,120-122], with the terminal ornithine and rhamnose serving as hydrophilic polar head groups that allow for stable insertion. The ability of the polyene moiety of pP7X, pP7, P9, and pP9 to span the plasma membrane partially, but not entirely, could explain the observed attenuated hemolytic activity relative to granadaene.

Additionally, calculated partition coefficients for more active lipids are in agreement with a dynamic and favorable lipophilic interaction with lipidic cellular domains (Table 3.1)[123].

The observation that P7, which is similar in length to pP7, is non-hemolytic (Supplementary Fig. 3.1) suggests an additional role for the terminal head groups in hemolytic activity. It is plausible that the terminal, hydrophilic hydroxyl group in P7 being imbedded within the highly hydrophobic lipid bilayer destabilizes the seven-alkene analog, whereas the hydrophobic TBS protecting group in pP7 allows for stable insertion into the cell's lipid bilayer. Our finding that P9, which does not have a TBS group but a terminal hydroxyl group, is hemolytic (Fig. 3.1e) suggests that a longer polyene chain (i.e. nine alkenes versus seven alkenes) stabilizes insertion of the polyene into the cell membrane. A limitation of our work is the present inability to synthesize compounds with polyene chains containing more than nine alkenes due to rapid denaturation during synthesis. Synthesis of analogs with longer polyenes, such as those with twelve alkenes like granadaene, will be essential in confirming the model we propose (Fig. 3.2).

Recently, microbial lipids have gained appreciation for their importance as antigens in the host response against bacterial infections[124]. Here, we show that granadaene kills cells of the adaptive immune system, including CD4+ T cells and B cells (Fig. 3.3). Death in these cells was marked by cell membrane permeability and damage, as indicated by rapid PI/AV positivity and SEM imaging. Our new findings with adaptive immune cells could at least partially explain why antibodies specific to granadaene never been isolated from infected patients or produced in the laboratory; the cytotoxic effect of the GBS ornithine rhamnopolyene to the very cells involved in antibody production inhibit their function. As such, granadaene is likely a poor candidate to serve as an antigen in a GBS vaccine formulation.

We hypothesized that a non-toxic analog with structural similarities to granadaene, namely the rhamnose, polyene chain, and amino acid, may serve as an antigen that would prompt an immune

response with cross-reactivity to granadaene during GBS infection. We show that compound R-P4 is non-toxic to CD4+ T cells and B cells and that these cells can respond to activating stimuli when exposed to R-P4 (Fig. 3.4). Thus, we selected R-P4 as the immunizing agent for our vaccination studies. We found that plasma from mice vaccinated and boosted with R-P4 contained class-switched antibodies that bound specifically to granadaene (Fig. 3.5b). In addition, plasma from R-P4-vaccinated mice inhibited hemolytic activity of granadaene *ex vivo* more than plasma from control only mice (Fig. 3.5c). Moreover, the amount of granadaene-bound IgG in plasma significantly correlated with granadaene inhibition (Supplementary Fig. 3.4). These findings suggest that vaccination with R-P4 generates granadaene-specific antibodies, which have toxin-neutralizing properties. The anti-virulence factor effect of R-P4 vaccination was further supported by results from infected mice; analog-vaccinated mice infected with hyper-hemolytic GBS experienced less bacteremia and bacterial dissemination to peripheral organs, including the spleen, lungs, and brain compared to adjuvant-only control mice (Fig. 3.5c). Because granadaene has been shown to promote GBS transmigration of the lung and blood brain barriers[33,34], our results suggest that vaccination with R-P4 limited GBS virulence by counteracting the pathogenic effects of this toxin. We hypothesize that the high degree of structural similarity between R-P4 and granadaene allowed for the production of antibodies with affinity for granadaene that dampened the activity of this toxin during GBS infection. Additional data on the dynamics of the humoral and cell-mediated response during immunization and the course of infection will lend greater insight into the mechanisms of protection conferred by this vaccine formulation and will inform the design of other vaccines that incorporate lipid antigens.

In conclusion, our findings with synthetic analogs reveal the structural components of granadaene that are important for host cell lysis. Additionally, we overcome granadaene-mediated cytotoxicity of T cells and B cells by creating a vaccine using a non-toxic granadaene analog, which prompted the generation of granadaene-binding antibodies and reduced the harmful effects of this toxin

during GBS infection. Collectively, these studies provide proof-of-concept for a novel strategy to counteract a cytotoxic microbial polyene that is critical to pathogenesis. These findings have broad application to understanding the biological activity of similar microbial lipid toxins and the development of targeted therapeutics against them.

3.5 Materials and Methods

3.5.1 *Ethics statement*

Written informed patient consent for donation of human blood was obtained with approval from the Seattle Children's Research Institute Institutional Review Board (protocol #11117) per the Principles in the WMA Declaration of Helsinki and Dept. of Health and Human Services Belmont Report. Children under the age of 18 were not recruited for donation of human blood.

All animal experiments were approved by the Seattle Children's Research Institutional Animal Care and Use Committee (protocol IACUC00036) and performed in strict accordance with the recommendations in the Guide for the Care and Use of Laboratory Animals of the National Institutes of Health (8th Edition).

3.5.2 *Chemicals*

Dimethyl sulfoxide (DMSO, Fisher Scientific), trifluoroacetic acid (TFA, Thermo Fisher Scientific), and Difco soluble starch (BD) were used to make DMSO + TFA (0.01%) + starch (DTS). All reagents used in the synthesis of granadaene analogs were purchased from standard chemical suppliers and used without further purification.

3.5.3 *Bacterial strains*

The wild-type (WT) GBS strains used in this study are A909 (serotype Ia) and NCTC10/84 (serotype V); these strains are clinical isolates obtained from infected newborns[125]. Isogenic non-

hemolytic Δ*cylE* mutants derived from A909 and NCTC10/84 have been previously described[21] and were used as non-hemolytic controls.

Cultures of GBS were grown in tryptic soy broth (TSB; Difco Laboratories) at 37 ºC in 5% CO_2. Culture growth for all bacterial strains was measured at 600 nm, and bacterial strains were washed twice in PBS before being used in experiments. Photographs of bacterial strains on blood agar (Remel) or Granada medium (Hardy Diagnostics) were captured with an SLR camera (EOS Rebel XSi 12.2MP; Cannon) with an 18–55 mm zoom lens and processed using Photoshop CC (Adobe).

3.5.4 *Isolation and purification of granadaene from GBS*

Granadaene was isolated from wildtype GBS A909 as described in Chapter 2 and in previous articles[23,75,126]. Briefly, 500 mL cultures of wildtype GBS A909 cultures were grown in Granada medium, and granadaene was extracted from the bacterial pellet using DMSO + 0.1% trifluoroacetic acid (TFA; Sigma-Aldrich). The extract was column-purified using high pressure liquid chromatography (HPLC) with a Vydac 214TP C4 column. Purified fractions were pooled, precipitated with NH_4OH (Scientific Products), washed twice with HPLC-grade water and then twice with DMSO, and lyophilized to dryness. Lyophilized granadaene was stored at -80 ºC, and working granadaene solutions were dissolved in DMSO + 0.1% TFA + 20% starch (DTS), as previously described[75]. The purification and isolation procedure were also performed on GBS A909Δ*cylE* (non-pigmented/non-hemolytic isogenic mutant of wildtype A909). Extract from A909Δ*cylE* was used as a control for granadaene in all experiments, along with the DTS solvent. ^{1}H NMR spectrum of purified samples was used as the criterion of purity and identity.

3.5.5 *Synthesis of granadaene analogs*

The entire procedure for the synthesis of granadaene analogs is in Appendix B.

General information. The synthetic approach was based on an iterative sequence of Horner-Wadsworth-Emmons olefination reactions. Although many other olefination reactions are known, this sequence was chosen for its preference toward *E* stereoisomers, which is desirable for synthesis of the target compounds. The complexity of the analysis of naturally occurring granadaene precluded an exact analysis of the stereochemistry of the polyene chain, which was postulated to be *E*. The stereochemical purity in such a long polyene is compromised and therefore many diastereoisomers could contribute to the hemolytic activity. Given this, we produced a mixture of diastereoisomers composed by the all *E*-diastereoisomer and minor amounts of other *Z*-containing diastereoisomers, thus more precisely mimicking natural granadaene.

Tetrahydrofuran (THF) was freshly distilled from Na. CH_2Cl_2 was freshly distilled from P_2O_5. Thin layer chromatography (TLC) was performed on aluminum-backed plates coated with silica gel 60 (230-240 mesh) with F_{254} indicator. The spots were visualized with UV light (254 nm). All chromatography purifications were performed with silica gel 60 (40-60 μm). NMR spectra were measured at room temperature. ^{1}H NMR spectra were recorded at 400, 500 and 600 MHz. Chemical shifts are reported in ppm using residual solvent peak as reference ($CHCl_3$: δ = 7.26 ppm, CH_3OH: δ = 3.31 ppm, DMSO: δ = 2.50 ppm). ^{13}C NMR spectra were recorded at 100, 125 and 150 MHz using broadband proton decoupling, and chemical shifts are reported in ppm using residual solvent peaks as reference ($CHCl_3$: δ = 77.16 ppm, CH_3OH: δ = 49.0 ppm, DMSO: δ = 39.51 ppm). Carbon multiplicities were assigned by DEPT techniques. High resolution mass spectra (HRMS) were recorded on a mass spectrometer using EI at 70 eV. Racemic ethyl 3-hydroxybutanoate was used in the synthesis of all granadaene derivatives, except for R-P4 owing to the presence of the D-rhamnose subunit, which can generate different diastereoisomers. In this case, (*3R*)- ethyl 3-hydroxybutanoate was used as starting material. The known compound ethyl 3-((tertbutyldimethylsilyl)oxy)butanoate was isolated as pure sample and showed NMR spectra matching those of previously reported[127].

General procedure for Horner-Wadsworth-Emmonds reaction (GP-1). A mixture of the corresponding phosphonate (2.5 mmol), and NaH (2.5 mmol, 60% purity) in THF (15 mL) was stirred at 0 ºC for 10 minutes. Then, the corresponding aldehyde (1 mmol) was added dropwise for 10 minutes, and the new mixture was stirred at room temperature for 0.5-1.5 h. Then, saturated aqueous NH_4Cl was added, and THF was removed under reduced pressure. The residue was solved in EtOAc, and the mixture was washed with saturated aqueous NH_4Cl and brine, dried over anhydrous Na_2SO_4, and the solvent was removed. Products were purified by flash chromatography on silica gel (EtOAc/Hexane mixtures) and characterized by spectroscopic techniques.

General procedure for DIBAL-H reduction of esters to alcohols (GP-2). To a solution of the corresponding ester (1 mmol) in THF (5 mL), DIBAL-H (2.5 mmol, 1 M in THF) was added, and the mixture was stirred at 0 ºC for 1-2 h. Then, the reaction was quenched with H_2O, diluted with EtOAc, and washed with 10% solution of HCl and brine. The mixture was dried over anhydrous Na_2SO_4 and the solvent removed. Products were purified by flash chromatography on silica gel (EtOAc/Hexane mixtures) and characterized by spectroscopic techniques.

General procedure for oxidation with Dess-Martin periodinane (GP-3). To a solution of the corresponding alcohol (1 mmol) in CH_2Cl_2 (15 mL) at 0ºC, Dess-Martin periodinane (DMP) (1.5 mmol) was added, and the mixture was stirred at room temperature for 1-2 h. Then, the solvent was removed, and EtOAc was added. The organic layer was washed with a 1:1 solution of saturated $NaHCO_3$ and 10% $Na_2S_2O_3$, dried over anhydrous Na_2SO_4, and the solvent removed. Products were purified by flash chromatography on silica gel (EtOAc/Hexane mixtures) and characterized by spectroscopic techniques.

General procedure for basic deprotection of esters (GP-4). To a solution of the corresponding ester (1 mmol) in wet MeOH (30 mL), a 2 M solution of KOH in MeOH (8-12 mmol) was added, and the mixture was stirred at room temperature for 4-6 h. Then, a few drops of water were added, and the

mixture was neutralized by addition of amberlyst 15 (110 mg, previously washed with CH_2Cl_2 and MeOH). Products were purified by flash chromatography on silica gel (CH_2Cl_2/MeOH) and characterized by spectroscopic techniques.

3.5.6 *Modeling granadaene and synthetic compounds and predicting lengths of polyene chains*

All compounds were drawn in ChemDraw software (Perkin Elmer). Structures underwent energy minimization in Chem3D software (Perkin Elmer) and were visualized as .mol files in Mercury software (The Cambridge Crystallographic Data Centre). Here, the distance between the first carbon to the last carbon of the last double bond in the polyene chain was measured to calculate the length of the polyene chain for each compound.

3.5.7 *Hemolytic assays*

Synthetic analogs of granadaene (table 1) were resuspended in DTS or DMSO to achieve a concentration of 0.02 M. To test for hemolysis, 3-5 µL of synthetic analogs were spotted onto a Red blood agar plate (TSA plate containing 5% sheep's blood, Remel). After allowing the spots to dry for about 10 minutes at room temperature, the blood agar plates incubated overnight at 37 ºC in 5% CO_2, as described[75]. Blood agar plates were placed on a light box, and photographs were captured with the digital SLR camera described above and processed using Photoshop CC (Adobe). Synthetic analogs were co-incubated with human red blood cells in PBS in a final volume of 100 µL at 250 µM, 125 µM and 62.5 µM for 1 hour at 37 °C. As described previously[75], hemoglobin release in cell supernatants was measured, and percent hemolysis relative to Triton X-100 (0.1%)-treated positive controls and PBS-treated negative controls was calculated.

3.5.8 *Isolation of CD4+ T cells and B cells from human adult blood*

Approximately 15 mL of blood was collected from healthy human adults into EDTA tubes (BD Biosciences). Immediately following collection, CD4+ cells or B cells were isolated from the blood

using the appropriate RosetteSep Enrichment Cocktail (StemCell) along with SepMate tubes (StemCell), per manufacturer instructions. Cells were then pelleted, and any residual red blood cells (RBC) were removed by re-suspending the cell pellet in RBC lysis solution (150 mM NH_4Cl, 1 mM $NaHCO_3$) for 15 minutes at room temperature. Following RBC lysis, cells were washed with Roswell Park Memorial Institute 1640 tissue culture medium containing L-glutamine (Corning; hereafter referred to as RPMI-G). Cell purity was assessed by examining the proportion of cells positive for the appropriate markers using flow cytometry. Briefly, approximately 1 x 10^6 cells from the purification preparation or 1 x 10^6 cells from whole blood (following two RBC lysis steps, as described above) were incubated with Fc receptor block (1:200, BD Biosciences) for 15 minutes at room temperature. Then, immunofluorescent antibodies were added to the cells and cells incubated for 30 minutes at room temperature. B cell preparations were stained with CD19-PerCP/Cy5.5 (3:100, BioLegend); CD4+ T cell preparations were stained with CD3-FITC (1:10, BD Biosciences), CD4-V450 (1:10, BD Biosciences) and CD8-PerCP/Cy5.5 (1:10, BD Biosciences). Stained cells were washed twice in FACS (fluorescence-activated cell sorting) buffer (1 mM EDTA, 25 mM HEPES, 1% BSA (w/v) in PBS) and were analyzed immediately on an LSR II flow cytometer (BD Biosciences). Single-stained fluorochrom-reactive AbC beads (Thermo Fisher) and unstained cells were used for compensation. Data were analyzed using FlowJo v. 10.1 (FlowJo, LLC).

3.5.9 *Testing bacterial strains, granadaene, and synthetic analogs for cytotoxicity*

T cells and B cells were isolated as described above. T cells or B cells were seeded at 2.5 x 10^6 cells/well in 90 µL RPMI-G. Hyper-hemolytic GBS (WT NCTC10/84) and non-hemolytic GBS (NCTC10/84Δ*cylE*) were grown to mid-exponential growth phase (OD_{600} = 0.3), washed twice in sterile PBS, and added to cells at a multiplicity of infection (MOI) of 10. MOIs were confirmed by dilution plating. Additionally, granadaene in DTS from WT GBS was added to cells at a final concentration of 0.5 µM, and R-P4 was added to cells at a final concentration of 20 µM. As positive

and negative controls for all assays, cells were incubated in 0.1% Triton X-100 (Sigma Aldrich) or sterile PBS, respectively. After 1 hour incubation at 37 ºC, cells were analyzed for cytotoxicity by the presence of cytoplasmic lactate dehydrogenase (LDH) in cell supernatants using the colorimetric LDH kit (Clontech), per the manufacturer's instructions. Percent cytotoxicity was calculated by normalizing to PBS-treated cells (0% cell death) and Triton X-100-treated cells (100% cell death), as described[24,72,75].

3.5.10 *Uptake of propidium iodide (PI) and annexin V (AV)*

PI uptake and AV staining were measured concurrently, as previously described[72]. Briefly, T cells and B cells were isolated as described above and were washed in PBS and resuspended in AV binding buffer (10 mM HEPES, 140 mM NaCl, 2.5 mM $CaCl_2$ in PBS) at a concentration of approximately 3.33 $x10^6$ cells/mL. Cells were then incubated with AV-Alexa Fluor 488 (1:20, Invitrogen) and PI (12.5 µg/mL, Life Technologies) for 15 minutes at room temperature, protected from light. Cells were then diluted by a factor of 5 in AV binding buffer into FACS tubes (BD Biosciences) and treated with hyper-hemolytic GBS or non-hemolytic GBS at an MOI of 10 or granadaene (0.5 µM) or an equivalent volume of GBSΔ*cyl*E extract. PI uptake and AV staining were measured using an LSR II flow cytometer (BD Biosciences) immediately following inoculation (0 min time point) and various times after inoculation (15, 30 min). Gates for PI positive (PI+) and AV positive (AV+) cells were determined using unstained and single-stained controls.

3.5.11 *Scanning electron microscopy*

Cells were washed in PBS and resuspended in one volume of ½ Karnovsky's fixative (2% paraformaldehyde, 2.5% glutaraldehyde, 2.5 mM $CaCl_2$ in 0.1 M Cacodylate buffer, pH 7.2). Then, the cells were centrifuged and resuspended in 1.4 mL ½ Karnovsky's fixative and allowed to incubate overnight at 4 °C. Samples were prepared for scanning electron microscopy as described

previously[72,75,83]. Images were obtained using a Sigma 500 variable pressure Field Emission Scanning Electron Microscope (FESEM) operating with Smart SEM (version 5.09).

3.5.12 *Stimulation of CD4+ T cells and B cells*

Primary human CD4+ T cells and B cells were isolated from the blood of healthy human adults, as described above. Cells were seeded at approximately 1 x 10^6 cells/mL in RPMI-G on a TC-treated 96-well plate (180 µL/well). CD4+ T cells were stimulated with immobilized anti-human CD3ε (0.5 µg, BD Biosciences) and PMA (10 ng/mL, Sigma), as previously described[130,131]. B cells were stimulated with human IL-4 (20 ng/mL, Sigma) and anti-human CD40 monoclonal antibody (5 µg/mL, Enzo, clone mAb 89), as previously described[132]. Immediately following stimulation, cells were treated with either PBS or R-P4 (20 µM) in technical triplicate. As controls, a group of CD4+ T cells and B cells received no stimulus and no treatment (designated as "PBS (unstimulated)"). After incubating for 48 hours at 37 °C, cells were treated with human Fc block (1:200, BD Biosciences), stained with anti-CD69-PE/Cy7 (10 µL/test, BD Biosciences, clone FN50), washed, and resuspended in DAPI (0.5 µM, Thermo). Cells were run on an LSR II flow cytometer (BD Biosciences). Unstained cells, single-stained DAPI+ cells, and single-stained PE/Cy7+ beads were used as compensation controls. Data were analyzed in FlowJo software, and gates for DAPI- and CD69+ events were determined using fluorescence minus one or unstained controls. For the gating strategy used to calculate percent CD69+ cells of single cells, see Supplementary Fig. 3.3.

3.5.13 *Vaccination*

The first vaccine emulsion was prepared by mixing Complete Freund's Adjuvant (CFA, Invivogen) and R-P4 (20 µM dissolved in sterile PBS) at a ratio of 1:1. For the first vaccination, 100 µL of the emulsion was injected (I.P.) into male (n = 12) and female (n = 12) C57BL6/J mice (obtained from Jackson Laboratories). Fourteen days after initial vaccination, mice were injected with 100 µL of

freshly prepared vaccine emulsion in Incomplete Freund's Adjuvant (IFA, Invivogen). Adjuvant-only emulsions were made by mixing the appropriate adjuvant in sterile PBS at a ratio of 1:1. Adjuvant-only control mice were injected (I.P.) in male (n = 12) and female (n =12) mice on the same schedule as analog-vaccinated mice.

3.5.14 *Immunoblots*

Blood was collected from 10 vaccinated mice and 10 adjuvant-only control C57BL6/J mice via cardiac puncture 21 days after initial vaccination. Blood was centrifuged at 3,000 x *g* for 15 minutes at 4 °C, and unpelleted plasma was collected and stored at -80 °C.

Granadaene (dissolved in DMSO + 0.1% trifluoroacetic acid) was diluted to 25 μM in PBS and was pipetted (4 μL) onto pre-cut squares of Immoblion-FL PVDF membrane (Sigma Aldrich). After drying for approximately 1 hour, membranes were treated with Odyssey blocking buffer in PBS (LI-COR) for 1 hour while shaking at room temperature. Blocking buffer was removed, and each membrane was probed with an aliquot of plasma from an analog-vaccinated or adjuvant-only mouse diluted 1:250 in buffer solution (1:1 Odyssey blocking buffer and PBS with 0.02% Tween 20). After shaking overnight at 4 °C, membranes were washed three times in wash solution (TBS + 0.02% Tween 20), and then probed with Alexa Fluor 680 goat anti-mouse IgG (Invitrogen) (1:2,500 in buffer solution). Membranes incubated with secondary antibody for 45 minutes at room temperature, protected from light. Then, membranes were washed three times in wash solution and twice in PBS and imaged using the LI-COR Odyssey Infrared Imaging System. Signal intensity of each spot was determined using Image J software.

3.5.15 *Granadaene ex vivo inhibition assay*

Diluted plasma (1:1000) from analog-vaccinated mice or adjuvant-control mice (n = 10/group) were pre-incubated with purified granadaene (0.3 μM in DTS) for 1 hour at room temperature. The

samples were then incubated with 100 µL of EDTA-treated human red blood cells (1% in PBS) for 1 hour at 37 ºC. As described previously[75], hemoglobin release in cell supernatants was measured using the SpectraMax i3x plate reader (absorbance at 420 nm), and percent hemolysis relative to Triton X-100 (0.1%)/granadaene-treated positive controls (100% hemolysis) and PBS-treated negative controls (0% hemolysis) was calculated.

3.5.16 *Murine model of GBS infection*

Twenty-one days after initial vaccination, analog-vaccinated (n = 24) and adjuvant-only mice (n = 24) were injected (I.P.) with approximately 1 x 10^8 CFU of GBS strain NCTC10/84 suspended in sterile PBS (100 µL injected). At 24 hours, all mice were euthanized. Blood was collected via cardiac puncture into heparin tubes (BD). Organs (brain, lung, and spleen) were collected in 1 mL sterile PBS and homogenized. GBS CFU in the blood and each organ was determined by dilution plating on tryptic soy agar (Difco Laboratories).

3.5.17 *Statistical analysis*

A value of $p < 0.05$ was considered significant. Non-significant p values are denoted as "ns" in figures. For *in vitro* assays, an unpaired, two-tailed Student's t test or one-way ANOVA with Tukey's posttest was employed as appropriate to analyze differences between treatment groups, unless otherwise noted. All *in vitro* experiments were performed three times (unless otherwise noted) in technical triplicate. The correlation between IgG signal intensity and granadaene inhibition was analyzed using a Pearson correlation test. Differences in CFU in blood and peripheral organs of vaccinated and unvaccinated mice were determined using Mann-Whitney test, as Gaussian distribution was not assumed in these datasets. GraphPad Prism (version 7.03) was used to compute all statistical tests.

3.6 ACKNOWLEDGEMENTS

3.6.1 *Competing interests*

The authors declare no competing interests.

3.6.2 *Author contributions*

B.A., P.H., J.M.C., and L.R. designed the experiments. B.A., P.H., C.W, P.Q., J.J., R.T, R.C., A.M., A.H., V.S.U., J.V., S.M., and M.C. performed the experiments. B.A., P.H., M.C., P.Q., J.R.G., A.M., J.M.C., and L. R. analyzed the results, and B.A., P.H., K.A.W., A.M., J.M.C., and L.R. wrote the manuscript. All authors reviewed the final version of the manuscript.

3.6.3 *Funding*

This work was supported by funding from the National Institutes of Health grants R01AI112619, R01AI133976, R01AI100989, and R21AI125907 and seed funds from Seattle Children's Research Institute to L.R. The NIH training grants T32AI007509 (PI: Lee Ann Campbell) supported C.W. and J.V. The content is solely the responsibility of the authors and does not necessarily represent the official views of the National Institutes of Health.

3.6.4 *Other*

Thanks to Shayla Nguyen and Anna Furuta for technical assistance, Bobbie Schneider, Sharmon Knecht, and Steve MacFarlane for their assistance with scanning electron microscopy**,** Connie Hughes for administrative support, and all those who donated blood for this work.

3.7 FIGURES AND TABLES

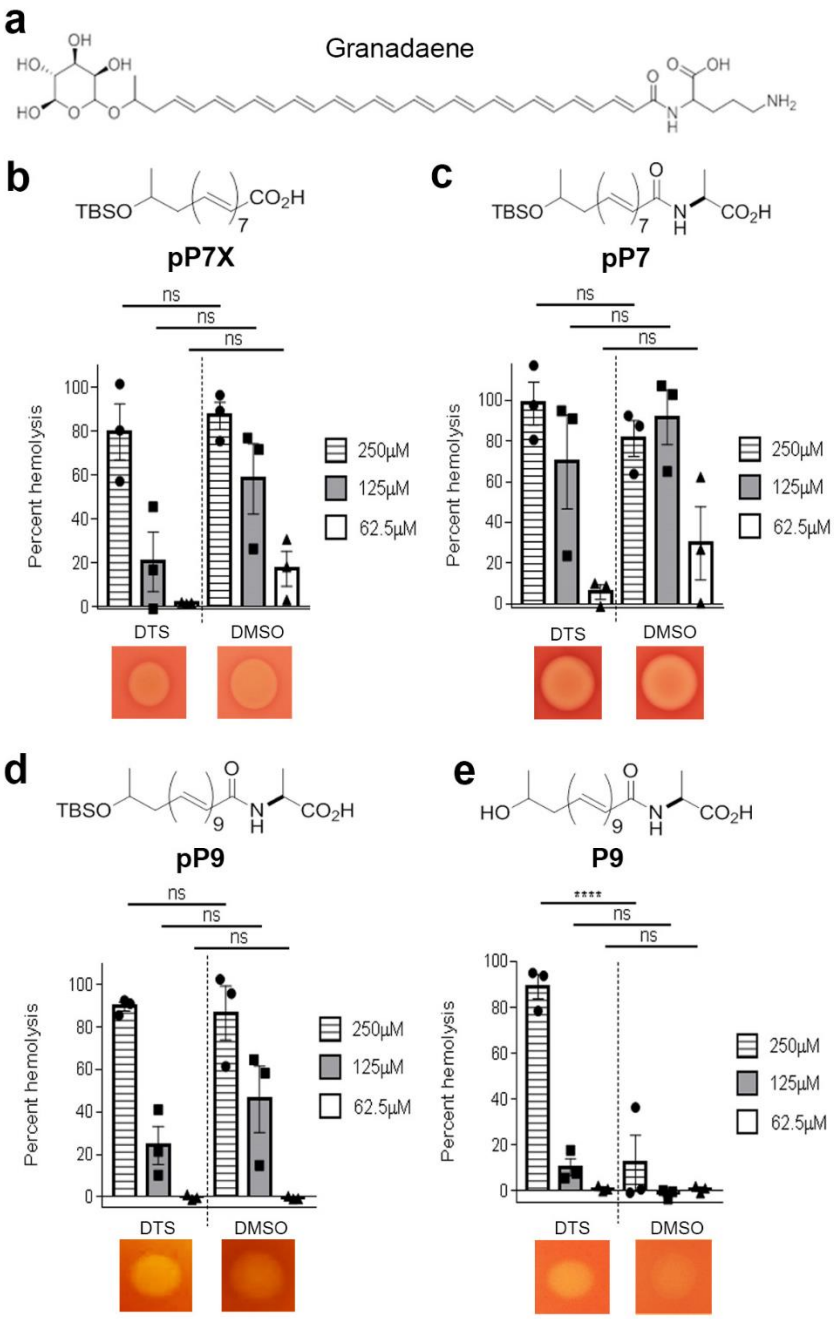

Figure 3.1. The polyene chain length is important for hemolytic activity.

(**a**) Granadaene contains a terminal rhamnose, a polyene chain consisting of twelve alkene bonds, and a terminal ornithine. (**b-e**) Synthetic analogs of granadaene (structures shown) were resuspended in DTS (DMSO + trifluroacetic acid (TFA, 0.1%) + starch (20%)) or DMSO. The analogs were co-

incubated with human red blood cells at 250 µM, 125 µM, and 62.5 µM for 1 hour at 37 °C, and hemoglobin release in cell supernatants was quantified to determine percent hemolysis relative to Triton X-100 (0.1%)-treated positive controls and PBS-treated negative controls. Mean and standard error from three independent experiments are shown. Differences in percent hemolysis between DTS and DMSO were analyzed at each concentration using a two-way ANOVA with Tukey's multiple comparisons test. Except for P9 ($p = 0.0044$ at 250 µM; $p = 0.0395$ at 125 µM), there was no significant difference in percent hemolysis between solvents. Additionally, 5 µL of each synthetic analog at 0.02 M concentration was spotted onto red blood agar plates and allowed to incubate at 37 °C overnight. The hemolytic effect of each compound on red blood agar is shown.

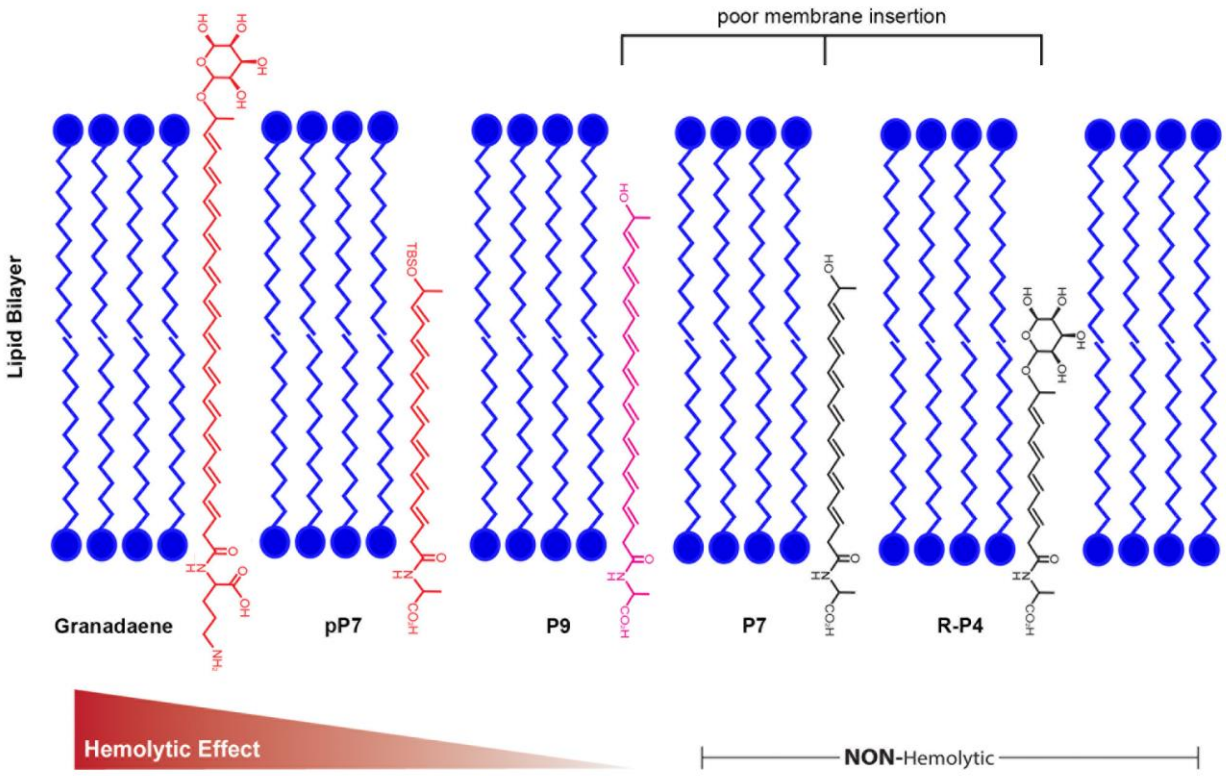

Figure 3.2. Proposed role of polyenes and polar head groups for granadaene-mediated hemolysis and cytolysis.

The polyene chain of granadaene spans the length of the target cell's lipid bilayer and the two polar head groups, rhamnose and ornithine, allow for stable insertion of the GBS ornithine rhamnopolyene into the cell membrane, leading to membrane disruption and hemolysis or cytolysis. Shorter polyenes such as those containing seven double bonds are hemolytic only when one polar end is replaced with a hydrophobic group (e.g. TBS), as in pP7, in which the molecule stably inserts in the membrane due to the compatibility between the hydrophobic lipid bilayer and the TBS group. However, if both polar ends are maintained in compounds with shorter polyenes, as in P7 or R-P4, no hemolytic activity is observed because stable insertion into the cell membrane is not favored. Once the polyene chain reaches a sufficient length, as in P9, some hemolytic activity is observed even when both polar head groups are maintained. Together, this suggests that the length of the polyene chain and polar head groups found in granadaene are key to stable membrane disruption of host cells.

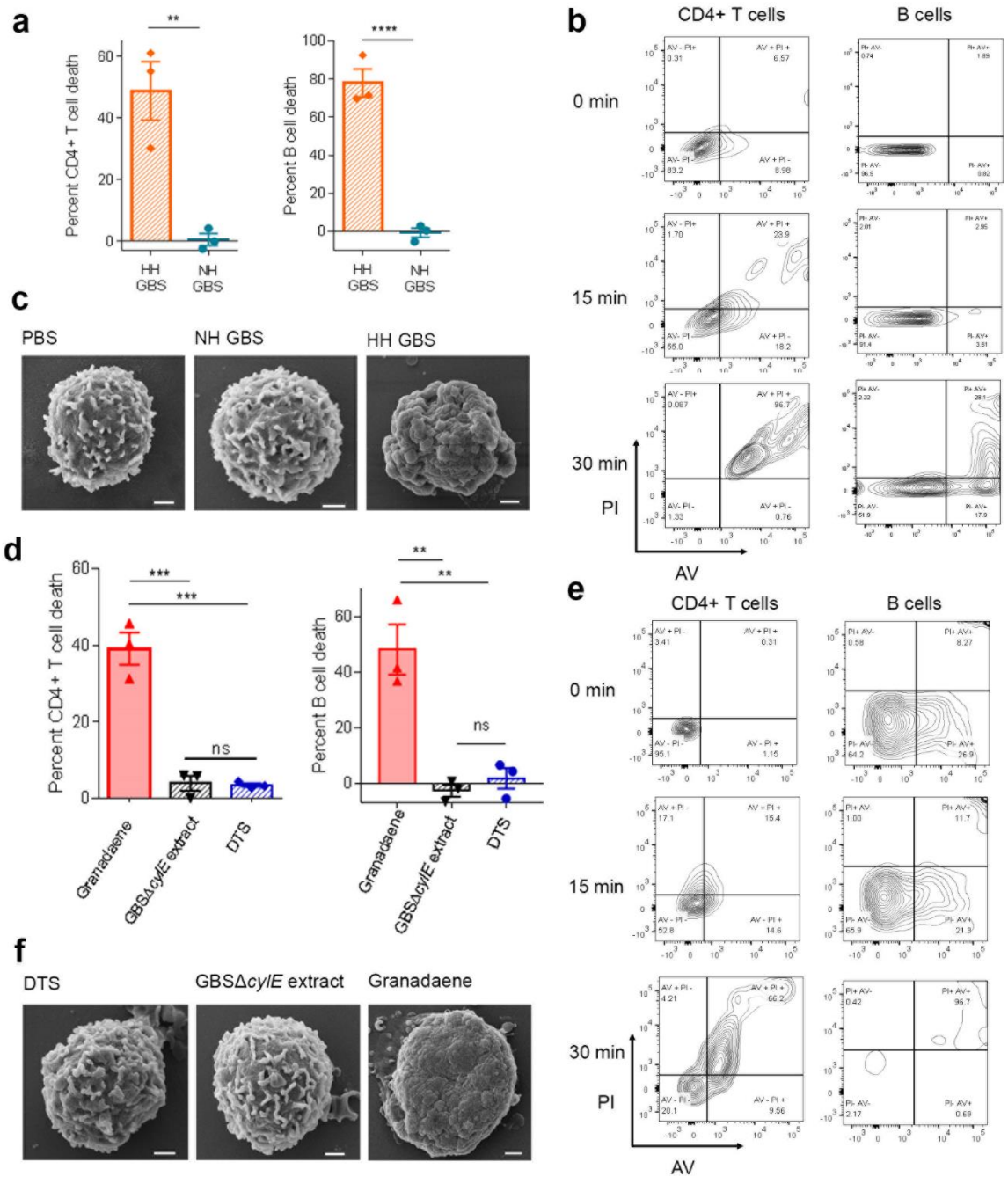

Figure 3.3. Granadaene is cytolytic to T cells and B cells.

(**a**) Primary human CD4+ T cells and B cells were incubated with either hyper-hemolytic GBS (HH GBS) or non-hemolytic GBS (NH GBS) at an MOI of 10 for 1 hour at 37 °C, and cytotoxicity was measured by the release of LDH into the cell supernatant relative to 100% lysis (Triton X-100 (0.1%)) and 0% lysis (PBS) controls. Mean and standard error from three independent experiments are shown. An unpaired t test was used to compare groups. CD4+ T cells: p = 0.0075, B cells: p = 0.0005. (**b**) PI

uptake and Annexin V staining were measured using flow cytometry in each cell type following incubation with hyper-hemolytic GBS at an MOI of 10 at the indicated time points. (**c**) CD4+ T cells were imaged using SEM following incubation with PBS, non-hemolytic GBS, or hyper-hemolytic GBS (MOI = 10) for 1 hour. Scale bars are 1 μm. (**d**) Primary human CD4+ T cells and B cells were co-incubated with purified granadaene (0.5 μM), equivalent amount of extract from non-hemolytic GBS (GBSΔ*cylE* extract), or solvent (DTS), and cell death was measured by LDH release in cell supernatants, as above. Mean and standard error from three independent experiments are shown. Groups were compared with one-way ANOVA with Tukey's post-test. CD4+ T cells: granadaene vs. Δ*cylE* extract: $p = 0.0002$, granadaene vs. DTS: $p = 0.0002$, Δ*cylE* extract vs. DTS: $p = 0.9928$. B cells: granadaene vs. Δ*cylE* extract: $p = 0.0020$, granadaene vs. DTS: $p= 0.0032$, Δ*cylE* extract vs. DTS: $p = 0.8513$. (**e**) PI uptake and Annexin V staining were measured using flow cytometry in each cell type following incubation with purified granadaene (0.5 μM) at the indicated time points. (**f**) CD4+ T cells were imaged using SEM following incubation with DTS, GBSΔ*cylE* extract, or granadaene (0.5 μM) for 1 hour. Scale bars are 1 μm.

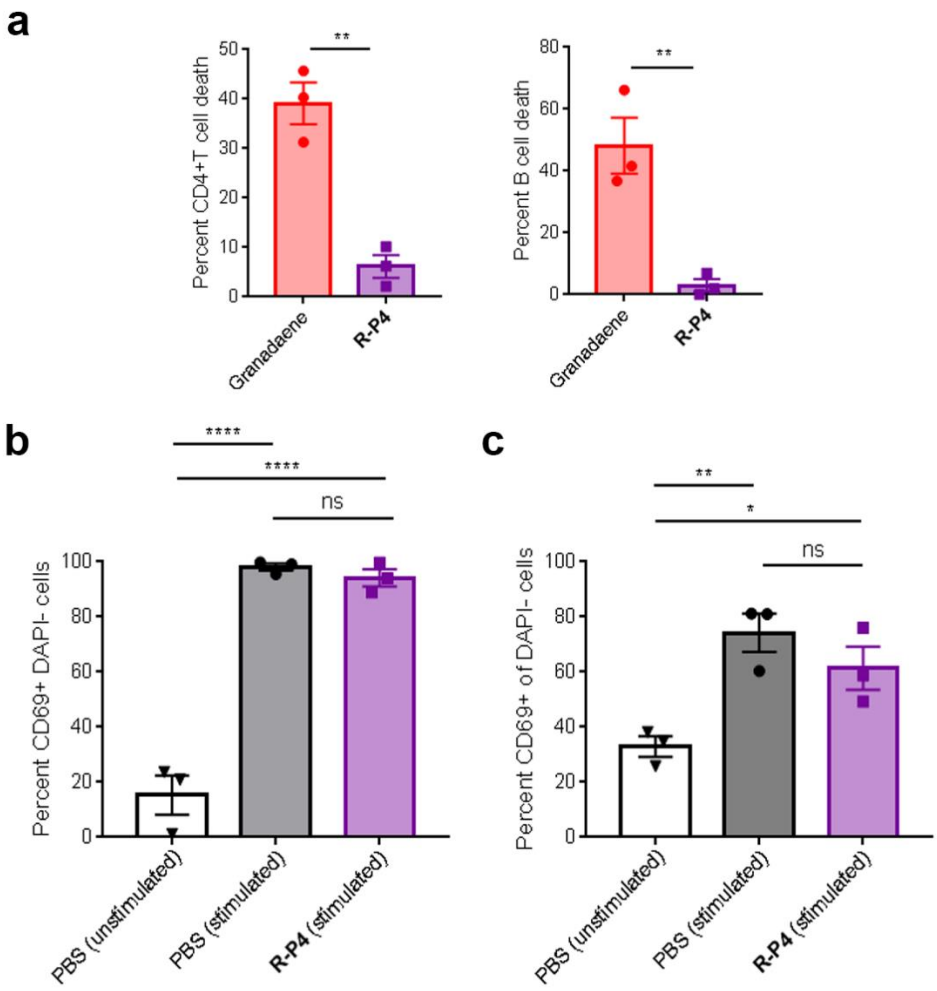

Figure 3.4. R-P4 is non-toxic to T cells and B cells.

(**a**) Primary human CD4+ T cells (left) and B cells (right) were incubated with R-P4 (20 μM) or granadaene (0.5 μM) for 1 hour at 37 °C, and cytotoxicity was measured by LDH release into cell supernatant relative to 100% lysis (Triton X-100 (0.1%)) and 0% lysis (PBS) controls. Mean and standard error from three independent experiments are shown. Groups were compared with an unpaired t test. CD4+ T cells: $p = 0.0024$, B cells: $p = 0.0084$. (**b**) Primary human CD4+ T cells were treated with PMA (10 ng/mL) and anti-CD3ε (100 μg/mL) (stimulated) or media alone (unstimulated). Then, cells were treated with either PBS or R-P4 (20 μM) and incubated at 37 °C for 48 hours. Cells were stained for CD69, resuspended in DAPI (0.5 μM), and analyzed by flow cytometry. Percent CD69+ of DAPI- cells from three independent experiments are represented with mean and standard error.

Treatment groups were compared using one-way ANOVA with Tukey's post-test. PBS (unstimulated) vs. PBS (stimulated): $p < 0.0001$, PBS (unstimulated) vs. R-P4 (stimulated): $p < 0.0001$, PBS (stimulated) vs. R-P4 (stimulated): $p = 0.8151$. (**c**) Primary human B cells were treated with IL-4 (20 ng/mL) and anti-CD40 (5 μg/mL) (stimulated) or media alone (unstimulated). Then, cells were treated with either PBS or R-P4 (20 μM) and incubated at 37 °C for 48 hours. Cells were stained for CD69, resuspended in DAPI (0.5 μM), and analyzed by flow cytometry. Percent CD69+ of DAPI- cells from three independent experiments are represented with mean and standard error. Treatment groups were compared using one-way ANOVA with Tukey's post-test. PBS (unstimulated) vs. PBS (stimulated): $p = 0.0091$, PBS (unstimulated) vs. R-P4 (stimulated): $p = 0.0453$, PBS (stimulated) vs. R-P4 (stimulated): $p = 0.3893$.

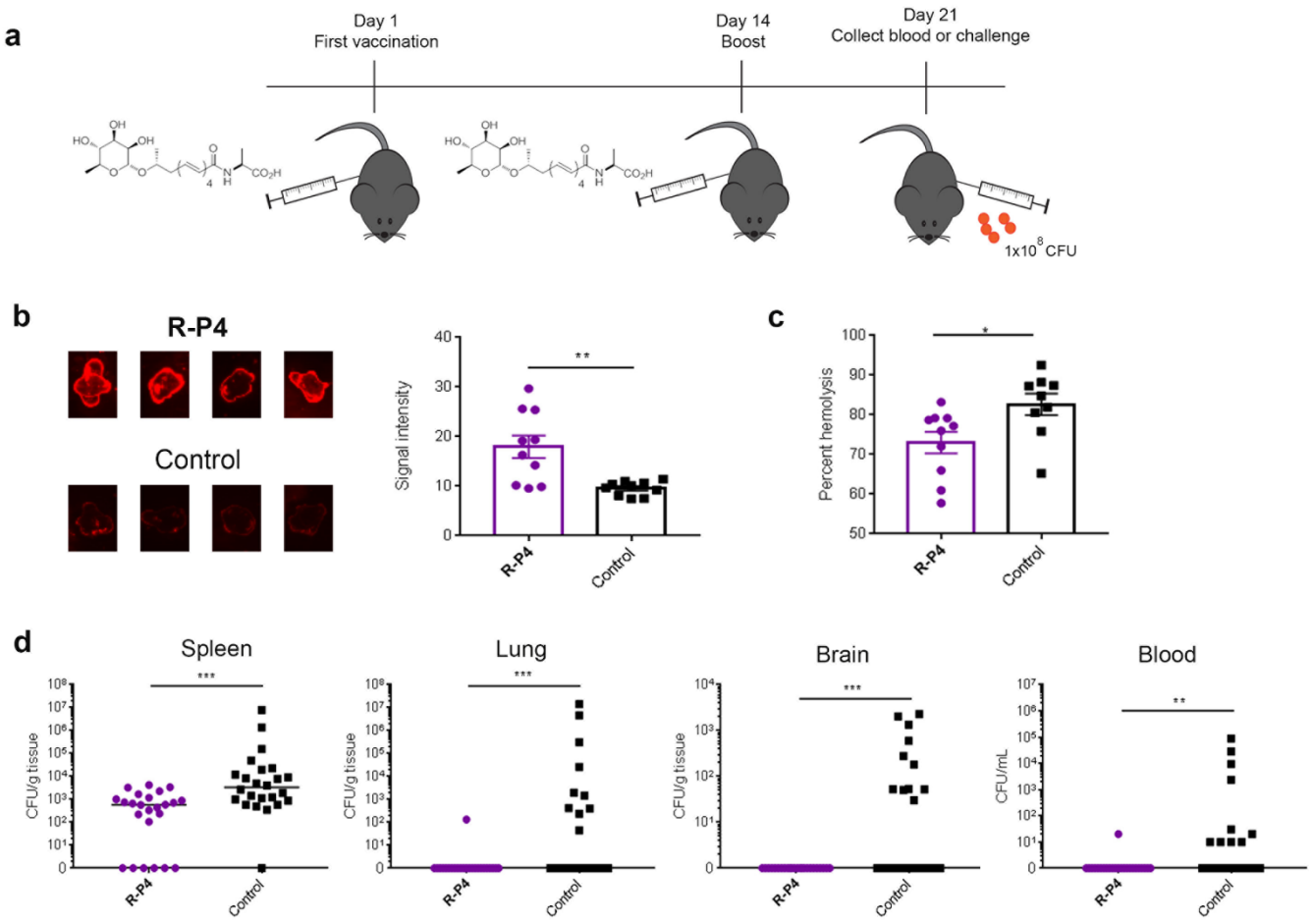

Figure 3.5. Vaccination with a non-toxic synthetic analog diminished GBS infection.

(**a**) Mice were vaccinated with an emulsion of R-P4 (10 μM in PBS) in complete Freund's adjuvant and were boosted 14 days after initial vaccination using R-P4 in incomplete Freund's adjuvant (see methods). At 21 days, vaccinated mice were euthanized for blood/plasma collection or were challenged (I.P.) with approximately 1 x 10^8 CFU of hyper-hemolytic GBS strain NCTC10/84. As controls, mice receiving adjuvant only were tested in parallel with the same schedule. (**b**) Approximately 4 μL solvent or purified granadaene (25 μM) was spotted on PVDF membranes, which were then blocked and probed with plasma from analog-vaccinated or adjuvant-only mice (n = 10/group). Subsequently, the membranes were probed with secondary goat anti-mouse IgG (Alexa Fluor 680) and analyzed on the Odyssey LI-COR Imaging System. Four representative spots from each group are shown. Signal intensity of each spot was determined using Image J software, and an unpaired t test was used to

compare signal intensity between groups ($p = 0.0020$). Mean and standard error are shown. (**c**) Plasma (diluted 1:1000) from analog-vaccinated mice or adjuvant-only only mice ($n = 10$/group) was pre-incubated with purified granadaene (0.3 μM) for 1 hour and then incubated with human red blood cells for 1 hour. Percent inhibition of granadaene hemolysis was calculated (see Materials and Methods), and an unpaired t test was used to compare hemolysis inhibition by R-P4 plasma vs. control plasma ($p = 0.0004$). Mean and standard error are shown. (**d**) GBS CFU recovered from the blood, spleen, lung, and brain of mice 24 hours post-infection were compared using the Mann-Whitney test. Blood: $p = 0.0025$, Spleen: $p = 0.0001$, Lung: $p = 0.0010$, Brain: $p = 0.0002$.

Table 3.1. The chemical structures, estimated polyene chain lengths, and calculated logarithm of the partition coefficient between n-octanol and water (cLogP) of synthetic analogs and granadaene are shown.

Compound name	Structure	Length of polyene chain (Å)	cLogP
pP1	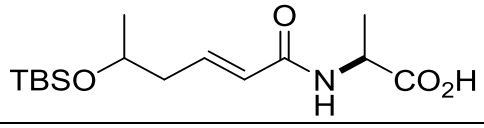	3.63	2.43
R-P4	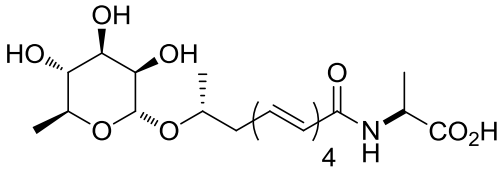	10.8	0.52
pP7X	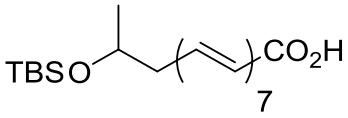	20.8	6.73
pP7	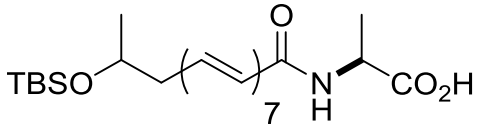	17.9	6.08
P7	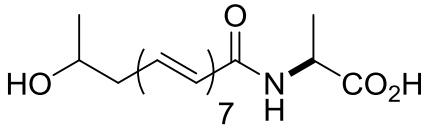	17.7	2.74
pP9	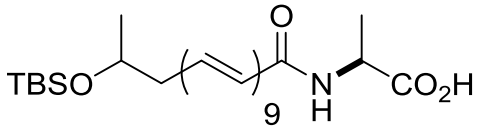	22.6	7.29
P9	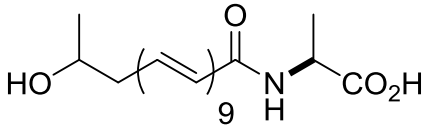	22.4	3.95
Granadaene	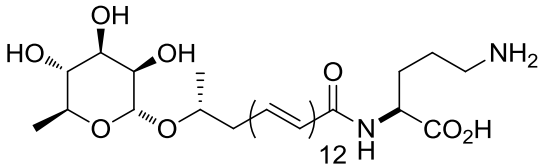	29.7	2.95

Chapter 4. HEMOLYTIC MEMBRANE VESICLES OF GROUP B STREPTOCOCCUS PROMOTE INFECTION

This chapter is from the following article:

Armistead, B., Quach, P., Snyder, J.M., Santana-Ufret, V., Rajagopal, L. Hemolytic membrane vesicles of Group B Streptococcus promote infection. *In preparation.*

4.1 ABSTRACT

Group B Streptococci (GBS) are β-hemolytic, Gram-positive bacteria that are frequently associated with fetal injury, preterm birth, spontaneous abortion, and neonatal infections. A key factor promoting GBS virulence is the β-hemolysin/cytolysin, a pigmented ornithine rhamnolipid (also known as granadaene) associated with the bacterial surface. A previous study indicated that GBS produce small, spherical, bilayered structures known as membrane vesicles (MVs), which contain virulence-associated proteins. Here, we show that purified MVs obtained from hemolytic GBS are pigmented and are hemolytic, even after protease treatment and in the absence of exogenous stabilizers, indicating that the hemolytic pigment is functionally active in MVs. Additionally, MVs from hemolytic GBS induced significantly greater cell death of neutrophils, T cells, and B cells compared to MVs from isogenic non-hemolytic GBS, which implicates MVs as a potential mechanism for hemolysin/pigment-mediated virulence. Finally, hemolytic MVs reduced oxidative killing of GBS and aggravated morbidity and mortality of neonatal mice infected with GBS. Collectively, these studies reveal a novel mechanism by which GBS deploy a crucial virulence factor during infection to promote bacterial dissemination and pathogenesis.

4.2 INTRODUCTION

Annually, at least 4 million preterm births or stillbirths and over 300,000 neonatal infections are attributable to Group B Streptococcus (GBS or *Streptococcus agalactiae*), a β-hemolytic, Gram positive bacterium that commonly colonizes the female lower genital tract [13,133]. Typically, GBS is transmitted to the fetus via ascending infection, in which the bacteria traffic from the lower genital tract into the amniotic cavity, greatly increasing the risk of preterm birth, fetal injury, and stillbirth. In addition, neonates can acquire GBS through the aspiration of infected vaginal fluids during birth, leading to severe infections including pneumonia, meningitis, or sepsis. A major determinant promoting invasive GBS infection is the β-hemolysin/cytolysin, a pigmented ornithine rhamnolipid also known as granadaene. Several studies have shown that granadaene facilitates GBS dissemination by weakening host barriers at the maternal-fetal interface[72,75], lung[31-33], and brain[34,35]. In addition, the hemolytic pigment is cytotoxic to several host immune cells, including macrophages[24], neutrophils[72], mast cells[83], T cells, and B cells (see Chapter 3).

Hemolytic activity of GBS is associated with the bacterial cell surface, and previous studies have shown that direct contact between GBS and red blood cells (RBCs) is required for hemolysis[18] and that GBS membrane fragments are pigmented[134]. Beyond this, little experimental evidence exists on whether or how granadaene may be released from the bacterial cell. A recent study demonstrated that GBS produce membrane vesicles (MVs), which are small spherical buds originating from the bacterial cell membrane[135]. GBS MVs were found to contain several GBS surface-associated virulence proteins, including hyaluronidase and metalloproteases, and intra-amniotic injection caused weakening of choriodecidual membranes and fetal injury in mice[135]. In other pathogens, MVs have been shown to act as vehicles for toxins and effector molecules, delivering these factors to host cell targets[133,136,137]. Here, we hypothesize that GBS deploy granadaene via the release of MVs, which exacerbates GBS infection. We show that MVs isolated from hemolytic GBS are pigmented, hemolytic, and cytotoxic

and aggravate morbidity and mortality in neonatal mice infected with non-hemolytic GBS. Collectively, these findings reveal a novel mechanism of granadaene delivery during GBS infection and further elucidates the function of this key virulence factor.

4.3 RESULTS

4.3.1 *GBS hemolytic pigment, granadaene, is released in membrane vesicles.*

To test the hypothesis that GBS hemolytic pigment associates with MVs, we isolated MVs from GBS strains that overexpress the hemolytic pigment, namely GBSA909Δ*covR* (lacks the hemolysin repressor CovR/S) and its isogenic non-hemolytic strain GBSΔ*covR*Δ*cylE*. Of note, hyper-hemolytic GBS strains, including those containing mutations in the *covR/S* two component system have been isolated from women in preterm labor[75] as well from patients with other manifestations of GBS infections [87-90]. Using SEM, we first confirmed that these GBS strains (Δ*covR* and Δ*covR*Δ*cylE*) produce MVs; these are seen as spherical structures proximal to and arising from GBS (Fig. 4.1 a, Supplementary Fig. 4.1 a, b), similar to those previously identified as MVs[135]. Ultracentrifugation of MVs from GBSA909Δ*covR* yielded a small pellet that was red/orange in color, unlike MVs from GBSΔ*covR*Δ*cylE*, indicating the presence of pigment in the MVs (Fig. 4.1 b, Supplementary Fig. 4.1 a). MV pellets were resuspended in PBS, homogenously dispersed by sonication, and then analyzed for hemolysis by spotting on red blood agar. As shown in Fig. 4.1 c, MVs from hyper-hemolytic GBS were indeed hemolytic, whereas MVs from non-hemolytic GBS were not. Similar results were also observed with wild-type hyper-hemolytic GBS strains such as NCTC10/84.

We then examined whether MVs from hemolytic GBS are cytolytic to host immune cells similar to live bacteria and purified granadaene. To this end, MVs from hyper-hemolytic GBSΔ*covR* (HH GBS MVs) or non-hemolytic GBSΔ*covR*Δ*cylE* (NH GBS MVs) were co-incubated with primary human neutrophils, CD4+ T cells, CD8+ T cells, or B cells, and cell death was measured by quantifying lactate dehydrogenase (LDH) release in cell supernatants. The results shown in Fig. 4.1 c indicate that

MVs from hyper-hemolytic GBS caused significantly greater cell death in all cell types compared to MVs from isogenic, non-hemolytic GBS. Collectively, these data demonstrate, for the first time, that GBS pigment is released from the bacterial cell surface with MVs, which induce hemolysis and cytolysis to host cells.

Next, we wondered whether the release of granadaene in MVs was dependent on a GBS-specific factor. To test this, we utilized the strain *L. lactis* p*cylX-K*, a Gram-positive bacterium which heterologously expresses granadaene, and the non-hemolytic/non-pigmented control strain *L. lactis* pEmpty (see Chapter 2, Fig. 2.1, 2.2). After isolating MVs from these strains as above, we noted that MVs from *L. lactis* p*cylX-K* were pigmented and hemolytic on red blood agar (Fig. 4.2, Supplementary Fig. 4.1 c), while MVs from *L. lactis* pEmpty were neither pigmented nor hemolytic (Supplementary Fig. 4.1 c). Together, these findings demonstrate that granadaene is released in membrane vesicles from Gram-positive bacteria and its association with MVs did not require any GBS-specific factor.

4.3.2 *Hemolytic activity of MVs containing granadaene is independent of proteins*

To confirm that protein or peptides do not contribute to the hemolytic activity observed in MVs, we tested hemolysis of MVs in the presence of proteinase K (PK). HH GBS MVs and *L. lactis* p*cylX-K* were subjected to proteinase K (PK, 0.25 mg/mL) treatment for 1 hour at 37°C. As a control, the activity of the PK used in these studies was verified by incubating it (at 0.25 mg/mL) with 100µg BSA. All samples were analyzed for protein content by resolving on a 12% SDS-PAGE followed by SYPRO Ruby staining. The data shown in Fig. 4.2 a confirm that proteins present in the MVs are susceptible to degradation by PK. Next, we resuspended HH GBS MVs and *L. lactis* p*cylX-K* with PK (PK, 0.25 mg/mL) and spotted onto a red blood agar plate or mixed with human RBCs. NH GBS MVs and *L. lactis* pEmpty were also included. We observed that treatment with PK did not diminish the hemolytic activity in MVs isolated from hyper-hemolytic GBS or *L. lactis* p*cylX-K* (Fig. 4.2 b, c). Taken together,

these data indicate that hemolytic activity observed with MVs did not require any MV-associated proteins.

4.3.3 *Hemolytic MVs prevent oxidative killing of GBS*

Next, we asked whether hemolytic MVs protect GBS against antimicrobial host defenses encountered during infection, such as reactive oxygen species (ROS) that are often produced by host cells such as macrophages and neutrophils. Based on previous observations that the hemolytic pigment of GBS has antioxidant properties[25], and MVs from *Helicobacter pylori* promote bacterial survival against ROS[138], we hypothesized that MVs derived from hyper-hemolytic GBS may protect GBS against oxidative killing. To test this hypothesis, we treated non-hemolytic GBS (GBSΔ*covR*Δ*cylE*) with H_2O_2 that was pre-incubated with either HH GBS MVs or NH GBS MVs. As controls, GBS was exposed to H_2O_2 alone (i.e. without MVs) or PBS only. After 1 hour, we quenched residual ROS with catalase and then enumerated surviving CFU. We observed that significantly more GBS survived H_2O_2 that had been pretreated with HH MVs when compared to NH MV (Fig. 4.3 a). These findings show that hemolytic pigment in membrane vesicles can quench ROS and thus dampen killing of GBS by H_2O_2, a major constituent of the oxidative burst response[139].

4.3.4 *Hemolytic MVs exacerbate GBS pathogenesis in neonatal mice*

Since our *in vitro* data indicated that hemolytic MVs promote GBS survival against ROS, we hypothesized that hemolytic MVs contribute to GBS pathogenesis *in vivo*. To this end, neonatal mice between 12-36 hours of age were inoculated (I.P.) with either a) HH MVs alone, b) HH MVs in the presence of non-hemolytic GBS, c) non-hemolytic GBS alone, or d) control saline. The mice were observed for morbidity and mortality symptoms for up to 7 days post-inoculation. The results in Fig. 4.3 b show that neonatal mice inoculated with HH MVs alone did not succumb to the challenge. However, the presence of HH MVs aggravated morbidity and mortality of neonatal mice treated with

non-hemolytic GBS when compared to mice inoculated with non-hemolytic GBS alone (Fig. 4.3 b). Histological examination of H & E stained sections was performed on the lungs from one mouse of each group obtained 24 hours post-inoculation. These analyses indicated that the neonatal lung from the mouse inoculated with HH MVs + non-hemolytic GBS had a few clusters of small basophilic structures reminiscent of bacteria, which was not observed in the other groups. Additionally, there was mild eosinophilic acellular material within the alveoli (consistent with fibrin) in the lungs of the neonate from the above group, which was generally minimal to absent in the lungs of neonates from the other groups (Fig. 4.3 c). These findings show that while MVs from hyper-hemolytic GBS alone were insufficient to induce morbidity and mortality in the neonatal host, they reduced survival and exacerbated lung injury in neonates infected with non-hemolytic GBS. Notably, simultaneous isolation of hemolytic and non-hemolytic GBS from human cases has been reported[88,90,140] including in neonates[140]. Together, these data indicate that hemolytic GBS MVs can exacerbate GBS pathogenesis and neonatal morbidity and mortality.

4.4 DISCUSSION

Group B Streptococci remain a leading etiological agent of infection in human newborns and are associated with preterm birth, stillbirth, and neonatal sepsis [2,3,13,17,112,141-148]. A major barrier to the development of new prevention strategies is the lack of understanding of virulence factors important for GBS pathogenesis. In this work, we add biochemical insight into a critical GBS virulence factor, the hemolytic pigment, and show how GBS may package and deploy this toxin to overcome host defenses and promote infection.

In 2013, Whidbey et al. showed that the GBS pigment (granadaene) is hemolytic in the presence of starch, demonstrating that the pigment and β-hemolysin of GBS were one in the same[75]. While this work represented a major advance in our understanding of GBS pathogenesis, the requirement for starch in purified pigment for hemolytic activity remained a mystery, as GBS does not produce starch

per se and yet are hemolytic. In the present study, we observed that membrane vesicles (MVs) isolated from hemolytic GBS or *L. lactis* expressing the GBS *cyl* genes[126] are hemolytic and cytolytic, even when MV-associated proteins are degraded by proteinase K (Fig. 4.1, 4.2). These findings demonstrate that exogenous, high-molecular-weight stabilizers such as starch are not essential for hemolysis and cytolysis when the pigment is associated with the bacterial membrane or membrane components. In addition, these data show that proteinaceous components of the bacterial membrane are also themselves not necessary for hemolytic activity, suggesting that positioning within the membrane may itself provide sufficient stabilization for pigment activity.

Our findings in MVs support previous data indicating that the hemolytic pigment is localized to the bacterial surface[18,134] and reveal a novel mechanism by which GBS may release this toxin from the bacterial cell. Previous work showed that virulence-associated proteins such as extracellular matrix-degrading enzymes are packaged in GBS MVs and likely contribute to premature rupture of membranes, fetal injury, and preterm birth[135]. Although our findings in the neonatal mouse model suggest that hemolytic MVs themselves may not be pathogenic, our *in vitro* and *in vivo* findings show that the hemolytic pigment in MVs promotes GBS survival and pathogenesis, even for an attenuated, non-hemolytic strain (Fig. 4.3).

Recently, MVs have gained appreciation for their ability to promote bacterial survival by interfering with host defenses. For instance, *Staphylococcus aureus* MVs promoted bacterial survival by via neutrophil cytotoxicity[149], MVs from *Streptococcus pneumoniae* inhibited opsonophagocytic killing by sequestering complement components[149], and catalase-containing MVs from *Helicobacter pylori* decreased ROS-mediated killing[138]. Our data indicate that similar to *H. pylori*, MVs from GBS facilitate bacterial survival from oxidative killing, although protection is dependent on the presence of the hemolytic pigment in MVs (Fig. 4.3 a). It is likely that release of hemolytic MVs by GBS quenches ROS produced by the recruited macrophages or neutrophils, thereby attenuating host defenses and promoting GBS dissemination.

In summary, we identify a heretofore undescribed mechanism of pigment toxin-mediated virulence during GBS infection. Our results imply that GBS releases the hemolytic pigment via MVs, which quench microbicidal oxidants and enable bacteria to survive and disseminate. As ROS production by neutrophils is critical to clearance of GBS by the host[25,68,72], our findings provide new insight into how GBS overcomes hostile host environments and also lay a foundation for future studies examining the role of GBS MVs in immune evasion.

4.5 Materials and Methods

4.5.1 *Ethics statement*

Written informed patient consent for donation of human blood was obtained with approval from the Seattle Children's Research Institute Institutional Review Board (protocol #11117) per the Principles in the WMA Declaration of Helsinki and Dept. of Health and Human Services Belmont Report. Children under the age of 18 were not recruited for donation of human blood.

All animal experiments were approved by the Seattle Children's Research Institutional Animal Care and Use Committee (protocol IACUC00036) and performed in strict accordance with the recommendations in the Guide for the Care and Use of Laboratory Animals of the National Institutes of Health (8th Edition).

4.5.2 *Bacterial strains*

GBSΔ*covR* and GBSΔ*covR*Δ*cylE* were derived from the wild-type strain A909, as described[35,85]. A909 is a clinical isolate obtained from an infected human neonate and is classified as serotype Ia[99]. All GBS liquid cultures were grown in tryptic soy broth (TSB, Difco Laboratories) at 37 °C, 5% CO_2. *L. lactis* pcylX-K and *L. lactis* pEmpty were generated as described[126], and were grown in TSB at 37 °C, 5% CO_2 with 5 μg/mL chloramphenicol (Sigma-Aldrich).

4.5.3 *Isolation of MVs from GBS and L. lactis*

Membrane vesicles (MVs) were isolated from GBS using methods previously described [135], with slight modification. Cultures (15 mL) of GBSΔ*covR*, GBSΔ*covR*Δ*cylE*, *L. lactis* p*cylX-K*, and *L. lactis* pEmpty were grown to stationary phase (OD_{600nm} of 1). Each turbid culture was centrifuged at 12,000 x *g* for 30 minutes at 4 °C. The supernatants were collected and passed through a 0.22 µm syringe-driven filter (EMD Millipore) to remove residual bacterial cells. Then, the filtrate was added to a 10 kDa Amicon Ultra-15 filter device (EMD Millipore), which was centrifuged at 4,000 x *g* for 15 minutes. The concentrated solute was recovered, and the MVs were pelleted by ultracentrifugation (150,000 x *g* for 3 hours at 4 °C). Most of the supernatant was removed without disturbing the pellet. The pellets containing MV's were resuspended in sterile PBS and were normalized among all strains to 5 mg/mL.

4.5.4 *Scanning electron microscopy of MVs*

Bacteria were centrifuged, washed twice with PBS, and resuspended in one volume of ½ Karnovsky's fixative (2% paraformaldehyde, 2.5% glutaraldehyde, 2.5mM CaCl2 in 0.1M Cacodylate buffer, pH 7.2 [150]). Then, the bacterial cells were centrifuged and resuspended in 1.4 mL ½ Karnovsky's fixative and allowed to incubate overnight at 4°C. At the Fred Hutchinson Cancer Research Center Electron Microscopy Core, samples were prepared for scanning electron microscopy as described previously[72,75,83,151]. Images were obtained using a Sigma 500 variable pressure Field Emission Scanning Electron Microscope (FESEM) operating with Smart SEM (version 5.09).

4.5.5 *Verification of proteinase K activity*

Proteinase K (PK, Gene Choice) was resuspended in proteinase K buffer (20 nM Tris, pH 8.0, 1 mM $CaCl_2$) at a concentration of 2.5 mg/mL. Then, 1.5 µL PK (2.5 mg/mL) or 1.5 µL PBS was added to a 13.5 µL aliquot of 100 µg BSA in PBS or to a 13.5 µL resuspension of MVs from GBSΔ*covR* in

PBS. As a control, 1.5 µL (2.5 mg/mL) PK was resuspended in PBS. Each resuspension was incubated for 1 hour at 37 °C. To analyze for the presence of PK, each resuspension was analyzed by 12% SDS-PAGE followed by SYPRO Ruby staining.

4.5.6 *Testing MVs for hemolysis*

On a blood agar TSA plate, 10 µL of MV resuspension was sonicated (10 min) and then spotted and allowed to dry for approximately 10 minutes. The plate was incubated at 37 °C in 5% CO_2 overnight, and then analyzed for a zone of hemolysis. To test the effect of PK on MV hemolysis, 13.5 µL sonicated MV resuspension was mixed with 1.5 µL of PK (2.5 mg/mL, final concentration = 0.25 mg/mL) or PBS. Then, 10 µL was spotted and allowed to dry for approximately 10 minutes. The plate was incubated at 37 °C in 5% CO_2 overnight, and then analyzed for hemolysis. As described above, plates were placed on a light box, and photographs were captured with the digital SLR camera described above and processed using Photoshop CC (Adobe).

To quantify hemolytic activity of MVs, a hemolytic assay was performed as described previously with purified pigment/control extracts[19]. Briefly, human red blood cells in PBS were co-incubated with 10 µL sonicated MV resuspensions (5 mg/mL) from GBSΔ*covR* (or non-hemolytic control MVs) in the presence of PK (0.25 mg/mL) or PBS for 1 hour at 37 °C. Hemoglobin release in cell supernatants was measured, and percent hemolysis was determined relative to Triton X-100 (0.1%)-treated positive controls and PBS-treated negative controls.

4.5.7 *Testing MVs for cytotoxicity*

Primary human neutrophils, CD4+ T cells, CD8+ T cells, and B cells were isolated as described above. Neutrophils were seeded into 96-well plates at 2.5 $x10^5$ cells/well in 90 µL RPMI-G, and T and B cells were seeded at 2.5 x 10^6 cells/well in 90 µL RPMI-G. MVs (10 µL, 5 mg/mL) isolated from GBSΔ*covR* and GBSΔ*covR*ΔcylE were added to seeded cells and allowed to incubate at 37°C

(neutrophils = 3 hrs, T cells and B cells = 1 hr). As positive and negative controls, neutrophils were incubated in 0.1% Triton X-100 (Sigma Aldrich) or sterile PBS, respectively. Cells were analyzed for cytotoxicity by the presence of cytoplasmic lactate dehydrogenase (LDH) in cell supernatants using the colorimetric LDH kit (Clontech), per the manufacturer's instructions. Percent cytotoxicity was calculated by normalizing to PBS-treated cells (0% cell death) and Triton X-100-treated cells (100% cell death), as previously described [24,72,75].

4.5.8 *Oxidative killing assay*

MVs isolated from GBSΔ*covR* or GBSΔ*covR*Δ*cylE* were resuspended in sterile PBS at 5 mg/mL, 1.23 mg of each MV type was co-incubated with 0.06% H_2O_2 (Sigma Aldrich) for 45 minutes while rocking (500 µL total volume). PBS (no MVs) + 0.06% H_2O_2 and PBS-only (no MVs, no H_2O_2) conditions were included as positive and negative controls, respectively. Meanwhile, GBSΔ*covR*Δ*cylE* overnight cultures were sub-cultured in TSB, grown to mid-log phase (OD_{600} 0.3), washed twice in sterile PBS, and normalized to approximately 2 $x10^8$ CFU/mL in PBS. Then, approximately $1x10^8$ CFU (500 µL) was added to the pre-incubated MVs (and controls), bringing the final H_2O_2 concentration to 0.03%, as previously described for oxidative killing assays with GBS[25]. The mixtures incubated at 37 °C, 5% CO_2 for 1 hour, and then 1000 units of catalase (from bovine liver, Sigma-Aldrich) were added to each reaction condition to quench remaining H_2O_2 (as previously described[25]), and surviving CFU were enumerated by dilution plating onto TSA.

4.5.9 *Murine model of neonatal MV and GBS inoculation*

Neonatal C57BL/6J mice between 12-36 hours of age were pooled and randomly assigned to dams. Each group of neonates was then designated as an experimental group (hyper-hemolytic MVs + non-hemolytic GBS, n = 6; PBS + non-hemolytic GBS, n = 6; hyper-hemolytic MVs + PBS, n = 5; or PBS + PBS, n = 7). According to the assigned experimental group, neonates were injected (I.P.) with

50 µL hyper-hemolytic MVs (5 mg/mL from GBSΔ*covR*) or PBS and 10 µL non-hemolytic GBS (GBSΔ*covR*Δ*cylE*, 10^8 CFU/mL) or PBS and returned to their assigned dam. Neonates were monitored twice daily for 7 days for signs of morbidity and mortality. Moribund neonates were euthanized. At 24 hours post-inoculation, one randomly selected neonate from each experimental group was euthanized via decapitation and the lungs were harvested, stored in 10% buffered formalin (Fisher Scientific), paraffin embedded, sectioned at 4-5 µm, stained for hematoxylin and eosin (H&E), and analyzed for histology by J.M.S who was blinded to group assignment. Lack of formalin inflation (difficult in this neonatal age) complicated critical assessment of the interstitium. Mice euthanized for the purpose of histological analysis were censored from the survival analysis. Images of lungs were acquired from glass slides scanned in bright field with a 20X objective using a Nanozoomer Digital Pathology slide scanner (Hamamatsu; Bridgewater, New Jersey) and plated in Adobe Photoshop Elements. Image brightness was adjusted using levels (white balance), with manipulations applied to the entire image, and a scale bar placed.

4.5.10 *Statistical analysis*

A p value < 0.05 was considered significant. Unless otherwise noted, an unpaired t test or one-way ANOVA with Tukey's post-test was used to compare groups in *in vitro* assays. Survival data was plotted on a Kaplan-Meier curve, and the log-rank test was used to determine differences in survival between groups. GraphPad Prism (version 7.03) was used to compute all statistical tests.

4.6 ACKNOWLEDGEMENTS

4.6.1 *Competing interests*

The authors declare no competing interest.

4.6.2 *Author contributions*

B.A. and L.R. designed experiments. B.A., P.Q., and V.S.U. performed experiments. B.A., J.M.S., and L.R. analyzed data. B.A. and L.R. wrote the manuscript.

4.6.3 *Funding*

This work was supported by funding from the National Institutes of Health grants R01AI112619, R01AI133976, R01AI100989, and R21AI125907 and seed funds from Seattle Children's Research Institute to L.R. The NIH training grants T32AI007509 (PI: Lee Ann Campbell) supported C.W. The content is solely the responsibility of the authors and does not necessarily represent the official views of the National Institutes of Health.

4.6.4 *Other*

We thank Dr. Anirban Banerjee for expert advice, Meghan Garrett for technical assistance, and Connie Hughes for administrative support.

4.7 FIGURES AND TABLES

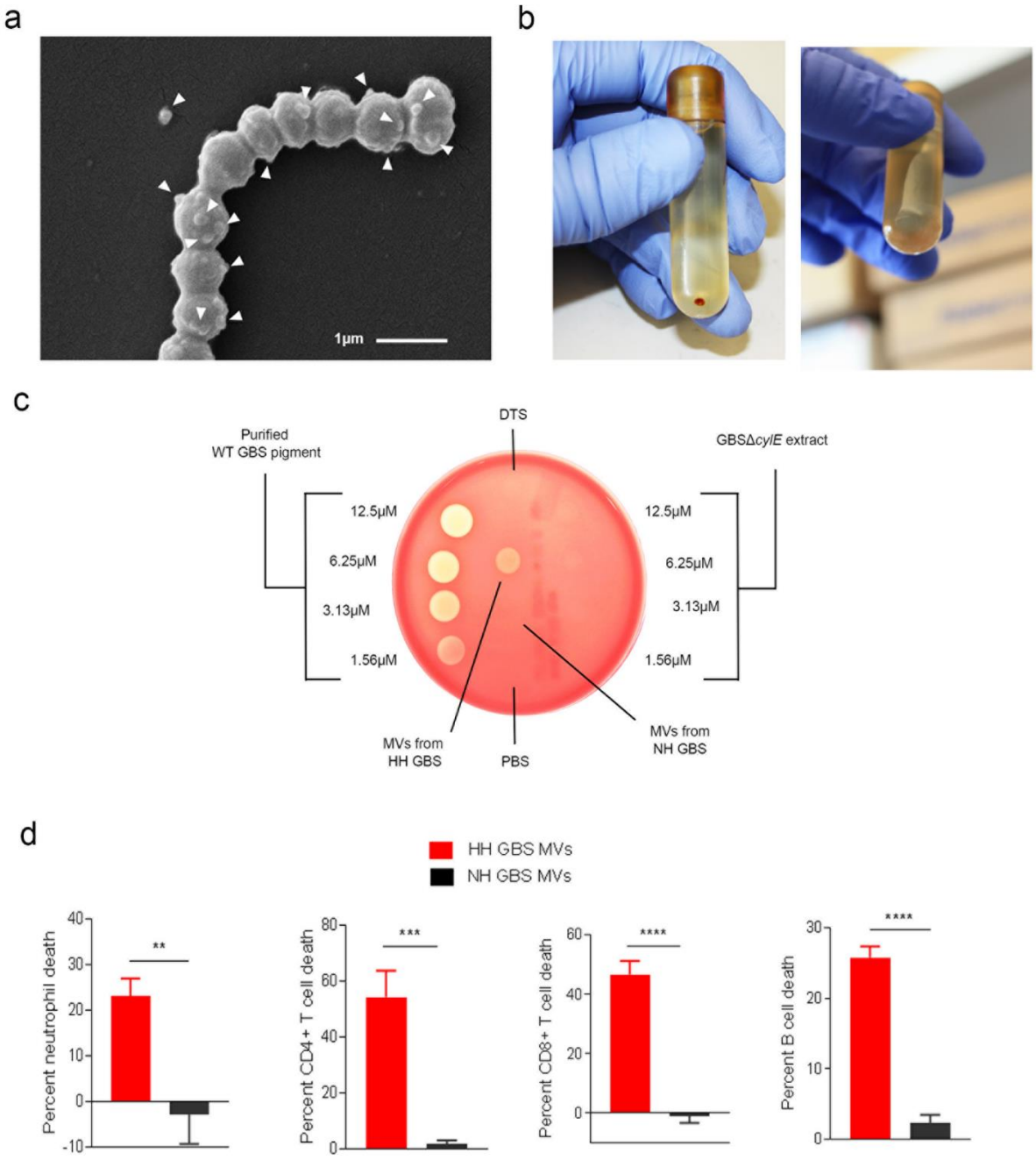

Figure 4.1. Membrane vesicles isolated from hemolytic GBS are hemolytic and cytolytic.

(**a**) Hyper-hemolytic GBS (GBSΔ*covR*) were centrifuged, fixed, and analyzed by SEM. Arrowheads indicate MVs, which are seen as spherical structures emerging from the surface of bacterial cells. (**b**)

MVs from hyper-hemolytic GBS (HH GBS, GBSΔ*covR*) or non-hemolytic GBS (NH GBS, GBSΔ*covR*Δ*cylE*) were resuspended in PBS, sonicated, and 10 µL was spotted onto red blood agar. Purified GBS pigment and equivalent amount of GBSΔ*cylE* extract in DTS at various dilutions were spotted (10 µL) for comparison. (**c**) Primary human neutrophils, CD4+ T cells, CD8+ T cells, or B cells were incubated with MVs from hyper-hemolytic GBS or non-hemolytic GBS (final concentration = 0.5 mg/mL), and cell death was measured by LDH release into the supernatant relative to Triton X-100 (0.1%)- and PBS-treated controls. Mean and SEM are shown from three experiments performed in technical triplicate. Groups were compared with unpaired, two-tailed Student's t test. Neutrophils: $p = 0.0042$, CD4+ T cells: $p = 0.0005$, CD8+ T cells: $p < 0.0001$, B cells: $p < 0.0001$.

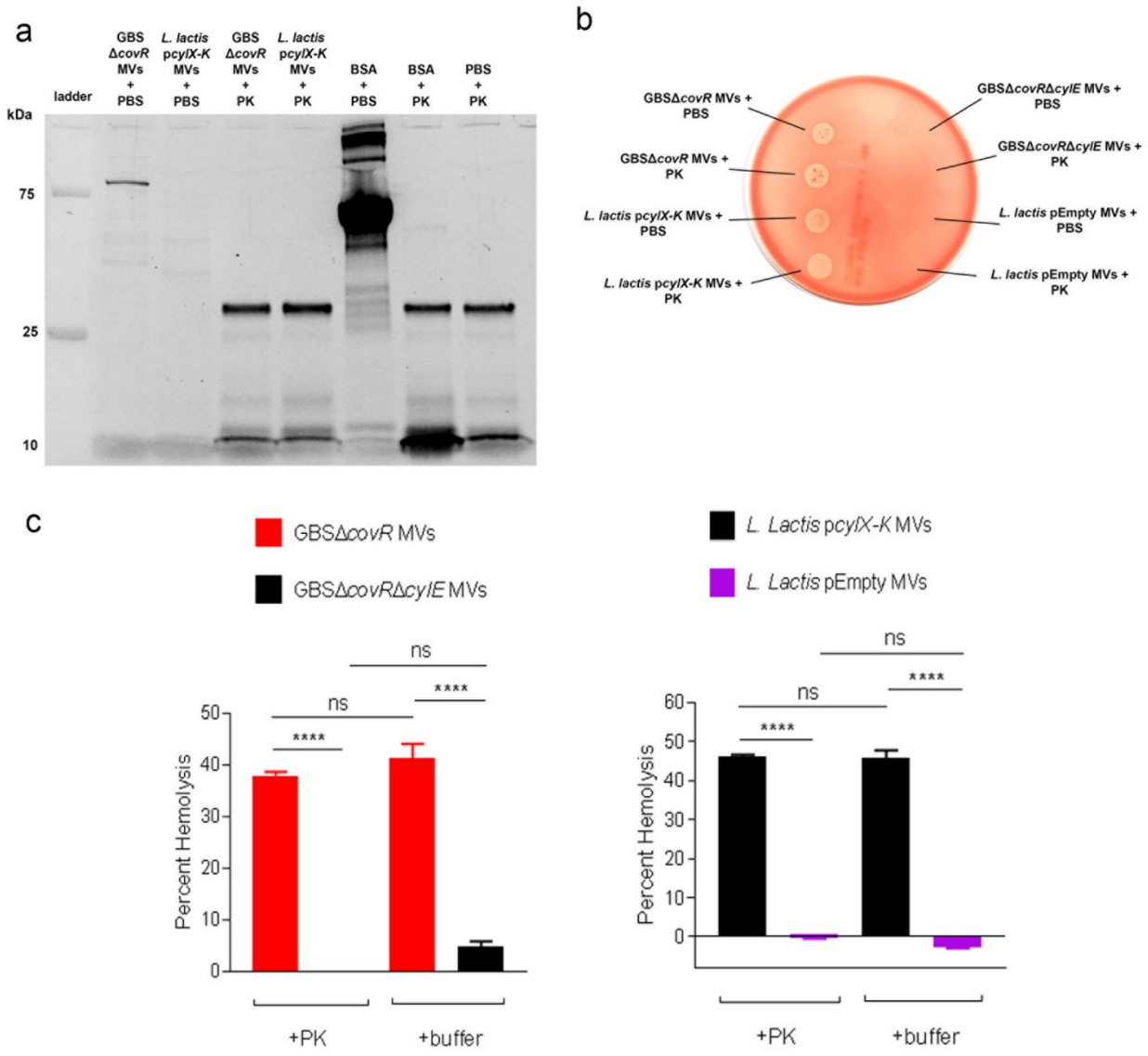

Figure 4.2. MVs are hemolytic after treatment with protease.

(**a**) Proteins in MVs isolated from GBS and *L. lactis* p*cylX- K* were subjected to proteinase K (PK) treatment by incubating GBSΔ*covR* MVs or *L. lactis* p*cylX-K* MVs with PK (0.25 mg/mL) or equivalent volume of PBS for 1 hour at 37 °C. The activity of PK was confirmed by incubating BSA (100 µg) with PK (0.25 mg/mL) for 1 hour at 37 °C. Samples were analyzed for protein content by resolving on a 12% SDS-PAGE followed by SYPRO Ruby staining. (**b**) MVs from GBSΔ*covR*, GBSΔ*covR*Δ*cylE, L. lactis* p*cylX-K*, or *L. lactis* pEmpty were treated with proteinase K (PK, final concentration 0.25 mg/mL) or an equivalent volume of PBS for 1 hour at 37°C, and 10 µL of each was

spotted on blood agar. (**c**) MVs from GBSΔ*covR*, GBSΔ*covR*Δ*cylE*, *L. lactis* p*cylX-K, or L. lactis* pEmpty were mixed with human erythrocytes in the presence of PBS or PK (0.25 mg/mL) for 1 hour, and percent hemolysis was determined relative to Triton X-100 (0.1%)-treated positive controls. One-way ANOVA with Tukey's post-test was used. Mean and SEM from three experiments performed in triplicate are shown. * indicates $p < 0.05$, *** indicates $p < 0.001$, **** indicates $p < 0.0001$, ns indicates not significant, or $p \geq 0.05$.

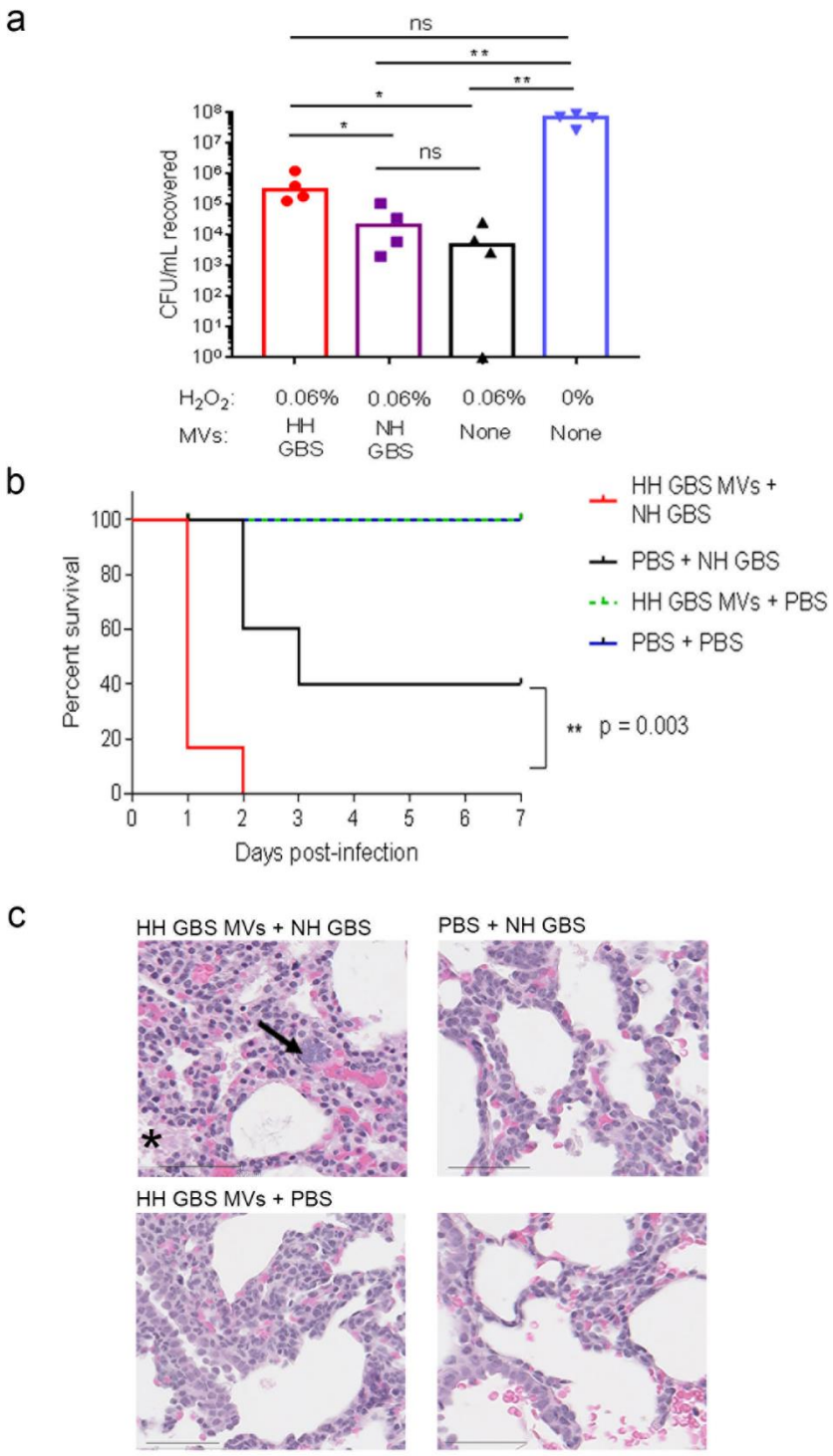

Figure 4.3. Hemolytic MVs dampen oxidative killing and exacerbate GBS pathogenesis in neonatal mice.

(**a**) MVs were isolated from hyper-hemolytic (HH) GBSΔ*covR* or non-hemolytic (NH) GBSΔ*covR*Δ*covR* were pre-incubated with 0.06% H_2O_2 for 45 min and then incubated with NH GBS

at 37 °C for 1 hour. Following incubation, remaining H_2O_2 was quenched with 1,000 units of catalase, and surviving CFU were enumerated by dilution plating onto TSA. A group consisting of no MVs + H_2O_2 and no MVs + no H_2O_2 were included as positive and negative controls, respectively. Treatment groups were compared using a Kruskal-Wallis test with multiple comparisons corrected for false discovery. HH GBS MVs + H_2O_2 vs. no MVs + H_2O_2: p = 0.0170; HH GBS MVs + H_2O_2 vs. NH GBS MVs + H_2O_2: p = 0.0395. NH GBS MVs + H_2O_2 vs. no MVs + H_2O_2: p > 0.9999; HH GBS MVs + H_2O_2 vs. PBS only: p = 0.0822; NH GBS MVs + H_2O_2 vs. PBS only: p = 0.0032; no MVs + H_2O_2 + PBS: p = 0.0015. Line at median. (**b**) Kaplain-Meier plot depicts survival of neonatal mice inoculated with MVs alone or GBS strains alone or GBS strains with MVs, as indicated. Survival between groups was compared using the log-rank test. (**c**) Lungs from neonatal mice in each treatment group were harvested at 24 hours post-treatment, fixed, sectioned, and stained for H & E. Arrow represents aggregate of small basophilic circular structures (consistent with bacteria), and asterisk indicates eosinophilic material within the alveoli (fibrin). Scale bar is 50 µm.

Chapter 5. HYALURONIDASE OF GROUP B STREPTOCOCCUS ATTENUATES NEUTROPHIL FUNCTION AND PROMOTES INVASION OF THE AMNIOTIC CAVITY, FETAL BACTEREMIA, AND PRETERM LABOR

This chapter is from the following article:

Coleman, M.*, **Armistead, B.***, Orvis, A., Quach, P., Brokaw, A., Gendrin, C., Ogle, J., Merillat, S., Dacanay, M., Wu, T-Y, Munson, J., Baldessari, A., Vornhagen, J., Furuta, A., Nguyen, S., Adams Waldorf, K.M., Rajagopal, L. Hyaluronidase of Group B Streptococcus attenuates neutrophil function and promotes invasion of the amniotic cavity, cervical ripening, and preterm labor. *In preparation*.

* These authors contributed equally to this work.

5.1 ABSTRACT

Invasive bacterial infections during pregnancy are a major risk factor for preterm birth, stillbirth and fetal injury. Group B Streptococci (GBS) are gram-positive bacteria that commonly reside as commensal organisms in the vagina but infect the amniotic fluid and induce preterm birth or stillbirth. A better understanding of how GBS virulence factors evade host defenses leading to adverse pregnancy outcomes is necessary for the development of preventive strategies. Using a unique chronically catheterized nonhuman primate model that closely emulates human pregnancy and informs temporal events surrounding amniotic cavity invasion and preterm labor, we show that the GBS hyaluronidase (HylB) significantly promotes microbial invasion of the amniotic cavity, fetal bacteremia, and preterm labor. Although delayed cytokine responses were observed in animals inoculated with the HylB-proficient strain, increased prostaglandin levels in these animals likely promoted cervical ripening and preterm labor in these animals. Furthermore, we show that HylB promotes GBS resistance to neutrophil killing and dampens ROS production. Collectively, our studies demonstrate how a bacterial enzyme enables GBS to blunt host defenses to cause microbial invasion of the amniotic cavity, fetal bacteremia, and preterm labor.

5.2 INTRODUCTION

Globally, invasive bacterial infections are a leading cause of stillbirths and preterm births [152-154]. Group B Streptococci (GBS) or *Streptococcus agalactiae* are β-hemolytic, gram-positive bacteria that commonly exist as commensal organisms in the recto-vaginal tract of healthy adult women. However, GBS can be transmitted to neonates during birth or ascend into the uterus during pregnancy, resulting in fetal injury, stillbirth, preterm birth, or early neonatal infection [3,145,155]. Some countries have implemented protocols to screen women for GBS colonization in the third trimester of pregnancy and to subsequently administer antibiotics to GBS-positive women during labor and delivery (known as intrapartum antibiotic prophylaxis). Although these measures have decreased the incidence of neonatal GBS disease in the first week of life [112,156], they fail to prevent adverse pregnancy outcomes that occur prior to labor and delivery that result in preterm births or stillbirths [112,157-159]. Recent reports have indicated that by conservative estimates, approximately 147,000 stillbirths and 3.5 million preterm births each year are attributed to GBS infections [13]. A better understanding of how GBS evades host defenses during ascending infection is pivotal for the development of improved preventive therapies.

Host factors important for responses to microbial infection include hyaluronan (HA). HA is a major constituent of the host extracellular matrix and exists as a high-molecular weight glucosaminoglycan polymer that assists in cell migration, cell-cell signaling and responses to injury and infection [160,161]. During infection or injury, high molecular weight HA (HMW-HA) is degraded by host hyaluronidases or reactive oxygen species (ROS) to low molecular weight HA (LMW-HA, comprising HA tetramers or pentamers) which are pro-inflammatory in nature and mediate cytokine responses through signaling via Toll-like receptors (TLRs), such as TLR-2 and TLR-4 [162,163]. Interestingly, certain bacterial pathogens including GBS also secrete a hyaluronidase enzyme [42,164]. The GBS hyaluronidase (HylB, encoded by the *hylB* gene) was identified in 1950 as an exolytic

enzyme [165] that breaks down HA to HA disaccharides [36]. Recently, GBS HylB-generated HA disaccharides were shown to block TLR-2 and TLR-4 signaling in macrophages and dampen cytokine responses[43]. Subsequently, we observed that clinical GBS isolates associated with preterm labor or neonatal infections exhibit increased hyaluronidase activity when compared to commensal GBS isolates obtained from rectovaginal swabs of healthy women [46]. We also noted that GBS hyaluronidase dampened uterine immune responses and promoted ascending infection and preterm birth in pregnant mouse models of GBS infection[46].

However, the pregnant mouse and other lower mammalian models of pregnancy exhibit dissimilarities to many aspects of human pregnancy including differences in reproductive anatomy, placentation, mechanism of onset of labor and sensitivity to pathogens. In contrast, the closest animal model for studies related to human pregnancy is the pregnant non-human primate (NHP) [166-169]. Similarities of NHP to humans include reproductive anatomy, type and structure of placenta (hemomonochorial), number of fetuses (singleton), long gestational period (160-170 days), initiation of labor (hormonal control of parturition), sensitivity to pathogens, and the developmental timeline of the fetal lung and brain [168,169]. In the chronically catheterized pregnant NHP model [30,73] we inoculate bacteria at the choriodecidual space, which is between the uterine muscle and the placental membranes, where bacteria first encounter the maternal-fetal interface during ascending infection from the lower genital tract [73,153].

Previous studies using the above NHP model revealed that hyper-hemolytic and hyper-pigmented GBS (lacking the hemolysin transcriptional repressor CovR, GBSΔ*covR*) invaded the amniotic cavity and induced preterm labor in a hemolysin-dependent manner [30]. Here, we used a non-hemolytic GBS strain (Serotype V, GB37) that exhibits increased hyaluronidase activity [41] to address how hyaluronidase expression (in the absence of hemolytic activity) may affect immune evasion, fetal injury and preterm labor. Our studies reveal that pregnant NHP inoculated with GB37 exhibited rapid MIAC and preterm labor in contrast to animals inoculated with the isogenic GB37Δ*hylB* (lacking

hyaluronidase expression). Although MIAC correlated with increased neutrophil recruitment to the choriodecidual space, the ability of hylauronidase to dampen neutrophil ROS production and increase GBS resistance to neutrophil killing likely enabled MIAC and fetal bacteremia. Infection with hyaluronidase-proficient GBS was also associated with increased prostaglandin levels that likely promoted cervical ripening. Collectively, our studies reveal that a secreted bacterial hyaluronidase can impact multiple host pathways to promote GBS MIAC and preterm labor.

5.3 RESULTS

5.3.1 *HylB promotes adverse pregnancy outcomes in a choriodecidual model of GBS infection*

To elucidate how hyaluronidase promotes GBS infection during pregnancy, we used a chronically catheterized nonhuman primate (*Macaca nemistrina*) model that closely emulates human pregnancy and defines temporal events during MIAC and preterm labor[72]. Ten animals received choriodecidual inoculations of 1-3 x 10^8 colony forming units (CFU) of either hyaluronidase-proficient wild-type GBS (strain GB37, n = 5) or an isogenic hyaluronidase-deficient GBS (strain GB37Δ*hylB*, n = 5). Notably, neither the wild-type GB37 nor the mutant strain exhibit hemolysis/pigmentation. Controls included NHP that received saline (n = 6 total; n = 4 described previously[73]). Preterm labor and/or microbial invasion of the amniotic cavity (MIAC) (Table 1) were the primary outcomes of our study, as either of these events induces adverse pregnancy outcomes. In GBS-inoculated animals, Cesarean section was performed at the onset of preterm labor (defined as progressive cervical dilation associated with increased uterine activity (hourly contraction area >10,000 mmHg*sec/hr)) or at three days post-GBS inoculation if preterm labor did not occur, as described previously[72].

We found that GB37 induced preterm labor in 4/5 (80%) animals compared to 1/5 (20%) animals inoculated with hyaluronidase-deficient strain GB37Δ*hylB* or 0/7 (0%) saline controls (Table 5.1, Fig. 5.1). Further, all GB37-inoculated animals (5/5, 100%) experienced microbial invasion of the amniotic cavity in contrast to 1/5 animals (20%) inoculated with GB37Δ*hylB* and 0/7 (0%) saline

controls (Table 5.1, Fig. 5.1). The phenotype of the bacterial colonies recovered from the animals was similar to the inoculum strain in all cases. In the GB37 group, GBS CFU was recovered from the amniotic fluid (AF) as early as 6 hours post-inoculation in two animals (GB37 #1 and GB37 #2), which was followed by preterm labor at 26 and 41 hours post-inoculation, respectively (Fig. 5.1, Supplementary Fig. 5.1). GBS was recovered from the AF at 12 hours post-inoculation in GB37 #3 and GB37 #4. At 48 hours post-inoculation, the AF of GB37 #3 was significantly turbid due to MIAC, although contractions exceeding 10,000 mmHg*sec/hr and cervical dilation did not occur at this time. To avoid *in utero* fetal death due to sepsis, we proceeded with Cesarean section prior to the defined study endpoint (preterm labor) at 49 hours post-inoculation for this animal. In GB37 #5, although GBS was not detected in the AF until 48 hours post-inoculation, infection and contractions progressed rapidly after this point, and the NHP was close to delivering the fetus at 70 hours post-inoculation (early on day 3 post-inoculation). In the GB37Δ*hylB* group, only one animal exhibited preterm labor and MIAC (GB37Δ*hylB* #5), wherein GBS was detected in the AF at 24 hours post-inoculation and the animal experienced preterm labor within 70 hours of inoculation (Fig. 5.1, Supplementary Fig. 5.1). The remaining four animals in this group did not exhibit MIAC, preterm labor, or other adverse outcomes, similar to saline controls (Fig. 5.1, Supplementary Fig. 5.1). Collectively, our results indicate that choriodecidual inoculation of a GBS strain with elevated hyaluronidase activity was significantly associated with adverse pregnancy outcomes when compared to inoculation with the isogenic hyaluronidase-deficient GBS strain or saline controls ($p = 0.0214$ GB37 vs. GB37Δ*hylB*; $p = 0.0005$ GB37 vs. saline).

5.3.2 *MIAC coincided with fetal bacteremia and inflammation despite low levels of pro-inflammatory cytokines in the amniotic fluid*

All cases of MIAC coincided with fetal bacteremia, and GBS CFU (ranging from 10^3-10^8 CFU/g) were recovered from several fetal organs, including the brain (Fig. 5.2 a). Of note, consistently

more bacteria were recovered from the fetal lung when compared to the other fetal organs (Fig. 5.2 a), similar to our previous observations with a hyper-hemolytic strain of GBS[72].

To determine the inflammatory milieu that can be associated with either the progression or clearance of GBS infection in the various groups, we measured cytokine levels in the AF during the course of the experiment. In the GB37 group, we noted that for three animals that experienced preterm labor within 48 hours post-inoculation (GB37 #1, GB37 #2, GB37 #4), AF levels IL-1β, IL-6, IL-8, and TNF-α remained relatively low (< 2,000 pg/mL) after the onset of MIAC (Fig. 5.1, Supplementary Fig. 5.1); this cytokine profile sharply contrasts to our prior studies using a hyper-hemolytic pigmented GBS strain (GBSΔ*covR*), wherein AF levels of IL-1β, IL-6, IL-8, and TNF-α increased immediately before MIAC was detected[72]. In the other two animals that experienced preterm labor after 48 hours post-GBS inoculation (GB37 #3, GB37 #5), a spike in levels of IL-1 β (3,000-6,000 pg/mL), IL-6 (3,500-8,000 pg/mL), and IL-8 (1,500-8,000 pg/mL) occurred between 24 and 48 hours after MIAC was detected. In contrast, for the GB37Δ*hylB* group, the levels of IL-1β, IL-6, IL-8, and TNF-α remained low (< 2,000 pg/mL) and were comparable to the saline-inoculated animals throughout the experiment (Fig. 5.1, Supplementary Fig. 5.1), with the exception of GB37Δ*hylB* #5, which experienced MIAC and preterm labor. Notably, there was no statistical difference in the peak AF cytokine levels among all treatment groups (Table 5.1). In addition, compared to our previously published GBSΔ*covR*-inoculated animals[72], the GB37 group had significantly lower peak AF levels of IL-6 ($p = 0.0090$) and IL-8 ($p = 0.0163$). These results suggest that increased AF cytokines are not necessarily a predictive signature of preterm labor, particularly during infection with immunosuppressive hyaluronidase-expressing GBS strains.

We also measured cytokines in fetal tissues and plasma at the study endpoint (Fig. 5.2 b, Table 5.1). As fetal tissue lysates were not obtained from historical saline animals (n = 4) reported previously[72], only saline animals performed in the current study (n = 2) were included in these analyses.

Overall, the GB37-infected fetuses exhibited increased IL-1β in the lung ($p = 0.0536$); IL-6 in the lung ($p = 0.0242$), spleen ($p = 0.0678$), and kidney ($p = 0.0536$); IL-8 in the lung ($p = 0.0530$); and TNF-α in the lung ($p = 0.0536$) when compared to GB37Δ*hylB* (with the highest cytokines observed in GB37Δ*hylB* #5, which had MIAC and preterm labor). Higher levels of the following cytokines were also observed in GB37- versus saline-treated animals: IL-1β in the kidney ($p = 0.0852$); IL-6 in the spleen ($p = 0.0726$), liver ($p = 0.0353$), and plasma ($p = 0.0490$) ; IL-8 in the lung ($p = 0.0383$) and spleen ($p = 0.0305$); and TNF-α in the liver ($p = 0.0418$). The significant increase in proinflammatory cytokines in the fetal lung wherein higher bacterial burden was also detected suggests that immune suppression due to HylB may be more evident in the immunotolerant placental tissues rather than fetal tissues.

Haemotoxylin and eosin (H&E) staining of neonatal lungs supported these findings. Lungs from the GB37 group showed minimal (GB37 #4) and moderate to severe (GB37 #1, #2, #3, and #5) neutrophilic deep alveolar pneumonia with intracellular and extracellular bacteria and abundant aspirated material and fibrin (Supplementary Fig. 5.2). In contrast, H&E staining of the GB37Δ*hylB* group showed overall minimal neutrophilic inflammation in the fetal lung. The only animal with MIAC in this group, GB37Δ*hylB* #5, exhibited moderate and mixed cell-type inflammation and aspirated bacteria within the lung (Supplementary Fig. 5.2). Collectively, these analyses reveal that choriodecidual inoculation of hyaluronidase-expressing GBS resulted in increased cytokines and inflammation in fetal tissues compared to choriodecidual inoculation with GBS lacking hyaluronidase. This immune response may, in part, be driven by pathogen-associated molecular patterns (PAMPs) associated with bacterial invasion of the fetal tissues.

5.3.3 *HylB-expressing GBS induced greater infiltration of phagocytes to the maternal-fetal interface*

To gain insight into the nature of the immune cells present at the maternal-fetal interface, we performed flow cytometry on various samples obtained at the experimental endpoint. Of note, while saline controls performed as a part of the current study (n = 2) are included, historical saline controls (n = 4) were not included in these analyses, as similar samples were not available and/or such analyses were not previously performed. At Cesarean section, biopsies were obtained from the placental membranes (the chorionic villi and the choriodecidual membranes at the inoculation site) and the uterus (upper uterus, mid-uterus, and lower uterus adjacent to the inoculation site) (Fig. 5.3 a). Maternal and fetal blood (from the umbilical cord) were also collected. Placental and uterine tissues were processed to obtain single cells, and then treated with one of four fluorescent antibody panels (Supplementary Table 5.1) designed to screen for various immune cell types, including monocytes, neutrophils, mast cells, DCs, NK cells, T cells, and B cells. Stained single cells were analyzed by flow cytometry, and specific immune cell populations were determined by gating on size, single cells, and known phenotypic markers for each cell type (see materials and methods). Because only two saline controls were included, we examined the data for statistical differences between the GB37 and GB37Δ*hylB* groups.

These analyses revealed a trend for elevated levels of neutrophils (CD44+/CD66+) in the mid- and upper uterine segments, choriodecidual membranes (inoculation site) and maternal blood of GB37-treated NHP compared to GB37Δ*hylB* or saline controls ($p < 0.1$, Fig 5.3 b). No differences in neutrophil frequency was seen in the chorionic villi, lower uterus, or fetal blood between the GBS treatment groups. Notably, a trend towards increased monocytes (CD45+/CD14+) was also seen in the upper and mid-uterine segments of GB37 animals compared to GB37Δ*hylB* or saline controls. Elevated

levels of CD8+ T cells (CD3+/CD4-/CD8+) were also seen in the chorionic villi and choriodecidual membranes of GB37-inoculated animals compared to GB37Δ*hylB*-inoculated animals.

We also examined the placental membranes by H&E staining to assess inflammation and tissue injury. Placentas from the GB37 group exhibited moderate to severe predominantly neutrophilic inflammation with areas of edema, mild regional hemorrhage, and fibrinous necrosis (Supplementary Fig. 5.3). Conversely, placental sections from the GB37Δ*hylB* group had minimal to mild neutrophilic and mixed cell-type inflammation, except for GB37Δ*hylB* #5, which had moderate to severe neutrophilic inflammation (Supplementary Fig. 5.3). Collectively, our flow cytometry and placental histology results indicate that levels of neutrophils and possibly monocytes are increased in the reproductive tissues of animals inoculated with GB37 versus GB37Δ*hylB* and saline controls.

5.3.4 *Digital spatial profiling of the placenta revealed minimal immune signatures to GBS hyaluronidase*

To obtain greater spatial resolution of the cellular events and signaling cascades at the maternal-fetal interface, we analyzed placental membranes from each animal (including n = 2 historical salines) using the GeoMx Digital Spatial Profiling (DSP) platform (NanoString Technologies) (Fig. 5.4 a). Briefly, formalin fixed paraffin embedded (FFPE) sections of choriodecidual membranes from animals inoculated with GB37 (n = 5), GB37Δ*hylB* (n = 5), or saline (n = 4; n = 2 from current study, n = 2 historical controls) were incubated with primary antibodies reactive to pan cytokeratin (Pan-CK, green), fibroblast activation protein (FAP, yellow), and GBS (red) to visualize the overall tissue architecture and bacterial invasion by fluorescence microscopy. Next, regions of interest (ROIs) comprising the decidua, chorion, and amnion in each animal were selected (Fig 5.4 b), and 62 antibody probes coupled to photocleavable oligonucleotide tags were hybridized and serially photocleaved within each ROI and then collected and quantified. Counts were mapped to tissue location to yield a spatially-resolved profile of analyte abundance, which is represented in Fig. 5.4 c.

Intriguingly, while GBS was detected in the decidua of all GB37-treated animals and only one GB37Δ*hylB* animal (GB37Δ*hylB* #5) (Supplementary Fig. 5.1), no significant differences in inflammation-associated analytes (e.g. CD45, CD68, CD34, CD40L, STING, TGF-β1, CD86, CD56) were detected between the GBS groups in any tissue type (amnion, chorion, decidua) (Fig. 5.1, Supplementary Fig. 5.4). Conversely, some markers associated with inflammation were significantly lower in GB37 animals compared to saline controls, including the macrophage marker CD14 in the decidua and amnion and T cell co-stimulatory molecule CD86 in decidua, chorion, and amnion (Fig. 5.4 c, Supplementary Fig. 5.5). These data indicate that even in tissues sites where GB37 were detected by fluorescent microscopy (Fig. 5.4 b), some inflammatory markers were dampened relative to baseline. However, a nearly 9-fold significant increase in Ki67 and a significant decrease in the cell cycle regulatory protein PTEN in the decidua of GB37-inoculated animals compared to saline controls suggest that pathology-associated cell proliferation may have occurred at these infected tissue sites[170-172]. Together, DSP showed no indication that choriodecidual inoculation with GB37 induced a pro-inflammatory phenotype in the amnion, chorion, or decidua.

5.3.5 *HylB promotes resistance to antimicrobial effects of neutrophils*

Given our observations of increased neutrophil recruitment in the choriodecidual membranes and uterus of GB37-infected animals (Fig. 5.3), yet minimal pro-inflammatory events in the placenta (Fig. 5.4 c), we asked whether GBS hyaluronidase plays a role in dampening neutrophil defenses, which are critical in protecting the host against GBS infection[72,173]. We previously observed that hyper-hemolytic strains of GBS circumvented the neutrophil response, in part, by inducing neutrophil cell death[72]. To test whether hyaluronidase-expressing GBS killed neutrophils more readily than GBS lacking hyaluronidase, we isolated primary human neutrophils from fresh adult human blood and exposed them to strains GB37 and GB37Δ*hylB* at a multiplicity of infection (MOI) of 100, 10, and 1

for 4 hours and measured cytotoxicity by the release of lactate dehydrogenase (LDH), as described[72,83]. No significant differences in cell death were observed between neutrophils treated with the two strains at MOI 100, 10, and 1, and minimal cell death (< 0.02%) was observed relative to Triton X 100-treated positive controls and PBS-treated negative controls (Fig. 5.5 a).

Next, we asked whether hyaluronidase may enable GBS to resist the microbicidal activity of neutrophils. To this end, we compared the survival of GB37, GB37Δ*hylB,* and GB37*ΔcpsE* (lacks capsule, enhancing susceptibility to neutrophil killing[72]) in the presence of purified human neutrophils. We found significantly less neutrophil killing of GB37 compared to GB37Δ*hylB* or GB37Δ*cpsE* (Fig. 5.5 b), indicating that hyaluronidase enables GBS to subvert this critical host defense.

To understand the mechanisms by which HylB may facilitate GBS resistance to neutrophil killing, we measured the production of reactive oxygen species (ROS) in neutrophils in the presence of hyaluronidase proficient or deficient GBS. The production of ROS is critical for the microbicidal action of neutrophils[174]. To measure ROS production, we pretreated human neutrophils with dihydrorhodamine 123 (DHR), which converts to fluorescent monohydrorhodamine (MHR) in the presence of ROS. Neutrophils pretreated with DHR were exposed to GB37, GB37Δ*hylB,* or GB37*ΔcpsE*, and MHR fluorescence was measured after 60 minutes by flow cytometry. Increased ROS-positive cells were noted in neutrophils exposed to GB37Δ*hylB* and GB37*ΔcpsE* compared to GB37 (Fig. 5.5 c), demonstrating that HylB may have blunted the ability of neutrophils to generate ROS.

Because HylB has been shown to degrade HA into dimers that inhibit TLR-2/4 pro-inflammatory signaling in murine macrophages[43], we wondered whether HylB-mediated TLR-2/4 interference could explain the differences in neutrophil ROS production induced by GB37 and GB37Δ*hylB*. To test this, we grew GB37 and GB37Δ*hylB* to stationary phase and incubated filtered supernatants from each strain with HA for 18 hours to allow for enzymatic digestion of HA into

disaccharides, as described[43]. Next, we pre-treated human neutrophils with 10 μg/mL anti-TLR-2 antibody (Invivogen) and 10 μg/mL anti-TLR-4 antibody (Invivogen) or vehicle control. Neutrophils were then pre-treated with DHR as above, exposed to the digested HA solutions from each strain for 60 minutes, and then analyzed for ROS production by flow cytometry. Greater ROS-positive events were seen in neutrophils treated with GB37Δ*hylB*-HA digests compared to neutrophils treated with GB37-HA digests (Fig. 5.5 d), suggesting that HylB dampens neutrophil activation. Among neutrophils treated with GB37Δ*hylB*-HA digest, we observed significantly less ROS production in neutrophils treated with anti-TLR-2 and anti-TLR-4 antibodies compared to those without TLR inhibitors. These data show that pro-inflammatory HA fragments promote ROS production in neutrophils that is, in part, mediated via TLR-2/4 signaling. Taken together, our data are the first to demonstrate that HylB promotes GBS resistance to neutrophils, leading to adverse pregnancy outcomes.

5.4 DISCUSSION

A complete understanding of the mechanisms that GBS use to subvert host defenses in its transition from asymptomatic colonizer to invasive pathogen is essential for the development of improved treatment and prevention strategies for GBS-associated preterm birth, stillbirth, fetal injury and neonatal infection. We previously showed that hyaluronidase (HylB) activity was greater in GBS strains isolated from cases of preterm birth and neonatal infection compared to commensal isolates[46] and that HylB facilitated ascending GBS infection in mice[46]. Here, we utilize a chronically catheterized pregnant NHP model, which more closely emulates human pregnancy than lower animal models[166-169], to elucidate how HylB influences uterine responses and immune mechanisms throughout the course of

infection, starting from the time of inoculation until labor. Our data indicate that HylB is a crucial virulence factor that enables GBS to rapidly invade the amniotic cavity and cause preterm labor.

During infection, host hyaluronidases promote immune surveillance by cleaving HA fragments into pro-inflammatory multimers that interact with pattern recognition receptors (PRRs) such as TLR-2 and TLR-4 on macrophages, dendritic cells, and endothelial cells[163,175-177]. Recently, it was shown that GBS evades HA-mediated immune activation by secreting their own hyaluronidase, HylB, which degrades HA into non-stimulatory disaccharide fragments that interfered with TLR-2/4 signaling in murine macrophages[43]. These results were supported by our recent studies in mice, which indicated that vaginal GBS inoculation with a HylB-proficient strain dampened expression of pro-inflammatory cytokines such as TNF-α and IL-6 in the uterus, leading to ascending infection[46]. Similarly, levels of TNF-α, IL-8, and IL-6 were lower in immortalized endometrial cells infected with WT GBS compared to GBSΔ*hylB*[46].

Given these data and that intraamniotic inflammation is associated with preterm labor[178], we hypothesized that choriodecidual inoculation of pregnant NHP with GB37, a non-pigmented/non-hemolytic clinical isolate of GBS with high HylB activity, would result in immune suppression leading to MIAC, fetal sepsis, and stillbirth rather than preterm labor per se. Surprisingly, we found MIAC and a potential stillbirth without preterm labor in only one NHP in the GB37 group (GB37 #3), whereas the other four GB37-infected animals experienced MIAC and preterm labor (Table 5.1, Fig. 5.1, Supplementary Fig. 5.1). In contrast, only one NHP inoculated with GB37Δ*hylB* experienced MIAC and preterm labor (GB37Δ*hylB* #5), while the other four showed minimal differences in contraction patters and neutrophil infiltration from saline controls (Fig. 5.1, Supplementary Fig. 5.1). Notably, GB37Δ*hylB* #5 exhibited a strong nocturnal pattern of contractions prior to GBS inoculation compared to other animals (Supplementary Fig. 5.1), which could indicate that this animal had a lower threshold for labor and was unable to contain bacterial trafficking. Nevertheless, clear differences in pregnancy

outcomes in GB37-treated animals versus the GB37Δ*hylB* group and the saline controls were observed. Intriguingly, however, minimal differences in peak AF cytokines (Table 5.1) and inflammatory placental immune signaling cascades (Fig. 5.4) were detected among the groups. These results are in stark contrast to our previous findings following choriodecidual inoculation with a hyper-hemolytic/hyper-pigmented GBS strain in a pregnant NHP, which showed significantly higher levels of IL-6 and IL-8 in the AF and up-regulation of inflammation-associated genes in the placenta compared to NHP inoculated with a non-hemolytic strain and saline controls[72]. The two studies also differ in fetal outcomes; MIAC and systemic fetal inflammation was observed in only three of five (60%) of NHP inoculated with the pro-inflammatory, hyper-hemolytic GBS strain in contrast to all five (100%) of the GB37-inoculated animals.

Our observation that GB37 readily invaded the amniotic cavity despite greater recruitment of neutrophils to the choriodecidual membranes and some uterine segments (Fig. 5.3) suggested that GBS may use HylB to overcome antimicrobial action of neutrophils or other infiltrating immune cells at the maternal-fetal interface. Indeed, our *in vitro* data showed that GB37 dampened ROS generation and promoted resistance to neutrophil killing, at least in part by interfering with TLR-2/4 signaling (Fig. 5.5). Notably, the HylB-mediated mechanism of neutrophil evasion is distinct from that conferred by the hemolytic pigment, which induces neutrophil necrosis and decreases GBS's susceptibility to neutrophil extracellular traps (NETs)[72]. These findings indicate that GBS promote pathogenesis by evading neutrophils via multiple distinct mechanisms.

One limitation to our study is our inability to observe the cellular events at the placenta and uterus immediately after inoculation if preterm labor does not occur. Accordingly, it is possible that we did not capture events that may lend greater insight into the kinetics of HylB-mediated immune suppression. For instance, as GB37Δ*hylB* lacks the ability to degrade HA into anti-inflammatory dimers[43], choriodecidual inoculation of GB37Δ*hylB* may have induced rapid recruitment of neutrophils

via controlled inflammation, resulting in swift clearance of this strain before MIAC could occur (in all animals except GB37Δ*hylB* #5). This idea is supported by our previous findings in an intraperitoneal murine model of infection, in which we observed greater neutrophil recruitment to the peritoneal fluid of GB37Δ*hylB*-inoculated mice at 2 hours post-infection and less bacterial dissemination at 48 hours post-infection compared to GB37-inoculated mice[41]. In the present study, bacterial clearance and resolution of inflammation at the choriodecidua in four out of five GB37Δ*hylB*-treated NHP could explain the lower neutrophil frequencies at the choriodecidual membranes and uterine segments between the GBS groups at the experimental endpoint. A time-controlled experiment in the NHP pregnancy model would lend greater insight into the differences in neutrophil recruitment and inflammatory events immediately following choriodecidual infection with GB37 or GB37Δ*hylB*.

Given the *in vivo* and *in vitro* data obtained in this study, we propose that GBS use HylB to dampen pro-inflammatory cascades and microbicidal activity of first-line innate immune defenses such as neutrophils, thereby promoting bacterial replication and invasion of the amniotic cavity and fetus. We hypothesize that once bacteria have invaded the fetal niche, other pro-inflammatory, surface-associated bacterial factors (e.g. capsular polysaccharides[179], surface immunogenic protein[180], pilus[181]) overcome the immune-dampening effects of GBS HylB-digested HA fragments, triggering host PRRs and resulting in systemic fetal inflammation. Our previous studies show that the GBS hemolytic pigment toxin causes rapid inflammation in the AF and placental membrane disruption[24,72,75], which leads to preterm birth but clearance of GBS in some cases[72]. In contrast, our results in this study indicate that GBS use HylB to suppress inflammatory responses to facilitate bacterial replication and dissemination into the amniotic cavity and fetus.

A remaining conundrum is why GB37 inoculation resulted in preterm birth in four of five animals despite immunosuppressive activity of this strain. One possibility is that although pro-inflammatory responses in the amniotic fluid and placenta were dampened, the systemic inflammatory

response in GB37-inoculated fetuses may have triggered parturition in these animals. Notably, peak levels of IL-6 in the fetal blood were higher in the GB37 group (1,049 pg/mL) compared to the GB37Δ*hylB* group (3.64 pg/mL) and saline controls (3.64 pg/mL) (Table 5.1), and fetal inflammatory response syndrome (plasma IL-6 > 11 pg/mL), is associated with preterm labor regardless of the inflammatory state of the amniotic fluid[182]. Thus, inflammatory events in the fetus may have played a role in the early onset of labor in GB37 animals. It is also possible that GBS HylB interfered with other host HA-mediated pathways in addition to immune surveillance mechanisms. Several host hyaluronidases have functions in maintaining healthy pregnancy, such as supporting the structural development of the placenta[183,184] or signaling the onset of labor through cervical ripening[185-187]. In fact, intracervical administration of exogenous hyaluronidase is a method to induce labor in humans[186,188]. Moreover, increased prostaglandin levels in the GB37 group (Table 5.1) indicate that cervical ripening may have occurred in these animals[189]. In short, the high frequency of preterm birth we observed in this study may have been facilitated by fetal inflammatory response syndrome, disruption of HA homeostasis at critical sites at the maternal-fetal-interface, and/or heretofore unidentified mechanisms involved in parturition. Further research on the effect of HylB on these and other host pathways during choriodecidual GBS infection is critical to understanding the multifaceted etiologies of GBS-associated preterm labor.

Together, the work in this chapter establishes HylB as a potent virulence factor that allows GBS to circumvent neutrophil responses, invade the amniotic cavity, and cause fetal bacteremia and preterm labor in an animal model that closely resembles human pregnancy. Accordingly, these results point to HylB as a potential therapeutic target for invasive GBS disease during pregnancy. Interestingly, several known hyaluronidase inhibitors exist and have been proposed as therapeutics for other HA-mediated pathology, including sexually transmitted infections[190,191], venom wounds[192,193], and cancer[194-196]. Identification of a HylB-specific inhibitor could lead to new treatments for GBS and have far-reaching impacts on maternal and neonatal health worldwide.

5.5 MATERIALS AND METHODS

5.5.1 *Study design*

NHP animals: A sample size of n = 5 was predefined (prior to beginning of study) to provide an estimated 80% power in achieving statistically significant results in comparisons among and between animals in each treatment group (ANOVA with alpha level of 0.025). Two-sided unpaired tests were used in the final analyses.

Rationale and design of study: The objective of this study was to determine if expression of hyaluronidase by GBS promoted GBS invasion of the amniotic fluid and fetus and/or preterm labor (PTL). Ten animals received choriodecidual inoculations of 1-3 x 10^8 colony forming units (CFU) of either hyaluronidase-expressing GBS (GB37) or an isogenic hyaluronidase deficient strain (GB37Δ*hylB*). The results from each treatment group were compared to one another and to saline controls (n = 6), four of which were previously described [73]. The primary outcomes of this study are shown in Table 1. Of note, the primary outcome, denoted as "adverse outcome," was a composite of preterm labor and/or MIAC, as both are poor outcomes of pregnancy.

5.5.2 *Ethics statement*

Written informed patient consent for donation of human blood was obtained with approval from the Seattle Children's Research Institute Institutional Review Board (protocol #11117) per the Principles in the WMA Declaration of Helsinki and Dept. of Health and Human Services Belmont Report. Children under the age of 18 were not recruited for donation of human blood.

Written informed patient consent for donation of human maternal blood and cord blood was obtained with approval from the University of Washington Institutional Review Board (protocol #

34004) per the Principles in the WMA Declaration of Helsinki and Dept. of Health and Human Services Belmont Report.

All animal experiments were carried out in strict accordance with the recommendations in the Guide for the Care and Use of Laboratory animals of the National Research Council and the Weatherall report, "The use of non-human primates in research." The protocol was approved by the University of Washington Institutional Animal Care and Use Committee (Permit number: 4165-01). All surgery was performed under general anesthesia and all efforts were made to minimize pain and distress.

5.5.3 *Chemicals*

Unless indicated otherwise, all chemicals were purchased from Sigma-Aldrich.

5.5.4 *Bacterial strains*

GBS strains used in the non-human primate (NHP) model were derived from strain GB37 (serotype V, multilocus sequence type-1), which was isolated from the blood of a septic human neonate with early onset disease in [197]. This strain is neither hemolytic nor pigmented [198], but exhibits increased hyaluronidase activity compared to other GBS clinical isolates [41]. The isogenic strain GB37Δ*hylB* lacks hyaluronidase and was described previously [41]. The isogenic strain GB37Δ*cpsE* was derived from wild-type GB37 using methods described previously [46,199] . Briefly, approximately 1.0-kb of DNA flanking either side of the *cpsE* gene was PCR amplified using GB37 genomic DNA as template and the primers (for 1KB upstream: 5'-ATTTAAAGATACCCCCAATACAAGAGCCCCTTACTTCC-3' and 5'-GGGGCTCTTGTATTGGGGGTATCTTTAAATACTG3'; for 1KB downstream: 5'-AAAGGATCCAATCCAAAAATGTCTCAAAAATTAG-3' and 5'-AAAAAGCTTTCCTCCTATTAACAAATAC3'). The region encoding kanamycin resistance was PCR amplified from the plasmid pCIV2 [200] using primers (5'-CAAATTTTCATTATACTAAAACAATTCATCCAG-3' and 5'-

GGATGAATTGTTTTAGTATAATGAAAATTTGTCTGG-3') . All PCR fragments were ligated using the Gibson Assembly cloning kit (New England Biolabs) into the linearized temperature-sensitive vector pHY304 [201]. The resulting plasmid was then electroporated into electrocompetent GB37, and selection for the double crossover mutant with an allelic replacement of *cpsE* with the gene conferring kanamycin resistance was performed as previously described [199].

Cultures of GBS were grown in tryptic soy broth (TSB) or tryptic soy agar (TSA, Difco Laboratories) at 37 °C with 5% CO_2. For inoculations in the NHP model, GBS strains were grown to mid-log phase (OD_{600} = 0.27), and 1 x 10^8 CFU in 1mL sterile PBS was inoculated into the choriodecidual space, as described below and previously [72,73]. Similarly, for *in vitro* studies, GBS strains were grown to mid-log phase (OD_{600} = 0.27), washed, and resuspended in sterile PBS prior to infection unless otherwise noted.

5.5.5 *Chronically catheterized NHP model*

As described [72], pregnant pigtail macaques (*Macaca nemestrina*) were time-mated and fetal age was determined using early ultrasound. Animals were provided drinking water at all times and were fed commercial monkey chow, supplemented daily with fruits and vegetables. Temperature in animal quarters was maintained between 72 °F and 82 °F. Each animal was conditioned to a nylon jacket/tether system for several weeks before surgery, which allowed for free movement within the cage while protecting the catheters.

Between days 116 and 125 of pregnancy (term = 172 days), NHP were catheterized by laparotomic surgical implantation into the maternal femoral vein, amniotic cavity, and choriodecidual interface in the lower uterine segment (i.e., between the uterine muscle and fetal membranes, external to amniotic cavity) as described [72,73,202]. Choriodecidual and amniotic fluid catheters were made of polyvinyl tubing, and maternal artery and vein catheters were made of silicone tubing. Fetal ECG electrodes and a maternal temperature probe (AD Instruments) were also implanted. Post-operative

analgesia was provided via a fentanyl patch applied one day prior to surgery, in addition to post-operative indomethacin or ketoprofen as described [72,73].

Following surgery, each animal was placed in the jacket and tether with the catheters/electrodes tracked through the tether system. Cefazolin and either terbutaline sulfate or atosiban (0.12 mg/kg/hr) were administered intravenously to reduce postoperative infection risk and uterine activity. Cefazolin, terbutaline, or atosiban were stopped at least 72 hours prior to experimental start (97% of drugs eliminated) and represented approximately a 7- to 10-day period of postoperative terbutaline administration. To allow for recovery, experiments began approximately two weeks after catheterization surgery (equivalent to approximately 30 to 31 weeks human gestation).

The experiment was initiated when a catheterized pregnant NHP received one of two experimental treatments: choriodecidual inoculation of either GBS strain GB37 (n = 5) or the isogenic strain GB37Δ*hylB* (n = 5, does not produce hyaluronidase). Two chronically catheterized NHP that were inoculated with sterile saline were also included, along with five saline controls performed in previous studies [73,203].

AF and maternal blood were collected for culture, cytokine, and prostaglandin analysis during each experiment. Intra-amniotic pressure was continuously recorded, digitized, and analyzed as described [72,73]. The integrated area under the curve for intrauterine pressure was used as a measure of uterine activity and reported as the hourly contraction area (HCA; mmHg*sec/hr) over 24 hours. Preterm labor was defined as progressive cervical dilation associated with increased uterine activity (hourly contraction area >10,000 mmHg*sec/hr). Cesarean section was performed at the following experimental endpoints to allow for tissue collection: 1) preterm labor, 2) three days post-GBS inoculation if preterm labor did not occur, or 3) seven days post-saline inoculation [73,204]. After Cesarean section, fetuses were euthanized by barbiturate overdose (1-2mL, 390 mg/mL, Beuthanasia-D Special,

Schering-Plough Health Corp.), followed by exsanguination and fetal necropsy [73,204]. Complete gross and histopathologic examinations were performed.

AF (~4 mL) and maternal blood (~3 mL, in EDTA tubes, BD Biosciences) were sampled before (at -24 and -0.25 hours) and after inoculation (0.75, +6, +12, +24 hours and then every 12 hours until Cesarean section for fetal necropsy). To quantify bacterial invasion of the amniotic cavity, AF (200 μL) from each sampling was serially diluted by a factor of 10, and dilutions were plated on TSA, incubated overnight at 37 °C, 5% CO_2, and GBS CFU were enumerated. For cytokine and prostaglandin (PG) analysis, samples of AF and material blood were centrifuged for 5 min at 300 x *g* immediately after collection, and indomethacin (0.3 mM) was added to supernatants to halt PG metabolism prior to freezing at -80 °C.

Fetal blood was obtained during Cesarean section, and fetal tissues were obtained and weighed during necropsy. To analyze bacterial dissemination into fetal organs, fetal tissues were homogenized in sterile PBS on ice using a hand-held tissue homogenizer (Tissue Tearor, Biospec Products, Inc.) in 10 to 30 second pulses until the samples were completely homogenous. Subsequently, 10-fold serial dilutions were plated on TSA and incubated overnight at 37 °C, 5% CO_2, and GBS CFU were enumerated, as described [204]. To analyze fetal inflammatory cytokines, fetal organ homogenates were diluted 1:1 in lysis buffer (150 mM NaCl, 15 mM Tris, 1 mM MgCl2, 1 mM CaCl2, 1% Triton X-100, supplemented with cOmplete, Mini, EDTA-free protease inhibitor cocktail (Roche)) and incubated overnight at 4 °C. Then, lysates were centrifuged at 600 x *g* for 5 min at 4 °C, and supernatants were analyzed immediately or stored at -80 °C for later analysis. Cytokine (IL-1β, TNF-α, IL-6, and IL-8) levels were determined using ProcartaPlex cytokine kits (ThermoFisher), per manufacturer instructions. Prostaglandin E2 (PGE2) and prostaglandin F2-alpha (PGF2α) were determined using commercially available ELISA kits (Cayman Chemical), per manufacturer instructions.

5.5.6 *Placental and fetal lung histology*

A board-certified veterinary pathologist (A.B.) was blinded to the experimental groups and performed histopathologic examination of the fetal and placental tissues. H&E-stained, full-thickness paraffin sections (placental disc, umbilical cord, fetal membrane roll) were examined from each case to exclude inflammation, necrosis, fetal vascular thrombosis, or other histopathological findings. Chorioamnionitis was diagnosed by the presence of a neutrophilic infiltrate at the chorion-decidua junction (mild) or amniochorion junction (moderate or severe). For histologic examination of the fetal lung, two to three randomly selected fixed fetal lung tissues were embedded in paraffin and sections stained with hematoxylin and eosin (H&E). Regions of interest within each tissue were outlined corresponding to the amnion, chorion and decidua within the chorioamniotic membranes and alveoli within the fetal lung.

5.5.7 *Flow cytometry of placental tissues, uterine tissues, maternal blood, and fetal blood*

Intact placental segments, including chorioamniotic membranes and chorionic villi (CV), as well as biopsies from the myometrium (lower uterus, mid-uterus, and upper uterus) were obtained during Cesarean section and stored in RPMI 1640 with L-glutamine (Corning, hereafter referred to as RPMI-g) on ice for approximately 30 min prior to tissue processing. Maternal and fetal blood (approx. 1 mL) were also collected during Cesarean section and stored in 1X red blood cell (RBC) lysis buffer (150 mM NH_4Cl, 0.1 mM $NaHCO_3$, 1.27 mM EDTA in distilled, deionized H_2O) on ice.

Placental and uterine tissues were washed twice with PBS, then weighed. Digestion buffer (20 mM HEPES, 30 mM $NaHCO_3$, 150 µg/mL DNase I (Roche), 1 mg/mL hyaluronidase from bovine testes, 10 mg/mL BSA, 0.75 mg/mL Collagenase A (Roche), 100 µg/mL streptomycin, 100 U/mL penicillin in RPMI-g) was added to each tissue at 10 mL/g tissue, and then each tissue was minced to approximately 1 cm^3, transferred to a 50 mL conical tube, and incubated at 37 °C for 1 hour while

shaking at 300 rpm. During the incubation, blood samples were washed 3 to 5 times in 1X RBC lysis buffer (until RBCs were visibly absent from cell pellets), resuspended in RPMI-g supplemented with 10% heat-inactivated fetal bovine serum (Gibco) and 5% penicillin/streptomycin (hereafter referred to as RPMI-g + FBS + p/s) and stored at 4 °C. Following digestion, macerated placental and uterine tissues were washed once (300 x *g*, 5 minutes), resuspended in RPMI-g + FBS + p/s, and then progressively passed through a 280 μm metal sieve and a 40 μm nylon screen. Single cells were pelleted and resuspended in RPMI-g + FBS + p/s. Cell suspensions from all tissues and blood were counted using a TC20 cell counter (BioRad), diluted to approximately 1.5 x 10^7 cells/mL in RPMI-g + FBS + p/s, and stored at 4 °C overnight.

Cell suspensions were transferred to wells of a 96-well plate (approximately 3 x 10^6 cells/well), washed once with FACS buffer (300 x *g*, 5 minutes), and then incubated in 100 μL human Fc block (1:200, BD Biosciences) for 15 min at room temperature. Cells were then resuspended in 100 μL of the appropriate extracellular panel (Supplementary Table 1) and incubated for 15 to 25 minutes at room temperature, protected from light. Cells were washed twice in FACS buffer, then resuspended in 200 μL fixation/permeabilization working solution from the Intracellular Fixation & Permeabilization Buffer Set (eBioscience). After incubating for 30 minutes at room temperature, protected from light, cells were washed twice in fixation/permeabilization buffer (Fixation & Permeabilization Buffer Set, eBioscience) and then resuspended in 100 μL of the appropriate intracellular panel (Supplementary Table 2). Cells stained for 30-35 minutes at room temperature, protected from light, and were washed twice in fixation/permeabilization buffer, resuspended in 100 μL FACS buffer, and aliquoted into FACS tubes containing 700 μL FACS buffer. Cells were analyzed for intracellular and extracellular markers using an LSRII flow cytometer (BD Biosciences), and unstained cells and single-stained compensation beads (BD Biosciences) were used for compensation. Data were analyzed using FlowJo software version 10.1 (FlowJo).

5.5.8 *Digital Spatial Profiling*

GeoMx Digital Spatial Profiling (DSP) was performed at NanoString Technologies in Seattle, WA, USA. Formalin fixed paraffin embedded (FFPE) placental sections from animals from each group were incubated with fluorescent probes and a multiplex cocktail of primary antibodies with photocleavable oligonucleotides (i.e. the validated DSP human-immune oncology protein panel, NanoString Technologies). The fluorescent markers included anti-pan cytokeratin-Alexa Fluor 488 (Pan-CK, clone AE1/AE3, Novusbio), anti-fibroblast activation protein-Alexa-Fluor 594 (FAP, clone SP325, Abcam), SYTO 83 for nuclei visualization (ThermoFisher), and anti-GBS-Alexa Fluor 647 (clone ab53584, Abcam). Sections were magnified to 20X, and regions of interest (ROIs) comprising the decidua, chorion, and amnion from each animal were selected based on tissue morphology (Fig. 5.4 b). Each ROI was then exposed to UV illumination with a double digital mirror device (DDMD) molecule, which cleaved the DNA oligos into the aqueous layer above the tissue slice. The oligos in the eluent were collected via microcapillary aspiration and transferred to an individual well of a microtiter plate. Oligos were then hybridized to nCounter optical barcodes (NanoString Technologies) to permit *ex situ* digital counting of each analyte. Briefly, hybridization of oligos to optical barcodes were performed at 65 °C in a thermocycler. Following hybridization, samples were processed using the nCounter Prep Station and Digital Analyzer. Data were normalized to technical controls and area. To generate signal-to-noise ratios, data were calculated relative to isotype controls.

5.5.9 *Isolation of neutrophils from adult human blood*

As described[72], 5-15 mL of human adult blood was collected independently from healthy human adults into EDTA tubes (BD Biosciences). Immediately following collection, neutrophils were isolated using a MACSxpress neutrophil isolation kit, per the manufacturer's instructions (Miltenyi Biotec). Cells were then pelleted, and any residual red blood cells (RBC) were removed by re-suspending the cell pellet in RBC lysis buffer for 15 minutes at room temperature. After RBC lysis,

cells were washed with RPMI-G. Neutrophil purity in the prepared cell suspension was assessed by examining the proportion of cells positive for the neutrophil cell markers CD15 (PerCP/Cy5.5, clone HI98, BD Biosciences) and CD16 (FITC, clone 3G8, BD Biosciences) by flow cytometry. Briefly, approximately 1 x 10^6 cells from the neutrophil purification preparation or 1 x 10^6 cells from whole blood (following two RBC lysis steps, as described above) were incubated with human Fc block (1:200, BD Biosciences) for 15 minutes at room temperature. Then, immunofluorescent antibodies were added to the cells at concentrations recommended by the manufacturer (1:10, CD15-PerCP/Cy5.5; 1:200, CD16-FITC), and cells incubated for 30 minutes at room temperature. Stained cells were washed twice in FACS buffer and were analyzed immediately on an LSR II flow cytometer (BD Biosciences). Single-stained flurochrome-reactive AbC beads and unstained cells were used for compensation. Data were analyzed using FlowJo v. 10.1 (FlowJo, LLC).

5.5.10 *Neutrophil cell death assay*

Neutrophils were isolated from fresh human blood as described above and washed with RPMI-g. Neutrophils were seeded in a 96-well plate at approximately 1 x 10^5 cells/well in 100 μL RPMI-g, and then exposed to GB37 or GB37Δ*hylB* at MOI 100, 10, or 1 for 4 hours at 37 °C. Cell death was measured by the release of the cytoplasmic enzyme lactate dehydrogenase (LDH) into cell supernatants using the LDH Assay Kit (Takara) per manufacturer instructions. Percent cell death was calculated relative to 0.1% Triton X-100-treated positive controls (100% cell death) and PBS-treated negative controls (0% cell death).

5.5.11 *Neutrophil killing assay*

As above, neutrophils were isolated from fresh human blood and washed with RPMI-g. Then, approximately 1 x 10^6 neutrophils were incubated with GB37, GB37Δ*hylB*, or capsule-deficient GB37Δ*cpsE* at MOI 1 in RPMI for 1 hour at 37 °C as described[72,205]. Triton X-100 (0.1%) was added

to lyse neutrophils and release intracellular bacteria and total bacteria (intracellular and extracellular) were enumerated by serial dilution plating on TSA. Percent killing was calculated as the number of CFU recovered in the presence of neutrophils over the number of CFU recovered in the absence of neutrophils (x 100).

5.5.12 *Measurement of ROS production by neutrophils*

Neutrophils were isolated as described above, resuspended in HBSS at 1 x 10^6 cells/mL and pre-incubated with 84 μM dihydrorhodamine 123 (DHR in 0.28% DMSO) at 37 °C for 20 minutes, as described[72]. Approximately 5 x 10^5 pre-treated neutrophils were exposed to GB37, GB37Δ*hylB*, or GB37Δ*cpsE* (MOI 100) for 60 minutes, and the fluorescence intensity of cells (which measures DHR oxidation by ROS to fluorescent MHR) was measured immediately by flow cytometry using an LSR II (BD Biosciences). Data are representative of 2 experiments with neutrophils obtained from independent donors and were analyzed using FlowJo v. 10.1 (FlowJo, LLC).

5.5.13 *Measurement of TLR2-/4 signaling on ROS production by neutrophils*

Neutrophils were isolated as above, resuspended to 1 x 10^7 cells/mL in HBSS, and treated with 10 μg/mL anti-human-TLR-2 antibody (maba2-htlr2, Invivogen) and 10 μg/mL anti-human-TLR-4 antibody (mabg-htlr4, Invivogen) in HBSS or equal volume of HBSS for 15 minutes at room temperature. Then, neutrophils were diluted to 1 x 10^6 cells/mL in HBSS and treated with 84 μM dihydrorhodamine 123 (DHR) at 37 °C for 20 minutes as above. Then, approximately 5 x 10^5 neutrophils were exposed to GB37 or GB37Δ*hylB* for 60 minutes, the fluorescence intensity of cells was measured by flow cytometry as above (LSR II, BD Biosciences), and data were analyzed using FlowJo v. 10.1 (FlowJo, LLC).

5.5.14 *Statistical analyses*

For *in vivo* studies (NHP experiments) the primary study outcomes were compared using Barnard's test. Changes in peak AF cytokines and prostaglandins were compared using an analysis of one-way ANOVA with Bonferroni's correction. These analyses were performed using Intercooled STATA 8.2 for Windows (StatCorp) or SciStatCalc. CFU in fetal tissues were compared using the Mann-Whitney test, as normal distribution was not assumed in these samples. Similarly, cytokine levels in fetal tissues were not assumed to have equal distribution and were thus compared using test Kruskal-Wallis test with Dunn's multiple comparison test. Welch's test was used to compare immune cell populations detected by flow cytometry in GB37 vs. GB37Δ*hylB* animals. A mixed linear model controlling for false discovery rate was used to compare differences in DSP analyte abundance among GB37, GB37Δ*hylB*, and saline. In all cases, results were considered significantly different if $p < 0.05$. However, because of the limited number of samples per group in NHP experiments, we also report trends (i.e. p values between 0.05 and 0.100) as described previously for NHP experiments[206]. For *in vitro* experiments with greater than two comparison groups, Kruskal-Wallis test or one-way ANOVA was performed with Dunn's or Tukey's post-test, respectively, and as indicated in figure legends. For *in vitro* experiments with two comparison groups, a student's t test was performed. All statistical tests were unpaired and two-sided. These analyses were performed using GraphPad Prism version 6.0 (GraphPad Software, www.graphpad.com).

5.6 ACKNOWLEDGEMENTS

5.6.1 *Competing interests*

The authors declare no competing interests.

5.6.2 *Author contributions*

L.R., K.A.W., M.C., B.A., C.G., and J.V. designed the experiments. M.C., B.A., A.O., P.Q., A.B., C.G., J.O., S.M., M.D., W.T-Y., J.M., A.B., A.F., S.N., K.A.W., and L.R. performed the experiments. M.C., B.A., A.O., P.Q., C.G., S.M., M.D., K.A.W., and L.R. analyzed the results, and D.M.A. and S.D.M. provided strain GB37. B.A., M.C., K.A.W., and L.R. wrote the manuscript.

5.6.3 *Funding*

This work was supported by funding from the National Institutes of Health grants R01AI112619, R01AI133976, R01AI100989, and R21AI125907 and seed funds from Seattle Children's Research Institute to L.R. The NIH training grants T32AI007509 (PI: Lee Ann Campbell) supported C.W. and J.V. The content is solely the responsibility of the authors and does not necessarily represent the official views of the National Institutes of Health.

5.6.4 *Other*

We thank Connie Hughes for administrative support.

5.7 FIGURES AND TABLES

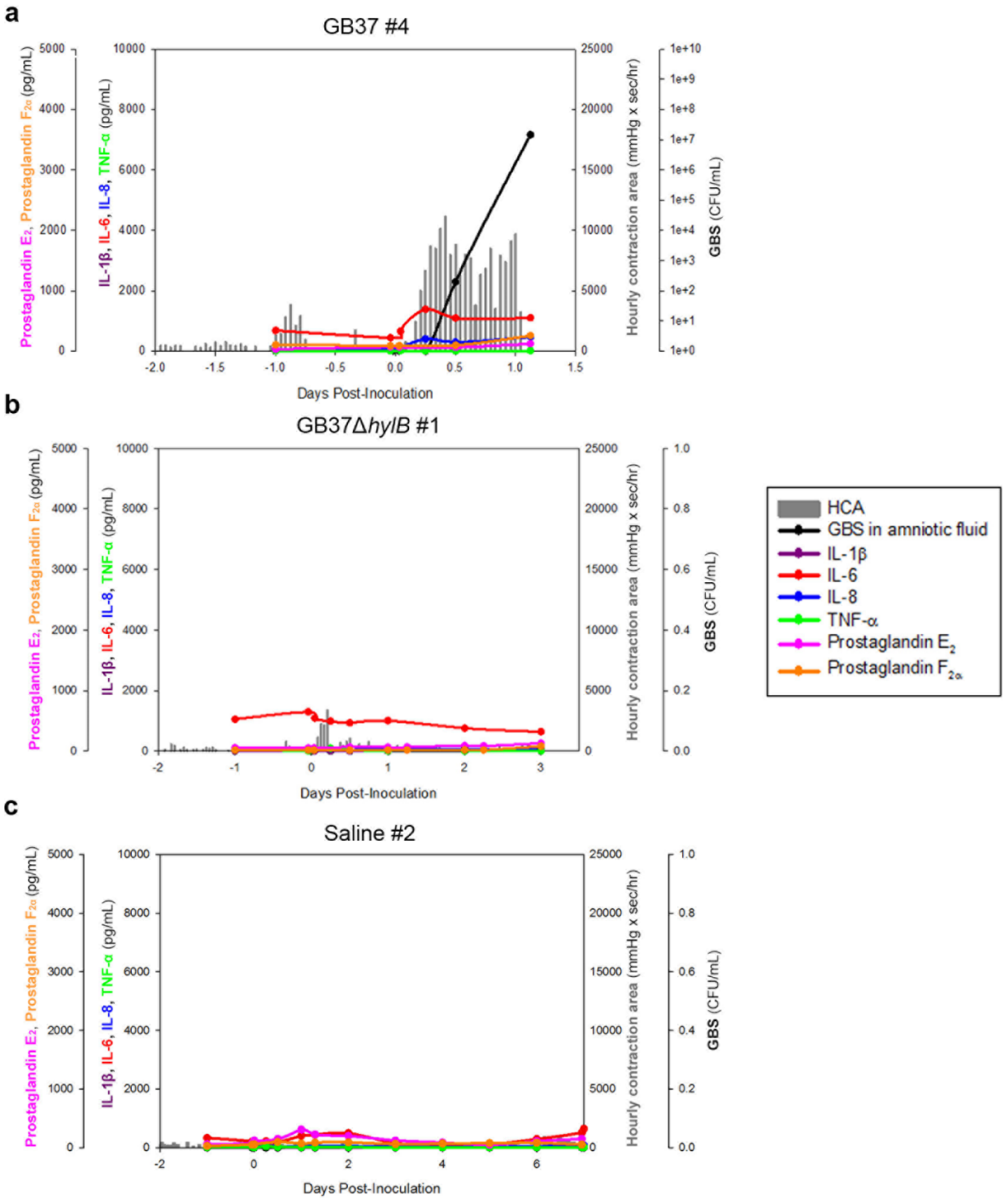

Figure 5.1. GBS HylB promotes MIAC and preterm labor.

Chronically catheterized pregnant pigtail macaques (*Macaca nemestrina*) received choriodecidual inoculations a GBS train that over-produces HylB (GB37, n = 5), an isogenic GBS strain lacking HylB (GB37Δ*hylB*, n = 5), or saline (n = 6) at 118 to 125 days gestation (term, 172 days). Hourly contraction area (HCA; vertical gray lines), cytokines (IL-1β, IL-6, IL-8, and TNF-α), prostaglandins (PGE_2 and $PGF_{2\alpha}$), and GBS CFU from the AF are shown from representative animals that received GB37 (**a**), GB37Δ*hylB* (**b**), or saline (**c**).

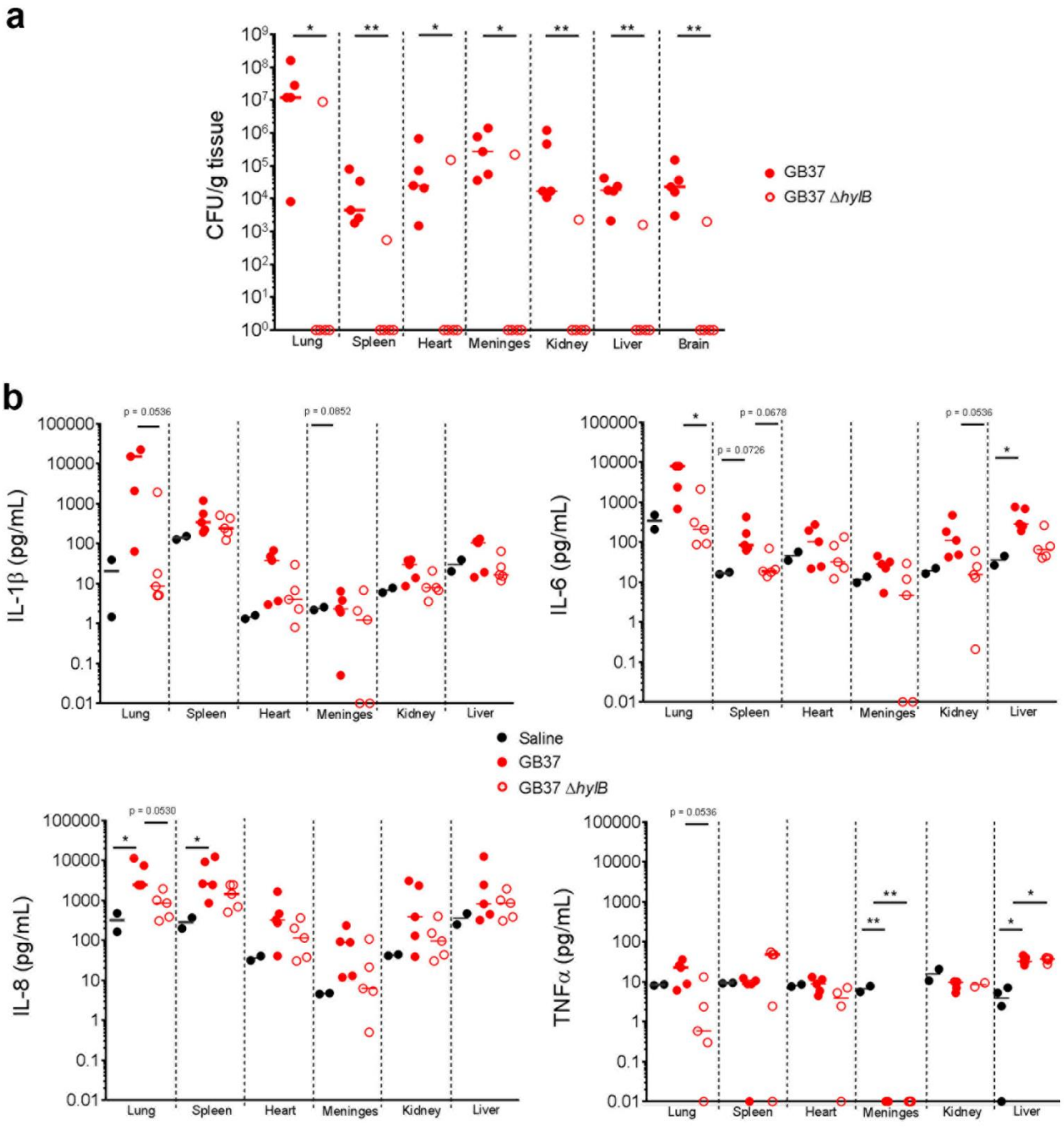

Figure 5.2. MIAC coincided with fetal bacteremia and systemic fetal inflammation.

At Cesarean section, fetal tissues were harvested from chronically catheterized pregnant NHP that received a choriodecidual inoculation of saline, GB37, or GB37Δ*hylB*. (**a**) The number of GBS CFU

obtained from various fetal tissues is shown. Note that GBS was recovered from all fetal tissues of all animals that experienced MIAC and preterm birth, including all (5/5) GB37-inoculated animals and one of five GB37Δ*hylB*-inoculated animals (GB37Δ*hylB* #5). Differences in CFU between treatment groups were analyzed using the Mann-Whitney test. * indicates $p < 0.05$, and ** indicates $p < 0.01$. (**b**) Lysates from fetal tissues were examined by Luminex to evaluate differences in levels of fetal cytokines. A Kruskal-Wallis test with Dunn's multiple comparisons test was performed. * indicates $p < 0.05$.

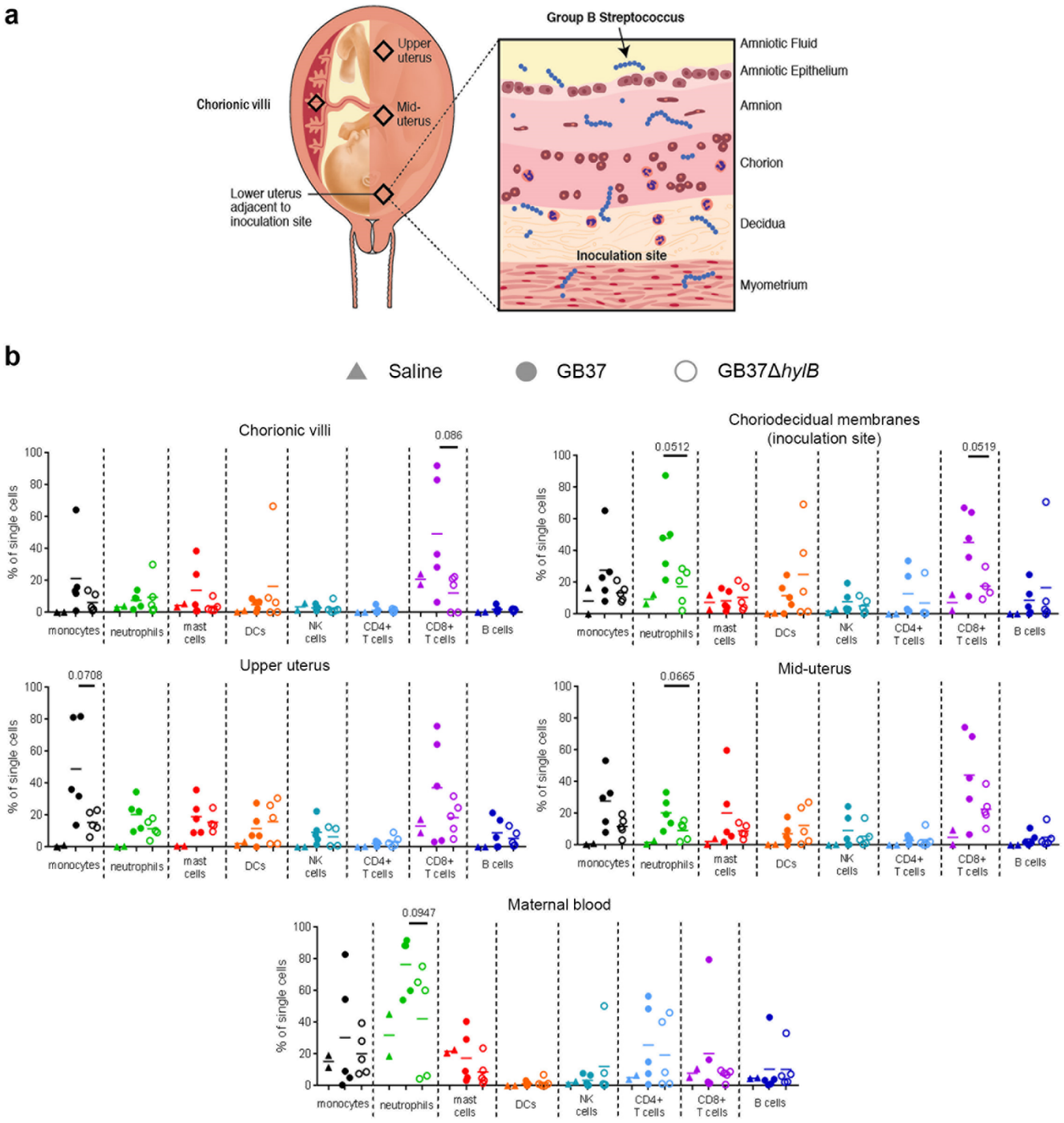

Figure 5.3. GB37-inoculated NHP experienced enhanced infiltration of CD8+ T cells and phagocytes to the maternal-fetal interface.

At Cesarean section, biopsies from the uterus and placenta as well as maternal and fetal blood were obtained. (**a**) A schematic depicting the biopsy sites is shown. (**b**) Samples were processed into single-

cell suspensions, stained, and analyzed by flow cytometry for various immune cell markers (indicated in the figure). A Welch's test was used to inspect for differences in immune cell populations between GB37- and GB37Δ*hylB*-treated animals at each site.

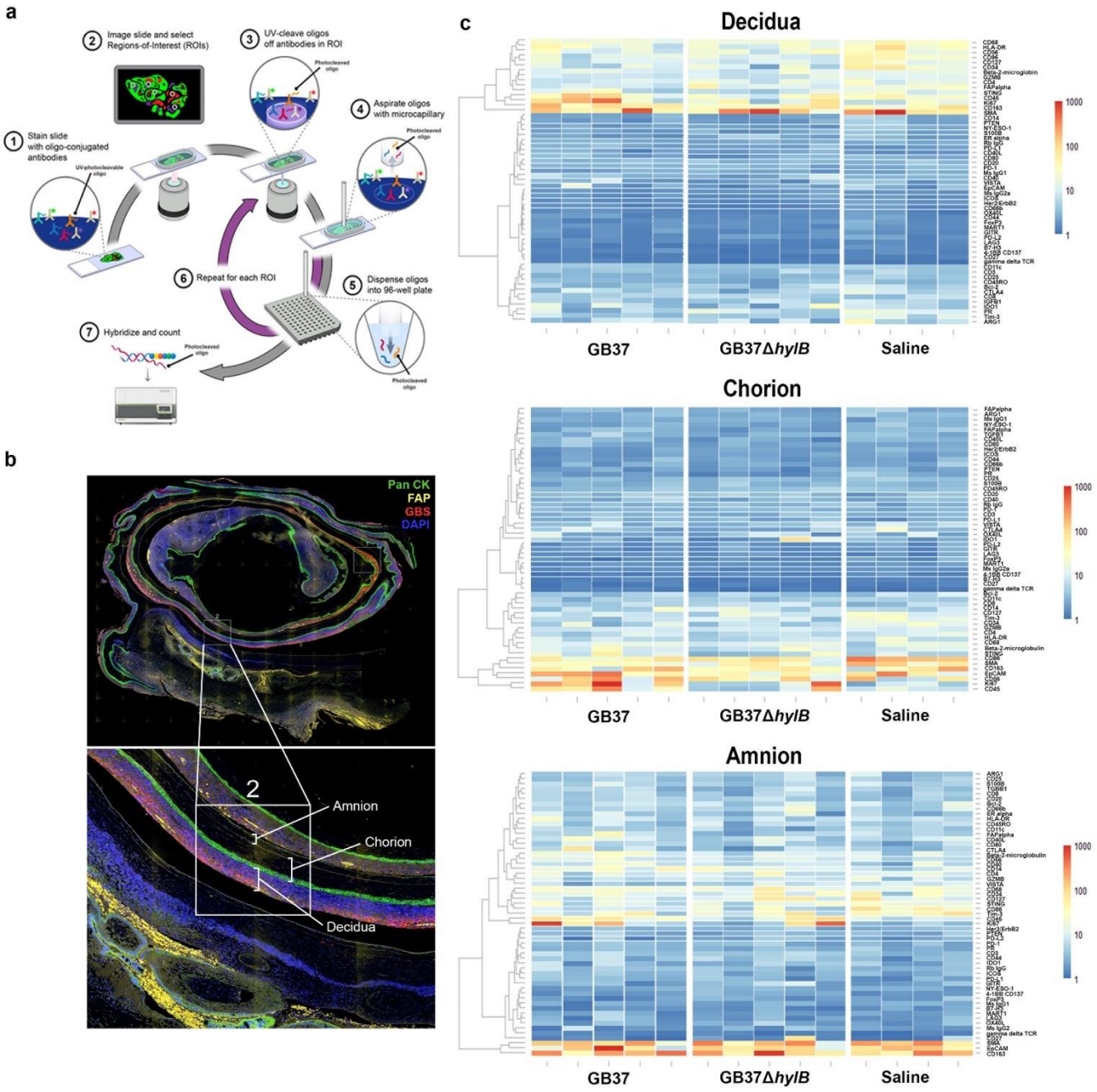

Figure 5.4. Digital Spatial Profiling (DSP) of placental tissues revealed minimal immune signatures to GBS hyaluronidase.

(**a**) The workflow for the DSP platform allows for spatial resolution of immunological pathways in the placenta. First, formalin fixed paraffin embedded placental sections are treated with fluorescent antibodies so that tissue architecture and bacterial invasion can be visualized. Then, sections are treated

with a panel of 62 oligo-conjugated antibodies reactive to immunological markers. Slides are imaged, and regions of interest (ROIs) are selected. At each ROI, UV light is used to cleave the antibody-conjugated oligos, which are then aspirated, dispensed into a 96-well plate format, hybridized, and then quantified. (**b**) A representative placental section from a GB37-treated NHP (GB37 #2) is shown. We treated each placental section with fluorescent anti-pan cytokeratin (Pan CK, green), anti-fibronectin attachment protein (FAP, yellow), anti-GBS (red), and DAPI (blue) and then identified the decidua, chorion, and amnion within each section as distinct ROIs. Each discrete ROI (i.e. chorion, amnion, and decidua) was analyzed for analyte abundance. (**c**) Heatmaps showing analyte abundance (normalized by signal-to-noise ratio) in the decidua, chorion, and amnion of each animal in the GB37 group (n = 5), GB37ΔhylB group (n = 5), and saline group (n = 4) are shown.

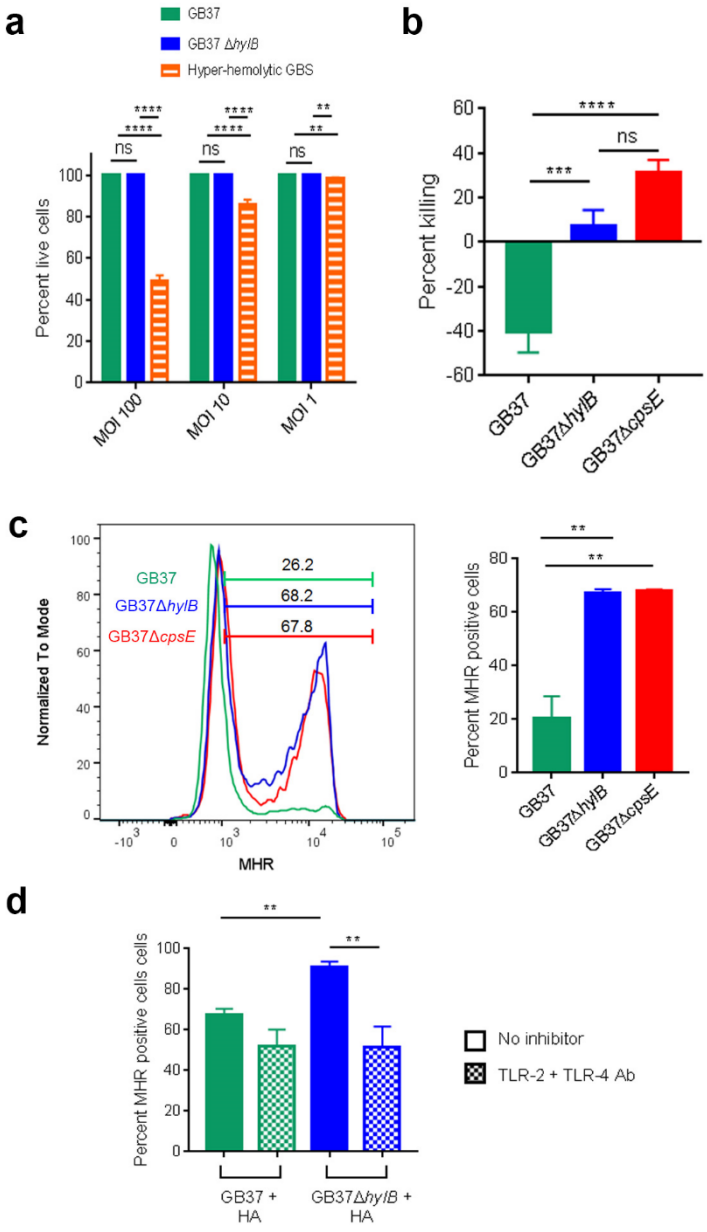

Figure 5.5. GBS HylB evades neutrophil killing independently of cell death by interfering with TLR-2/4 signaling.

(**a**) Primary human neutrophils were isolated from fresh blood, exposed to GB37 or GB37Δ*hylB* at MOIs 100, 10, or 1 for 4 hours, and then examined by LDH release. Percent live cells was calculated relative to Triton X-100-treated positive controls (0% live cells) and PBS-treated negative controls (100% live cells). An unpaired t test was used to examine differences between treatment groups at each

MOI. (**b**) GB37, GB37Δ*hylB*, or GB37Δ*cpsE* (more sensitive to neutrophil killing[72]) were exposed to primary human neutrophils isolated from fresh blood (MOI 1) for 4 hours in the absence of serum. Percent killing was calculated as the number of CFU recovered after incubation with neutrophils out of the number of the number CFU recovered after incubation without neutrophils (x 100). Differences among groups were determined by one-way ANOVA. (**c**) Primary human neutrophils were isolated as above, pre-treated with dihydrorhodamine 123 (DHR), and then exposed to GB37, GB37Δ*hylB*, or GB37Δ*cpsE* (MOI 100). The conversion of DHR to fluorescent MHR indicates ROS production in cells and was measured by flow cytometry at 60 minutes post-infection. Differences among treatment groups were determined by one-way ANOVA. (**d**) Filtered supernatants of stationary phase GB37 or GB37Δ*hylB* liquid cultures were incubated with HA for 18 hours to allow for enzymatic digestion of HA. Meanwhile, primary human neutrophils were pre-treated with 0 μg/mL anti-TLR-2 antibody (Invivogen) plus 10 μg/mL anti-TLR-4 antibody (Invivogen) or vehicle control. Neutrophils were treated with DHR, and then exposed to the digested HA solutions from each strain for 60 minutes. As above, ROS production in cells was measured by detecting fluorescent MHR via flow cytometry. Differences in MHR positive cells among treatment groups were determined by one-way ANOVA. * indicates $p < 0.05$, ** indicates $p < 0.01$, *** indicates $p < 0.001$, **** indicates $p < 0.0001$, ns indicates $p \geq 0.05$.

Table 5.1. Summary of pregnancy outcomes, cytokines, and prostaglandins in pregnant NHPs. The primary outcomes are shown as number (%) and were compared among groups using Barnard's test. AF cytokines and prostaglandins and fetal plasma cytokines are expressed as mean peak (SEM) in pg/mL. Hourly contraction area (HCA) is expressed in mmH* sec/hr. Cytokines (IL-1β, TNF-α, IL-6, and IL-8) and prostaglandins (PG_{E2} and $PG_{F2\alpha}$) were compared using one-way ANOVA with Bonferroni's correction. Statistical analyses were conducted using Intercooled STATA 8.2 for Windows 2000 (StataCorp) or SciStatCalc, and p values < 0.05 are listed in bold. NS indicates p > 0.100.

	Saline (n=6)	GB37 (n=5)	GB37Δ*hylB* (n=5)	*P* value Saline vs. GB37	*P* value GB37 vs. GB37Δ*hylB*	*P* value Saline vs. GBS GB37Δ*hylB*
Primary and composite outcomes						
Adverse outcome[#]	0 (0%)	5 (100%)	1 (20%)	**0.0009**	**0.0214**	NS
Preterm labor[@]	0 (0%)	4 (80%)	1 (20%)	**0.0117**	0.1094	NS
MIAC and Fetal bacteremia	0 (0%)	5 (100%)	1 (20%)	**0.0009**	**0.0214**	NS
Peak contractions, amniotic fluid cytokines, and prostaglandins						
Hourly contraction area	1326.7 (506.58)	5606.0 (1165.1)	3087.4 (1050.0)	**0.0370**	NS	NS
IL-1β	31.61 (20.59)	1754.8 (1112.7)	597.65 (583.42)	0.086	NS	NS
TNF-α	26.13 (11.44)	574.58 (285.82)	97.58 (39.43)	0.070	NS	NS

IL-6	7091.1 (2642.2)	2827.8 (1331.3)	2404.1 (1356.5)	NS	NS	NS
IL-8	888.07 (321.53)	2120.5 (1383.3)	1629.7 (1498.2)	NS	NS	NS
PGE_2	509.83 (247.84)	1160.9 (647.40)	289.23 (116.69)	NS	NS	NS
$PGF_{2\alpha}$	424.31 (169.64)	1808.1 (887.27)	164.93 (45.91)	NS	0.077	NS
Fetal cytokines*						
IL-1 β	0.80 (0.60)	2.152 (0.8584)	1.128 (0.8645)	NS	NS	NS
TNF- α	2.268 (1.127)	0.01 (0.0)	0.01 (0.0)	**0.035**	NS	**0.035**
IL-6	3.639 (1.852)	1049.6 (722.10)	44.74 (41.58)	**0.049**	NS	NS
IL-8	574.06 (314.04)	2648.8 (1674.1)	2576.2 (1551.3)	NS	NS	NS

Chapter 6. CONCLUSIONS AND FINAL THOUGHTS

6.1 SUMMARY OF FINDINGS

The work in this dissertation addresses several key questions regarding two GBS virulence factors, namely the hemolytic pigment (granadaene) and the secreted hyaluronidase (HylB). The results detailed in the chapters provide new insight into the complex mechanisms by which GBS utilizes these virulence factors for its survival and pathogenesis. These findings also have relevance to the development of targeted treatment strategies to prevent invasive GBS disease.

Hemolytic activity was first described in GBS over a century ago[77,78], yet the molecular identity of this major virulence factor was only discovered in 2013[75]. While recent research into the mechanisms of granadaene-mediated virulence have enhanced our understanding of GBS disease[24,72,75,83], several outstanding questions remained regarding its biosynthetic and evolutionary origins, the chemical moieties important for activity, and how GBS deploys granadaene during infection. In Chapter 2, we show that introduction of the *cyl* genes necessary for granadaene production in GBS are sufficient for toxin production in a non-hemolytic Gram-positive bacterium, *Lactococcus lactis*. Further, through phylogenetic analysis of the *cyl* genes, we propose novel roles for *cyl* gene products in granadaene biosynthesis and conclude that similar, potentially toxic lipid toxins may be encoded by other Gram-positive bacteria. In Chapter 3, we overcome challenges associated with studying the basis of granadaene's toxic activity through the synthesis of granadaene-inspired analogs, which revealed that the polyene chain length is central to hemolysis. In addition, we demonstrate that incorporation of a non-toxic granadaene analog into a vaccine formulation is a viable strategy for diminishing the effects of granadaene during GBS infection. Finally, in Chapter 4, we show that hemolytic GBS release membrane vesicles containing granadaene; these hemolytic MVs quench

reactive oxygen species and promote bacterial survival and dissemination. Together, these chapters offer new insight into the hemolytic pigment toxin produced by GBS and provide the basis for future studies centered on optimizing a vaccine to mitigate its pathogenic effects.

Hyaluronan (HA) is a major constituent of the mammalian extracellular matrix, and several HA-cleaving enzymes, known as hyaluronidases, are secreted by the host to assist in critical cellular functions, including cell migration, cell-to-cell signaling, and immune surveillance[160,161]. Many pathogenic Gram-positive bacteria secrete their own hyaluronidases, which likely interfere with host HA homeostasis to cause disease[164]. Previous reports have shown that GBS hyaluronidase (HylB) cleaves host HA into dimers, which block TLR-2/4 signaling and diminish the inflammatory response to GBS[43]. In addition, studies in pregnant mice indicated that HylB-mediated immune suppression facilitates ascending GBS infection and fetal demise[46]. In Chapter 5, we utilize a highly relevant non-human primate (NHP) model of pregnancy to demonstrate that GBS HylB modulates immune responses at the maternal-fetal interface to induce bacterial invasion of the amniotic cavity, fetal bacteremia, and preterm labor. Our use of a non-hemolytic GBS strain that exhibits increased hyaluronidase activity[41] establishes HylB as a critical virulence factor during pregnancy, independently of granadaene activity. This is pertinent to clinical infection, as some GBS strains associated with invasive disease are non-hemolytic. Accordingly, our results point to HylB as a potential therapeutic target to prevent intrauterine infection of GBS and associated fetal bacteremia and preterm labor.

Collectively, this dissertation offers insight into two functionally distinct virulence factors that each subvert host processes to promote GBS survival and disease. Additional discussions of future research on each of these factors are presented below.

6.2 NEXT STEPS FOR RESEARCH ON THE HEMOLYTIC PIGMENT, GRANADAENE

Our findings in Chapter 2 suggest that granadaene can potentially function across a physiologically diverse group of organisms if they possess a Gram-positive-type cell wall structure.

Furthermore, our phyletic analyses revealed that the ancient *cyl* operon likely evolved in free-living bacteria, and a range of Gram-positive bacteria may produce granadaene or heretofore undescribed granadaene-like hemolytic/cytolytic toxins. A recent report linked *cyl* gene expression with granadaene production and hemolysis in several *Acidipropionibacterium* species used for industrial applications, including cheese production, probiotics, and food preservation[98]. Together with our data in Chapter 2, these findings raise concerns that *cyl*-encoded toxins could pose a potential consumer health risk. Further studies examining presence and nature of polyenic lipid toxins produced by bacteria encoding the *cyl* gene cluster, particularly those of industrial importance, are warranted.

The discovery of a granadaene-targeted, lipid analog-based vaccine in Chapter 3 presents an exciting opportunity for further research into the mechanisms of immunoprotection conferred by this and other amphiphilic antigens. We observed that vaccination with the R-P4 analog resulted in the production of IgG that bound to granadaene and inhibited hemolytic activity *ex vivo*, indicating that vaccination induced a protective antibody response. Whether the vaccine induced the production of other granadaene-binding antibody isotypes or prompted antibody-independent effector functions remains to be studied. In addition, discovering which moieties of R-P4 are immunogenic and identifying the binding epitope of granadaene-specific antibodies will be crucial to vaccine optimization. Notably, it is unknown whether humans naturally acquire granadaene-specific antibodies following colonization and clearance of GBS. Protective effects of naturally acquired antibodies specific to the GBS capsular polysaccharide are well described[47-49] and have informed the design of capsular-based GBS vaccines for human clinical trials[50-53]. Thus, the identification and characterization of granadaene-specific antibodies acquired during colonization and/or infection in humans may reveal key information for vaccine design. Finally, testing and optimizing the safety and efficacy of the analog vaccine in other relevant modes of GBS infection, including ascending infection, intrauterine infection, and neonatal infection, is essential.

Our results in Chapter 4 indicate that hemolytic MVs facilitate bacterial dissemination in neonatal mice. While this model is highly relevant to GBS infection in early life, questions remain regarding the role of hemolytic MVs in disrupting pregnancy. Our previous studies have shown that production of granadaene by GBS facilitates placental membrane disruption and neutrophil evasion at the maternal-fetal interface, which promotes microbial invasion of the amniotic cavity and fetal injury[24,72,75]. Furthermore, reports of sterile intraamniotic inflammation in humans[207] may indicate that pathogenic bacteria deliver pro-inflammatory toxins to the maternal-fetal interface prior to ascending infection. Further research assessing the effect of hemolytic MVs on placental membrane disruption, bacterial invasion of the amniotic cavity, fetal injury, and preterm birth will be key to understanding the role of hemolytic MVs in GBS-associated adverse pregnancy outcomes.

6.3 NEXT STEPS FOR GBS HYALURONIDASE RESEARCH

In Chapter 5, we propose that choriodecidual inoculation with the hyaluronidase-deficient GBS strain prompted rapid recruitment of neutrophils, controlled inflammation, and bacterial clearance, resulting in normal, term pregnancy in 4/5 animals. We postulate this because unlike the wild-type strain, GBS lacking hyaluronidase are unable to cleave HA into dimers that block immune surveillance mechanisms, namely TLR-2 and TLR-4[43]. Yet because our study design prevented us from examining the placental immune milieu in the short time following choriodecidual inoculation with this strain if preterm labor did not occur, we cannot definitively conclude that early pro-inflammatory events in these tissues resulted in bacterial clearance. Time-controlled studies in the NHP model, in which the placental tissues are examined soon after infection using methods described in Chapter 5, will further illuminate the immunological events at the maternal-fetal interface that result in bacterial clearance or alternatively permit microbial invasion of the amniotic cavity.

Another significant area of interest is the role of TLR-2 and TLR-4 in HylB-mediated immune evasion during *in vivo* infection. Although *in vitro* studies clearly demonstrate that HylB degrades HA

into disaccharides that block TLR-2/4 signaling (Chapter 5)[43], immune surveillance mechanisms in *in vivo* systems are complex and may exhibit functional redundancy. Experiments in pregnant mouse models lacking these host cell receptors will be critical to understanding the whether HylB modulates the immune system exclusively through these two receptors, or if other mechanisms of immune evasion are at play.

Aside from hindering host immune surveillance mechanisms, it is possible that other effects of HylB contributed to the profound differences in pregnancy outcomes we observed between NHP inoculated with wild-type and hyaluronidase-deficient GBS. For instance, degradation of HA within the placental membranes could disrupt vasculature and barrier integrity[208], potentially facilitating bacterial transmigration into the amniotic cavity. In addition, host regulation of hyaluronic acid levels in the cervix is essential to cervical ripening, a process that allows cervical distention necessary for successful vaginal delivery[185-187]. HA disruption in the cervix and preterm birth has been reported following HSV-2 infection[209], and cervical HA regulation during preterm labor is thought to be distinct from that occurring at term[210]. Although it is unknown whether HylB contributes to GBS-associated preterm birth by inducing cervical ripening, we observed increased prostaglandin levels in NHP infected with the hyaluronidase-proficient GBS strain, indicating that premature cervical ripening may have occurred in these animals[189]. Further study into the effects of HylB on tissue integrity in the placenta and cervix may provide further insight into the multifaceted etiologies of GBS intrauterine infection and associated preterm birth.

Finally, our findings in Chapter 5 show that GBS HylB is a potent virulence factor and a potential drug target. Several hyaluronidase inhibitors exist and have been proposed as therapeutics for HA-mediated conditions in humans, including cancer[194-196], wound healing[192,193], and even sexually transmitted infections[190,191]. Little attention has been paid to identifying a HylB-specific inhibitor, but this could be accomplished via high-throughput *in vitro* screening of candidate compounds, including known hyaluronidase inhibitors.

6.4 FINAL THOUGHTS ON REDUCING THE GLOBAL BURDEN OF GBS DISEASE

Group B Streptococcus remains a leading cause of preterm labor, stillbirth, fetal injury, and neonatal infection throughout the world across all income groups. Despite the successes of screening programs and intrapartum antibiotic prophylaxis in preventing GBS disease in the first week of life, these protocols fail to capture and stop late-onset disease and adverse events prior to 37 weeks gestation, including ascending infection, stillbirth, fetal injury, and preterm labor. Thus, improved prevention and treatment strategies are an urgent global health priority. The work in this dissertation attempts to make a step toward this goal. Although the journey ahead is long, continued collaboration among scientists, health care workers, community stakeholders, for-profit and non-profit organizations, and government agencies can lead to the eradication of GBS as a human pathogen.

BIBLIOGRAPHY

1 Madrid, L. *et al.* Infant Group B Streptococcal Disease Incidence and Serotypes Worldwide: Systematic Review and Meta-analyses. *Clin Infect Dis* **65**, S160-S172, doi:10.1093/cid/cix656 (2017).

2 Seale, A. C. *et al.* Stillbirth With Group B Streptococcus Disease Worldwide: Systematic Review and Meta-analyses. *Clin Infect Dis* **65**, S125-S132, doi:10.1093/cid/cix585 (2017).

3 Bianchi-Jassir, F. *et al.* Preterm Birth Associated With Group B Streptococcus Maternal Colonization Worldwide: Systematic Review and Meta-analyses. *Clin Infect Dis* **65**, S133-S142, doi:10.1093/cid/cix661 (2017).

4 Hall, J. *et al.* Maternal Disease With Group B Streptococcus and Serotype Distribution Worldwide: Systematic Review and Meta-analyses. *Clin Infect Dis* **65**, S112-S124, doi:10.1093/cid/cix660 (2017).

5 Skoff, T. H. *et al.* Increasing burden of invasive group B streptococcal disease in nonpregnant adults, 1990-2007. *Clin Infect Dis* **49**, 85-92, doi:10.1086/599369 (2009).

6 Ballard, M. S. *et al.* The changing epidemiology of group B streptococcus bloodstream infection: a multi-national population-based assessment. *Infect Dis (Lond)* **48**, 386-391, doi:10.3109/23744235.2015.1131330 (2016).

7 Sendi, P., Johansson, L. & Norrby-Teglund, A. Invasive group B Streptococcal disease in non-pregnant adults : a review with emphasis on skin and soft-tissue infections. *Infection* **36**, 100-111, doi:10.1007/s15010-007-7251-0 (2008).

8 Siemens, N. *et al.* Prothrombotic and Proinflammatory Activities of the beta-Hemolytic Group B Streptococcal Pigment. *J Innate Immun*, 1-13, doi:10.1159/000504002 (2019).

9 Puopolo, K. M. *et al.* Management of Infants at Risk for Group B Streptococcal Disease. *Pediatrics* **144**, doi:10.1542/peds.2019-1881 (2019).

10 Leroux-Roels, G. *et al.* Safety and immunogenicity of a second dose of an investigational maternal trivalent Group B streptococcus vaccine in non-pregnant women 4-6 years after a first dose: results from a phase 2 trial. *Clin Infect Dis*, doi:10.1093/cid/ciz737 (2019).

11 Edwards, M. S. & Baker, C. J. Group B Streptococcal Disease: Interim Prevention at 50 Years and Counting. *Clin Infect Dis*, doi:10.1093/cid/ciz738 (2019).

12 Russell, N. J. *et al.* Maternal Colonization With Group B Streptococcus and Serotype Distribution Worldwide: Systematic Review and Meta-analyses. *Clin Infect Dis* **65**, S100-S111, doi:10.1093/cid/cix658 (2017).

13 Seale, A. C. *et al.* Estimates of the Burden of Group B Streptococcal Disease Worldwide for Pregnant Women, Stillbirths, and Children. *Clin Infect Dis* **65**, S200-S219, doi:10.1093/cid/cix664 (2017).

14 Le Doare, K. *et al.* Intrapartum Antibiotic Chemoprophylaxis Policies for the Prevention of Group B Streptococcal Disease Worldwide: Systematic Review. *Clin Infect Dis* **65**, S143-S151, doi:10.1093/cid/cix654 (2017).

15 CDC. (1998).

16 CDC. Active Bacterial Core Surveillance Report, Emerging Infections Program Network, Group B Streptococcus, 2016. (2016).

17 Phares, C. R. *et al.* Epidemiology of invasive group B streptococcal disease in the United States, 1999-2005. *JAMA* **299**, 2056-2065, doi:10.1001/jama.299.17.2056 (2008).

18 Platt, M. W. In vivo hemolytic activity of group B streptococcus is dependent on erythrocyte-bacteria contact and independent of a carrier molecule. *Curr Microbiol* **31**, 5-9 (1995).

19 Whidbey, C. *et al.* A hemolytic pigment of Group B Streptococcus allows bacterial penetration of human placenta. *J Exp Med* **210**, 1265-1281, doi:10.1084/jem.20122753 (2013).

20 Spellerberg, B. *et al.* Identification of genetic determinants for the hemolytic activity of Streptococcus agalactiae by ISS1 transposition. *J Bacteriol* **181**, 3212-3219 (1999).

21 Pritzlaff, C. A. *et al.* Genetic basis for the beta-haemolytic/cytolytic activity of group B Streptococcus. *Mol Microbiol* **39**, 236-247 (2001).

22 Lamy, M. C. *et al.* CovS/CovR of group B streptococcus: a two-component global regulatory system involved in virulence. *Mol Microbiol* **54**, 1250-1268, doi:10.1111/j.1365-2958.2004.04365.x (2004).

23 Rosa-Fraile, M., Rodriguez-Granger, J., Haidour-Benamin, A., Cuerva, J. M. & Sampedro, A. Granadaene: proposed structure of the group B Streptococcus polyenic pigment. *Appl Environ Microbiol* **72**, 6367-6370, doi:10.1128/AEM.00756-06 (2006).

24 Whidbey, C. *et al.* A streptococcal lipid toxin induces membrane permeabilization and pyroptosis leading to fetal injury. *EMBO Mol Med* **7**, 488-505, doi:10.15252/emmm.201404883 (2015).

25 Liu, G. Y. *et al.* Sword and shield: linked group B streptococcal beta-hemolysin/cytolysin and carotenoid pigment function to subvert host phagocyte defense. *Proc Natl Acad Sci U S A* **101**, 14491-14496, doi:10.1073/pnas.0406143101 (2004).

26 Carey, A. J. *et al.* Infection and cellular defense dynamics in a novel 17beta-estradiol murine model of chronic human group B streptococcus genital tract colonization reveal a role for hemolysin in persistence and neutrophil accumulation. *J Immunol* **192**, 1718-1731, doi:10.4049/jimmunol.1202811 (2014).

27 Patras, K. A. *et al.* Group B Streptococcus CovR regulation modulates host immune signalling pathways to promote vaginal colonization. *Cell Microbiol* **15**, 1154-1167, doi:10.1111/cmi.12105 (2013).

28 Gendrin, C. *et al.* Mast cell degranulation by a hemolytic lipid toxin decreases GBS colonization and infection. *Sci Adv* **1**, e1400225, doi:10.1126/sciadv.1400225 (2015).

29 Randis, T. M. *et al.* Group B Streptococcus beta-hemolysin/cytolysin breaches maternal-fetal barriers to cause preterm birth and intrauterine fetal demise in vivo. *J Infect Dis* **210**, 265-273, doi:10.1093/infdis/jiu067 (2014).

30 Boldenow, E. *et al.* Group B Streptococcus circumvents neutrophils and neutrophil extracellular traps during amniotic cavity invasion and preterm labor. *Sci Immunol* **1**, doi:10.1126/sciimmunol.aah4576 (2016).

31 Nizet, V. *et al.* Group B streptococcal beta-hemolysin expression is associated with injury of lung epithelial cells. *Infect Immun* **64**, 3818-3826 (1996).

32 Gibson, R. L., Nizet, V. & Rubens, C. E. Group B streptococcal beta-hemolysin promotes injury of lung microvascular endothelial cells. *Pediatr Res* **45**, 626-634, doi:10.1203/00006450-199905010-00003 (1999).

33 Doran, K. S., Chang, J. C., Benoit, V. M., Eckmann, L. & Nizet, V. Group B streptococcal beta-hemolysin/cytolysin promotes invasion of human lung epithelial cells and the release of interleukin-8. *J Infect Dis* **185**, 196-203, doi:10.1086/338475 (2002).
34 Doran, K. S., Liu, G. Y. & Nizet, V. Group B streptococcal beta-hemolysin/cytolysin activates neutrophil signaling pathways in brain endothelium and contributes to development of meningitis. *J Clin Invest* **112**, 736-744, doi:10.1172/JCI17335 (2003).
35 Lembo, A. *et al.* Regulation of CovR expression in Group B Streptococcus impacts blood-brain barrier penetration. *Mol Microbiol* **77**, 431-443, doi:10.1111/j.1365-2958.2010.07215.x (2010).
36 Pritchard, D. G., Lin, B., Willingham, T. R. & Baker, J. R. Characterization of the group B streptococcal hyaluronate lyase. *Arch Biochem Biophys* **315**, 431-437 (1994).
37 Milligan, T. W., Baker, C. J., Straus, D. C. & Mattingly, S. J. Association of elevated levels of extracellular neuraminidase with clinical isolates of type III group B streptococci. *Infect Immun* **21**, 738-746 (1978).
38 Pritchard, D. G. & Lin, B. Group B streptococcal neuraminidase is actually a hyaluronidase. *Infect Immun* **61**, 3234-3239 (1993).
39 Jones, N. *et al.* Multilocus sequence typing system for group B streptococcus. *J Clin Microbiol* **41**, 2530-2536 (2003).
40 Musser, J. M., Mattingly, S. J., Quentin, R., Goudeau, A. & Selander, R. K. Identification of a high-virulence clone of type III Streptococcus agalactiae (group B Streptococcus) causing invasive neonatal disease. *Proc Natl Acad Sci U S A* **86**, 4731-4735 (1989).
41 Gendrin, C. *et al.* A Nonhemolytic Group B Streptococcus Strain Exhibits Hypervirulence. *The Journal of infectious diseases* **217**, 983-987, doi:10.1093/infdis/jix646 (2018).
42 Wang, Z. *et al.* Two novel functions of hyaluronidase from Streptococcus agalactiae are enhanced intracellular survival and inhibition of proinflammatory cytokine expression. *Infect Immun* **82**, 2615-2625, doi:10.1128/IAI.00022-14 (2014).
43 Kolar, S. L. *et al.* Group B Streptococcus Evades Host Immunity by Degrading Hyaluronan. *Cell Host Microbe* **18**, 694-704, doi:10.1016/j.chom.2015.11.001 (2015).
44 Jiang, D., Liang, J. & Noble, P. W. Hyaluronan as an immune regulator in human diseases. *Physiol Rev* **91**, 221-264, doi:10.1152/physrev.00052.2009 (2011).
45 Jiang, D., Liang, J. & Noble, P. W. Hyaluronan in tissue injury and repair. *Annu Rev Cell Dev Biol* **23**, 435-461, doi:10.1146/annurev.cellbio.23.090506.123337 (2007).
46 Vornhagen, J. *et al.* Bacterial Hyaluronidase Promotes Ascending GBS Infection and Preterm Birth. *MBio* **7**, doi:10.1128/mBio.00781-16 (2016).
47 Baker, C. J. & Kasper, D. L. Correlation of maternal antibody deficiency with susceptibility to neonatal group B streptococcal infection. *N Engl J Med* **294**, 753-756, doi:10.1056/NEJM197604012941404 (1976).
48 Kwatra, G. *et al.* Natural acquired humoral immunity against serotype-specific group B Streptococcus rectovaginal colonization acquisition in pregnant women. *Clin Microbiol Infect* **21**, 568 e513-521, doi:10.1016/j.cmi.2015.01.030 (2015).
49 Baker, C. J. *et al.* Maternal antibody at delivery protects neonates from early onset group B streptococcal disease. *J Infect Dis* **209**, 781-788, doi:10.1093/infdis/jit549 (2014).
50 Baker, C. J. *et al.* Safety and immunogenicity of a bivalent group B streptococcal conjugate vaccine for serotypes II and III. *J Infect Dis* **188**, 66-73, doi:10.1086/375536 (2003).
51 Baker, C. J., Rench, M. A. & McInnes, P. Immunization of pregnant women with group B streptococcal type III capsular polysaccharide-tetanus toxoid conjugate vaccine. *Vaccine* **21**, 3468-3472 (2003).
52 Baker, C. J. *et al.* Safety and immunogenicity of capsular polysaccharide-tetanus toxoid conjugate vaccines for group B streptococcal types Ia and Ib. *J Infect Dis* **179**, 142-150, doi:10.1086/314574 (1999).
53 Baker, C. J. *et al.* Immune response of healthy women to 2 different group B streptococcal type V capsular polysaccharide-protein conjugate vaccines. *J Infect Dis* **189**, 1103-1112, doi:10.1086/382193 (2004).
54 GlaxoSmithKline. (2017).
55 Novartis. (ClinicalTrials.gov, 2014).
56 Novartis. (ClinicalTrials.gov, 2014).
57 Bellais, S. *et al.* Capsular switching in group B Streptococcus CC17 hypervirulent clone: a future challenge for polysaccharide vaccine development. *J Infect Dis* **206**, 1745-1752, doi:10.1093/infdis/jis605 (2012).
58 Neemuchwala, A., Teatero, S., Athey, T. B., McGeer, A. & Fittipaldi, N. Capsular Switching and Other Large-Scale Recombination Events in Invasive Sequence Type 1 Group B Streptococcus. *Emerg Infect Dis* **22**, 1941-1944, doi:10.3201//eid2211.152064 (2016).
59 Manning, S. D. *et al.* Naturally occurring antibodies for the group B streptococcal surface immunogenic protein (Sip) in pregnant women and newborn babies. *Vaccine* **24**, 6905-6912, doi:10.1016/j.vaccine.2006.06.020 (2006).
60 Lin, S. M. *et al.* Vaccination With a Latch Peptide Provides Serotype-Independent Protection Against Group B Streptococcus Infection in Mice. *J Infect Dis* **217**, 93-102, doi:10.1093/infdis/jix565 (2017).
61 Santillan, D. A. *et al.* Efficacy of polymeric encapsulated C5a peptidase-based group B streptococcus vaccines in a murine model. *Am J Obstet Gynecol* **205**, 249 e241-248, doi:10.1016/j.ajog.2011.06.024 (2011).
62 Santillan, D. A., Andracki, M. E. & Hunter, S. K. Protective immunization in mice against group B streptococci using encapsulated C5a peptidase. *Am J Obstet Gynecol* **198**, 114 e111-116, doi:10.1016/j.ajog.2007.06.003 (2008).
63 Stalhammar-Carlemalm, M., Waldemarsson, J., Johnsson, E., Areschoug, T. & Lindahl, G. Nonimmunodominant regions are effective as building blocks in a streptococcal fusion protein vaccine. *Cell Host Microbe* **2**, 427-434, doi:10.1016/j.chom.2007.10.003 (2007).
64 Maione, D. *et al.* Identification of a universal Group B streptococcus vaccine by multiple genome screen. *Science* **309**, 148-150, doi:10.1126/science.1109869 (2005).
65 Clarke, D. *et al.* Group B Streptococcus Induces a Robust IFN-gamma Response by CD4(+) T Cells in an In Vitro and In Vivo Model. *J Immunol Res* **2016**, 5290604, doi:10.1155/2016/5290604 (2016).
66 Patras, K. A., Rosler, B., Thoman, M. L. & Doran, K. S. Characterization of host immunity during persistent vaginal colonization by Group B Streptococcus. *Mucosal Immunol* **8**, 1339-1348, doi:10.1038/mi.2015.23 (2015).
67 de Goffau, M. C. *et al.* Human placenta has no microbiome but can contain potential pathogens. *Nature* **572**, 329-334, doi:10.1038/s41586-019-1451-5 (2019).
68 Doster, R. S., Sutton, J. A., Rogers, L. M., Aronoff, D. M. & Gaddy, J. A. Streptococcus agalactiae Induces Placental Macrophages To Release Extracellular Traps Loaded with Tissue Remodeling Enzymes via an Oxidative Burst-Dependent Mechanism. *mBio* **9**, doi:10.1128/mBio.02084-18 (2018).
69 Sutton, J. A. *et al.* Protein kinase D mediates inflammatory responses of human placental macrophages to Group B Streptococcus. *Am J Reprod Immunol* **81**, e13075, doi:10.1111/aji.13075 (2019).
70 Rogers, L. M. *et al.* Decidual stromal cell-derived PGE2 regulates macrophage responses to microbial threat. *Am J Reprod Immunol* **80**, e13032, doi:10.1111/aji.13032 (2018).

71 Kothary, V. *et al.* Group B Streptococcus Induces Neutrophil Recruitment to Gestational Tissues and Elaboration of Extracellular Traps and Nutritional Immunity. *Front Cell Infect Microbiol* **7**, 19, doi:10.3389/fcimb.2017.00019 (2017).
72 Boldenow, E., Gendrin, C., Ngo, L., Bierle, C., Vornhagen, J., Coleman, M., Merillat, S., Armistead, B., Whidbey, C., Alishetti, V., Santana-Ufret,V., Ogle, J., Gough, M., Srinouanprachanh, S., MacDonald, J., Bammler, T., Bansal, A., Liggitt, H., Rajagopal, L., Adams Waldorf, K. . Group B Streptococcus circumvents neutrophils and neutrophil extracellular traps during amniotic cavity invasion and preterm labor. *Science Immunology* **1** (2016).
73 Adams Waldorf, K. M. *et al.* Choriodecidual group B streptococcal inoculation induces fetal lung injury without intra-amniotic infection and preterm labor in Macaca nemestrina. *PLoS One* **6**, e28972, doi:10.1371/journal.pone.0028972 (2011).
74 Lawn, J. E. *et al.* Group B Streptococcal Disease Worldwide for Pregnant Women, Stillbirths, and Children: Why, What, and How to Undertake Estimates? *Clin Infect Dis* **65**, S89-S99, doi:10.1093/cid/cix653 (2017).
75 Whidbey, C. *et al.* A hemolytic pigment of Group B Streptococcus allows bacterial penetration of human placenta. *J Exp Med* **210**, 1265-1281, doi:10.1084/jem.20122753 (2013).
76 Russell, N. J. *et al.* Risk of Early-Onset Neonatal Group B Streptococcal Disease With Maternal Colonization Worldwide: Systematic Review and Meta-analyses. *Clin Infect Dis* **65**, S152-S159, doi:10.1093/cid/cix655 (2017).
77 Brown, J. H. The Cultural Differentiation of Beta Hemolytic Streptococci of Human and Bovine Origin. *J Exp Med* **31**, 35-47 (1920).
78 Ayers, S. H. R., P. . Differentiation of Hemolytic Streptococci from Human and Bovine Sources by the Hydrolysis of Sodium Hippurate. *The Journal of Infectious Diseases* **30**, 388-399 (1922).
79 Spellerberg, B., Martin, S., Brandt, C. & Lutticken, R. The cyl genes of *Streptococcus agalactiae* are involved in the production of pigment. *FEMS Microbiol Lett* **188**, 125-128 (2000).
80 Hamon, M. A., Ribet, D., Stavru, F. & Cossart, P. Listeriolysin O: the Swiss army knife of Listeria. *Trends Microbiol* **20**, 360-368, doi:10.1016/j.tim.2012.04.006 (2012).
81 Seilie, E. S. & Bubeck Wardenburg, J. Staphylococcus aureus pore-forming toxins: The interface of pathogen and host complexity. *Semin Cell Dev Biol* **72**, 101-116, doi:10.1016/j.semcdb.2017.04.003 (2017).
82 Cavanagh, D., Fitzgerald, G. F. & McAuliffe, O. From field to fermentation: the origins of Lactococcus lactis and its domestication to the dairy environment. *Food Microbiol* **47**, 45-61, doi:10.1016/j.fm.2014.11.001 (2015).
83 Gendrin, C. *et al.* Mast cell degranulation by a hemolytic lipid toxin decreases GBS colonization and infection. *Sci Adv* **1**, e1400225, doi:10.1126/sciadv.1400225 (2015).
84 Chaffin, D. O. & Rubens, C. E. Blue/white screening of recombinant plasmids in Gram-positive bacteria by interruption of alkaline phosphatase gene (phoZ) expression. *Gene* **219**, 91-99 (1998).
85 Rajagopal, L., Vo, A., Silvestroni, A. & Rubens, C. E. Regulation of cytotoxin expression by converging eukaryotic-type and two-component signalling mechanisms in Streptococcus agalactiae. *Mol Microbiol* **62**, 941-957, doi:10.1111/j.1365-2958.2006.05431.x (2006).
86 Jiang, S. M., Cieslewicz, M. J., Kasper, D. L. & Wessels, M. R. Regulation of virulence by a two-component system in group B streptococcus. *J Bacteriol* **187**, 1105-1113, doi:10.1128/JB.187.3.1105-1113.2005 (2005).
87 Almeida, A. *et al.* Whole-Genome Comparison Uncovers Genomic Mutations between Group B Streptococci Sampled from Infected Newborns and Their Mothers. *J Bacteriol* **197**, 3354-3366, doi:10.1128/JB.00429-15 (2015).
88 Lupo, A., Ruppen, C., Hemphill, A., Spellerberg, B. & Sendi, P. Phenotypic and molecular characterization of hyperpigmented group B Streptococci. *Int J Med Microbiol* **304**, 717-724, doi:10.1016/j.ijmm.2014.05.003 (2014).
89 Whidbey, C. *et al.* A Hyperhemolytic/Hyperpigmented Group B Streptococcus Strain with a CovR Mutation Isolated from an Adolescent Patient with Sore Throat. *Clin Res Infect Dis* **2** (2015).
90 Sendi, P. *et al.* Bacterial phenotype variants in group B streptococcal toxic shock syndrome. *Emerg Infect Dis* **15**, 223-232 (2009).
91 Almeida, A. *et al.* Parallel Evolution of Group B Streptococcus Hypervirulent Clonal Complex 17 Unveils New Pathoadaptive Mutations. *mSystems* **2**, doi:10.1128/mSystems.00074-17 (2017).
92 Kikuchi, G., Motokawa, Y., Yoshida, T. & Hiraga, K. Glycine cleavage system: reaction mechanism, physiological significance, and hyperglycinemia. *Proc Jpn Acad Ser B Phys Biol Sci* **84**, 246-263, doi:10.2183/pjab.84.246 (2008).
93 Rajagopal, L., Sundari, C. S., Balasubramanian, D. & Sonti, R. V. The bacterial pigment xanthomonadin offers protection against photodamage. *FEBS Lett* **415**, 125-128, doi:10.1016/s0014-5793(97)01109-5 (1997).
94 Madden, K. S. *et al.* Using Nature's polyenes as templates: studies of synthetic xanthomonadin analogues and realising their potential as antioxidants. *Org Biomol Chem* **17**, 3752-3759, doi:10.1039/c9ob00275h (2019).
95 Slouf, V. *et al.* Photoprotection in a purple phototrophic bacterium mediated by oxygen-dependent alteration of carotenoid excited-state properties. *Proc Natl Acad Sci U S A* **109**, 8570-8575, doi:10.1073/pnas.1201413109 (2012).
96 Howardwilliams, C., Pridmore, R., Downes, M. T. & Vincent, W. F. Microbial Biomass, Photosynthesis and Chlorophyll-a Related Pigments in the Ponds of the Mcmurdo Ice Shelf, Antarctica. *Antarctic Science* **1**, 125-131, doi:Doi 10.1017/S0954102089000192 (1989).
97 Vanberg, C., Lutnaes, B. F., Langsrud, T., Nes, I. F. & Holo, H. Propionibacterium jensenii produces the polyene pigment granadaene and has hemolytic properties similar to those of Streptococcus agalactiae. *Applied and Environmental Microbiology* **73**, 5501-5506, doi:AEM.00545-07 [pii]
10.1128/AEM.00545-07 (2007).
98 Deptula, P. *et al.* Red-Brown Pigmentation of Acidipropionibacterium jensenii Is Tied to Haemolytic Activity and cyl-Like Gene Cluster. *Microorganisms* **7**, doi:10.3390/microorganisms7110512 (2019).
99 Lancefield, R. C., McCarty, M. & Everly, W. N. Multiple mouse-protective antibodies directed against group B streptococci. Special reference to antibodies effective against protein antigens. *J Exp Med* **142**, 165-179 (1975).
100 de la Rosa, M. *et al.* New Granada Medium for detection and identification of group B streptococci. *J Clin Microbiol* **30**, 1019-1021 (1992).
101 Altschul, S. F. *et al.* Gapped BLAST and PSI-BLAST: a new generation of protein database search programs. *Nucleic Acids Res* **25**, 3389-3402, doi:10.1093/nar/25.17.3389 (1997).
102 Lassmann, T., Frings, O. & Sonnhammer, E. L. Kalign2: high-performance multiple alignment of protein and nucleotide sequences allowing external features. *Nucleic Acids Res* **37**, 858-865, doi:10.1093/nar/gkn1006 (2009).
103 Price, M. N., Dehal, P. S. & Arkin, A. P. FastTree 2--approximately maximum-likelihood trees for large alignments. *PLoS One* **5**, e9490, doi:10.1371/journal.pone.0009490 (2010).
104 Csardi, G. & Nepusz, T. The igraph software package for complex network research. **Complex Systems**, 9 (2006).
105 Forquin, M. P. *et al.* The putative glycosyltransferase-encoding gene cylJ and the group B Streptococcus (GBS)-specific gene cylK modulate hemolysin production and virulence of GBS. *Infect Immun* **75**, 2063-2066, doi:10.1128/IAI.01565-06 (2007).
106 Gottschalk, B. *et al.* Transport of multidrug resistance substrates by the Streptococcus agalactiae hemolysin transporter. *J Bacteriol* **188**, 5984-5992, doi:10.1128/JB.00768-05 (2006).

107 George, K. M., Pascopella, L., Welty, D. M. & Small, P. L. A Mycobacterium ulcerans toxin, mycolactone, causes apoptosis in guinea pig ulcers and tissue culture cells. *Infect Immun* **68**, 877-883, doi:10.1128/iai.68.2.877-883.2000 (2000).
108 Nitenberg, M. *et al.* The potent effect of mycolactone on lipid membranes. *PLoS Pathog* **14**, e1006814, doi:10.1371/journal.ppat.1006814 (2018).
109 Zulianello, L. *et al.* Rhamnolipids are virulence factors that promote early infiltration of primary human airway epithelia by Pseudomonas aeruginosa. *Infect Immun* **74**, 3134-3147, doi:10.1128/IAI.01772-05 (2006).
110 McClure, C. D. & Schiller, N. L. Effects of Pseudomonas aeruginosa rhamnolipids on human monocyte-derived macrophages. *J Leukoc Biol* **51**, 97-102, doi:10.1002/jlb.51.2.97 (1992).
111 Lynch, A. *et al.* The Bacteroidales produce an N-acylated derivative of glycine with both cholesterol-solubilising and hemolytic activity. *Sci Rep* **7**, 13270, doi:10.1038/s41598-017-13774-6 (2017).
112 Schrag, S. J. *et al.* Group B streptococcal disease in the era of intrapartum antibiotic prophylaxis. *N Engl J Med* **342**, 15-20, doi:10.1056/NEJM200001063420103 (2000).
113 Khan, M. A., Faiz, A. & Ashshi, A. M. Maternal colonization of group B streptococcus: prevalence, associated factors and antimicrobial resistance. *Ann Saudi Med* **35**, 423-427, doi:10.5144/0256-4947.2015.423 (2015).
114 Castor, M. L. *et al.* Antibiotic resistance patterns in invasive group B streptococcal isolates. *Infect Dis Obstet Gynecol* **2008**, 727505, doi:10.1155/2008/727505 (2008).
115 Madden, K. S., Mosa, F. A. & Whiting, A. Non-isoprenoid polyene natural products--structures and synthetic strategies. *Org Biomol Chem* **12**, 7877-7899, doi:10.1039/c4ob01337a (2014).
116 Paradas, M. *et al.* Clarifying the structure of granadaene: total synthesis of related analogue [2]-granadaene and confirmation of its absolute stereochemistry. *Bioorg Med Chem* **20**, 6655-6661, doi:10.1016/j.bmc.2012.09.017 (2012).
117 Crowley, L. C., Marfell, B. J., Scott, A. P. & Waterhouse, N. J. Quantitation of Apoptosis and Necrosis by Annexin V Binding, Propidium Iodide Uptake, and Flow Cytometry. *Cold Spring Harb Protoc* **2016**, doi:10.1101/pdb.prot087288 (2016).
118 Pietkiewicz, S., Schmidt, J. H. & Lavrik, I. N. Quantification of apoptosis and necroptosis at the single cell level by a combination of Imaging Flow Cytometry with classical Annexin V/propidium iodide staining. *J Immunol Methods* **423**, 99-103, doi:10.1016/j.jim.2015.04.025 (2015).
119 Cibrian, D. & Sanchez-Madrid, F. CD69: from activation marker to metabolic gatekeeper. *Eur J Immunol* **47**, 946-953, doi:10.1002/eji.201646837 (2017).
120 Andersen, O. S. & Koeppe, R. E., 2nd. Bilayer thickness and membrane protein function: an energetic perspective. *Annu Rev Biophys Biomol Struct* **36**, 107-130, doi:10.1146/annurev.biophys.36.040306.132643 (2007).
121 Mitra, K., Ubarretxena-Belandia, I., Taguchi, T., Warren, G. & Engelman, D. M. Modulation of the bilayer thickness of exocytic pathway membranes by membrane proteins rather than cholesterol. *Proc Natl Acad Sci U S A* **101**, 4083-4088, doi:10.1073/pnas.0307332101 (2004).
122 Nagle, J. F. & Tristram-Nagle, S. Structure of lipid bilayers. *Biochim Biophys Acta* **1469**, 159-195, doi:10.1016/s0304-4157(00)00016-2 (2000).
123 Horobin, R. W. Where do dyes go inside living cells? Predicting uptake, intracellular localisation, and accumulation using QSAR models. *Color Technol* **130**, 155-173, doi:10.1111/cote.12093 (2014).
124 Gras, S., Van Rhijn, I., Shahine, A. & Le Nours, J. Molecular recognition of microbial lipid-based antigens by T cells. *Cell Mol Life Sci* **75**, 1623-1639, doi:10.1007/s00018-018-2749-4 (2018).
125 Wilkinson, H. W. Nontypable group B streptococci isolated from human sources. *J Clin Microbiol* **6**, 183-184 (1977).
126 Armistead, B. *et al.* The cyl Genes Reveal the Biosynthetic and Evolutionary Origins of the Group B Streptococcus Hemolytic Lipid, Granadaene. *Front Microbiol* **10**, 3123, doi:10.3389/fmicb.2019.03123 (2019).
127 Fortunati, T., D'Acunto, M., Caruso, T. & Spinella, A. Chemoenzymatic preparation of musky macrolactones. *Tetrahedron* **71**, 2357-2362, doi:10.1016/j.tet.2015.03.007 (2015).
128 Sivasubramanian, K., Kaanumalle, L. S., Uppili, S. & Ramamurthy, V. Value of zeolites in asymmetric induction during photocyclization of pyridones, cyclohexadienones and naphthalenones. *Org Biomol Chem* **5**, 1569-1576, doi:10.1039/b702572f (2007).
129 Wang, G., Huang, Z. & Negishi, E. Highly stereoselective and efficient synthesis of ω-heterofunctional di- and trienoic esters for Horner–Wadsworth–Emmons reaction via alkyne hydrozirconation and Pd-catalyzed alkenylation. *Tetrahedron Letters* **50**, 3220-3223, doi:10.1016/j.tetlet.2009.02.023 (2009).
130 Dumont, F. J., Staruch, M. J., Fischer, P., DaSilva, C. & Camacho, R. Inhibition of T cell activation by pharmacologic disruption of the MEK1/ERK MAP kinase or calcineurin signaling pathways results in differential modulation of cytokine production. *J Immunol* **160**, 2579-2589 (1998).
131 Bjorndahl, J. M., Sung, S. S., Hansen, J. A. & Fu, S. M. Human T cell activation: differential response to anti-CD28 as compared to anti-CD3 monoclonal antibodies. *Eur J Immunol* **19**, 881-887, doi:10.1002/eji.1830190515 (1989).
132 Van Belle, K. *et al.* Comparative In Vitro Immune Stimulation Analysis of Primary Human B Cells and B Cell Lines. *J Immunol Res* **2016**, 5281823, doi:10.1155/2016/5281823 (2016).
133 Edmond, K. M. *et al.* Group B streptococcal disease in infants aged younger than 3 months: systematic review and meta-analysis. *Lancet* **379**, 547-556, doi:10.1016/S0140-6736(11)61651-6 (2012).
134 Merritt, K. & Jacobs, N. J. Characterization and incidence of pigment production by human clinical group B streptococci. *J Clin Microbiol* **8**, 105-107 (1978).
135 Surve, M. V. *et al.* Membrane Vesicles of Group B Streptococcus Disrupt Feto-Maternal Barrier Leading to Preterm Birth. *PLoS Pathog* **12**, e1005816, doi:10.1371/journal.ppat.1005816 (2016).
136 Brameyer, S. *et al.* Outer Membrane Vesicles Facilitate Trafficking of the Hydrophobic Signaling Molecule CAI-1 between Vibrio harveyi Cells. *J Bacteriol* **200**, doi:10.1128/JB.00740-17 (2018).
137 Bomberger, J. M. *et al.* Long-distance delivery of bacterial virulence factors by Pseudomonas aeruginosa outer membrane vesicles. *PLoS Pathog* **5**, e1000382, doi:10.1371/journal.ppat.1000382 (2009).
138 Lekmeechai, S. *et al.* Helicobacter pylori Outer Membrane Vesicles Protect the Pathogen From Reactive Oxygen Species of the Respiratory Burst. *Front Microbiol* **9**, 1837, doi:10.3389/fmicb.2018.01837 (2018).
139 Forman, H. J. & Torres, M. Reactive oxygen species and cell signaling: respiratory burst in macrophage signaling. *Am J Respir Crit Care Med* **166**, S4-8, doi:10.1164/rccm.2206007 (2002).
140 Sigge, A., Schmid, M., Mauerer, S. & Spellerberg, B. Heterogeneity of hemolysin expression during neonatal Streptococcus agalactiae sepsis. *J Clin Microbiol* **46**, 807-809, doi:10.1128/JCM.01963-07 (2008).
141 Slattery, M. M. & Morrison, J. J. Preterm delivery. *Lancet* **360**, 1489-1497, doi:10.1016/S0140-6736(02)11476-0 (2002).
142 Katz, J. *et al.* Mortality risk in preterm and small-for-gestational-age infants in low-income and middle-income countries: a pooled country analysis. *Lancet* **382**, 417-425, doi:10.1016/S0140-6736(13)60993-9 (2013).

143 Matorras, R. *et al.* Group B streptococcus and premature rupture of membranes and preterm delivery. *Gynecol Obstet Invest* **27**, 14-18 (1989).
144 Rubens, C. E., Gravett, M. G., Victora, C. G., Nunes, T. M. & Group, G. R. Global report on preterm birth and stillbirth (7 of 7): mobilizing resources to accelerate innovative solutions (Global Action Agenda). *BMC Pregnancy Childbirth* **10 Suppl 1**, S7, doi:10.1186/1471-2393-10-S1-S7 (2010).
145 Brigtsen, A. K. *et al.* Maternal Colonization with Group B Streptococcus Is Associated with an Increased Rate of Infants Transferred to the Neonatal Intensive Care Unit. *Neonatology* **108**, 157-163, doi:10.1159/000434716 (2015).
146 Verani, J. R. *et al.* Early-onset group B streptococcal disease in the United States: potential for further reduction. *Obstet Gynecol* **123**, 828-837, doi:10.1097/AOG.0000000000000163 (2014).
147 Ledger, W. J. Perinatal infections and fetal/neonatal brain injury. *Curr Opin Obstet Gynecol* **20**, 120-124, doi:10.1097/GCO.0b013e3282f734db (2008).
148 Kohli-Lynch, M. *et al.* Neurodevelopmental Impairment in Children After Group B Streptococcal Disease Worldwide: Systematic Review and Meta-analyses. *Clin Infect Dis* **65**, S190-S199, doi:10.1093/cid/cix663 (2017).
149 Askarian, F. *et al.* Staphylococcus aureus Membrane-Derived Vesicles Promote Bacterial Virulence and Confer Protective Immunity in Murine Infection Models. *Front Microbiol* **9**, 262, doi:10.3389/fmicb.2018.00262 (2018).
150 Glauert, A. M. *Practical methods in electron microscopy*. (North-Holland Pub. Co. ;
Sole distributors for the U.S.A., American Elsevier Pub. Co., 1972).
151 Braet, F., De Zanger, R. & Wisse, E. Drying cells for SEM, AFM and TEM by hexamethyldisilazane: a study on hepatic endothelial cells. *J Microsc* **186**, 84-87 (1997).
152 in *Preterm Birth: Causes, Consequences, and Prevention The National Academies Collection: Reports funded by National Institutes of Health* (eds R. E. Behrman & A. S. Butler) (2007).
153 Goldenberg, R. L., Hauth, J. C. & Andrews, W. W. Intrauterine infection and preterm delivery. *New England Journal of Medicine* **342**, 1500-1507, doi:10.1056/NEJM200005183422007 (2000).
154 Hillier, S. L., Krohn, M. A., Kiviat, N. B., Watts, D. H. & Eschenbach, D. A. Microbiologic causes and neonatal outcomes associated with chorioamnion infection. *American journal of obstetrics and gynecology* **165**, 955-961 (1991).
155 Campbell, J. R. *et al.* Group B streptococcal colonization and serotype-specific immunity in pregnant women at delivery. *Obstetrics and gynecology* **96**, 498-503, doi:S0029-7844(00)00977-7 [pii] (2000).
156 Centers for Disease, C. & Prevention. Perinatal group B streptococcal disease after universal screening recommendations--United States, 2003-2005. *MMWR Morb Mortal Wkly Rep* **56**, 701-705 (2007).
157 Verani, J. R., McGee, L. & Schrag, S. J. Prevention of perinatal group B streptococcal disease--revised guidelines from CDC, 2010. *MMWR Recomm Rep* **59**, 1-36, doi:rr5910a1 [pii] (2010).
158 Rivera, L. *et al.* Incidence and serotype distribution of invasive group B streptococcal disease in young infants: a multi-country observational study. *BMC Pediatr* **15**, 143, doi:10.1186/s12887-015-0460-2 (2015).
159 Berardi, A. *et al.* Group B streptococcal infections in the newborn infant and the potential value of maternal vaccination. *Expert Rev Anti Infect Ther* **13**, 1387-1399, doi:10.1586/14787210.2015.1079126 (2015).
160 Stern, R. & Jedrzejas, M. J. Hyaluronidases: their genomics, structures, and mechanisms of action. *Chem Rev* **106**, 818-839, doi:10.1021/cr050247k (2006).
161 Fallacara, A., Baldini, E., Manfredini, S. & Vertuani, S. Hyaluronic Acid in the Third Millennium. *Polymers (Basel)* **10**, doi:10.3390/polym10070701 (2018).
162 Litwiniuk, M., Krejner, A., Speyrer, M. S., Gauto, A. R. & Grzela, T. Hyaluronic Acid in Inflammation and Tissue Regeneration. *Wounds* **28**, 78-88 (2016).
163 Jiang, D. *et al.* Regulation of lung injury and repair by Toll-like receptors and hyaluronan. *Nat Med* **11**, 1173-1179, doi:10.1038/nm1315 (2005).
164 Hynes, W. L. & Walton, S. L. Hyaluronidases of Gram-positive bacteria. *FEMS Microbiol Lett* **183**, 201-207, doi:10.1111/j.1574-6968.2000.tb08958.x (2000).
165 Gochnauer, T. A. & Wilson, J. B. Hyaluronidase production in vitro by streptococci isolated from bovine mastitis cases. *American journal of veterinary research* **12**, 20-22 (1951).
166 Mitchell, B. F. & Taggart, M. J. Are animal models relevant to key aspects of human parturition? *Am J Physiol Regul Integr Comp Physiol* **297**, R525-545, doi:00153.2009 [pii]
10.1152/ajpregu.00153.2009 (2009).
167 Carter, A. M. Animal models of human placentation--a review. *Placenta* **28 Suppl A**, S41-47, doi:S0143-4004(06)00272-4 [pii]
10.1016/j.placenta.2006.11.002 (2007).
168 Adams Waldorf, K. M., Rubens, C. E. & Gravett, M. G. Use of nonhuman primate models to investigate mechanisms of infection-associated preterm birth. *BJOG : an international journal of obstetrics and gynaecology* **118**, 136-144, doi:10.1111/j.1471-0528.2010.02728.x (2011).
169 Gravett, M. G. *et al.* An experimental model for intraamniotic infection and preterm labor in rhesus monkeys. *American journal of obstetrics and gynecology* **171**, 1660-1667, doi:0002-9378(94)90418-9 [pii] (1994).
170 Sobecki, M. *et al.* The cell proliferation antigen Ki-67 organises heterochromatin. *Elife* **5**, e13722, doi:10.7554/eLife.13722 (2016).
171 Howitt, J. *et al.* Ndfip1 represses cell proliferation by controlling Pten localization and signaling specificity. *J Mol Cell Biol* **7**, 119-131, doi:10.1093/jmcb/mjv020 (2015).
172 Unek, G., Ozmen, A., Isenlik, B. S. & Korgun, E. T. The proliferation mechanism of normal and pathological human placentas. *Histol Histopathol* **32**, 339-349, doi:10.14670/HH-11-832 (2017).
173 Lin, J. *et al.* Neonatal neutrophils stimulated by group B Streptococcus induce a proinflammatory T-helper cell bias. *Pediatr Res* **83**, 739-746, doi:10.1038/pr.2017.272 (2018).
174 Hampton, M. B., Kettle, A. J. & Winterbourn, C. C. Inside the neutrophil phagosome: oxidants, myeloperoxidase, and bacterial killing. *Blood* **92**, 3007-3017 (1998).
175 Scheibner, K. A. *et al.* Hyaluronan fragments act as an endogenous danger signal by engaging TLR2. *J Immunol* **177**, 1272-1281, doi:10.4049/jimmunol.177.2.1272 (2006).
176 Taylor, K. R. *et al.* Hyaluronan fragments stimulate endothelial recognition of injury through TLR4. *J Biol Chem* **279**, 17079-17084, doi:10.1074/jbc.M310859200 (2004).
177 Termeer, C. *et al.* Oligosaccharides of Hyaluronan activate dendritic cells via toll-like receptor 4. *J Exp Med* **195**, 99-111, doi:10.1084/jem.20001858 (2002).
178 Romero, R., Dey, S. K. & Fisher, S. J. Preterm labor: one syndrome, many causes. *Science* **345**, 760-765, doi:10.1126/science.1251816 (2014).

179 von Hunolstein, C. *et al.* Soluble antigens from group B streptococci induce cytokine production in human blood cultures. *Infect Immun* **65**, 4017-4021 (1997).
180 Diaz-Dinamarca, D. A. *et al.* Surface Immunogenic Protein of Streptococcus Group B is an Agonist of Toll-Like Receptors 2 and 4 and a Potential Immune Adjuvant. *Vaccines (Basel)* **8**, doi:10.3390/vaccines8010029 (2020).
181 Banerjee, A. *et al.* Bacterial Pili exploit integrin machinery to promote immune activation and efficient blood-brain barrier penetration. *Nat Commun* **2**, 462, doi:10.1038/ncomms1474 (2011).
182 Gomez, R. *et al.* The fetal inflammatory response syndrome. *Am J Obstet Gynecol* **179**, 194-202, doi:10.1016/s0002-9378(98)70272-8 (1998).
183 Takahashi, H. *et al.* Extravillous trophoblast cell invasion is promoted by the CD44-hyaluronic acid interaction. *Placenta* **35**, 163-170, doi:10.1016/j.placenta.2013.12.009 (2014).
184 Lee, T. Y., Jamieson, A. M. & Schafer, I. A. Changes in the composition and structure of glycosaminoglycans in the human placenta during development. *Pediatr Res* **7**, 965-977, doi:10.1203/00006450-197312000-00005 (1973).
185 El Maradny, E. *et al.* The role of hyaluronic acid as a mediator and regulator of cervical ripening. *Hum Reprod* **12**, 1080-1088, doi:10.1093/humrep/12.5.1080 (1997).
186 Kavanagh, J., Kelly, A. J. & Thomas, J. Hyaluronidase for cervical ripening and induction of labour. *Cochrane Database Syst Rev*, CD003097, doi:10.1002/14651858.CD003097.pub2 (2006).
187 Mahendroo, M. Cervical hyaluronan biology in pregnancy, parturition and preterm birth. *Matrix Biol* **78-79**, 24-31, doi:10.1016/j.matbio.2018.03.002 (2019).
188 Spallicci, M. D. *et al.* Use of hyaluronidase for cervical ripening: a randomized trial. *Eur J Obstet Gynecol Reprod Biol* **130**, 46-50, doi:10.1016/j.ejogrb.2005.10.028 (2007).
189 Ekerhovd, E., Weijdegard, B., Brannstrom, M., Mattsby-Baltzer, I. & Norstrom, A. Nitric oxide induced cervical ripening in the human: Involvement of cyclic guanosine monophosphate, prostaglandin F(2 alpha), and prostaglandin E(2). *Am J Obstet Gynecol* **186**, 745-750, doi:10.1067/mob.2002.121327 (2002).
190 Anderson, R. A. *et al.* Evaluation of poly(styrene-4-sulfonate) as a preventive agent for conception and sexually transmitted diseases. *J Androl* **21**, 862-875 (2000).
191 Zaneveld, L. J. *et al.* Efficacy and safety of a new vaginal contraceptive antimicrobial formulation containing high molecular weight poly(sodium 4-styrenesulfonate). *Biol Reprod* **66**, 886-894, doi:10.1095/biolreprod66.4.886 (2002).
192 Kemparaju, K. & Girish, K. S. Snake venom hyaluronidase: a therapeutic target. *Cell Biochem Funct* **24**, 7-12, doi:10.1002/cbf.1261 (2006).
193 Oliveira-Mendes, B. B. R. *et al.* Inhibition of Tityus serrulatus venom hyaluronidase affects venom biodistribution. *PLoS Negl Trop Dis* **13**, e0007048, doi:10.1371/journal.pntd.0007048 (2019).
194 Botzki, A. *et al.* L-Ascorbic acid 6-hexadecanoate, a potent hyaluronidase inhibitor. X-ray structure and molecular modeling of enzyme-inhibitor complexes. *J Biol Chem* **279**, 45990-45997, doi:10.1074/jbc.M406146200 (2004).
195 Girish, K. S. & Kemparaju, K. The magic glue hyaluronan and its eraser hyaluronidase: a biological overview. *Life Sci* **80**, 1921-1943, doi:10.1016/j.lfs.2007.02.037 (2007).
196 Girish, K. S., Kemparaju, K., Nagaraju, S. & Vishwanath, B. S. Hyaluronidase inhibitors: a biological and therapeutic perspective. *Curr Med Chem* **16**, 2261-2288, doi:10.2174/092986709788453078 (2009).
197 Davies, H. D. *et al.* Antibodies to capsular polysaccharides of group B Streptococcus in pregnant Canadian women: relationship to colonization status and infection in the neonate. *The Journal of infectious diseases* **184**, 285-291, doi:10.1086/322029 (2001).
198 Singh, P., Aronoff, D. M., Davies, H. D. & Manning, S. D. Draft Genome Sequence of an Invasive Streptococcus agalactiae Isolate Lacking Pigmentation. *Genome Announc* **4**, doi:10.1128/genomeA.00015-16 (2016).
199 Rajagopal, L., Clancy, A. & Rubens, C. E. A eukaryotic type serine/threonine kinase and phosphatase in *Streptococcus agalactiae* reversibly phosphorylate an inorganic pyrophosphatase and affect growth, cell segregation, and virulence. *The Journal of biological chemistry* **278**, 14429-14441 (2003).
200 Okada, N., Geist, R. T. & Caparon, M. G. Positive transcriptional control of mry regulates virulence in the group A streptococcus. *Mol Microbiol* **7**, 893-903 (1993).
201 Chaffin, D. O., Beres, S. B., Yim, H. H. & Rubens, C. E. The serotype of type Ia and III group B streptococci is determined by the polymerase gene within the polycistronic capsule operon. *J Bacteriol* **182**, 4466-4477 (2000).
202 Vanderhoeven, J. P. *et al.* Group B streptococcal infection of the choriodecidua induces dysfunction of the cytokeratin network in amniotic epithelium: a pathway to membrane weakening. *PLoS Pathog* **10**, e1003920, doi:10.1371/journal.ppat.1003920 PPATHOGENS-D-13-01329 [pii] (2014).
203 Adams Waldorf, K. M. *et al.* Uterine overdistention induces preterm labor mediated by inflammation: observations in pregnant women and nonhuman primates. *American journal of obstetrics and gynecology* **213**, 830 e831-830 e819, doi:10.1016/j.ajog.2015.08.028 (2015).
204 Boldenow, E. *et al.* Group B Streptococcus Circumvents Neutrophils and Neutrophil Extracellular Traps during Amniotic Cavity Invasion and Preterm Labor. *Sci Immunol* **1** (2016).
205 Maisey, H. C. *et al.* A group B streptococcal pilus protein promotes phagocyte resistance and systemic virulence. *FASEB J* **22**, 1715-1724, doi:10.1096/fj.07-093963 (2008).
206 Rueda, C. M. *et al.* Lipopolysaccharide-Induced Chorioamnionitis Promotes IL-1-Dependent Inflammatory FOXP3+ CD4+ T Cells in the Fetal Rhesus Macaque. *J Immunol* **196**, 3706-3715, doi:10.4049/jimmunol.1502613 (2016).
207 Gervasi, M. T. *et al.* Midtrimester amniotic fluid concentrations of interleukin-6 and interferon-gamma-inducible protein-10: evidence for heterogeneity of intra-amniotic inflammation and associations with spontaneous early (<32 weeks) and late (>32 weeks) preterm delivery. *J Perinat Med* **40**, 329-343, doi:10.1515/jpm-2012-0034 (2012).
208 Ziganshina, M. M., Pavlovich, S. V., Bovin, N. V. & Sukhikh, G. T. Hyaluronic Acid in Vascular and Immune Homeostasis during Normal Pregnancy and Preeclampsia. *Acta Naturae* **8**, 59-71 (2016).
209 McGee, D. *et al.* Cervical HSV-2 infection causes cervical remodeling and increases risk for ascending infection and preterm birth. *PLoS One* **12**, e0188645, doi:10.1371/journal.pone.0188645 (2017).
210 Mahendroo, M. Cervical remodeling in term and preterm birth: insights from an animal model. *Reproduction* **143**, 429-438, doi:10.1530/REP-11-0466 (2012).
211 Duplantier, A. J. & Masamune, S. Pimaricin - Stereochemistry and Synthesis of Its Aglycon (Pimarolide) Methyl-Ester. *Journal of the American Chemical Society* **112**, 7079-7081, doi:DOI 10.1021/ja00175a063 (1990).
212 Nishizawa, M. *et al.* Synthesis and glycosylation shift of 1,1'-disaccharides. *Chem Pharm Bull (Tokyo)* **42**, 982-984, doi:10.1248/cpb.42.982 (1994).
213 de Bruyn, A., Anteunis, M., de Gussem, R. & Dutton, G. G. S. 1H-N.m.r. study of l-rhamnose, methyl α- l-rhamnopyranoside, and 4- O-β-d-galactopyranosyl- l-rhamnose in deuterium oxide. *Carbohydrate Research* **47**, 158-163 (1976).

214 Bebault, G. M., G.G.S., D. & Warfield, C. K. Synthesis of 4-O-α-l-rhamnopyranosyl-l-rhamnopyranose. *Carbohydrate Research* **34**, 174-179 (1974).

APPENDIX A

SUPPLEMENTARY FIGURES AND TABLES: CHAPTER 2

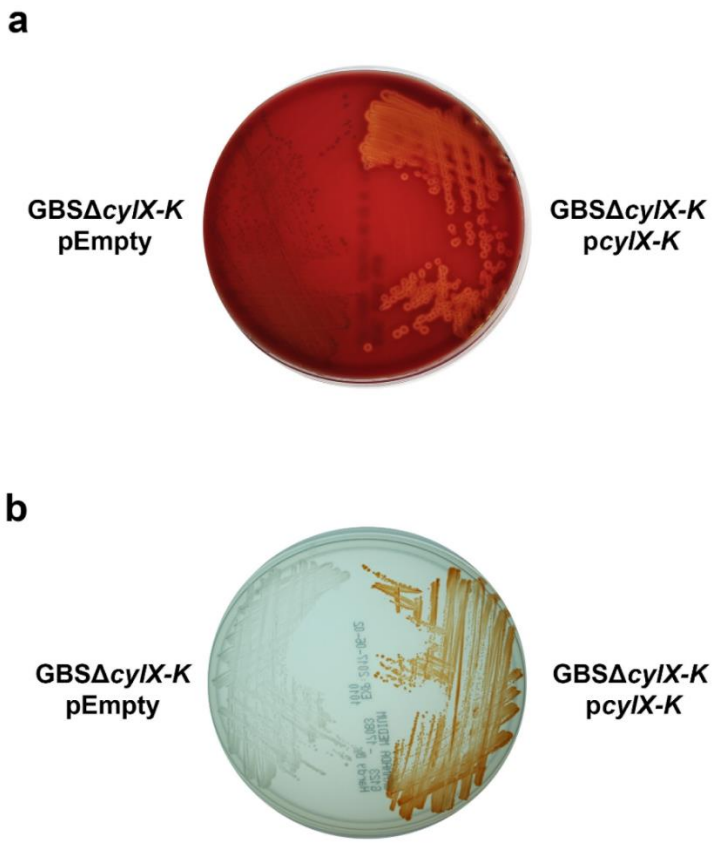

Supplementary Figure 2.1.

Complementation of the non-pigmented/non-hemolytic GBS strain lacking the *cyl* operon (GBSΔ*cylX-K*(8)) with the p*cylX-K* plasmid, but not the empty plasmid vector (pEmpty), restored hemolysis and pigmentation, as observed on red blood agar (a) and Granada agar (b).

E. coli MC1061 p*cylX-K*

Supplementary Figure 2.2.

Introduction of p*cylX-K* into E. coli MC1061 did not confer hemolysis.

Supplementary Figure 2.3.

The complete phylogenetic tree of the CylE protein. Clades with strong bootstrap support were collapsed into the filled triangles seen in Fig. 3.

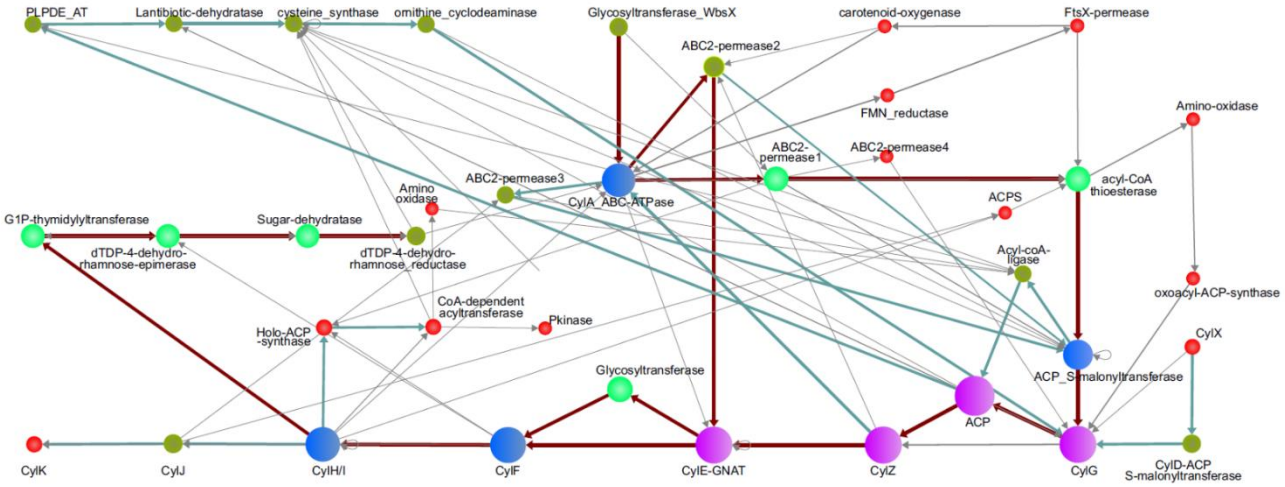

Supplementary Figure 2.4.

The operon network of *cyl* genes. Genes linked in operons are connected by arrows with the arrow-head pointing to the adjacent 3' gene. Node size and edge thickness are scaled based on the number of occurrences.

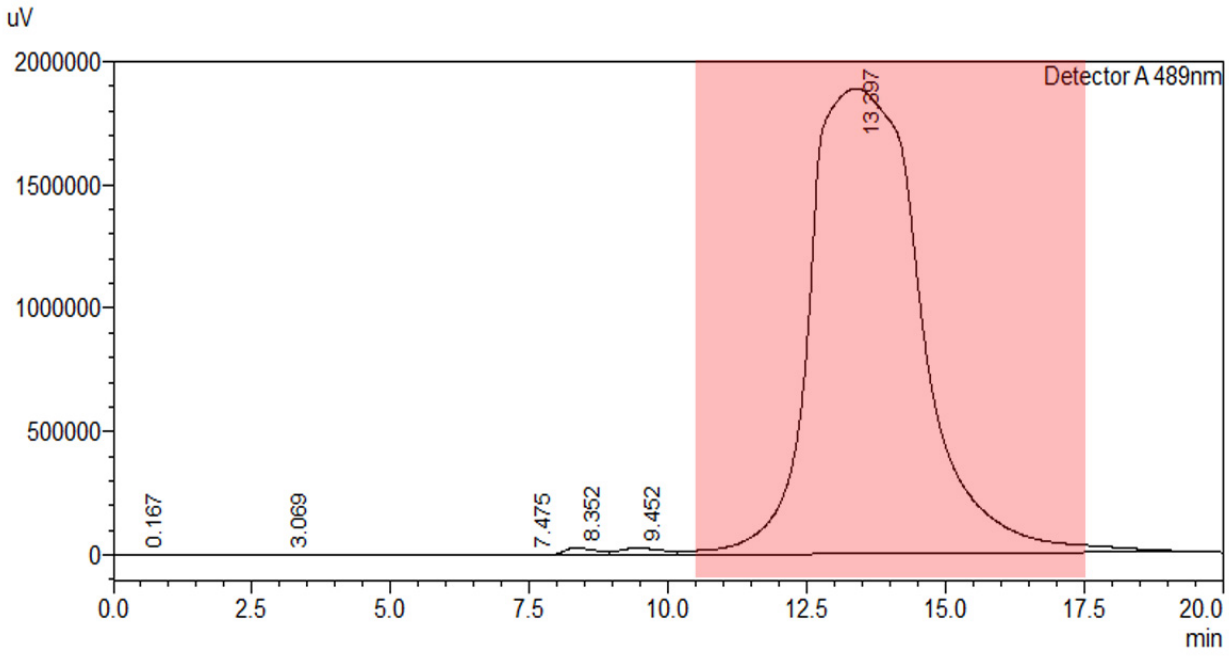

Supplementary Figure 2.5.

Representative chromatogram during HPLC purification of GBS pigment, granadaene. Fractions were collected from 10.5 minutes and 17.5 minutes of each HPLC run (represented by the shaded area) for samples from pigmented or nonpigmented GBS and *L. lactis*.

Supplementary Table 2.1.

Rare codons are abundant in the GBS *cyl* operon. The sequence of each gene in the *cyl* operon was analyzed using the rare codon sequence analysis tool at http://people.mbi.ucla.edu/sumchan/caltor.html. The frequency of each rare codon is listed.

Gene	Rare codons	Frequency
cylX	Arginine (CGG, AGG)	4
	Glycine (GGA, GGG)	5
	Isoleucine (AUA)	2
	Leucine (CUA)	2
	Threonine (ACG)	2
cylD	Arginine (AGG, AGA)	4
	Glycine (GGA, GGG)	5
	Isoleucine (AUA)	6
	Leucine (CUA)	3
cylG	Arginine (AGG, AGA)	6
	Glycine (GGA, GGG)	11
	Isoleucine (AUA)	5
	Leucine (CUA)	4
	Threonine (ACG)	2
acpC	Arginine (AGA)	1
	Glycine (GGA, GGG)	2
	Isoleucine (AUA)	5
	Leucine (CUA)	4
	Threonine (ACG)	1
cylZ	Arginine (AGA)	1
	Glycine (GGA)	1
	Isoleucine (AUA)	3
	Leucine (CUA)	2
	Proline (CCC)	1
cylA	Arginine (CGA, AGG, AGA)	8
	Glycine (GGA)	9
	Isoleucine (AUA)	4
	Leucine (CUA)	6
	Threonine (ACG)	4
cylB	Arginine (CGA, CGG, AGG, AGA)	4
	Glycine (GGA, GGG)	7
	Isoleucine (AUA)	3
	Leucine (CUA)	2
	Threonine (ACG)	4
cylE	Arginine (CGA, CGG, AGG, AGA)	25

	Glycine (GGA, GGG)	7
	Isoleucine (AUA)	11
	Leucine (CUA)	5
	Proline (CCC)	3
	Threonine (ACG)	3
cylF	Arginine (AGG, AGA)	7
	Glycine (GGA, GGG)	9
	Isoleucine (AUA)	3
	Leucine (CUA)	3
	Proline (CCC)	1
	Threonine (ACG)	1

Supplementary Table 2.2.

The primers listed above were used to amplify the GBS *cyl* operon for ligation into the multiple cloning site of the pDC123 (pEmpty) plasmid vector using Gibson Assembly. All primers were obtained from Sigma Aldrich.

Name	Sequence	T_m (°C)
cyl1_fwd	5' – CGCTAGGAGGAAACAAGGAAGAAGGTGATAATATGGGACG	79.1
cyl1_rev	5' – AAATAGTTAAATAATCCATAGCTGAATACTCTAGC	63.7
cyl2_fwd	5' – CTATGGATTATTTAACTATTTTAGGGATCGTTTC	65.6
cyl2_rev	5' – TTCCAGAAGAATAGGGCTGACATGCCAT	73.8
cyl3_fwd	5' – TCAGCCCTATTCTTCTGGAAAAGGAATCAATTTG	74.5
cyl3_rev	5' – CTTCATTTTGTTATTTACCAGTAGGAACAACATGTTGCG	74.7
pDC_fwd	5' – TGGTAAATAACAAAATGAAGAAAAAG	60.2
pDC_rev	5' – TTCCTTGTTTCCTCCTAGC	58.5

.

APPENDIX B

SUPPLEMENTARY FIGURES AND TABLES: CHAPTER 3

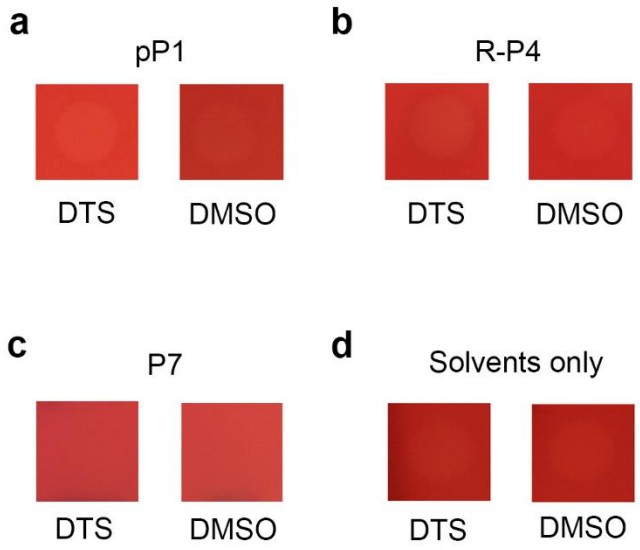

Supplementary Figure 3.1. Synthetic compounds pP1, R-P4, P7, and the solvents DMSO and DTS are not hemolytic.

(**a-c**) Each compound was resuspended in either DTS or DMSO at 0.02 M, and 5 µL was spotted onto red blood agar and incubated at 37 °C overnight. (**d**) 5 µL of the solvent (DTS or DMSO) was spotted onto red blood agar and incubated at 37 °C overnight.

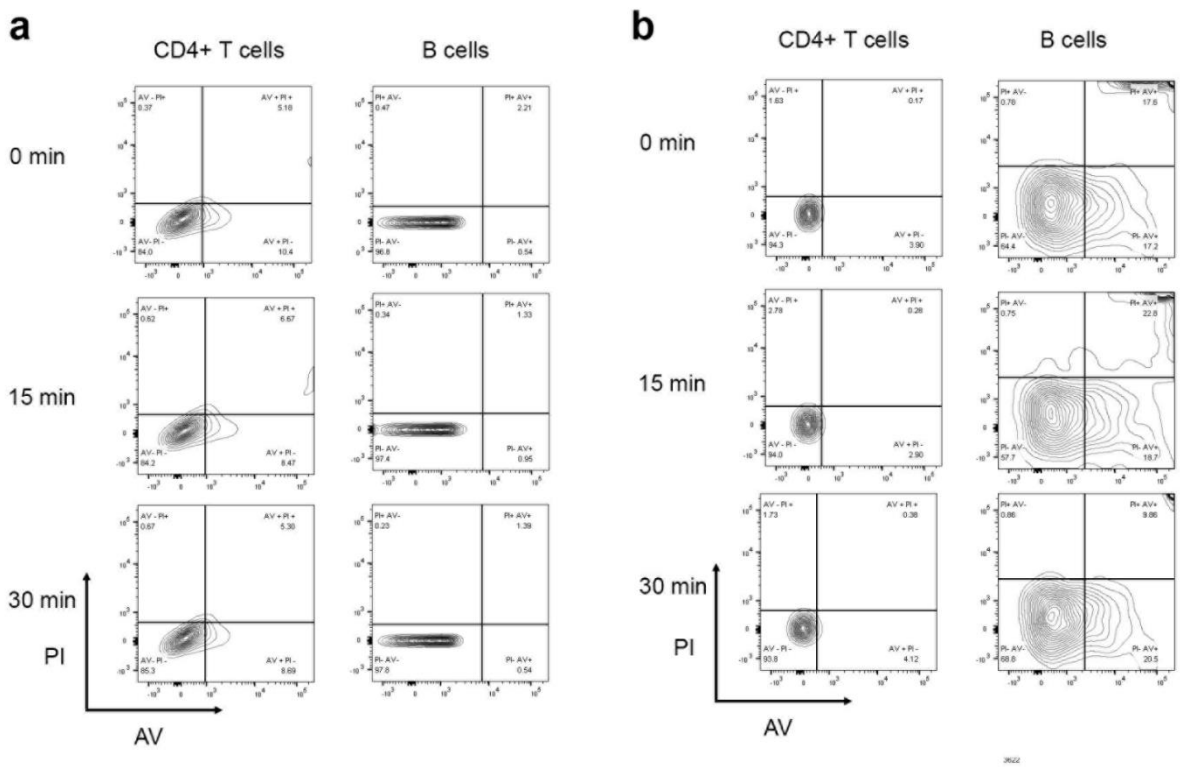

Supplementary Figure 3.2. Non-hemolytic GBS and its extract do not induce cell lysis.

PI uptake and Annexin V staining were measured using flow cytometry in CD4+ T cells and B cells following incubation with (**a**) non-hemolytic GBS at an MOI of 10 or with (**b**) GBSΔ*cylE* extract at the indicated time points.

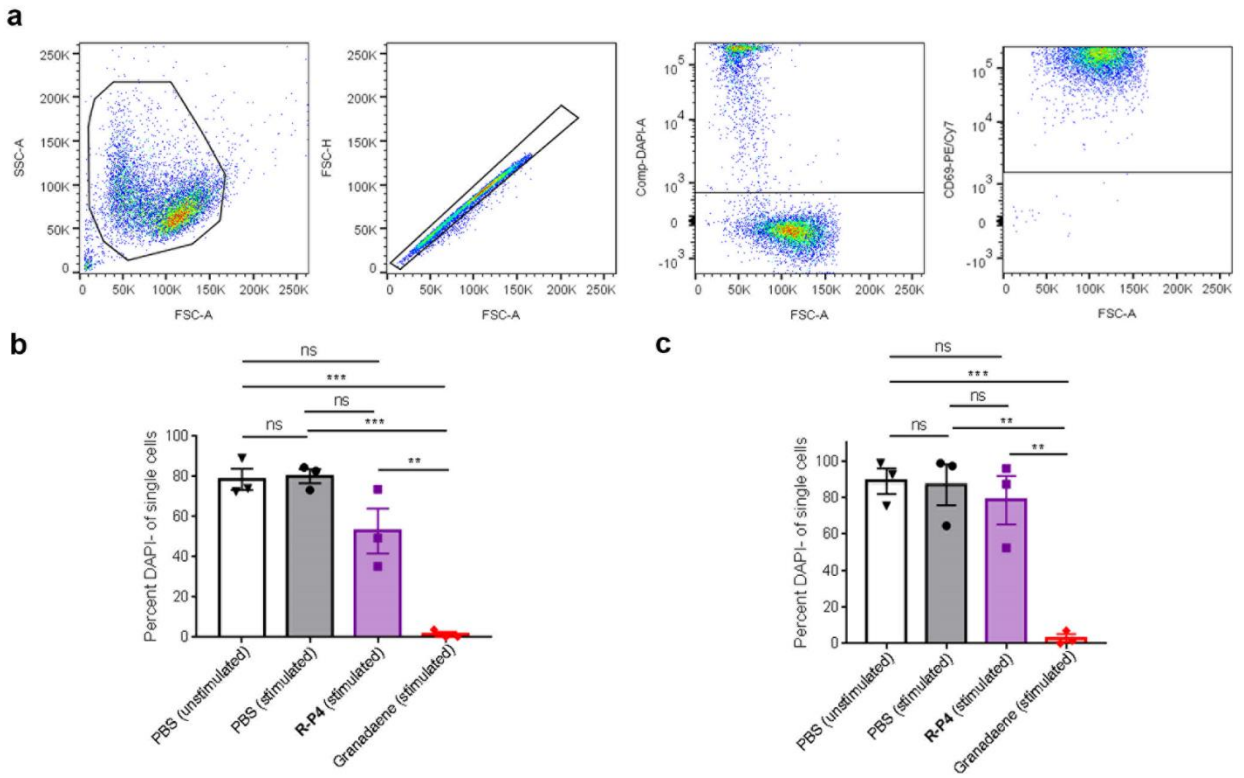

Supplementary Figure 3.3. Gating strategy for CD4+ T cell and B cell activation experiments. (**a**) The sequential gating strategy for CD4+ T cell and B cell activation experiments is shown (left to right) with example data from the PBS (stimulated) group in a CD4+ T cell experiment. Light scatter was used to include events based on size, then singlets. Then, live (DAPI-) events were analyzed for CD69. DAPI and CD69 gates were defined using fluorescence minus one or unstained controls. (**b**) Differences in the percent of DAPI- cells among each treatment group in CD4+ T cell experiments were determined using one-way ANOVA with Tukey's post-test. PBS (unstimulated) vs. PBS (stimulated): p = 0.9978, PBS (unstimulated) vs. R-P4 (stimulated): p = 0.0861, PBS (unstimulated) vs. granadaene: p = 0.0001, PBS (stimulated) vs. R-P4 (stimulated): p = 0.0669, PBS (stimulated) vs. granadaene (stimulated): p = 0.0001, R-P4 (stimulated) vs. granadaene: p = 0.0022. (**c**) Differences in the percent of DAPI- cells among each treatment group in B cell

experiments were determined using one-way ANOVA with Tukey's post-test. PBS (unstimulated) vs. PBS (stimulated): $p = 0.9986$, PBS (unstimulated) vs. R-P4 (stimulated): $p = 0.8612$, PBS (unstimulated) vs. granadaene: $p = 0.0009$, PBS (stimulated) vs. R-P4 (stimulated): $p = 0.9210$, PBS (stimulated) vs. granadaene (stimulated): $p = 0.0011$, R-P4 (stimulated) vs. granadaene: $p = 0.0021$.

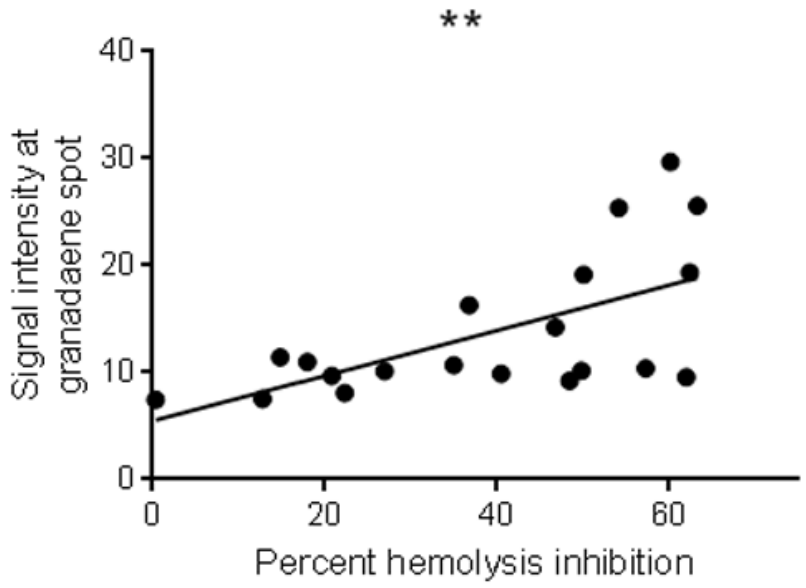

Supplementary Fig. 3.4. The amount of granadaene-bound IgG in mouse plasma is correlated with inhibition of granadaene activity *ex vivo*.

Immunoblots and inhibition of granadaene hemolysis using plasma samples from analog-vaccinated and adjuvant-only mice are shown in Fig. 3.5 b and c. A correlation analysis on these data was performed using the Pearson's correlation test ($p = 0.0040$).

*Synthesis of L-alanine derivative **3***

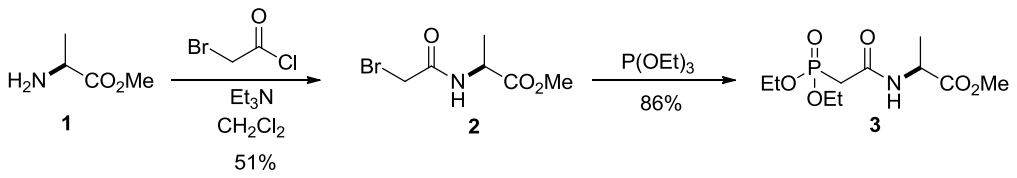

Scheme 1. Preparation of *L*-alanine derivative **3**.

Synthesis of α-bromoamide **2**: To a solution of *L*-alanine (**1**) (1.2 g, 8.6 mmol) in CH_2Cl_2 (50 mL), Et_3N (2.61 g, 25.8 mmol), and bromoacetyl chloride (2.03 g, 12.9 mmol) were added at 0 ºC. The mixture was stirred at room temperature for 2 h. Then, EtOAc was added and the mixture was washed with 10% aqueous HCl solution, sat. aq. $NaHCO_3$, and brine. The organic layer was dried over anhyd. Na_2SO_4, and the solvent removed. The residue was purified by flash chromatography (EtOAc/Hexane 3:7) to yield bromoamide **2** (0.99 g, 51%). Its ^{1}H and ^{13}C NMR spectra matched with those previously described[128].

Preparation of phosphonate **3**: To a sample of bromoamide **2** (0.99 g, 4.4 mmol), $P(OEt)_3$ (0.81 g, 4.9 mmol) was added, and the mixture was stirred at 100 ºC for 12 h. Phosphonate **3** was obtained without further purification (1.05 g, 86%). Brown oil. **^{1}H NMR (400 MHz, $CDCl_3$)** δ 7.22 (d, J = 7.3 Hz, 1H), 4.56 (quint, J = 7.2 Hz, 1H), 4.21–4.10 (m, 4H), 3.73 (s, 3H), 2.87 (d, $^2J_{H\text{-}P}$ = 20.7 Hz, 2H), 1.41 (d, J = 7.2 Hz, 3H), 1.33 (td, $^3J_{H\text{-}H}$ = 7.1; $^3J_{H\text{-}P}$ = 1.6 Hz, 6H). **^{13}C NMR (101 MHz, $CDCl_3$)** δ 172.9 (C), 163.7 (d, $^2J_{C\text{-}P}$ = 3.9 Hz, C), 62.9 (d, $^2J_{C\text{-}P}$ = 6.1 Hz, CH_2), 62.8 (d, $^2J_{C\text{-}P}$ = 6.2 Hz, CH_2), 52.4 (CH_3), 48.4 (CH), 35.1 (d, $^1J_{C\text{-}P}$ = 130.9 Hz, CH_2), 18.0 (CH_3), 16.3 (d, $^3J_{C\text{-}P}$ = 6.0 Hz, CH_3). **^{31}P NMR (202 MHz, $CDCl_3$)** δ 22.25. **HRMS (ESI):** $[M+Na]^+$ calcd. $C_{10}H_{20}NPO_6Na$: 304.0920, found: 304.0928.

Synthesis of pP1

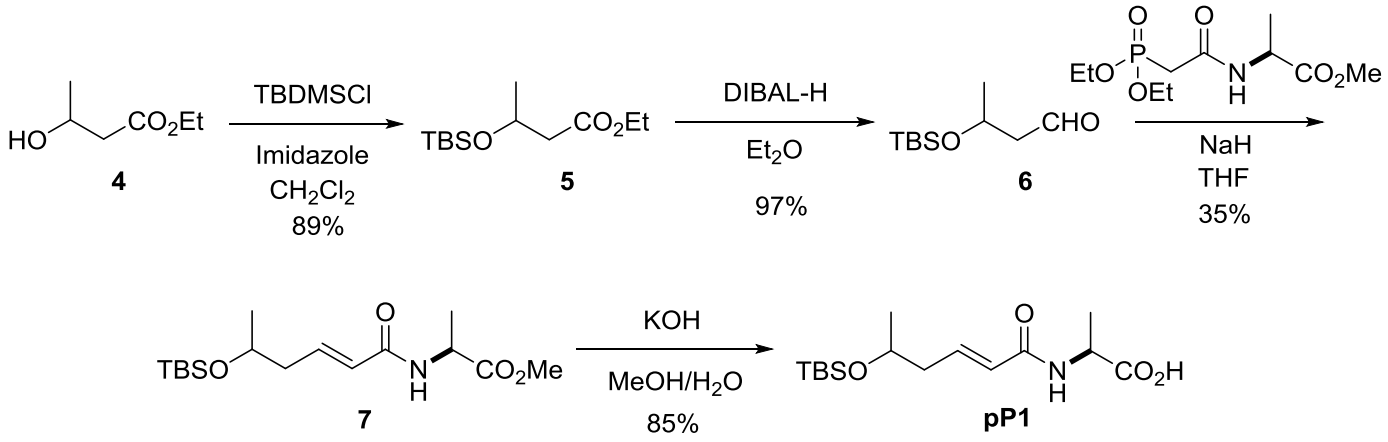

Scheme 2. Preparation of **pP1.**

Preparation of aldehyde **6**: To a solution of ester **5** (500 mg, 2.00 mmol) in Et_2O (2 mL), DIBAL-H (2.2 mL, 2.2 mmol, 1M in THF) was added, and the mixture was stirred at -78 ºC for 40 min. Then, the reaction was quenched with H_2O, diluted with EtOAc, and washed with 10% aqueous HCl solution, and brine. The mixture was dried over anhyd. Na_2SO_4 and the solvent removed. The residue was purified by flash chromatography (EtOAc/Hexane 1:9) to yield **6** (400 mg, 97%). Its ^{1}H and ^{13}C NMR spectra matched with those previously described[127].

Synthesis of ester **7**: According to GP-1, ester **7** was synthesized from aldehyde **6**, with a 35% yield. (EtOAc/Hexane 6:4). Colorless oil; **^{1}H NMR (500 MHz, $CDCl_3$)** δ 6.82 (dt, *J* = 15.2, 7.5 Hz, 1H), 6.15-6.04 (m, 1H), 5.83 (d, *J* = 15.3 Hz, 1H), 4.68 (quint, *J* = 7.2, 1H), 3.95–3.87 (m, 1H), 3.75 (s, 3H), 2.39–2.22 (m, 2H), 1.43 (d, *J* = 7.1 Hz, 3H), 1.15 (d, *J* = 6.0 Hz, 3H), 0.87 (s, 9H), 0.04 (s, 6H); **^{13}C NMR (125 MHz, $CDCl_3$)** δ 173.8 (C), 165.2 (C), 142.2 (CH), 125.3 (CH), 67.8 (CH), 52.6 (CH_3), 48.1 (CH), 42.6 (CH_2), 26.0 (CH_3), 23.8 (CH_3), 18.7 (CH_3), 18.2 (C), –4.42 (CH_3), –4.44 (CH_3); **HRMS (ESI):** $[M+H]^+$ calcd. $C_{16}H_{32}NO_4Si$: 330.2095, found: 330.2087.

Deprotection of compound **7**: According to GP-4, acid **pP1** was synthesized from compound **7**, with a 85% yield. (MeOH/CH_2Cl_2 1:9). Light brown oil; **^{1}H NMR (500 MHz, $CDCl_3$)** δ 9.49 (bs, 1H), 6.82 (dt, *J* = 15.2, 7.5 Hz, 1H), 6.57–6.36 (m, 1H), 5.82 (d, *J* = 15.3 Hz, 1H), 4.73–4.51 (m, 1H), 3.95–3.86 (m, 1H), 2.38–2.21 (m, 2H), 1.46 (d, *J* = 7.1 Hz, 3H), 1.13 (d, *J* = 6.1 Hz, 3H), 0.86 (s, 9H), 0.03 (s, 3H), 0.02 (s, 3H). **^{13}C NMR (126 MHz, $CDCl_3$)** δ 175.9 (C), 166.2 (C), 143.1 (CH), 124.9 (CH), 67.8 (CH), 48.5 (CH), 42.6 (CH_2), 26.0 (CH_3), 23.8 (CH_3), 18.3 (CH_3), 18.2 (C), –4.4 (CH_3), –4.6 (CH_3). **HRMS (ESI)**: $[M+H]^+$ calcd. $C_{15}H_{30}NO_4Si$: 316.1938, found: 316.1933. **Solubility**: CH_2Cl_2, $CHCl_3$ and DMSO among others.

Synthesis of R-P4

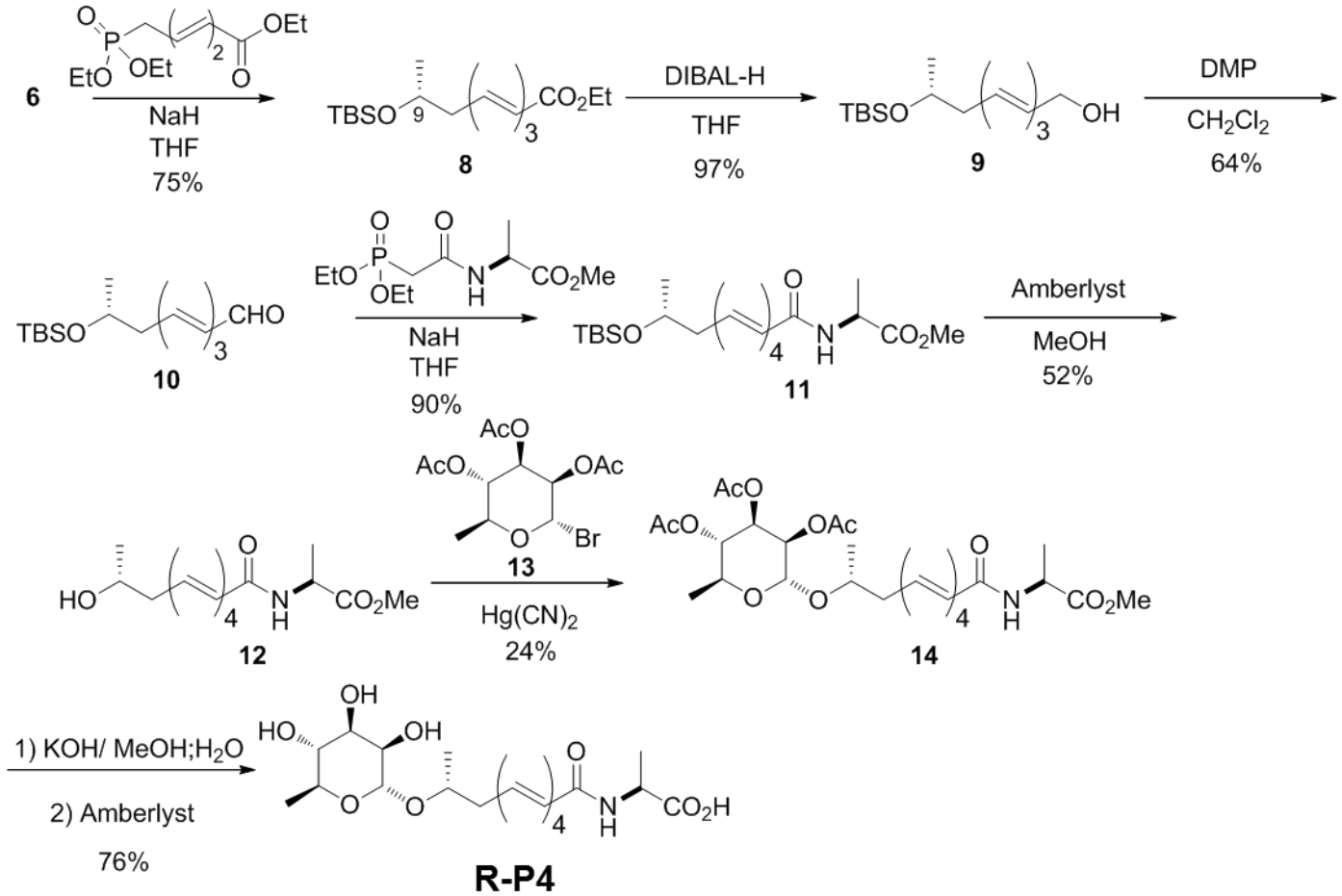

Scheme 3. Preparation of **R-P4.**

Synthesis of ester **(9*R*)-8**: According to GP-1, ester **(*9R*)-8** was synthesized from aldehyde **(*3R*)-6**, with a 75% yield. Colorless oil; $[\alpha]^{25}_{D}$ = + 2.6 (c = 0.01, $CHCl_3$). Its ^{1}H and ^{13}C NMR spectra matched with previously described[128,211].

Reduction of ester **(9*R*)-8** with DIBAL-H: According to GP-2, alcohol **(*9R*)-9** was prepared from ester **(*9R*)-8**, with a 97% yield (EtOAc/Hexane 1.5:8.5). Light yellow oil; $[\alpha]^{25}_{D}$ = +5.6 (c = 0.01, $CHCl_3$).

The mixture of isomers were separated by prep-HPLC ((EtOAc/Hexane 2:8)) and each isomer was isolated and characterized by ^{1}H- and ^{13}C-NMR. Signals were assigned using 2D-NMR spectra.

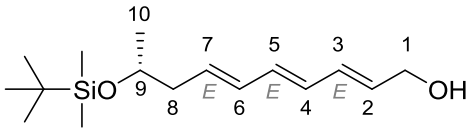

Major *E,E,E*-isomer, **^{1}H NMR (500 MHz, $CDCl_3$)** δ 6.27 (ddt, *J* = 15.2, 10.2, 1.4 Hz, 1H, 3-CH), 6.20 (dd, *J* = 14.8, 10.2 Hz, 1H, 4-CH), 6.13 (dd, *J* = 14.9, 10.4 Hz, 1H, 5-CH), 6.07 (ddt, *J* = 15.0, 10.2, 1.4 Hz, 1H, 6-CH), 5.82 (dt, *J* = 15.2, 6.0 Hz, 1H, 2-CH), 5.71 (dt, *J* = 15.0, 7.5 Hz, 1H, 7-CH), 4.19 (t, *J* = 5.2 Hz, 2H, 1-CH_2), 3.83 (h, *J* = 6.0 Hz, 1H, 9-CH), 2.29–2.15 (m, 2H, 8-CH_2), 1.13 (d, *J* = 6.1 Hz, 3H, 10-CH_3), 0.88 (s, 9H, $OSi(CH_3)_2C(CH_3)_3$), 0.04 (s, 3H, $OSi(CH_3)_2C(CH_3)_3$), 0.03 (s, 3H, $OSi(CH_3)_2C(CH_3)_3$). **^{13}C NMR (126 MHz, $CDCl_3$)** δ 133.7 (4-CH), 132.5 (7-CH), 132.3 (6-CH), 132.0 (3-CH), 131.4 (2-CH), 130.0 (5-CH), 68.7 (9-CH), 63.7 (1-CH_2), 43.3 (8-CH_2), 26.0 (CH_3, $OSi(CH_3)_2C(CH_3)_3$), 23.7 (10-CH_3), 18.3 (C, $OSi(CH_3)_2C(CH_3)_3$), –4.4 (CH_3, $OSi(CH_3)_2C(CH_3)_3$), –4.5 (CH_3, $OSi(CH_3)_2C(CH_3)_3$). **HRMS (ESI)**: $[M]^+$ calcd. $C_{16}H_{30}O_2Si$: 282.2015, found: 282.2026.

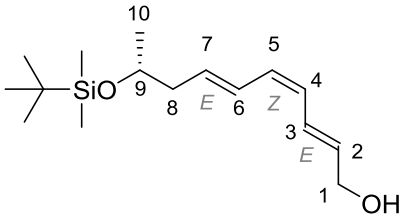

Minor *E,Z,E*-isomer, **^{1}H NMR (500 MHz, CDCl$_3$)** δ 6.71 (dd, *J* = 15.3, 10.6 Hz, 1H, 3-CH), 6.51 (dd, *J* = 15.1, 11.4 Hz, 1H, 6-CH), 5.98 (t, *J* = 10.9 Hz, 1H, 5-CH), 5.91 (t, *J* = 11.0 Hz, 1H, 4-CH), 5.84 (dt, *J* = 15.0, 5.9 Hz, 1H, 2-CH), 5.74 (dt, *J* = 15.0, 7.5 Hz, 1H, 7-CH), 4.24 (t, *J* = 5.2 Hz, 2H, 1-CH_2), 3.85 (h, *J* = 6.1 Hz, 1H, 9-CH), 2.37–2.19 (m, 2H, 8-CH_2), 1.14 (d, *J* = 6.1 Hz, 3H, 10-CH_3), 0.88 (s, 9H, OSi$(CH_3)_2$C$(CH_3)_3$), 0.04 (s, 3H, OSi$(CH_3)_2$C$(CH_3)_3$), 0.04 (s, 3H, OSi$(CH_3)_2$C$(CH_3)_3$). Carbon was assigned from the HSQC (quaternary carbon is not shown): **^{13}C NMR (126 MHz, CDCl$_3$)**: δ 133.3 (7-CH), 132.5 (2-CH), 130.4 (5-CH), 127.6 (6-CH), 126.9 (3-CH), 126.8 (4-CH), 68.5 (9-CH), 63.5 (1-CH_2), 43.4 (8-CH_2), 25.9 (CH_3, OSi$(CH_3)_2$C$(CH_3)_3$), 23.6 (10-CH_3), –4.5 (CH_3, OSi$(CH_3)_2$C$(CH_3)_3$).

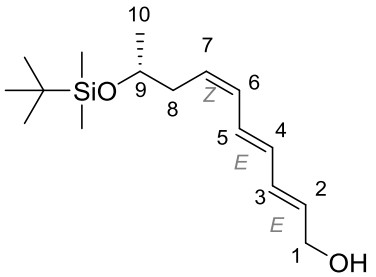

Minor *Z,E,E*-isomer **^{1}H NMR (500 MHz, CDCl$_3$)** δ 6.49 (dd, *J* = 14.8, 11.2 Hz, 1H, 5-CH), 6.31 (ddt, *J* = 15.1, 10.9, 1.8 Hz, 1H, 3-CH), 6.21 (dd, J = 15.0, 11.0 Hz, 1H, 4-CH), 6.09 (t, *J* = 10.3 Hz, 1H, 6-CH), 5.85 (dt, *J* = 15.3, 5.9 Hz, 1H, 2-CH), 5.51 (dt, *J* = 10.7, 5.9 Hz, 1H, 7-CH), 4.20 (t, *J* = 6.0 Hz, 2H, 1-CH_2), 3.85 (h, *J* = 6.0 Hz, 1H, 9-CH), 2.33 (m, 2H, 8-CH_2), 1.14 (d, *J* = 6.1 Hz, 3H, 10-CH_3), 0.88 (s, 9H, OSi$(CH_3)_2$C$(CH_3)_3$), 0.05 (s, 3H, OSi$(CH_3)_2$C$(CH_3)_3$), 0.04 (s, 3H, OSi$(CH_3)_2$C$(CH_3)_3$). Carbon was assigned from the HSQC (quaternary carbon is not shown): **^{13}C NMR (126 MHz, CDCl$_3$)**: δ 132.1 (4-CH), 132.0 (3-CH), 131.9 (2-CH), 129.9 (6-CH), 129.6 (7-CH), 129.2 (5-CH), 68.6 (9-CH), 63.5 (1-CH_2), 38.1 (8-CH_2), 26.0 (CH_3, OSi$(CH_3)_2$C$(CH_3)_3$), 23.6 (10-CH_3), –4.5 (CH_3, OSi$(CH_3)_2$C$(CH_3)_3$).

Preparation of aldehyde **(*9R*)-10**: According to GP-3, aldehyde **(*9R*)-10** was synthesized from alcohol **(*9R*)-9**, with a 64% yield (EtOAc/Hexane 0.5:9.5). Deep yellow oil; $[\alpha]^{25}_D$ = +9.1 (c =

0.01, $CHCl_3$); *E,E,E*-isomer: **^{1}H NMR (400 MHz, $CDCl_3$)** δ 9.55 (d, *J* = 7.9 Hz, 1H), 7.12 (dd, *J* = 15.3, 11.1 Hz, 1H), 6.65 (dd, *J* = 14.9, 10.6 Hz, 1H), 6.36 (dd, *J* = 14.9, 11.1 Hz, 1H), 6.24–6.10 (m, 2H), 6.03 (dt, *J* = 15.0, 7.4 Hz, 1H), 3.89 (h, *J* = 6.1 Hz, 1H), 2.32–2.26 (m, 2H), 1.15 (d, *J* = 6.1 Hz, 3H), 0.88 (s, 9H), 0.05 (s, 3H), 0.04 (s, 3H). **^{13}C NMR (101 MHz, $CDCl_3$)** δ 193.7 (CH), 152.4 (CH), 143.1 (CH), 139.0 (CH), 131.9 (CH), 131.0 (CH), 128.3 (CH), 68.4 (CH), 43.5 (CH_2), 26.0 (CH_3), 23.9 (CH_3), 18.3 (C), -4.3 (CH_3), -4.6 (CH_3). **HRMS (ESI):** $[M+Na]^+$ calcd. $C_{16}H_{28}O_2SiNa$: 303.1750, found: 303.1752.

Synthesis of ester **(10*R*)-11**: According to GP-1, ester **(*10R*)-11** was synthesized from aldehyde **(*9R*)-10** with a 90% yield (EtOAc/Hexane 2:8). The major isomer was isolated by prep-HPLC (EtOAc/Hexane 2:8). Light brown oil; $[\alpha]^{25}_D$ = +2.1 (c = 0.01, $CHCl_3$); *E,E,E,E isomer*: **^{1}H NMR (500 MHz, $CDCl_3$)** δ 7.27 (dd, *J* = 14.9, 11.3 Hz, 1H), 6.55 (dd, *J* = 14.8, 11.0 Hz, 1H), 6.36 (dd, *J* = 14.9, 10.7 Hz, 1H), 6.27 (dd, *J* = 14.8, 11.3 Hz, 1H), 6.19 (dd, *J* = 14.9, 11.0 Hz, 1H), 6.12 (dd, *J* = 15.1, 10.7 Hz, 1H), 6.02 (d, *J* = 7.5 Hz, 1H), 5.85 (d, *J* = 14.9 Hz, 1H), 5.83–5.78 (m, 1H), 4.70 (quint, *J* = 7.2 Hz, 1H), 3.85 (h, *J* = 6.0 Hz, 1H), 3.76 (s, 3H), 2.30–2.18 (m, 2H), 1.44 (d, *J* = 7.1 Hz, 3H), 1.13 (d, *J* = 6.1 Hz, 3H), 0.88 (s, 9H), 0.04 (s, 3H), 0.03 (s, 3H). **^{13}C NMR (126 MHz, $CDCl_3$)** δ 173.8 (C), 165.6 (C), 141.8 (CH), 140.4 (CH), 137.0 (CH), 134.7 (CH), 132.4 (CH), 130.3 (CH), 129.4 (CH), 122.3 (CH), 68.6 (CH), 52.7 (CH_3), 48.2 (CH), 43.5 (CH_2), 26.0 (CH_3), 23.8 (CH_3), 18.9 (CH_3), 18.3 (C), –4.4 (CH_3), –4.5 (CH_3). **HRMS (ESI):** $[M+Na]^+$ calcd. $C_{22}H_{37}NO_4SiNa$: 430.2384, found: 430.2399.

Preparation of alcohol **(10*R*)-12**: To a solution of ester **(*10R*)-11** (292 mg, 0.717 mmol) in MeOH (2 mL), amberlyst 15(H) was added (up to pH 5), and the mixture was stirred at room temperature

for 90 min. Then, the residue was purified by flash chromatography (MeOH/CH_2Cl_2 1:9) to yield **(*10R*)-12** (110 mg, 52%). Light yellow oil; $[\alpha]^{25}_D$ = –5.3 (c = 0.09, $CHCl_3$); The major isomer (all-*E*) was isolated by prep-HPLC (EtOAc/CH_2Cl_2 7:3): **^{1}H NMR (500 MHz, $CDCl_3$)** δ 7.27 (dd, *J* = 14.9, 11.3 Hz, 1H), 6.54 (dd, *J* = 14.8, 11.0 Hz, 1H), 6.37 (dd, *J* = 15.0, 10.5 Hz, 1H), 6.29 (dd, *J* = 14.8, 11.4 Hz, 1H), 6.26–6.17 (m, 2H), 6.04 (d, *J* = 7.4 Hz, 1H), 5.87 (d, *J* = 15.1 Hz, 1H), 5.84–5.79 (m, 1H), 4.70 (quint, *J* = 7.2 Hz, 1H), 3.88 (h, *J* = 6.4 Hz, 1H), 3.76 (s, 3H), 2.36–2.22 (m, 2H), 1.44 (d, *J* = 7.2 Hz, 3H), 1.21 (d, *J* = 6.2 Hz, 3H). **^{13}C NMR (126 MHz, $CDCl_3$)** δ 173.8 (C), 165.6 (C), 141.7 (CH), 140.1 (CH), 136.4 (CH), 133.5 (CH), 133.1 (CH), 131.0 (CH), 129.9 (CH), 122.6 (CH), 67.5 (CH), 52.7 (CH_3), 48.3 (CH), 43.0 (CH_2), 23.1 (CH_3), 18.9 (CH_3). **HRMS (ESI):** $[M+Na]^+$ calcd. $C_{16}H_{23}NO_4Na$: 316.1519, found: 316.1507.

Synthesis of rhamnose derivative **(10*R*)-14:** To a solution of alcohol **12** (114 mg, 0.389 mmol) and $Hg(CN)_2$ (98 mg, 0.39 mmol) in dry CH_3CN (2 mL), bromorhamnose **13** (206 mg, 0.585 mmol) was added in three portions during 3 h, and the mixture was stirred for additional 4 h. Then, the solvent was removed. The residue was solved in AcOEt and washed with 1M solution of KBr, saturated solution of $NaHCO_3$ and water. The organic layer was dried (anhyd Na_2SO_4) and the solvent was removed. The residue was submitted to flash chromatography (EtOAc/Hexane 3:7) to yield ester **(*10R*)-14** (52 mg, 24%). Brown oil; $[\alpha]^{25}_D$ -36.6 (c = 0.01, $CHCl_3$); *E,E,E,E* isomer: **^{1}H NMR (500 MHz, $CDCl_3$)** δ 7.26 (dd, *J* = 14.9, 11.3 Hz, 1H), 6.54 (dd, *J* = 14.4, 11.2 Hz, 1H), 6.40–6.14 (m, 4H), 6.05 (d, *J* = 7.4 Hz, 1H), 5.87 (d, *J* = 14.9 Hz, 1H), 5.79 (dt, *J* = 15.4, 7.6 Hz, 1H), 5.27 (dd, *J* = 10.2, 3.6 Hz, 1H), 5.17 (bs, 1H), 5.04 (t, *J* = 10.2 Hz, 1H), 4.83 (d, *J* = 1.8 Hz, 1H), 4.75–4.65 (quint, *J* = 7.2 Hz, 1H), 4.02–3.86 (m, 1H), 3.83–3.78 (m, 1H), 3.76 (s, 3H), 2.44–2.36 (m, 1H), 2.34–2.27 (m, 1H), 2.14 (s, 3H), 2.01 (s, 3H), 1.98 (s, 3H), 1.44 (d, *J* = 7.2 Hz, 3H),

1.17 (d, J = 6.3 Hz, 3H), 1.15 (d, J = 6.2 Hz, 3H). **^{13}C NMR (126 MHz, $CDCl_3$)** δ 173.7 (C), 170.2 (C), 170.0 (C), 165.4 (C), 141.5 (CH), 140.0 (CH), 136.3 (CH), 133.1 (CH), 132.9 (CH), 130.7 (CH), 129.6 (CH), 122.4 (CH), 95.1 (CH, $^1J_{C\text{-}H}$ = 170 Hz), 72.8 (CH), 71.1 (CH), 70.5 (CH), 69.2 (CH), 66.5 (CH), 52.5 (CH_3), 48.1 (CH), 40.4 (CH_2), 20.9 (CH_3), 20.8 (CH_3), 20.7 (CH_3), 18.9 (CH_3), 18.7 (CH_3), 17.3 (CH_3). **HRMS (ESI):** $[M+H]^+$ calcd $C_{28}H_{40}NO_{11}$: 566.2595, found: 566.2607.

Coupling constant values ($^3J_{H\text{-}H}$ and $^1J_{C\text{-}H}$) of the anomeric proton matched with those previously described for other α-rhamnopyranosyl derivatives [129,212-214].

Preparation of **R-P4**: To a solution of ester ***(10R)*-14** (27 mg, 0.05 mmol) in MeOH (1 mL), KOH 2M aqueous solution (0.29 mL, 0.57 mmol) was added and the mixture was stirred for 5 h. Then, washed amberlyst was added until pH 5, the mixture was submitted to flash chromatography (MeOH/CH_2Cl_2 1:1) to yield **R-P4** (15 mg, 76%). Light brown oil; $[\alpha]^{25}_{D}$ = –16.4 (c = 0.04, $CHCl_3$); Mixture of isomers. Data of major isomer are given: **^{1}H NMR (500 MHz, CD_3OD)** δ 7.18 (dd, J = 15.1, 11.0 Hz, 1H), 6.59 (dd, J = 14.8, 10.9 Hz, 1H), 6.44–6.32 (m, 2H), 6.27 (dd, J = 14.9, 10.9 Hz, 1H), 6.21 (dd, J = 15.2, 10.6 Hz, 1H), 6.07 (d, J = 14.8 Hz, 1H), 5.86 (dt, J = 14.8, 7.2 Hz, 1H), 4.34 (q, J = 7.6 Hz, 1H), 3.83 (m, 1H), 3.74 (bs, 1H), 3.68–3.61 (m, 2H), 3.37 (t, J = 9.5 Hz, 2H), 2.45–2.28 (m, 2H), 1.38 (d, J = 7.1 Hz, 3H), 1.23 (d, J = 6.4 Hz, 3H), 1.15 (d, J = 6.1 Hz, 3H). **^{13}C NMR (126 MHz, CD_3OD)** δ 179.4 (C), 168.0 (C), 141.7 (CH), 140.9 (CH), 137.6 (CH), 134.3 (CH), 134.0 (CH), 131.9 (CH), 131.1 (CH), 124.5 (CH), 99.3 (CH), 74.0 (CH), 73.4 (CH), 72.84 (CH), 72.4 (CH), 70.1 (CH), 51.6 (CH), 42.9 (CH_2), 19.19 (CH_3), 19.17 (CH_3), 17.9 (CH_3). **HRMS (ESI):** $[M+Na]^+$ calcd. $C_{21}H_{31}NO_8Na$: 448.1941, found: 448.1932. **Solubility**: MeOH, DMSO.

Synthesis of pP7X, pP7, and P7

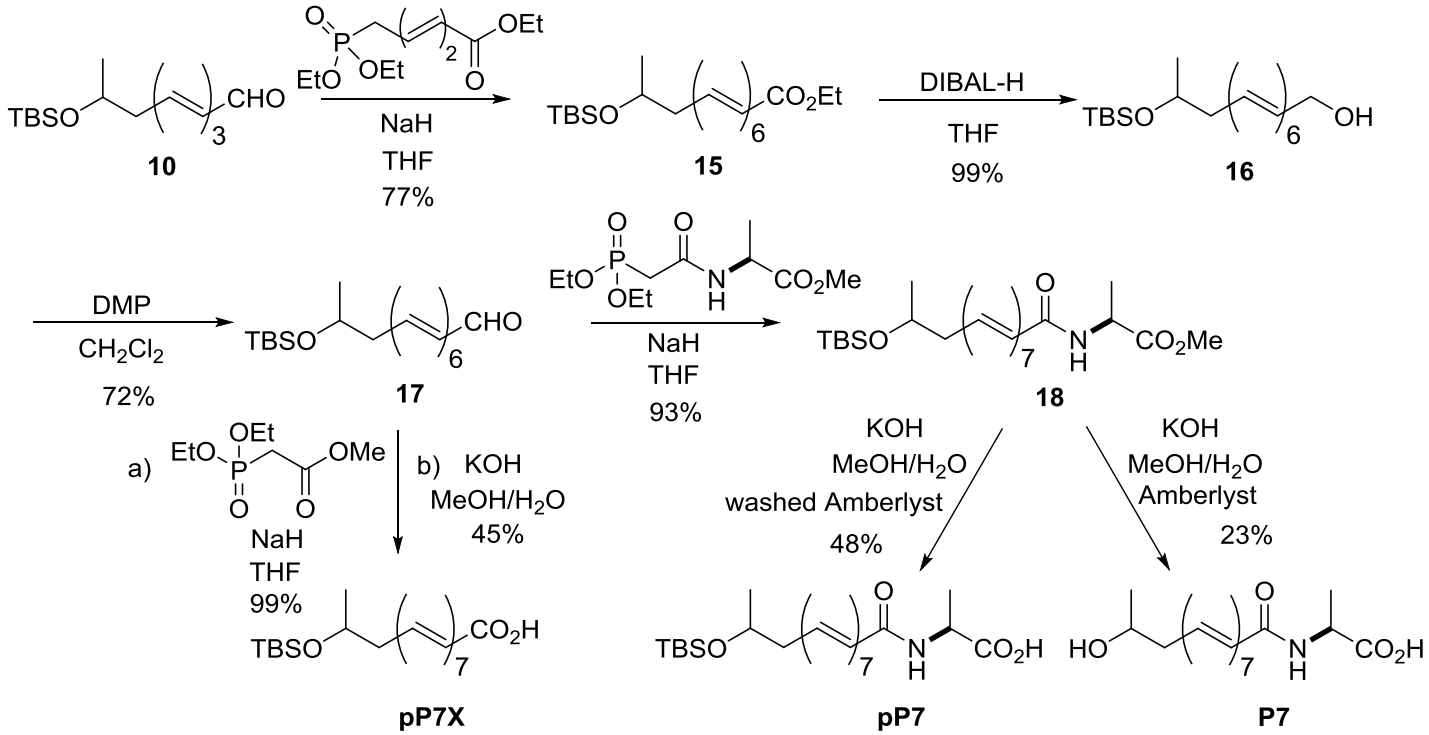

Scheme 4. Preparation of **pP7X**, **pP7** and **P7**.

Preparation of ester **15**: According to GP-1, polyene ester **15** was synthesized from racemic aldehyde **10**, with a 77% yield (EtOAc/Hexane 1:9). Yellow oil; *all-E* isomer: **^{1}H NMR (500 MHz, CDCl$_3$)** δ 7.31 (dd, *J* = 15.3, 11.0 Hz, 1H), 6.59 (dd, *J* = 14.8, 11.0 Hz, 1H), 6.44 (dd, *J* = 14.9, 10.7 Hz, 1H), 6.40–6.23 (m, 5H), 6.19 (dd, *J* = 14.7, 10.6 Hz, 1H), 6.18–6.05 (m, 1H), 5.85 (d, *J* = 15.2 Hz, 1H), 5.76 (dt, *J* = 15.1, 7.6 Hz, 1H), 4.20 (q, *J* = 7.1 Hz, 2H), 3.89–3.77 (m, 1H), 2.29–2.14 (m, 2H), 1.29 (t, *J* = 7.2 Hz, 3H), 1.12 (d, *J* = 6.2 Hz, 3H), 0.88 (s, 9H), 0.04 (s, 3H), 0.03 (s, 3H). **^{13}C NMR (126 MHz, CDCl$_3$)** δ 167.3 (C), 144.5 (CH), 140.9 (CH), 137.5 (CH), 136.0 (CH), 135.1 (CH), 133.4 (CH), 132.7 (CH), 132.0 (CH), 131.6 (CH), 131.0 (CH), 129.9 (CH), 120.5 (CH), 68.7 (CH), 60.4 (CH_2), 43.5 (CH_2), 26.0 (CH_3), 23.8 (CH_3), 18.3 (C), 14.5 (CH_3), –4.4 (CH_3), –4.6 (CH_3). **HRMS (ESI):** $[M+Na]^+$ calcd. $C_{24}H_{38}O_3SiNa$: 425.2482, found: 425.2486.

Reduction of ester **15** with DIBAL-H: According to GP-2, alcohol **16** was prepared from ester **15**, with a 99% yield (EtOAc/Hexane 3:7). Yellow oil; Mixture of isomers. Data of major isomer are given. **^{1}H NMR (400 MHz, $CDCl_3$)** δ 6.85–6.62 (m, 1H), 6.41–6.16 (m, 7H), 6.13–5.92 (m, 2H), 5.94–5.80 (m, 1H), 5.79–5.59 (m, 1H), 4.27–4.18 (bs, 2H), 3.93–3.79 (m, 1H), 2.33–2.17 (m, 2H), 1.15 (d, *J* = 6.2 Hz, 3H), 0.90 (s, 9H), 0.06 (s, 3H), 0.06 (s, 3H).**^{13}C NMR (101 MHz, $CDCl_3$)** δ 133.8 (CH), 133.7 (CH), 133.6 (CH), 133.5 (CH), 132.7 (CH), 132.5 (CH), 132.4 (CH), 132.3 (CH), 132.2 (CH), 131.9 (CH), 131.7 (CH), 131.2 (CH), 68.6 (CH), 63.4 (CH_2), 43.3 (CH_2), 25.9 (CH_3), 23.6 (C), 18.2 (CH_3), –4.5 (CH_3), –4.7 (CH_3). Due to the instability of this compound, a good mass spectrum could not be obtained.

Synthesis of aldehyde **17**: According to GP-3, aldehyde **17** was synthesized from alcohol **16**, with a 72% yield (EtOAc/Hexane 0.5:9.5). Yellow oil; *all-E* isomer: **^{1}H NMR (500 MHz, $CDCl_3$)** δ 9.56 (d, *J* = 8.0, 1H), 7.14 (dd, *J* = 15.1, 11.3 Hz, 1H), 6.71 (dd, *J* = 14.7, 11.2 Hz, 1H), 6.52 (dd, *J* = 14.7, 11.0 Hz, 1H), 6.50–6.39 (m, 2H), 6.38–6.35 (m, 1H), 6.34–6.26 (m, 2H), 6.21 (dd, *J* = 14.9, 10.8 Hz, 1H), 6.17–6.10 (m, 2H), 5.79 (dt, *J* = 15.1, 7.6 Hz, 1H), 3.85 (dt, *J* = 12.0, 5.9 Hz, 1H), 2.31–2.21 (m, 2H), 1.13 (d, *J* = 6.1 Hz, 3H), 0.88 (s, 9H), 0.04 (s, 3H), 0.03 (s, 3H). **^{13}C NMR (126 MHz, $CDCl_3$)** δ 193.6 (CH), 152.0 (CH), 143.0 (CH), 139.2 (CH), 137.1 (CH), 135.8 (CH), 134.0 (CH), 132.7 (CH), 131.8 (CH), 131.3 (CH), 130.87 (CH), 129.7 (CH), 68.7 (CH), 43.5 (CH_2), 26.0 (CH_3), 23.8 (CH_3), 18.3 (C), –4.4 (CH_3), –4.6 (CH_3). **HRMS (ESI):** $[M+Na]^+$ calcd. $C_{22}H_{34}O_2SiNa$: 381.2220, found 381.2229.

Preparation of derivative **pP7X**: According to GP-1, a polyene ester precursor was synthesized from aldehyde **17**, with a 99% yield (EtOAc/Hexane 0.5:9.5). Deep yellow oil; *all-E* isomer isolated by prep-HPLC (EtOAc/Hexane 1:9): **^{1}H NMR (500 MHz, $CDCl_3$)** δ 7.35 (dd, *J* = 15.3, 11.5 Hz, 1H), 6.63 (dd, *J* = 14.8, 11.2 Hz, 1H), 6.48 (dd, *J* = 14.7, 11.1 Hz, 1H), 6.43–6.21 (m, 8H), 6.14 (dd, *J* = 15.0, 10.3 Hz, 1H), 5.89 (d, *J* = 15.2 Hz, 1H), 5.77 (dt, *J* = 15.1, 7.6 Hz, 1H), 3.86 (h, *J* = 6.3 Hz, 1H), 3.77 (s, 3H), 2.3–2.22 (m, 2H), 1.15 (d, *J* = 6.0 Hz, 3H), 0.91 (s, 9H), 0.07 (s, 3H), 0.06 (s, 3H). **^{13}C NMR (126 MHz, $CDCl_3$)** δ 167.6 (C), 144.7 (CH), 141.0 (CH), 137.6 (CH), 136.0 (CH), 135.1 (CH), 134.5 (CH), 133.0 (CH), 132.6 (CH), 132.2 (CH), 132.2 (CH), 131.7 (CH), 131.1 (CH), 129.8 (CH), 119.9 (CH), 68.6 (CH), 51.5 (CH_3), 43.3 (CH_2), 25.9 (CH_3), 23.6 (CH_3), 18.2 (C), –4.5 (CH_3), –4.7 (CH_3). **HRMS (ESI):** $[M+H]^+$ calcd. $C_{25}H_{39}O_3Si$: 415.2663, found 415.2671. According to **GP-4** (using 24 mL of THF), this ester intermediate was transformed into **pP7X**, with a 45% yield. Preparative TLC ($MeOH/CH_2Cl_2$ 1:9). Prep-HPLC (EtOAc/Hexane 3:7). Light yellow oil; **^{1}H NMR (500 MHz, $CDCl_3$)** δ 7.40 (dd, *J* = 15.1, 11.4 Hz, 1H), 6.65 (t, *J* = 13.1 Hz, 1H), 6.56–6.19 (m, 9H), 6.11 (t, *J* = 11.7 Hz, 1H), 5.87 (d, *J* = 15.0 Hz, 1H), 3.89–3.81 (m, 1H), 2.35–2.18 (m, 2H), 1.15 (d, *J* = 6.1 Hz, 3H), 0.88 (s, 9H), 0.04 (s, 3H), 0.04 (s, 3H). **^{13}C NMR (126 MHz, $CDCl_3$)** δ 170.5 (C), 146.6 (CH), 141.9 (CH), 138.2 (CH), 136.2 (CH), 135.3 (CH), 133.1 (CH), 132.8 (CH), 132.6 (CH), 132.1 (CH), 131.7 (CH), 131.0 (CH), 130.2 (CH), 129.5 (CH), 118.9 (CH), 68.6 (CH), 43.3 (CH_2), 25.9 (CH_3), 23.6 (CH_3), 18.1 (C), –4.6 (CH_3), –4.7 (CH_3); **HRMS (ESI):** $[M–H]^+$ calcd. $C_{24}H_{35}O_3Si$: 399.2355, found 399.2361. **Solubility**: CH_2Cl_2, $CHCl_3$ and DMSO among others.

Synthesis of ester **18**: According to GP-1, polyene ester **18** was synthesized from aldehyde **17**, with a 93% yield (EtOAc/Hexane 3:7). Prep-HPLC (EtOAc/Hexane 1:1). Light orange oil; **^{1}H**

NMR (500 MHz, $CDCl_3$) δ 7.31 (dd, *J* = 15.3, 11.5 Hz, 1H), 6.69–6.52 (m, 2H), 6.50–6.39 (m, 2H), 6.39–6.27 (m, 6H), 6.13–6.08 (m, 1H), 6.01 (dd, *J* = 16.3, 10.9 Hz, 1H), 5.90 (d, *J* = 14.9 Hz, 1H), 4.72 (quint, *J* = 7.2 Hz, 1H), 3.93–3.83 (m, 1H), 3.79 (s, 3H), 2.44–2.23 (m, 2H), 1.47 (d, *J* = 7.1 Hz, 3H), 1.16 (d, *J* = 6.1 Hz, 3H), 0.90 (s, 9H), 0.07 (s, 3H), 0.06 (s, 3H). **^{13}C NMR (126 MHz, $CDCl_3$)** 173.7 (C), 165.5 (C), 141.5 (CH), 140.1 (CH), 136.8 (CH), 135.5 (CH), 133.7 (CH), 133.0 (CH), 132.8 (CH), 132.1 (CH), 130.9 (CH), 130.0 (CH), 129.9 (CH), 127.9 (CH), 127.7 (CH), 122.5 (CH), 68.5 (CH), 52.5 (CH_3), 48.1 (CH), 43.4 (CH_2), 25.9 (CH_3), 23.7 (CH_3), 18.7 (CH_3), 18.2 (C), –4.5 (CH_3), –4.7 (CH_3). **HRMS (ESI):** $[M+Na]^+$ calcd. $C_{28}H_{43}NO_4SiNa$: 508.2853, found 508.2869.

Preparation of **pP7**: According to GP-4 (using 12 mL of THF), **pP7** was synthesized from **18**, with a 48% yield ($MeOH/CH_2Cl_2$ 3:7). Prep-HPLC (EtOAc/Hexane 8:2). Deep orange oil. **^{1}H NMR (500 MHz, CD_3OD)** δ 7.24 (dd, *J* = 15.0, 11.4 Hz, 1H), 6.67 (dd, *J* = 14.7, 10.8 Hz, 1H), 6.52 (dd, J = 14.8, 10.3 Hz, 1H), 6.47–6.34 (m, 7H), 6.31–6.22 (m, 1H), 6.19–6.12 (m, 1H), 6.09 (d, *J* = 14.9 Hz, 1H), 5.77 (dt, *J* = 15.2, 7.6 Hz, 1H), 4.49 (bs, 1H), 4.00–3.86 (m, 1H), 2.25 (dd, *J* = 7.7, 5.8 Hz, 2H), 1.44 (d, *J* = 7.1 Hz, 3H), 1.15 (d, *J* = 6.0 Hz, 3H), 0.91 (s, 9H), 0.08 (s, 3H), 0.07 (s, 3H). **^{13}C NMR (126 MHz, CD_3OD)** δ 174.7 (C), 167.2 (C), 140.96 (CH), 140.94 (CH), 140.0 (CH), 136.8 (CH), 135.4 (CH), 134.5 (CH), 133.9 (CH), 132.8 (CH), 132.33 (CH), 132.28 (CH), 132.0 (CH), 131.8 (CH), 131.2 (CH), 129.9 (CH), 68.61 (CH), 42.93 (CH_2), 24.95 (CH_3) , 22.66 (CH_3), 17.55 (C), 16.40 (CH_3), -5.77 (CH_3), -5.91 (CH_3).One CH was not observed. **HRMS (ESI):** $[M+Na]^+$ calcd. $C_{27}H_{41}O_4NSiNa$: 494.2697, found 494.2706. **Solubility**: MeOH, DMSO.

Synthesis of **P7**: According to GP-4 (using 12 mL of THF, and adding non-washed Amberlyst), **P7** was synthesized from **18**, with a 23% yield. . Preparative TLC (EtOAc/Hexane 8:2). Yellow oil. **^{1}H NMR (500 MHz, CD_3OD)** δ 7.24 (dd, *J* = 14.7, 11.4 Hz, 1H), 6.67 (dd, *J* = 14.7, 11.1 Hz, 1H), 6.58–6.25 (m, 10H), 6.18 (t, *J* = 11.2 Hz, 1H), 6.08 (d, *J* = 14.9 Hz, 1H), 4.54–4.42 (m, 1H), 3.87–3.77 (m, 1H), 2.46–2.22 (m, 2H), 1.44 (d, *J* = 7.3 Hz, 3H), 1.19 (d, *J* = 6.2 Hz, 3H). **HRMS (ESI):** $[M–H]^+$ calcd. $C_{21}H_{26}O_4N$: 356.1867, found 356.1866. Owing to the unusual physical properties of this kind of compounds in terms of solubility, a clear ^{13}C NMR could not be obtained even using long acquisition times. HSQC 2D-NMR experiment has been carried out and attached to the ESI. **Solubility**: MeOH (partially), DMSO (0.02 M, fully soluble).

Synthesis of pP9 and P9

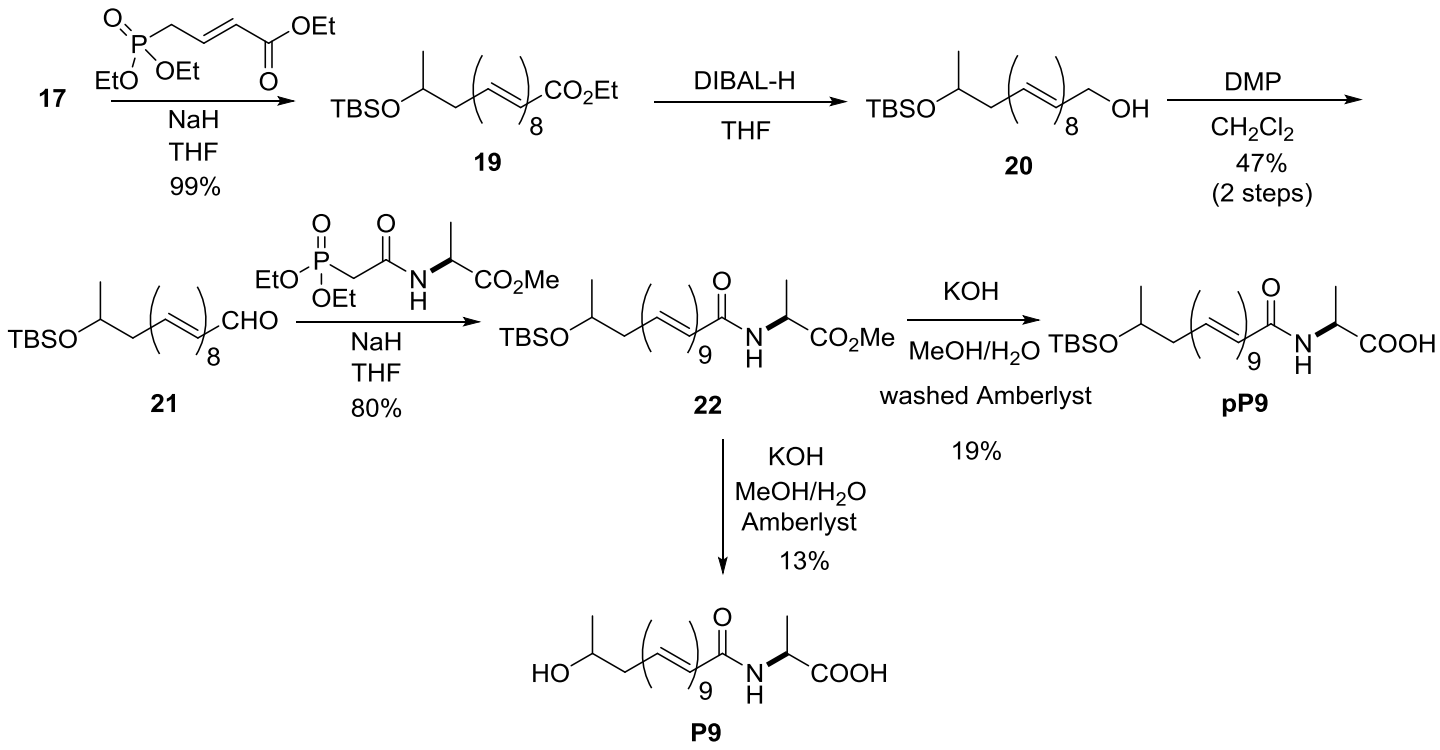

Scheme 5. Synthesis of **pP9** and **P9**.

Synthesis of ester **19**: According to GP-1, polyene ester **19** was synthesized from aldehyde **17**, with a 99% yield (EtOAc/Hexane 1:9). Deep orange oil; Mixture of isomers. Data of major isomer are given **^{1}H NMR (500 MHz, $CDCl_3$)** δ 7.35 (dd, *J* = 15.4, 11.5 Hz, 1H), 6.63 (dd, *J* = 14.7, 11.1 Hz, 1H), 6.53–6.44 (m, 1H), 6.44–6.20 (m, 10H), 6.13 (dd, *J* = 15.0, 10.1 Hz, 1H), 5.89 (dd, *J* = 15.2, 3.2 Hz, 1H), 5.76 (dt, *J* = 15.0, 7.5 Hz, 1H), 4.23 (q, *J* = 7.1 Hz, 2H), 3.86 (h, *J* = 6.3 Hz, 1H), 2.33–2.18 (m, 2H), 1.32 (t, *J* = 7.1 Hz, 3H), 1.15 (d, *J* = 6.1 Hz, 3H), 0.90 (s, 9H), 0.07 (s, 3H), 0.06 (s, 3H). **^{13}C NMR (125 MHz, $CDCl_3$)** δ 167.6 (C), 144.7 (CH), 141.0 (CH), 137.6 (CH), 136.0 (CH), 135.1 (CH), 134.6 (CH), 134.2 (CH), 132.8 (CH), 132.7 (CH), 132.5 (CH), 132.4 (CH), 131.8 (CH), 131.2 (CH), 129.9 (CH), 120.0 (CH), 68.6 (CH), 60.3 (CH_2), 51.5 (CH_3), 43.4

(CH_2), 25.9 (CH_3), 18.2 (C), 14.3 (CH_3), –4.5 (CH_3), –4.7 (CH_3). **HRMS (ESI)** m/z calcd for $C_{28}H_{42}O_3SiNa$ $[M+Na]^+$ 477.2795, found 477.2790.

Reduction of ester **19** with DIBAL-H: According to GP-2, alcohol **20** was prepared from ester **19**. This compound is highly unstable, and it was immediately used in the next step.

Synthesis of aldehyde **21**: According to GP-3, aldehyde **21** was synthesized from alcohol **20**, with a 47% yield (2 steps) (EtOAc/Hexane 1:9). Orange-red oil; Data of the major isomer (*all-E*-**21**) is given: **^{1}H NMR (500 MHz, $CDCl_3$)** δ 9.58 (d, *J* = 8.0 Hz, 1H), 7.16 (dd, *J* = 15.1, 11.3 Hz, 1H), 6.74 (dd, *J* = 14.7, 11.3 Hz, 1H), 6.56 (dd, *J* = 14.7, 11.1 Hz, 1H), 6.50–6.09 (m, 12H), 5.77 (dt, *J* = 15.1, 7.6 Hz, 1H), 3.86 (h, *J* = 6.1 Hz, 1H), 2.33–2.20 (m, 2H), 1.15 (d, *J* = 6.1 Hz, 3H), 0.90 (s, 9H), 0.07 (s, 3H), 0.06 (s, 3H).**^{13}C NMR (126 MHz, $CDCl_3$)** δ 193.5 (C), 151.9 (CH), 142.9 (CH), 139.2 (CH), 137.1 (CH), 135.9 (CH),135.1 (CH), 134.6 (CH), 133.2 (CH), 132.8 (CH), 132.5 (CH), 132.4 (CH), 132.3 (CH), 131.6 (CH), 131.2 (CH), 130.9 (CH), 129.9 (CH), 68.7 (CH), 43.5 (CH_2), 26.0 (CH_3), 23.8 (CH_3), 18.3 (C), –4.4 (CH_3), –4.5 (CH_3). **HRMS (EI):** $[M]^+$ calcd. $C_{26}H_{38}O_2Si$: 410.2641, found 410.2648.

Preparation of amide **22**: According to GP-1, polyene amide **22** was synthesized from aldehyde **21**, with an 80% yield (EtOAc/Hexane 3.5:6.5). Orange-red oil; *all-E* isomer: **^{1}H NMR (500 MHz, $CDCl_3$)** δ 7.28 (dd, *J* = 14.9, 11.5 Hz, 1H), 6.63–6.50 (m, 2H), 6.50–6.16 (m, 10H), 6.16–6.05 (m, 3H), 5.88 (d, *J* = 14.9 Hz, 1H), 5.81–5.67 (m, 1H), 4.70 (quint, *J* = 7.2 Hz, 1H), 3.91–3.79 (m, 1H), 3.76 (s, 3H), 2.34–2.14 (m, 2H), 1.44 (d, *J* = 7.1 Hz, 3H), 1.14 (d, *J* = 6.2 Hz, 3H), 0.88 (s, 9H), 0.05 (s, 3H), 0.04 (s, 3H). **^{13}C NMR (101 MHz, $CDCl_3$)** δ 173.7 (C), 165.4 (C), 141.5 (CH),

140.1 (CH), 136.9 (CH), 135.6 (CH), 134.8 (CH), 134.3 (CH), 134.1 (CH), 133.9 (CH), 133.0 (CH), 132.8 (CH), 132.7 (CH), 132.5 (CH), 132.1 (CH), 131.2 (CH), 130.0 (CH), 129.2 (CH), 127.9 (CH), 122.5 (CH), 68.6 (CH), 52.5 (CH_3), 48.1 (CH), 43.3 (CH_2), 25.9 (CH_3), 23.7 (CH_3), 18.7 (CH_3). 18.1 (C), -4.5 (CH_3), -4.7 (CH_3); HRMS (APCI) m/z calcd for $C_{32}H_{48}NO_4Si$ $[M+H]^+$ 538.3347, found 538.3351.

Saponification of amide **22** with KOH/MeOH: According to GP-4 (using 12 mL of THF), **pP9** was synthesized from **22**, with a 19% yield (MeOH/CH_2Cl_2 4:6). Orange-red oil; **^{1}H NMR (500 MHz, DMSO-*d*$_6$+0.1% TFA-*d*)** δ 8.34 (d, *J* = 7.5 Hz, 1H), 7.09 (dd, *J* = 14.9, 11.3 Hz, 1H), 6.75–6.64 (m, 1H), 6.61–6.22 (m, 14H), 6.18–6.06 (m, 2H), 4.31–4.23 (m, 1H), 3.91–3.81 (m, 1H), 2.25–2.12 (m, 2H), 1.28 (d, *J* = 7.4 Hz, 6H), 0.83 (s, 9H), –0.05 (s, 6H). **HRMS (ESI):** $[M–H]^+$ calcd. $C_{31}H_{44}NO_4Si$: 522.3045, found 522.3050. Owing to the unusual physical properties of this kind of compounds in terms of solubility, a clear ^{13}C NMR could not be obtained even using long acquisition times. **Solubility**: DMSO +0.1% TFA (0.02 M, fully soluble)

Synthesis of **P9**: According to GP-4 (using 12 mL of THF, and adding non-washed Amberlyst), **P9** was synthesized from **22**, with a 13% yield (MeOH/CH_2Cl_2 7:3). Deep orange oil; **^{1}H NMR (600 MHz, CD_3OD)** δ 7.32–7.08 (m, 1H), 6.91–5.89 (m, 16H), 5.82–5.69 (m, 1H), 4.41–4.28 (m, 1H), 2.39–2.11 (m, 2H), 1.25 (bs, 3H), 0.85 (bs, 3H); Owing to the unusual physical properties of this kind of compound in terms of solubility, a clear ^{13}C NMR could not be obtained in any solvent even using long acquisition times. **HRMS (ESI):** $[M–H]^+$ calcd. $C_{25}H_{30}NO_4$: 408.2180, found 408.2198. **Solubility**: DMSO +0.1% TFA (0.02 M)

^{1}H and ^{13}C NMR FOR NEW COMPOUNDS

^{1}H NMR **3** (400 MHz, $CDCl_3$)

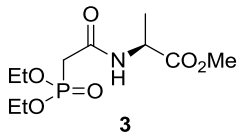

3

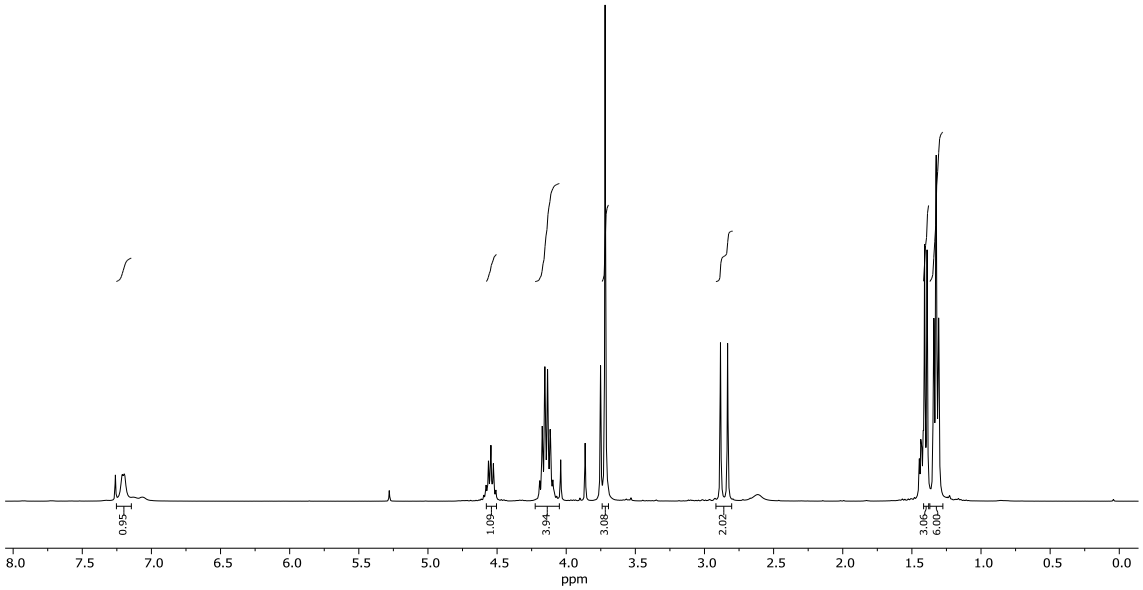

^{13}C NMR **3** (101 MHz, $CDCl_3$)

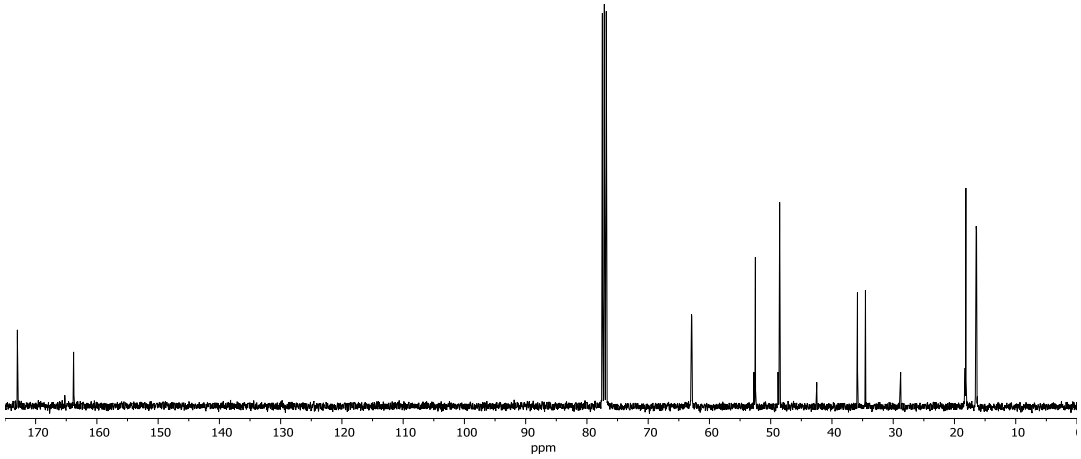

^{31}P NMR **3** (202 MHz, $CDCl_3$)

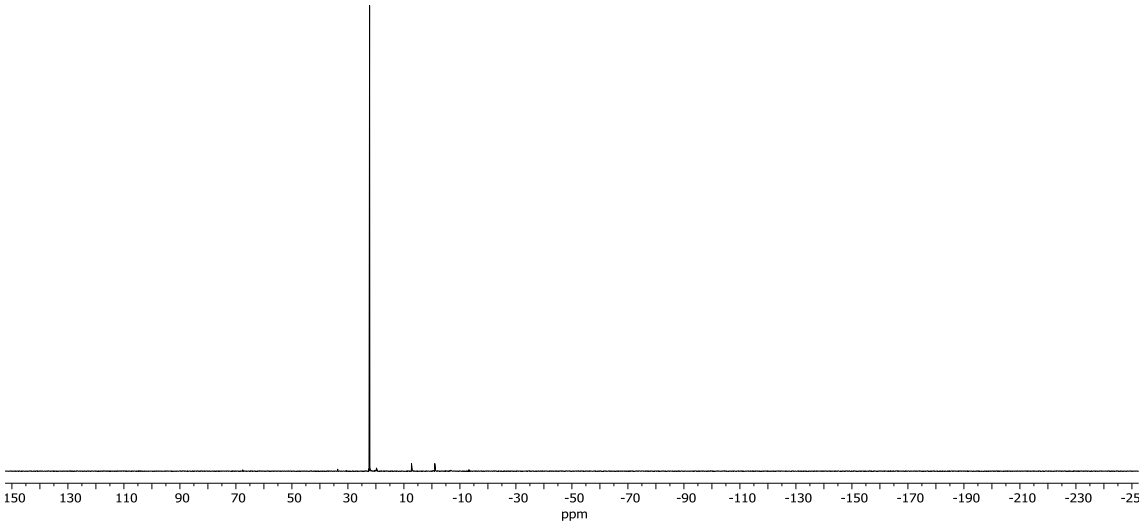

^{1}H NMR **7** (500 MHz, $CDCl_3$)

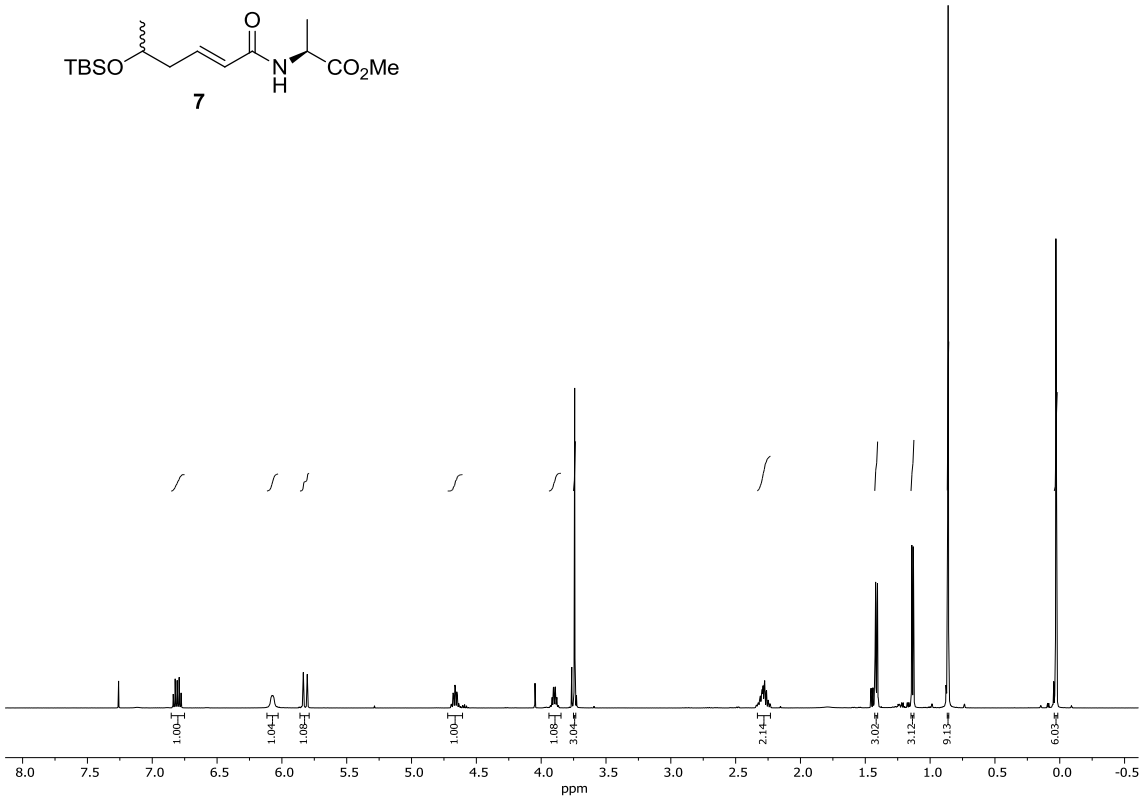

^{13}C NMR **7** (126 MHz, $CDCl_3$)

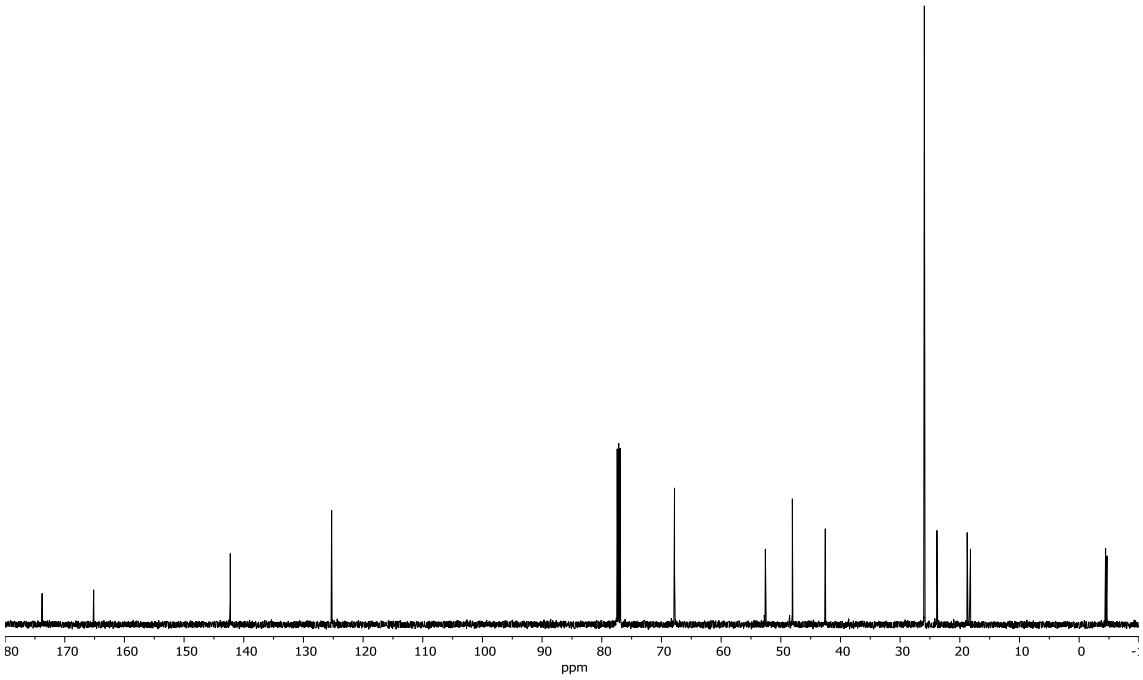

^{1}H NMR **pP1** (500 MHz, $CDCl_3$)

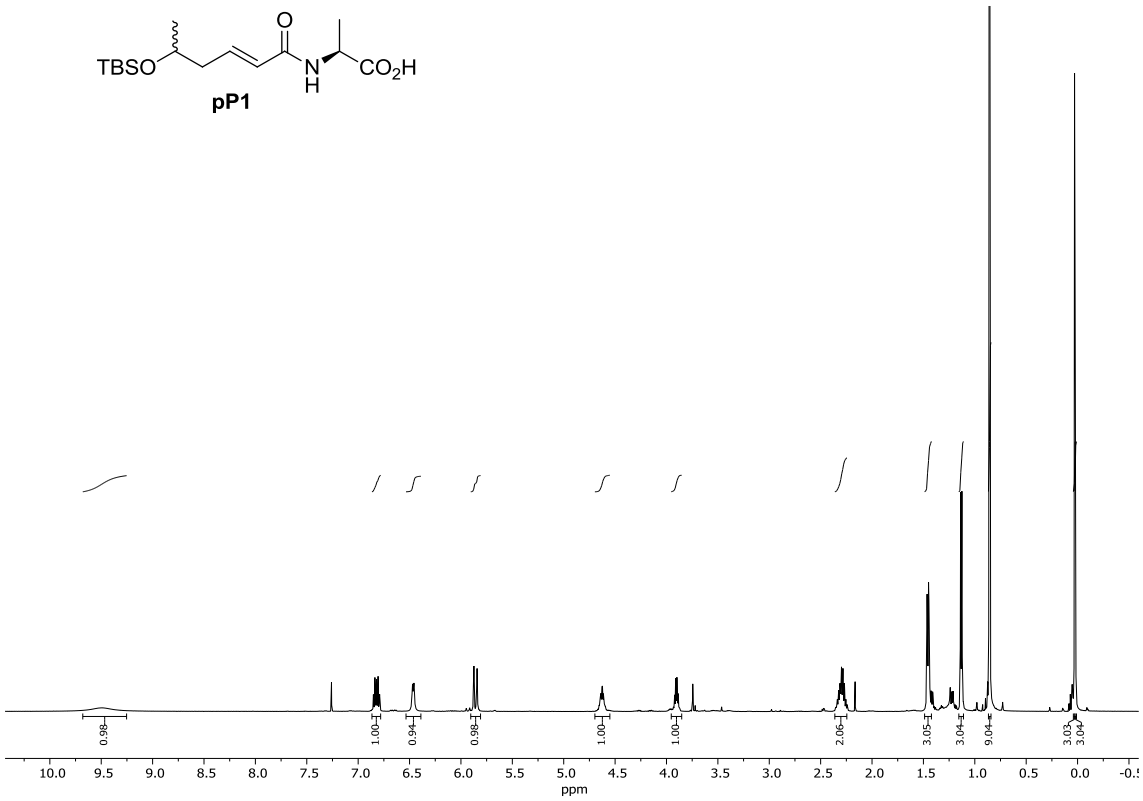

^{13}C NMR **pP1** (126 MHz, $CDCl_3$)

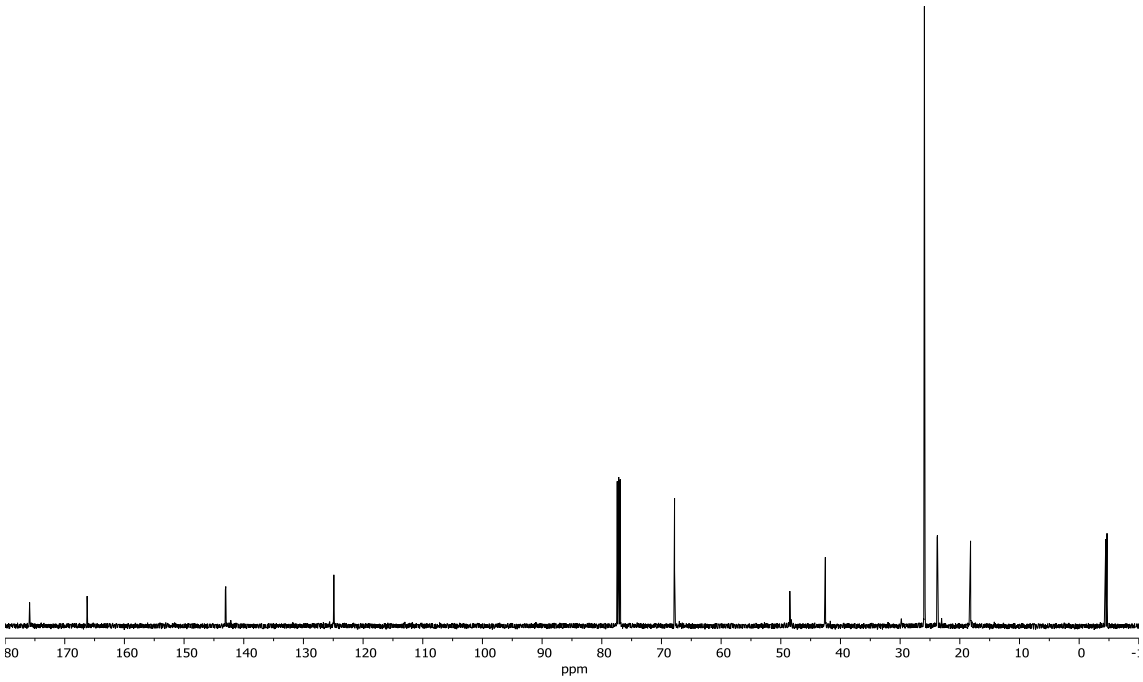
80
170
160
150
140
130
120
110
100
90
80
70
60
50
40
30
20
10
0
ppm

^{1}H NMR **9** major isomer (*E*,*E*,*E*-isomer) (500 MHz, $CDCl_3$)

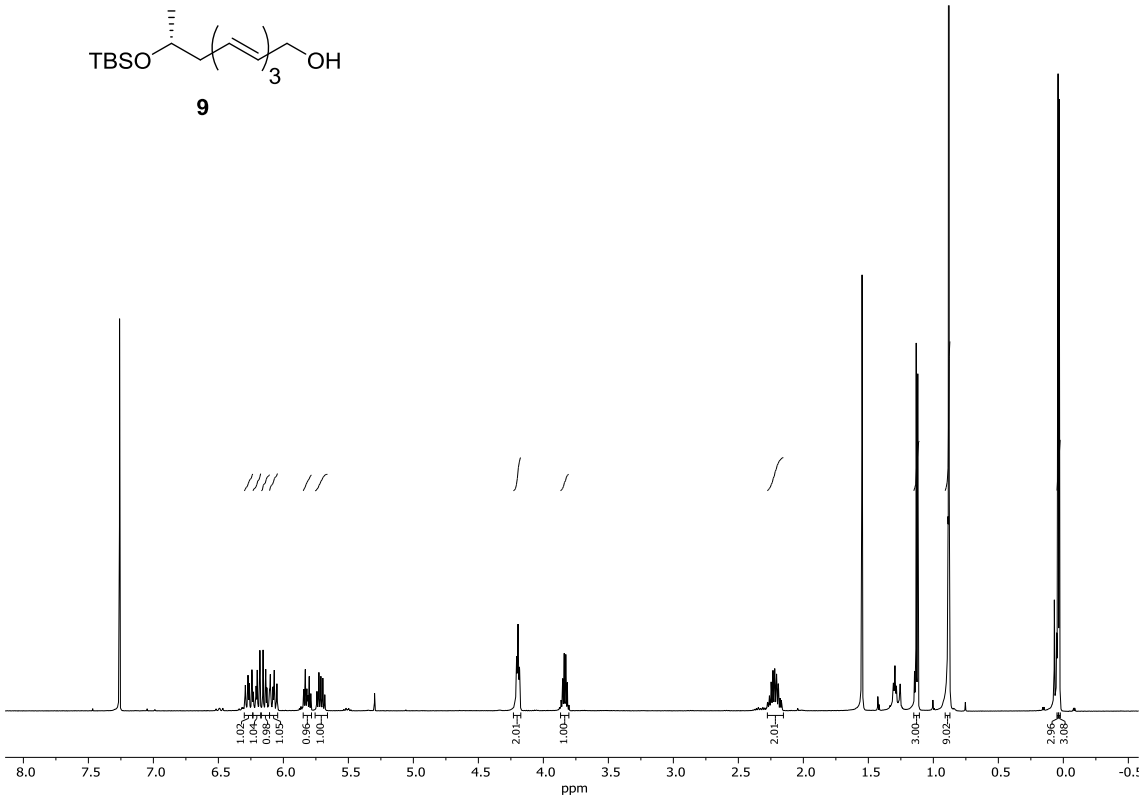

^{13}C NMR **9** major isomer (*E*,*E*,*E*-isomer) (126 MHz, $CDCl_3$)

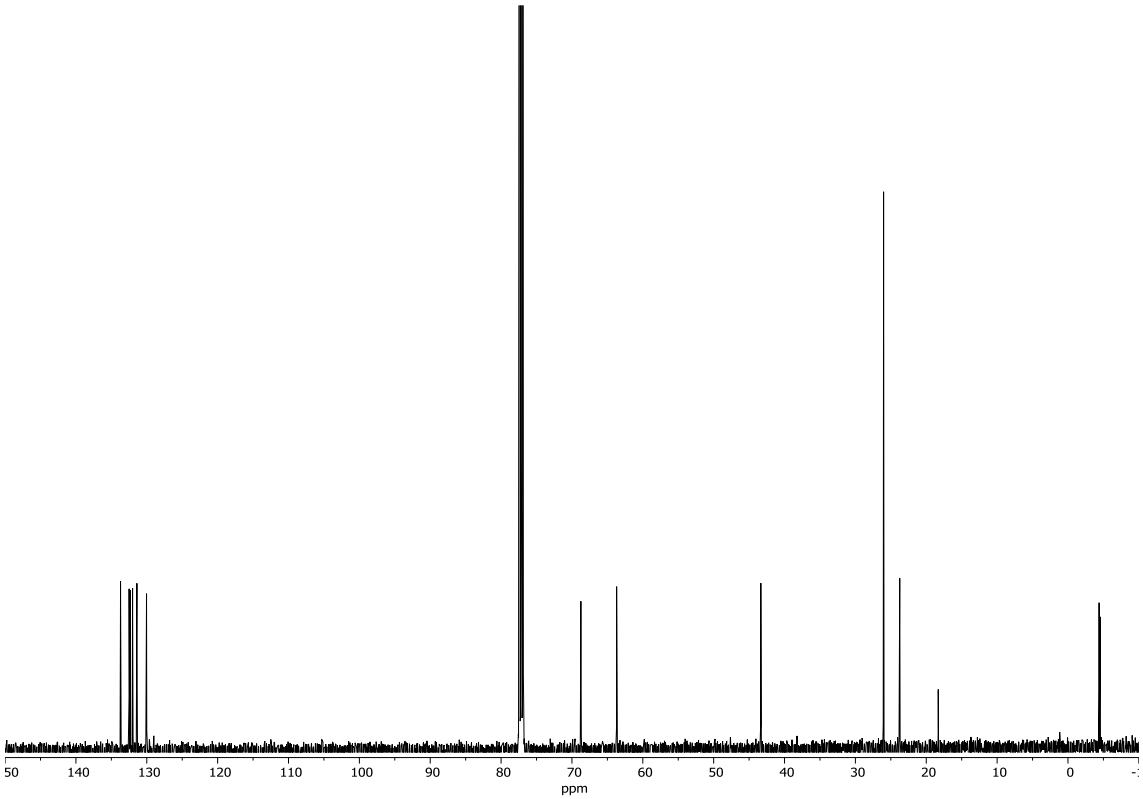

^{1}H NMR **9** minor isomer (*E*,*Z*,*E*-isomer) (500 MHz, $CDCl_3$)

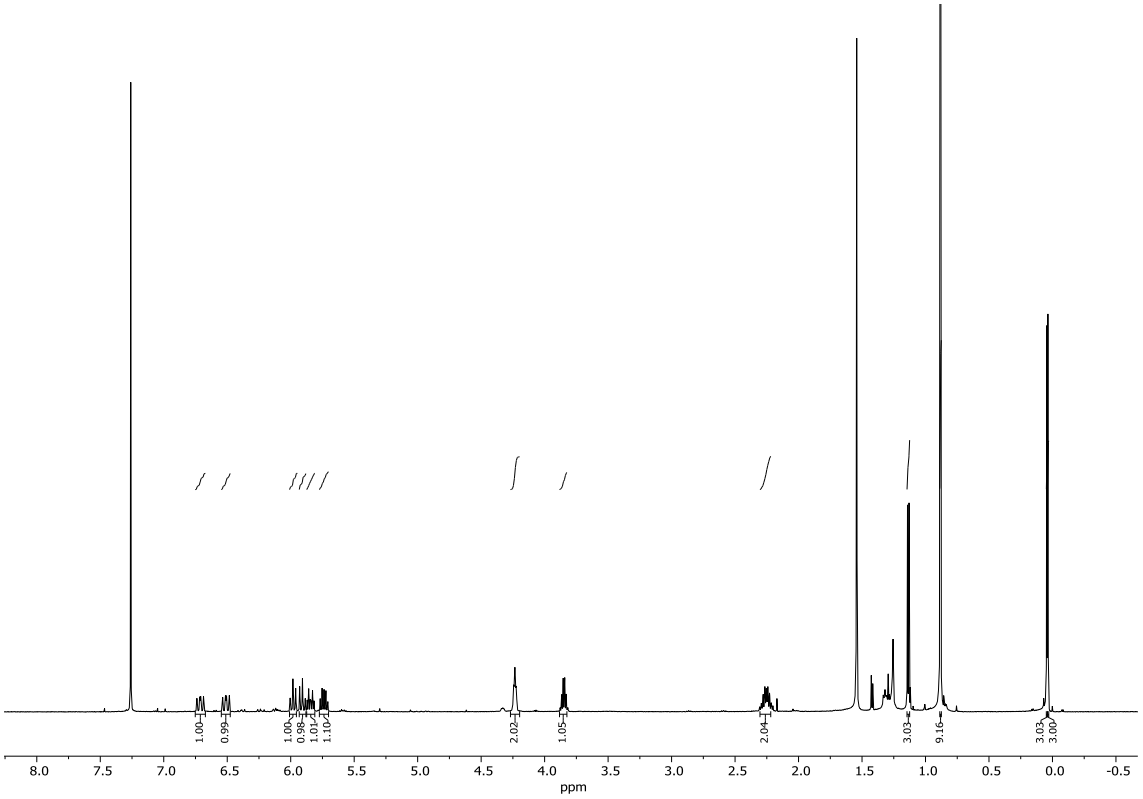

HSQC

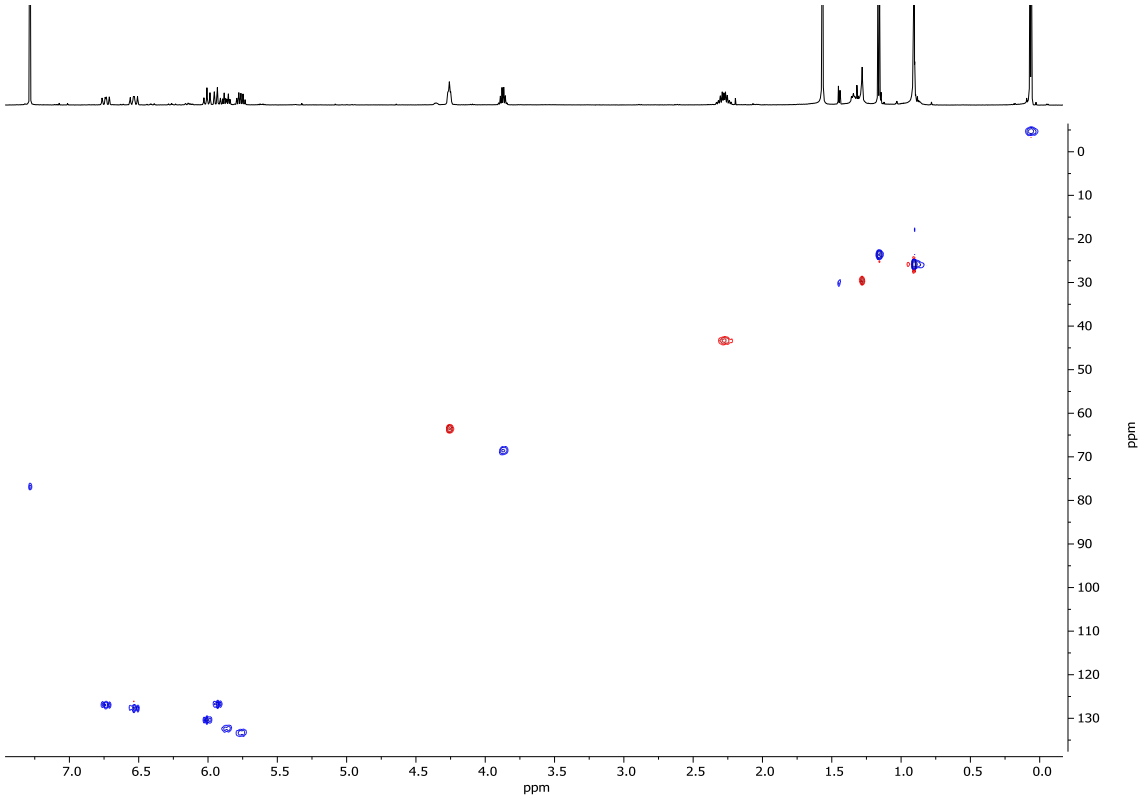
7.0
6.5
6.0
5.5
5.0
4.5
4.0
3.5
3.0
2.5
2.0
1.5
1.0
0.5
0.0
ppm
0
10
20
30
40
50
60
70
80
90
100
110
120
130
ppm

^{1}H NMR **9** minor isomer (*Z,E,E*-isomer) (500 MHz, $CDCl_3$)

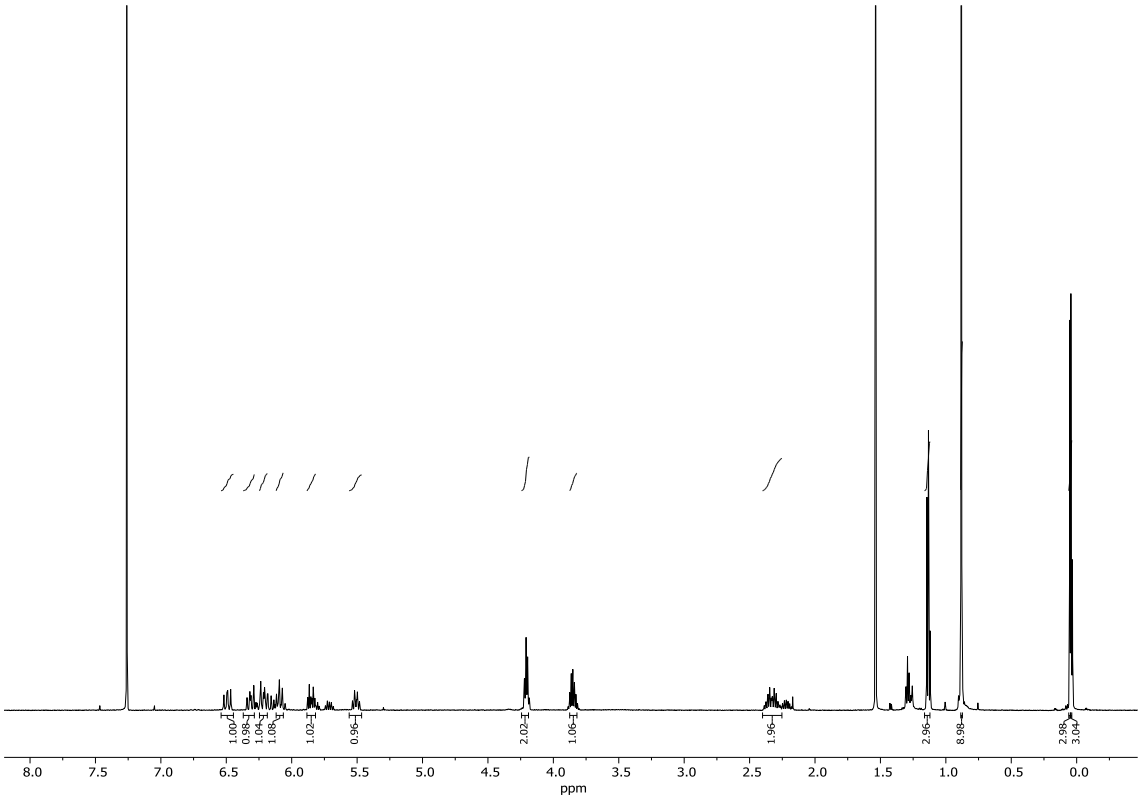

HSQC

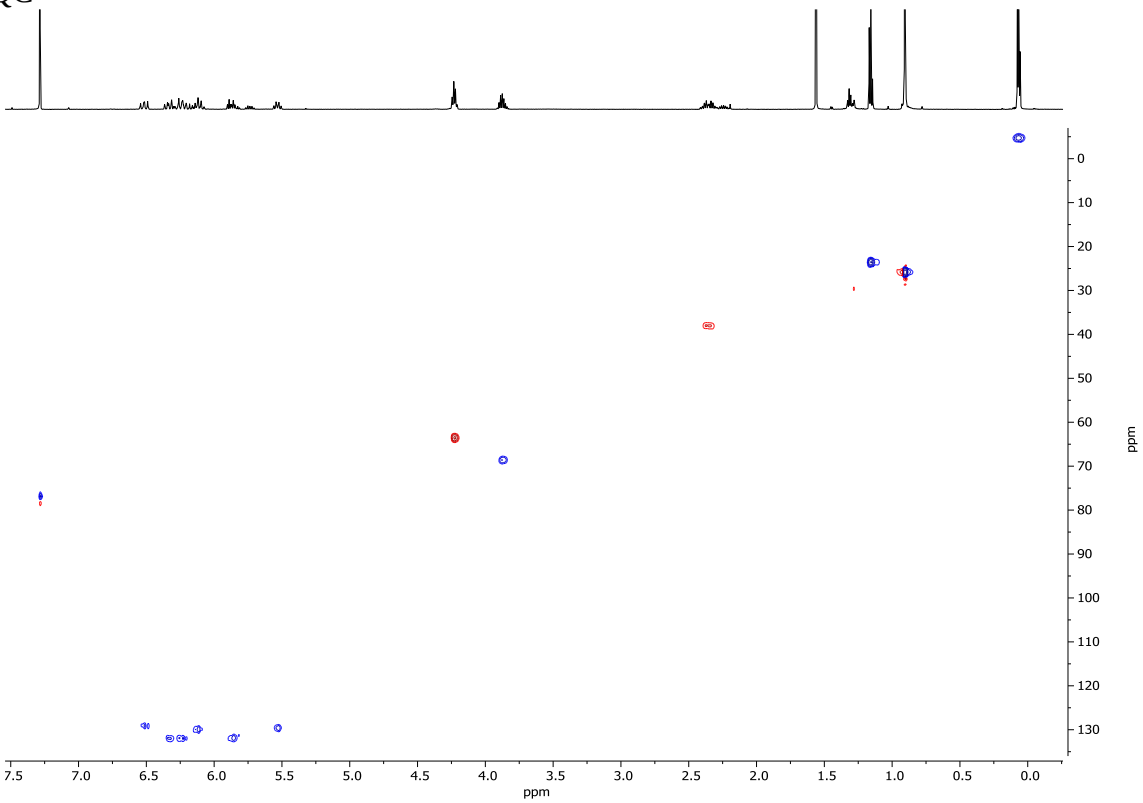

^{1}H NMR **10** *E*,*E*,*E*-isomer (400 MHz, $CDCl_3$)

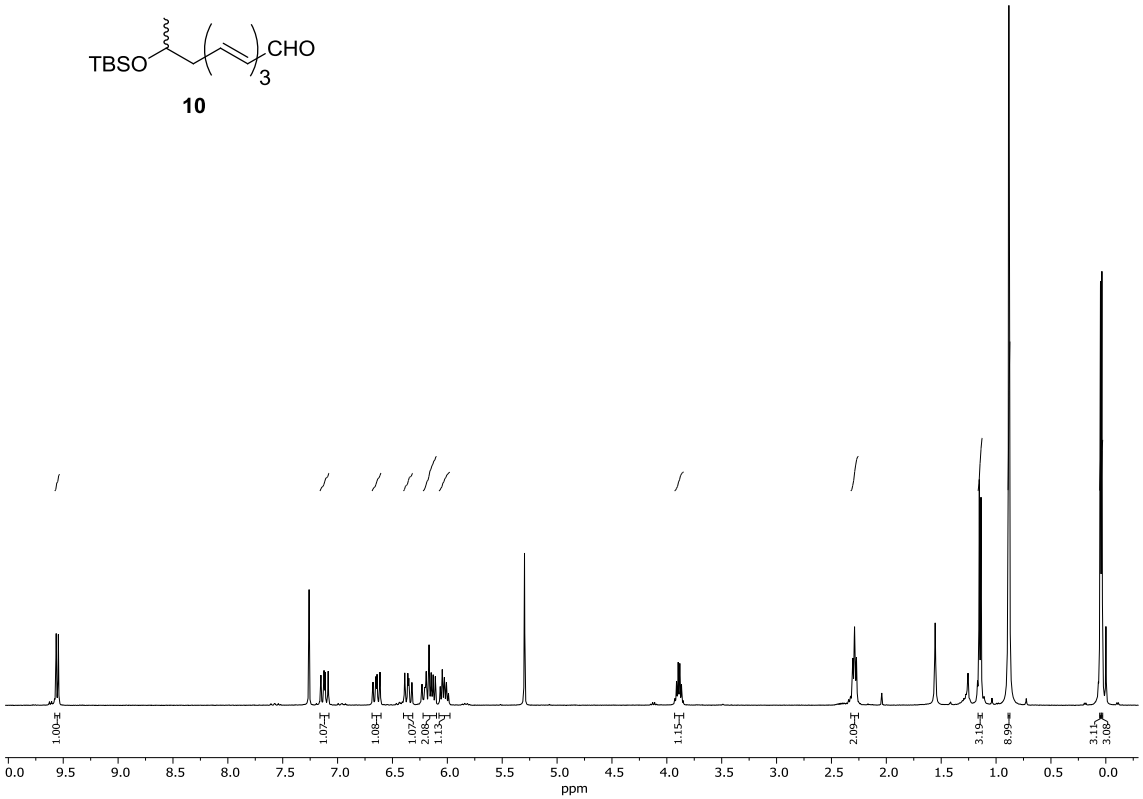

^{13}C NMR **10** *E*,*E*,*E*-isomer (101 MHz, $CDCl_3$)

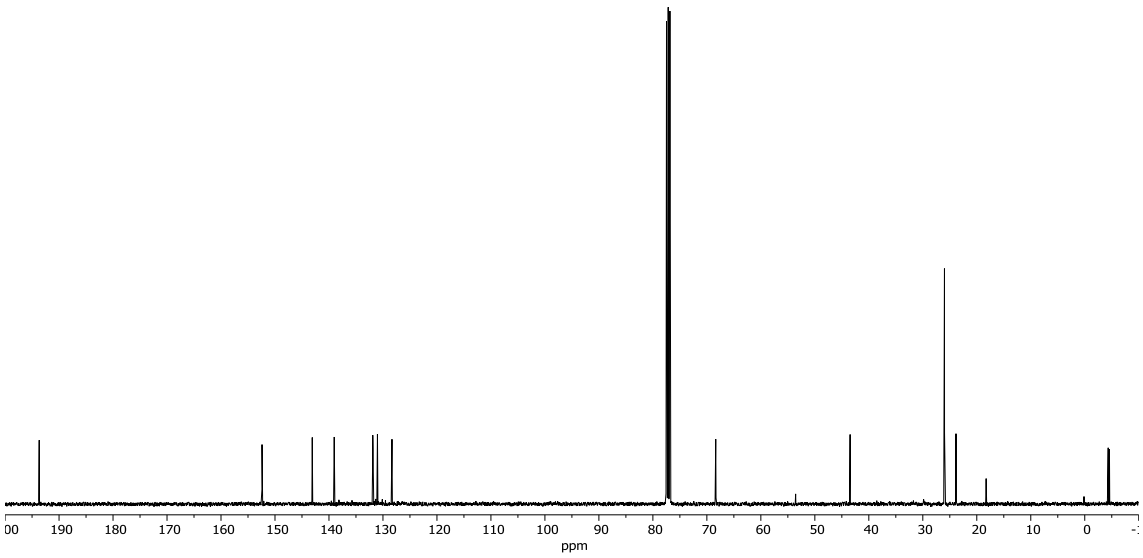

^{1}H NMR **11** *E*,*E*,*E*,*E*-isomer (500 MHz, $CDCl_3$)

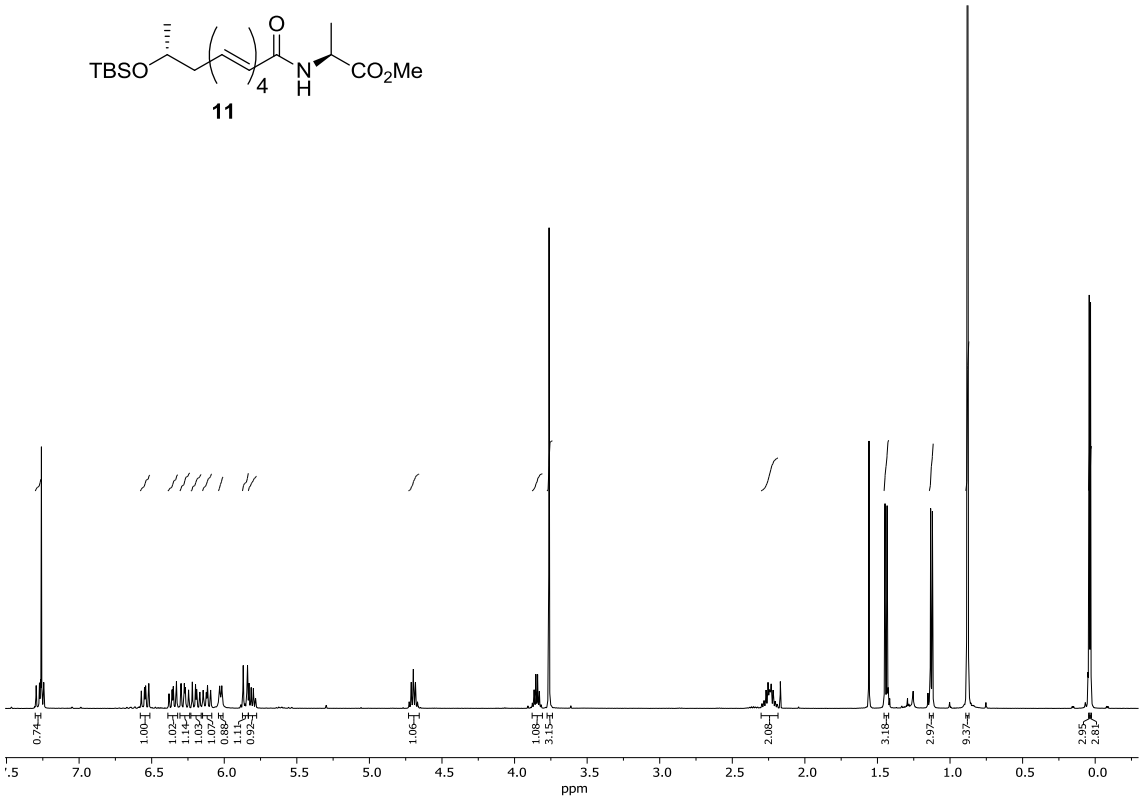

^{13}C NMR **11** *E*,*E*,*E*,*E*-isomer (126 MHz, $CDCl_3$)

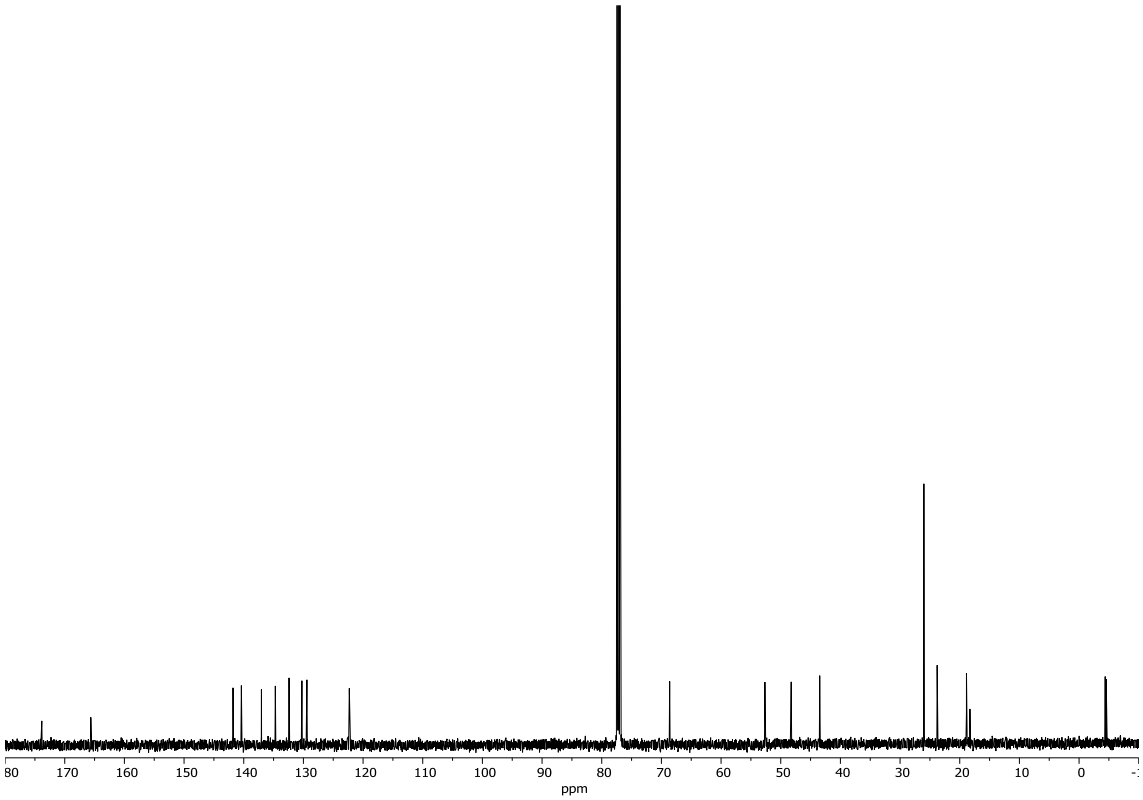

^{1}H NMR **12** *E*,*E*,*E*,*E*-isomer (500 MHz, $CDCl_3$)

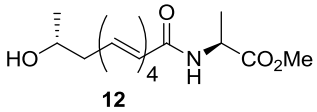

12

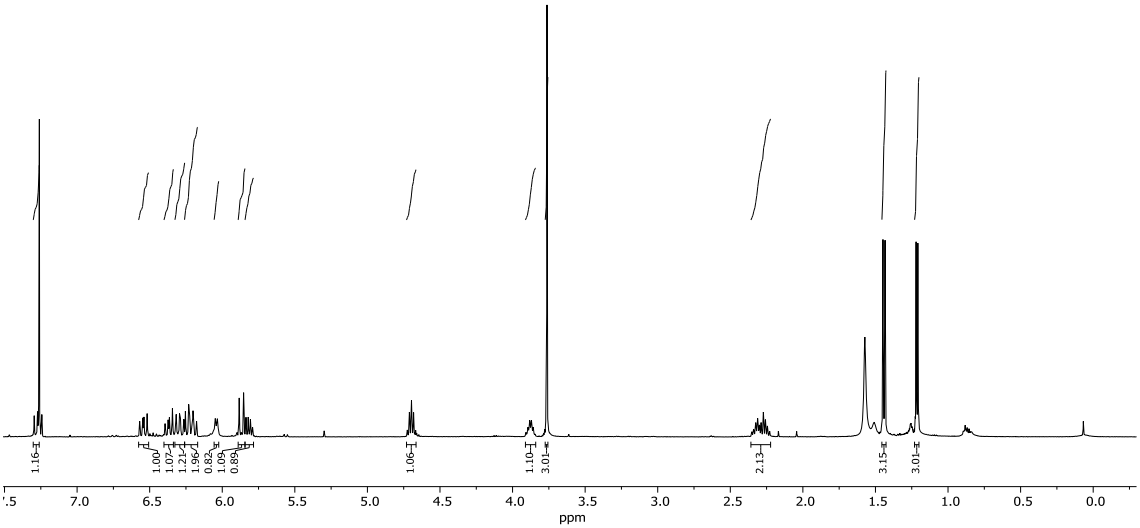

^{13}C NMR **12** *E*,*E*,*E*,*E*-isomer (126 MHz, $CDCl_3$)

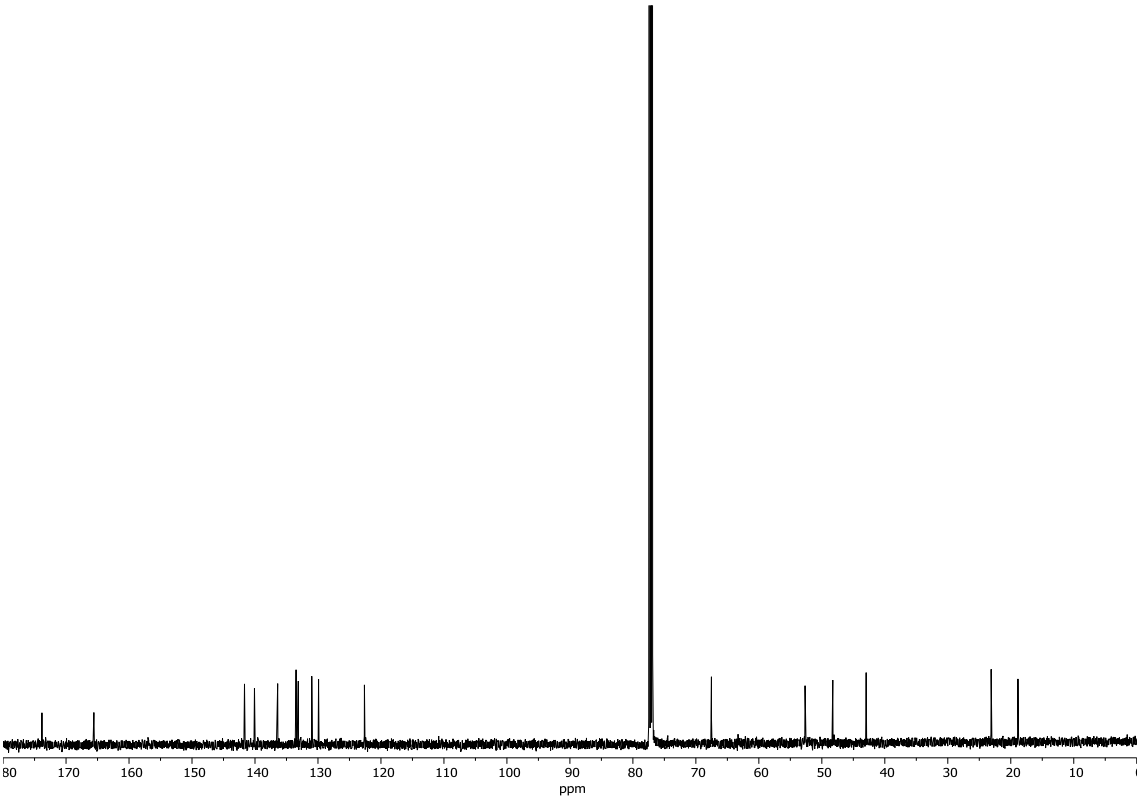

^{1}H NMR **14** *E*,*E*,*E*,*E*-isomer (500 MHz, $CDCl_3$)

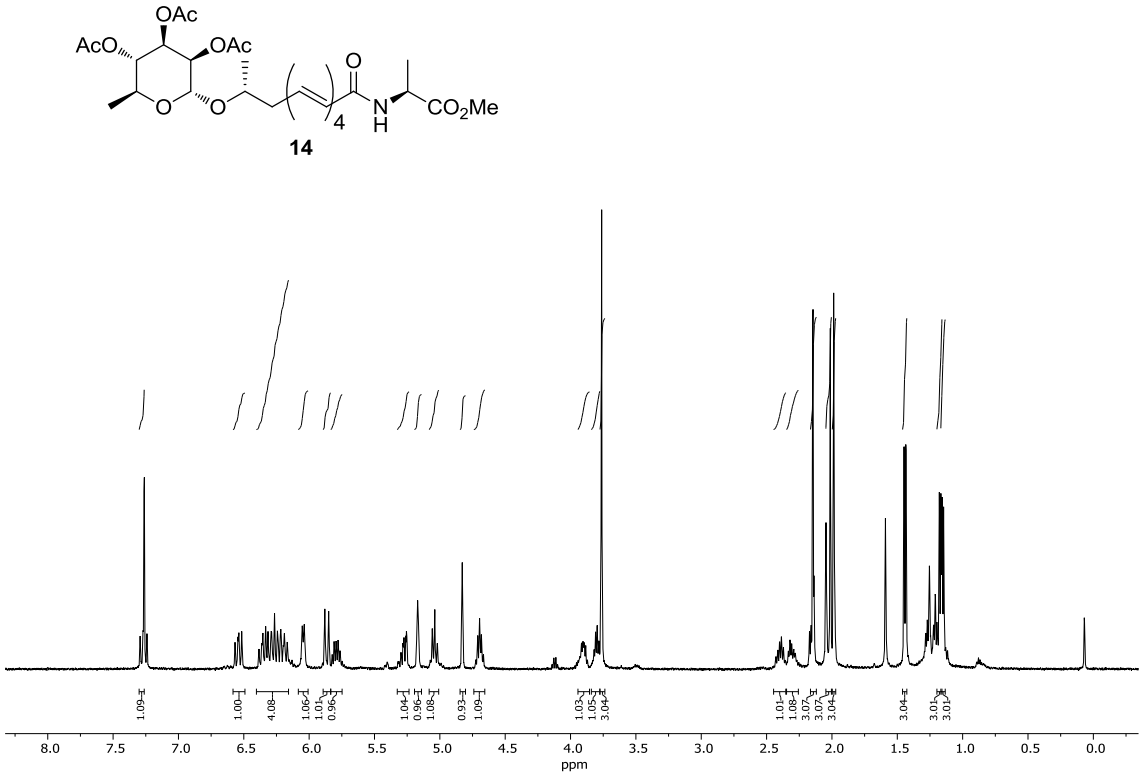

^{13}C NMR **14** *E*,*E*,*E*,*E*-isomer (126 MHz, $CDCl_3$)

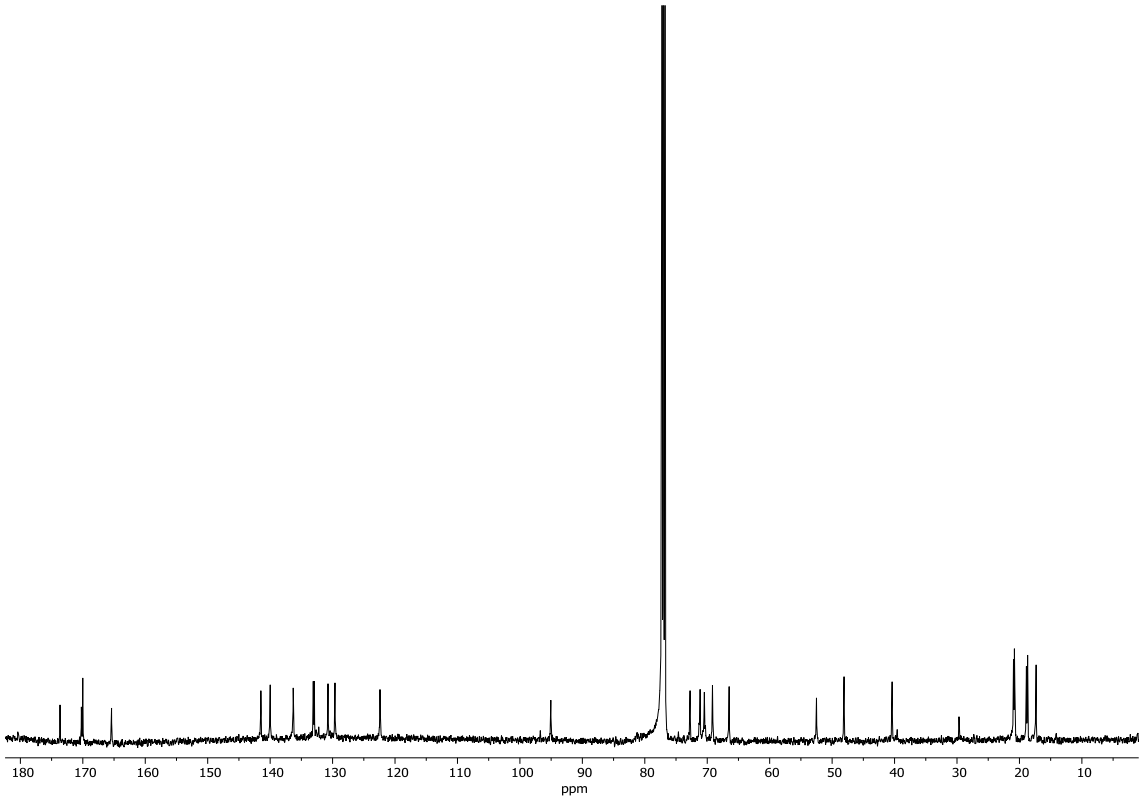

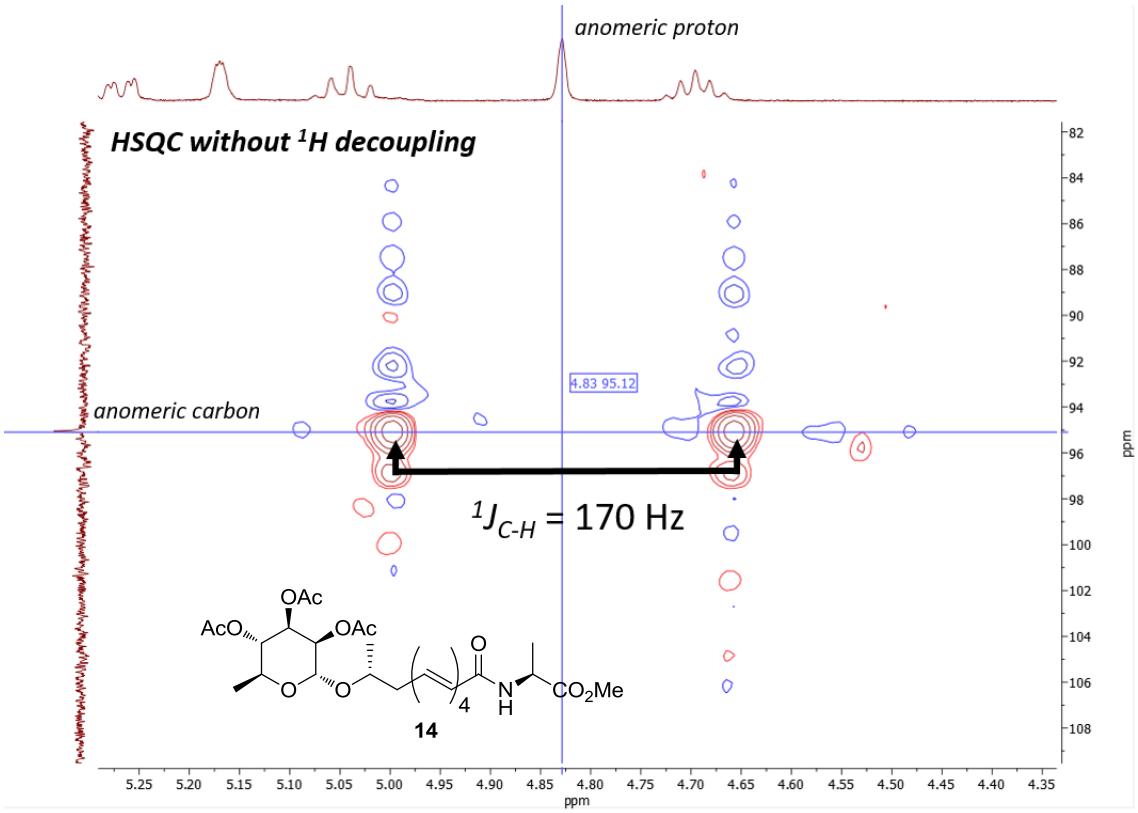

^{1}H NMR **14** (mixture of isomers) (500 MHz, $CDCl_3$)

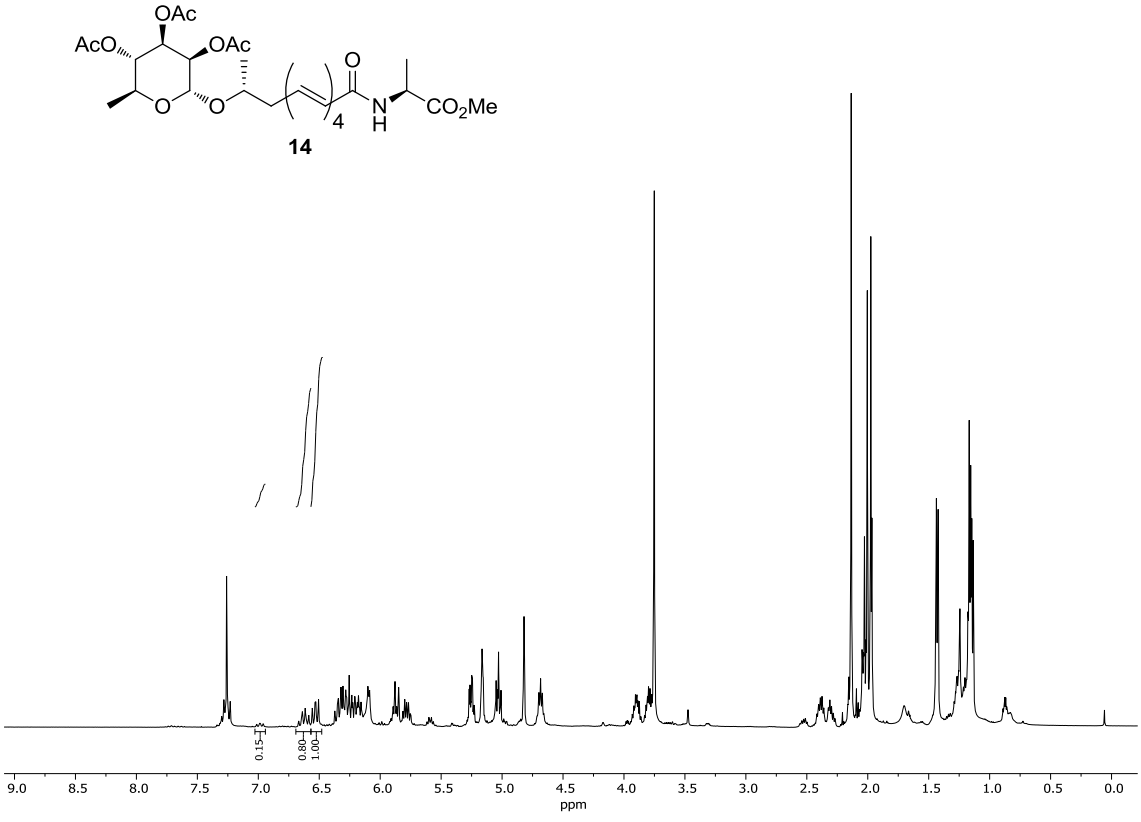

^{1}H NMR **R-P4** vaccine isomer (500 MHz, Methanol-d_4)

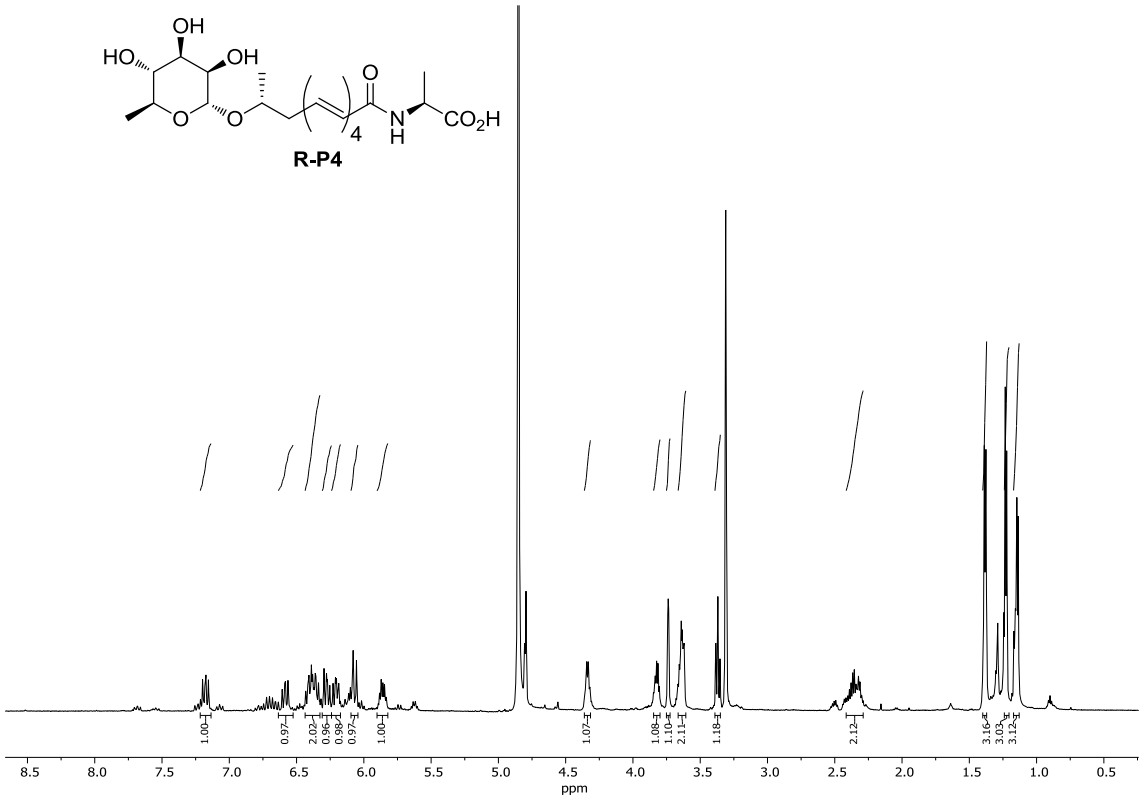

^{13}C NMR **R-P4** (126 MHz, Methanol-d_4)

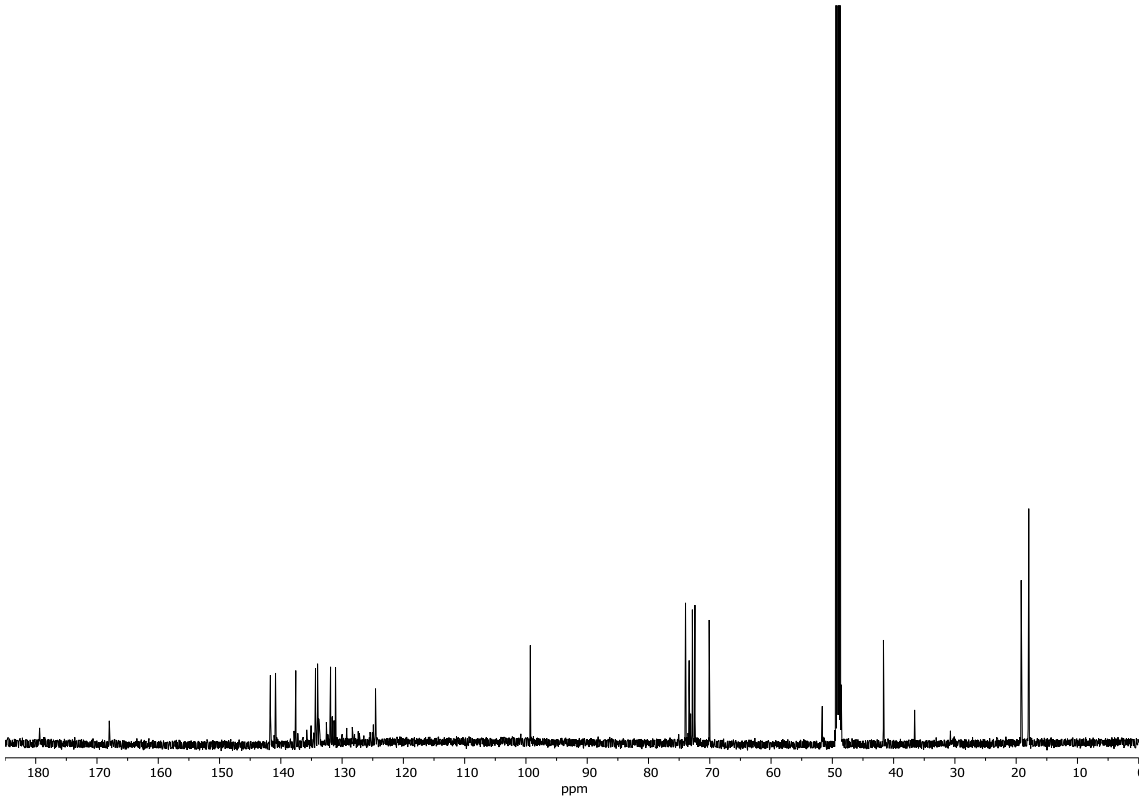

^{1}H NMR *all-E* **15** (500 MHz, $CDCl_3$)

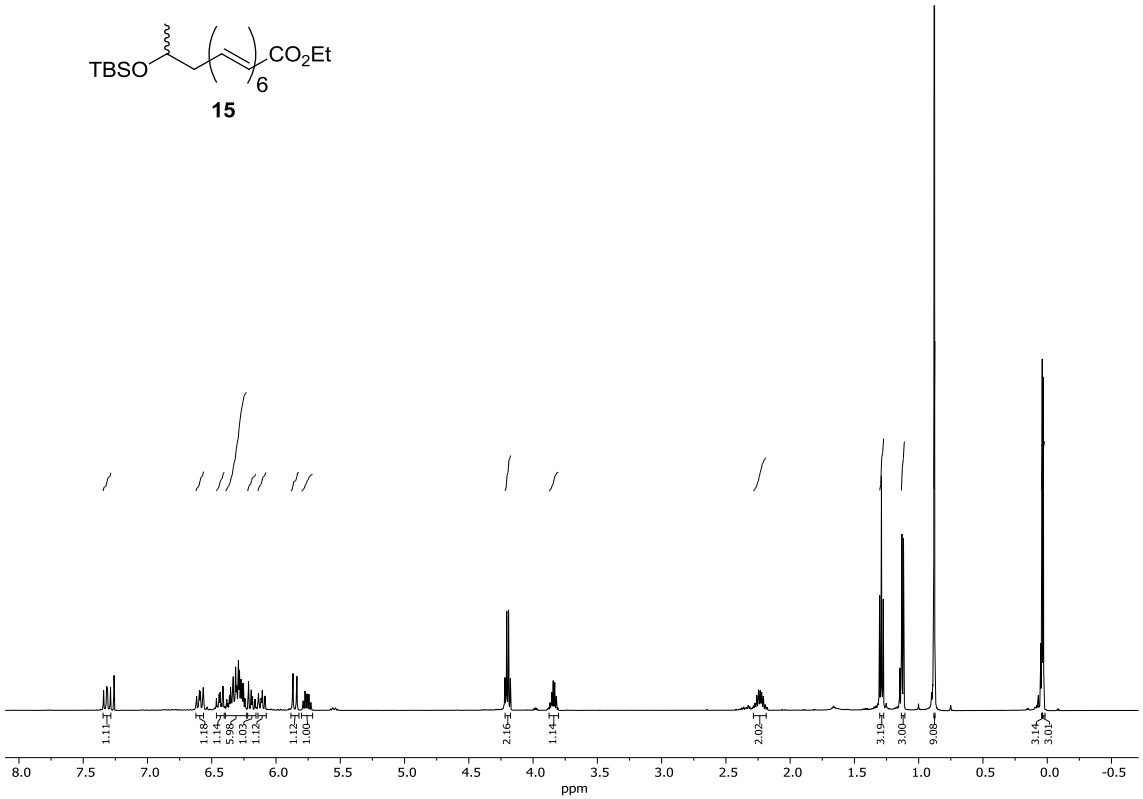

^{13}C NMR *all-E* **15** (126 MHz, $CDCl_3$)

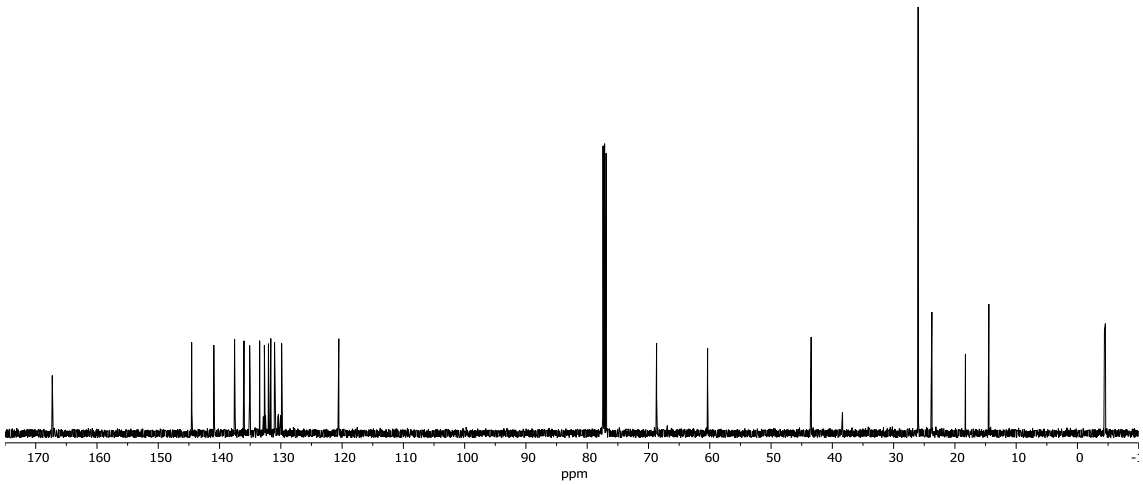

^{1}H NMR **16** (400 MHz, $CDCl_3$)

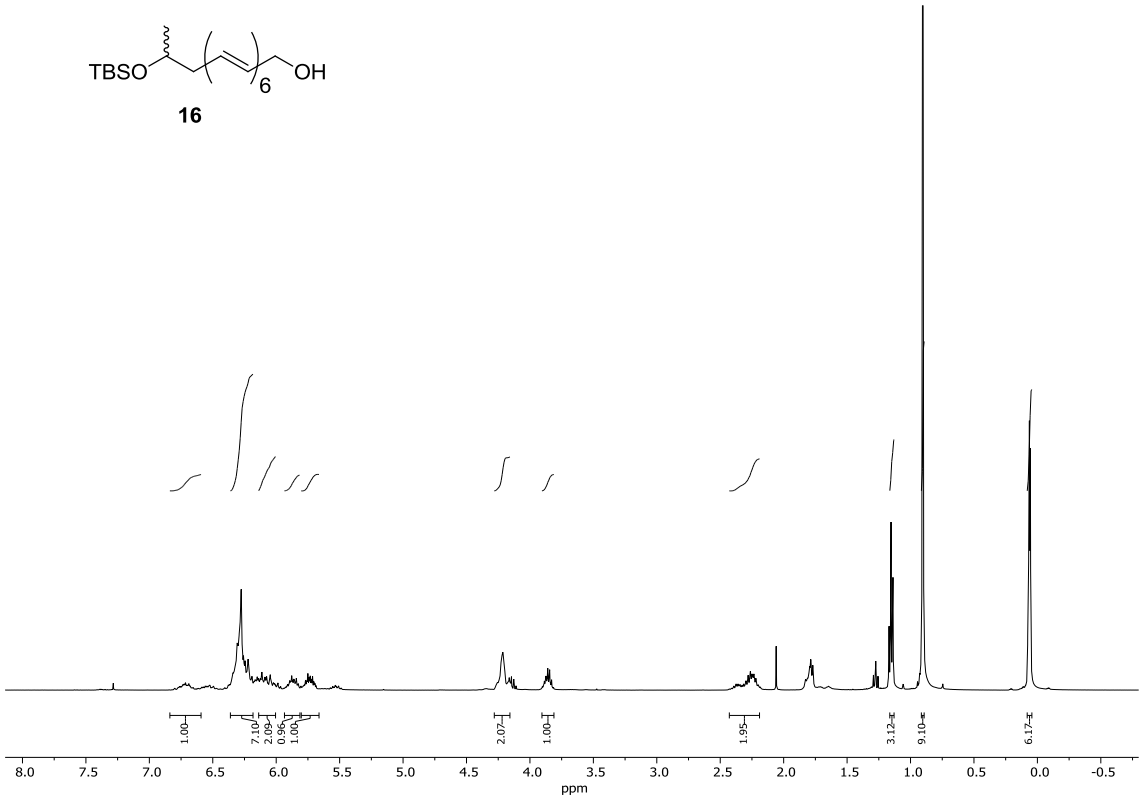

^{13}C NMR **16** (101 MHz, $CDCl_3$)

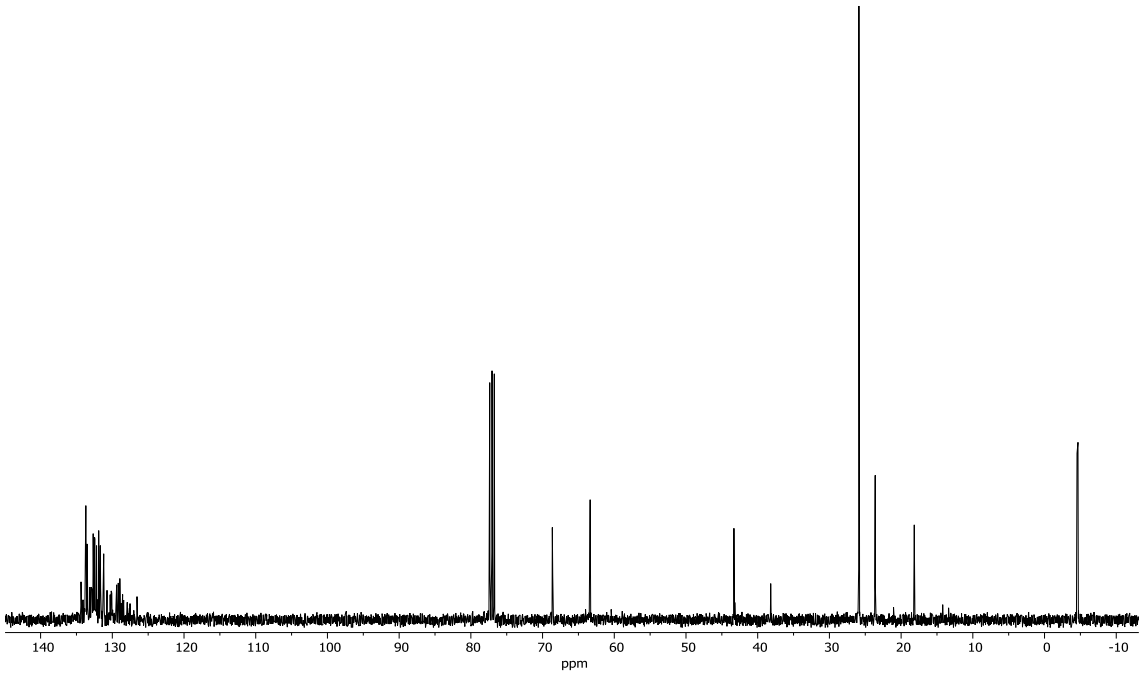

^{1}H NMR *all-E* **17** (500 MHz, $CDCl_3$)

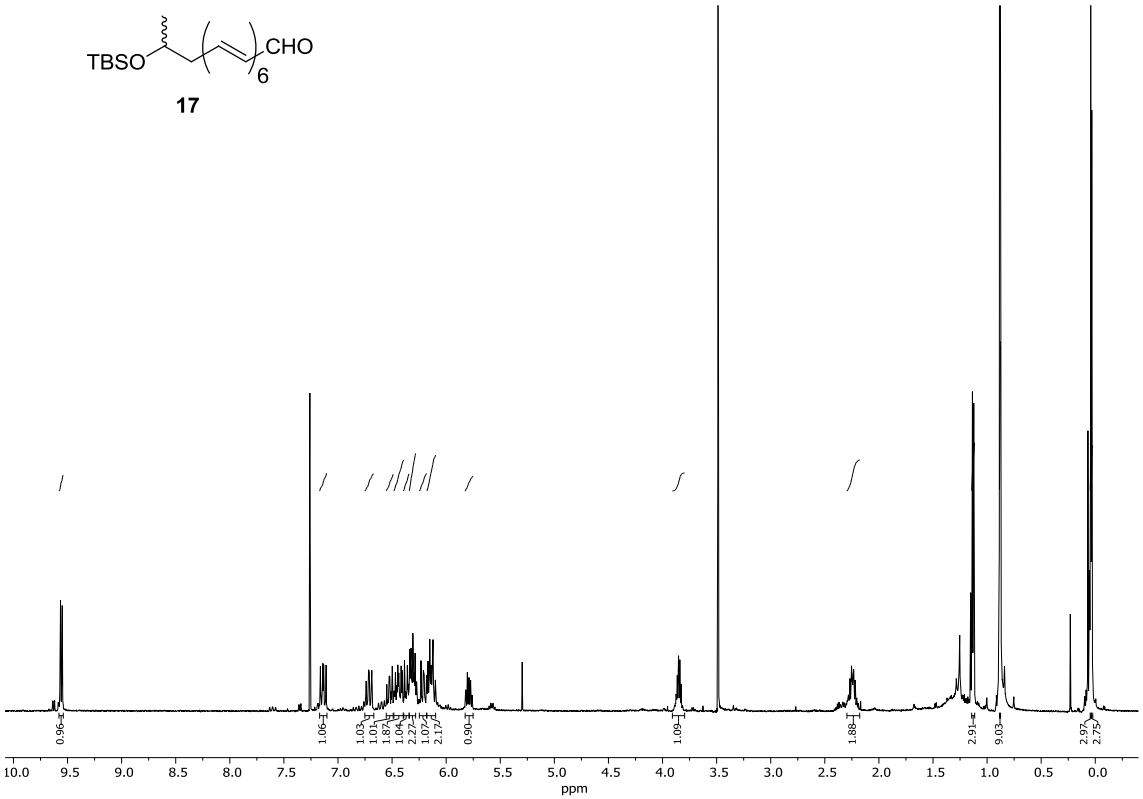

^{13}C NMR *all-E* **17** (126 MHz, $CDCl_3$)

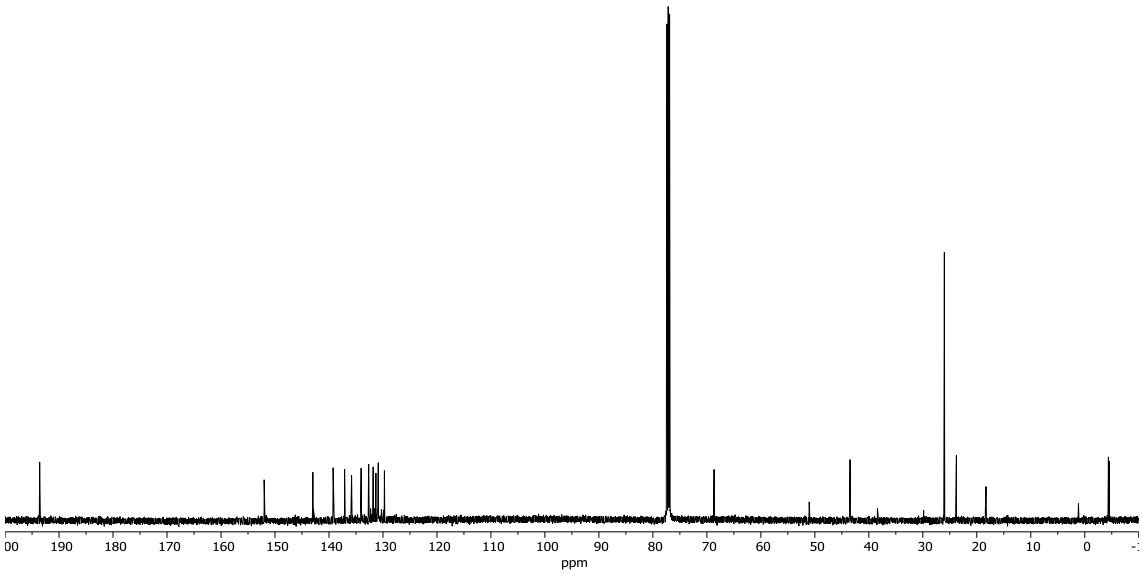

^{1}H NMR (500 MHz, $CDCl_3$) *all-E* isomer

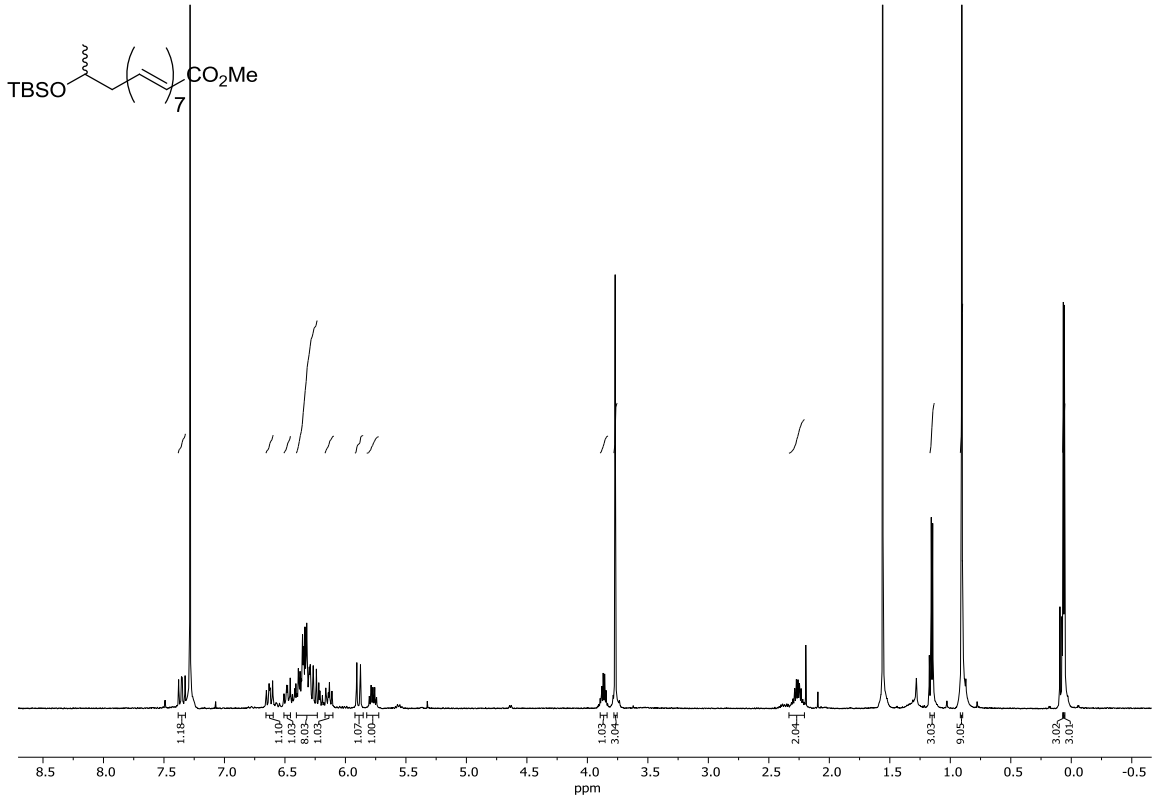

^{13}C NMR (126 MHz, $CDCl_3$) *all-E* isomer

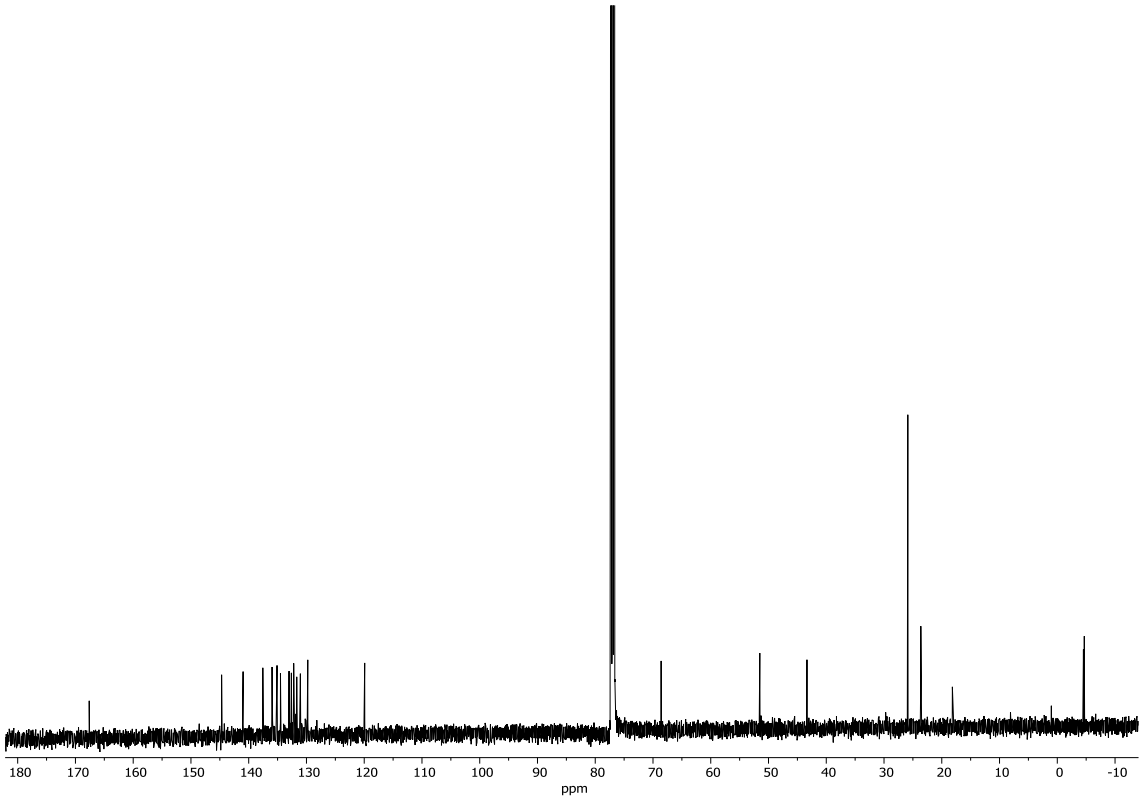

^{1}H NMR **pP7X** (500 MHz, Methanol-d_4)

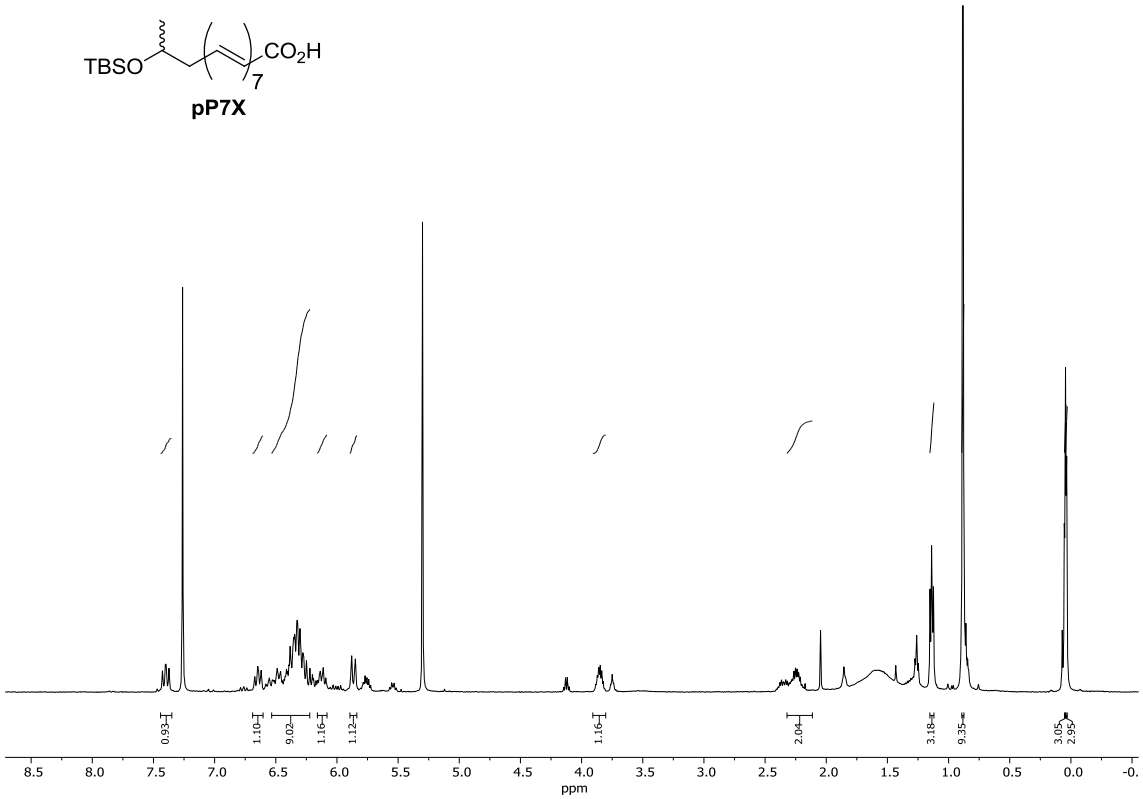

^{13}C NMR **pP7X** (126 MHz, Methanol-d_4)

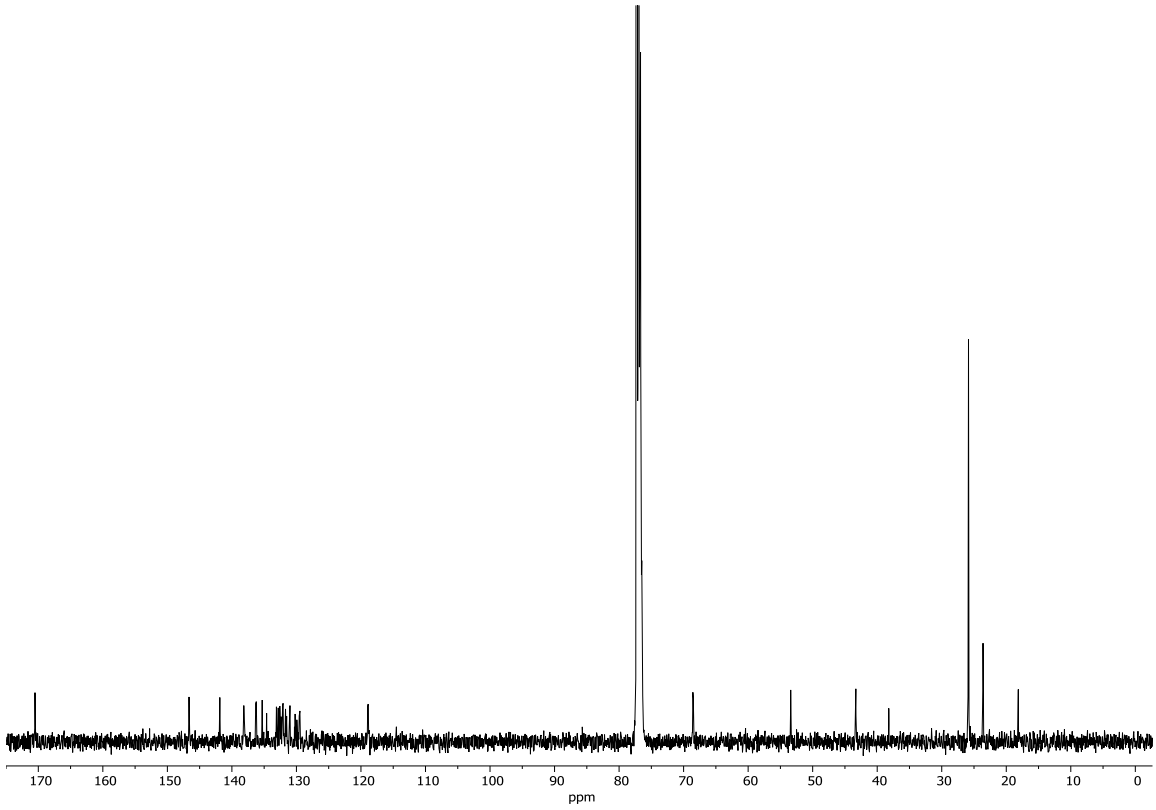

^{1}H NMR **18** (500 MHz, $CDCl_3$)

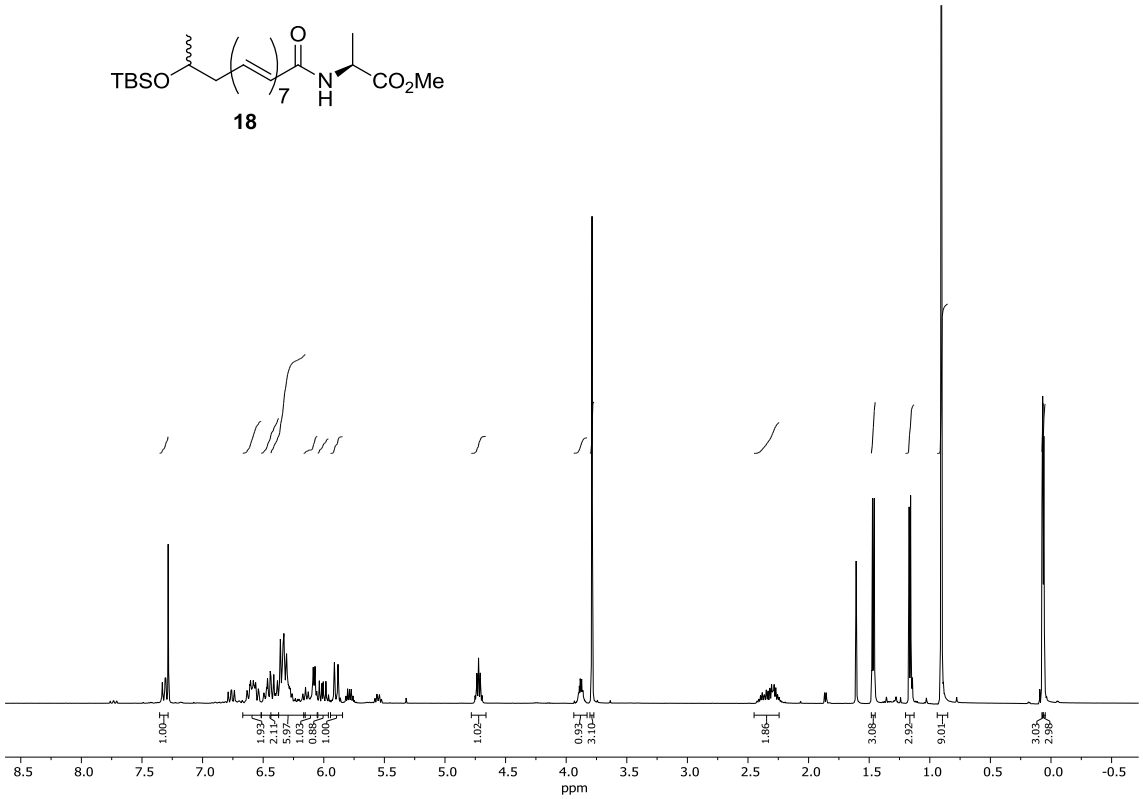

^{13}C NMR **18** (126 MHz, $CDCl_3$)

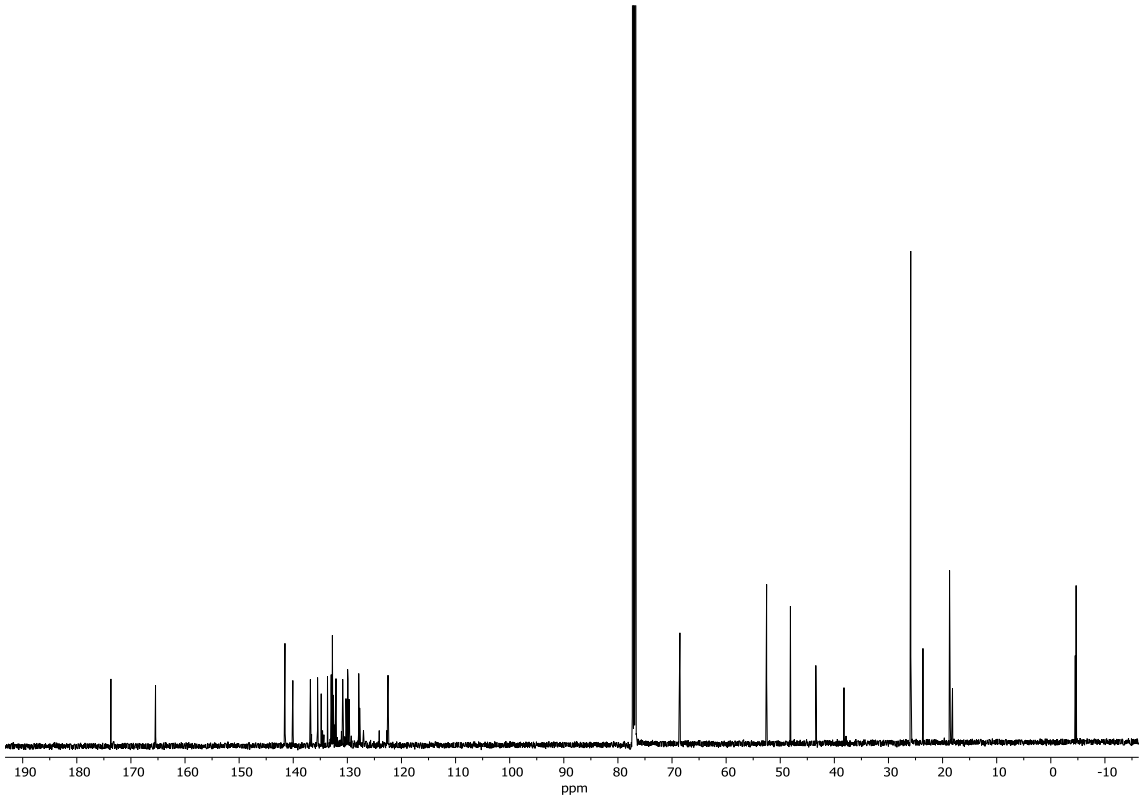

^{1}H NMR **pP7** (500 MHz, Methanol-d_4)

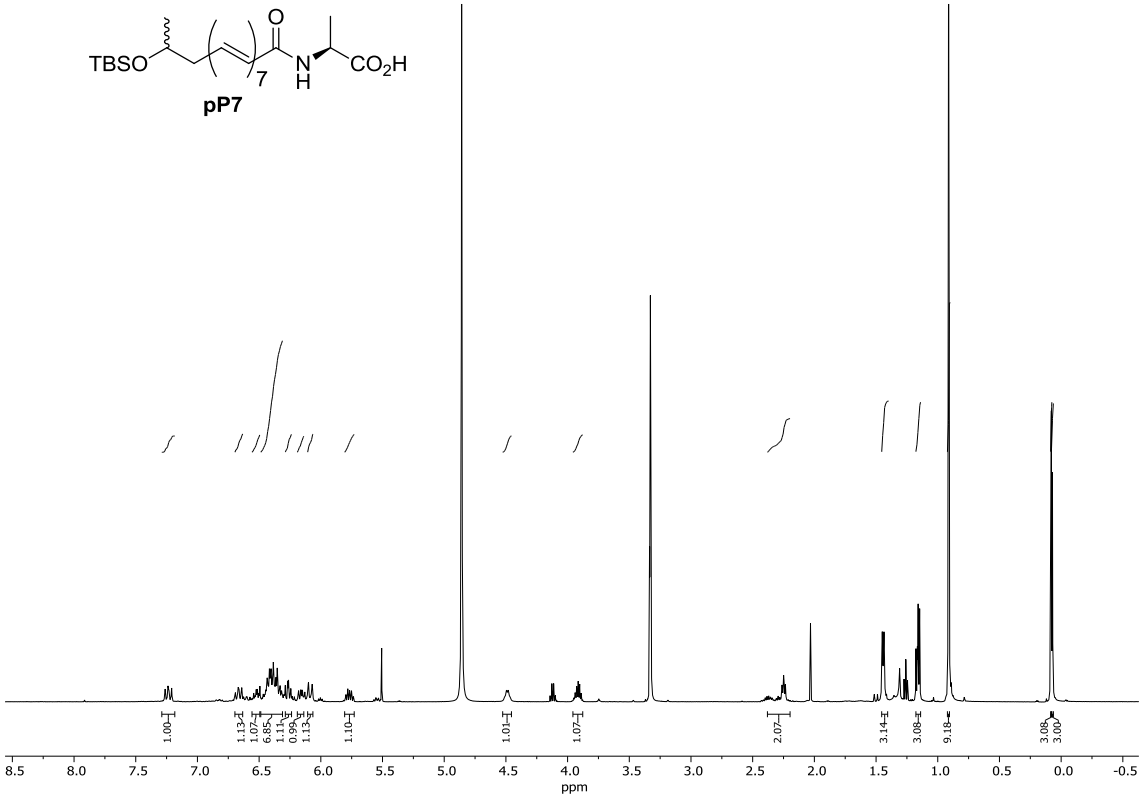

^{13}C NMR **pP7** (126 MHz, Methanol-d_4)

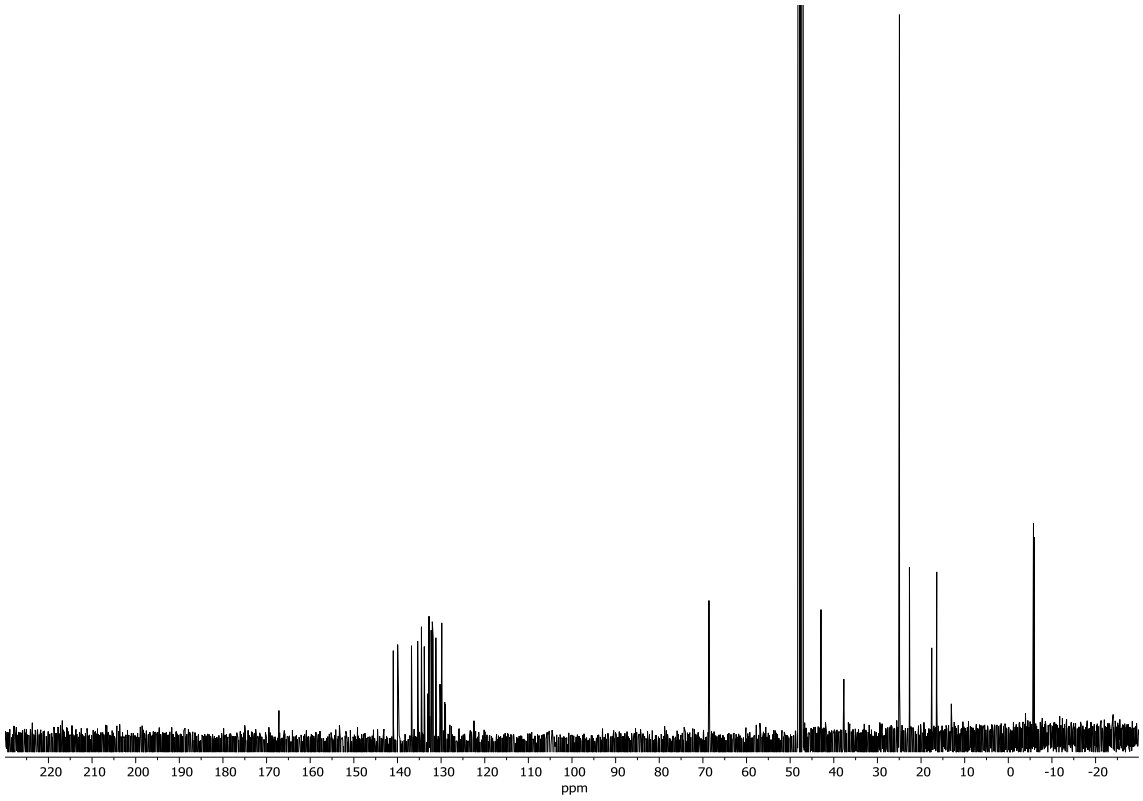
220 210 200 190 180 170 160 150 140 130 120 110 100 90 80 70 60 50 40 30 20 10 0 -10 -20
ppm

^{1}H NMR **P7** (500 MHz, Methanol-*d*$_4$)

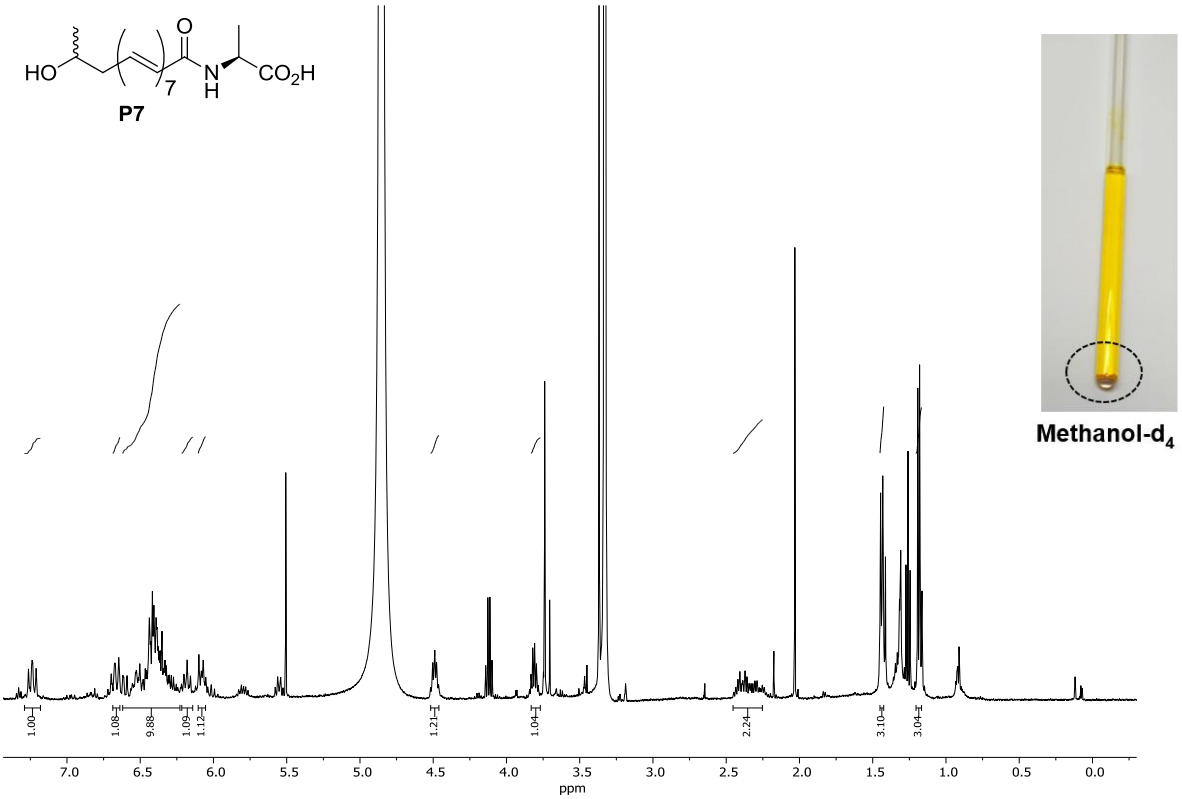

^{13}C NMR **P7** (500 MHz, Methanol-*d*$_4$)

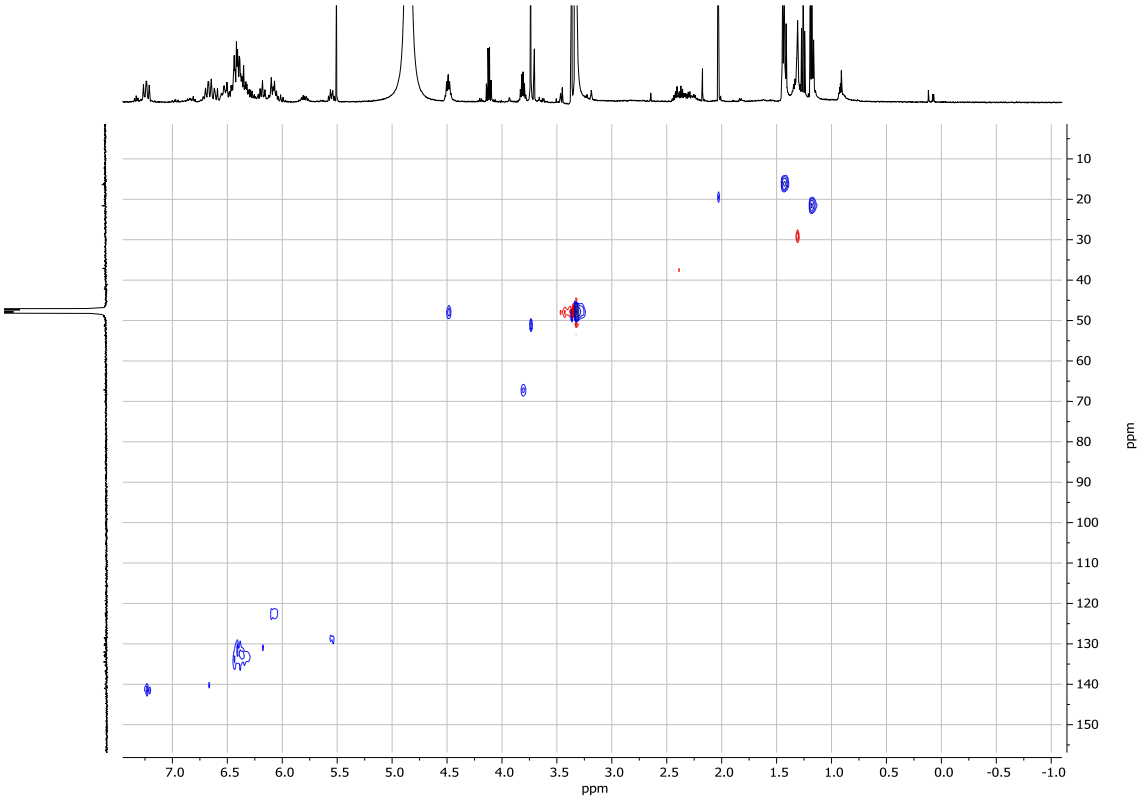

^{1}H NMR *all-E* **19** (500 MHz, $CDCl_3$)

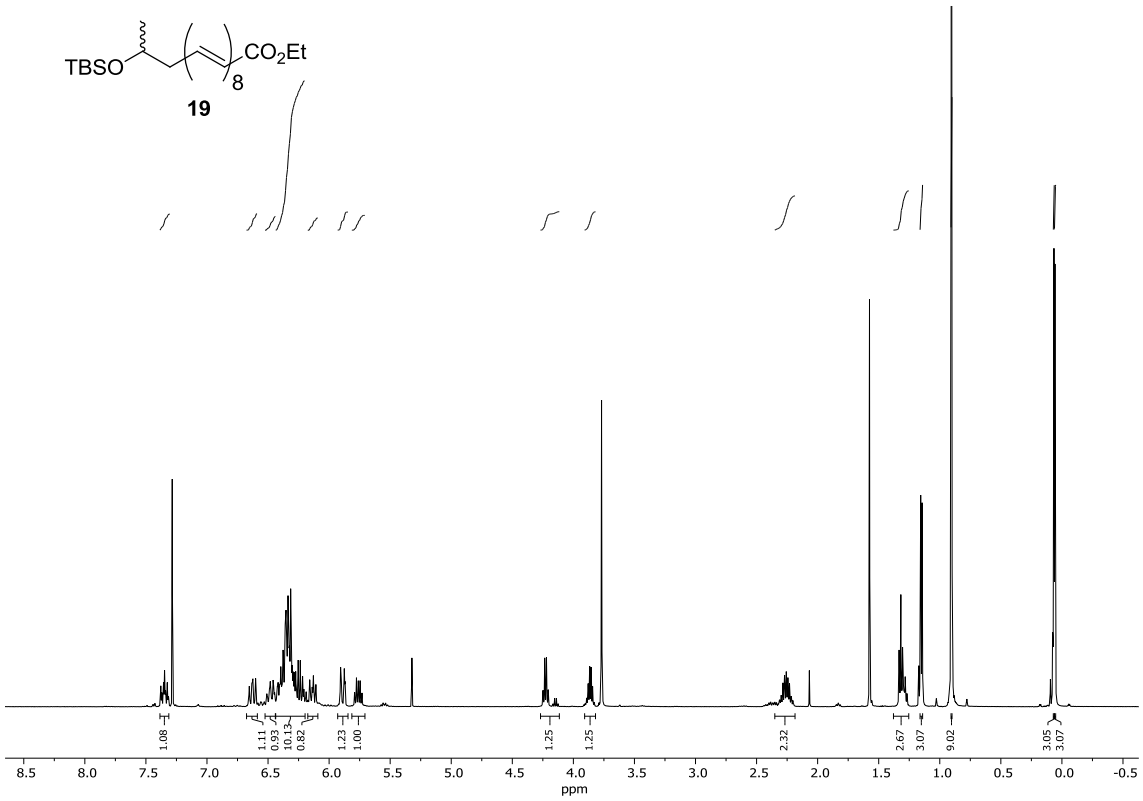

^{13}C NMR *all-E* **19** (126 MHz, $CDCl_3$)

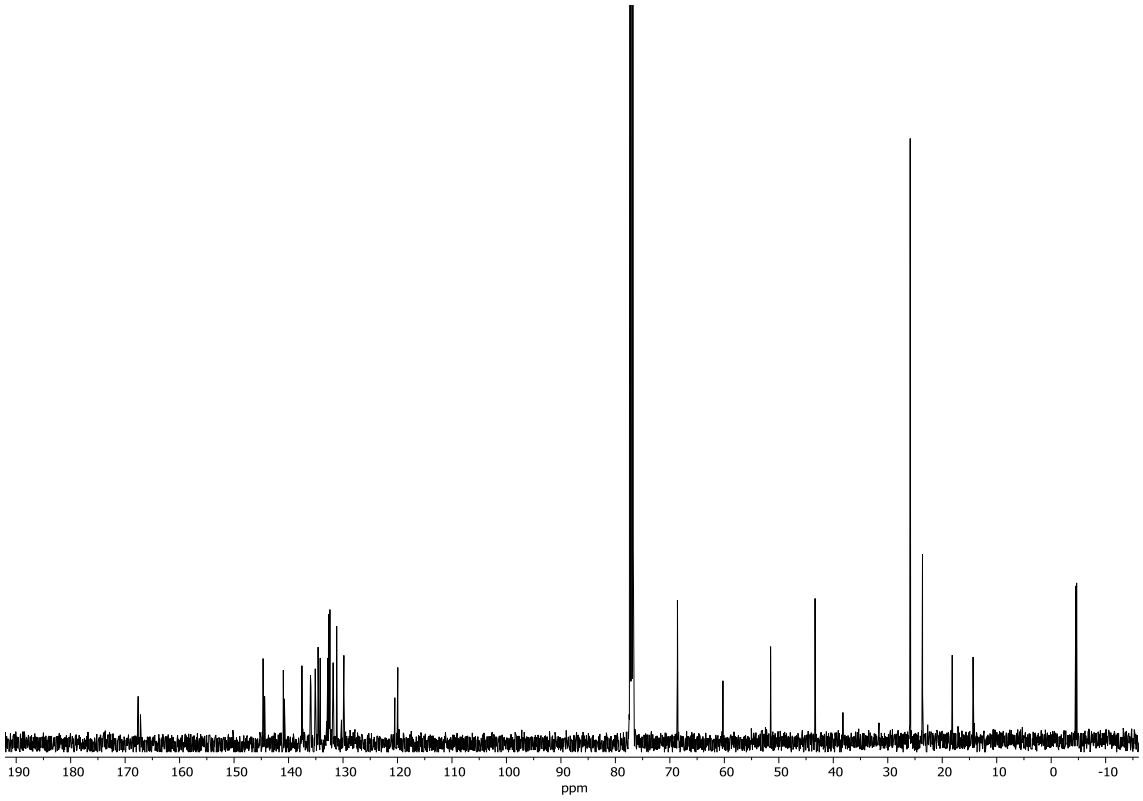
190
180
170
160
150
140
130
120
110
100
90
80
70
60
50
40
30
20
10
0
-10
ppm

^{1}H NMR **21** (500 MHz, $CDCl_3$)

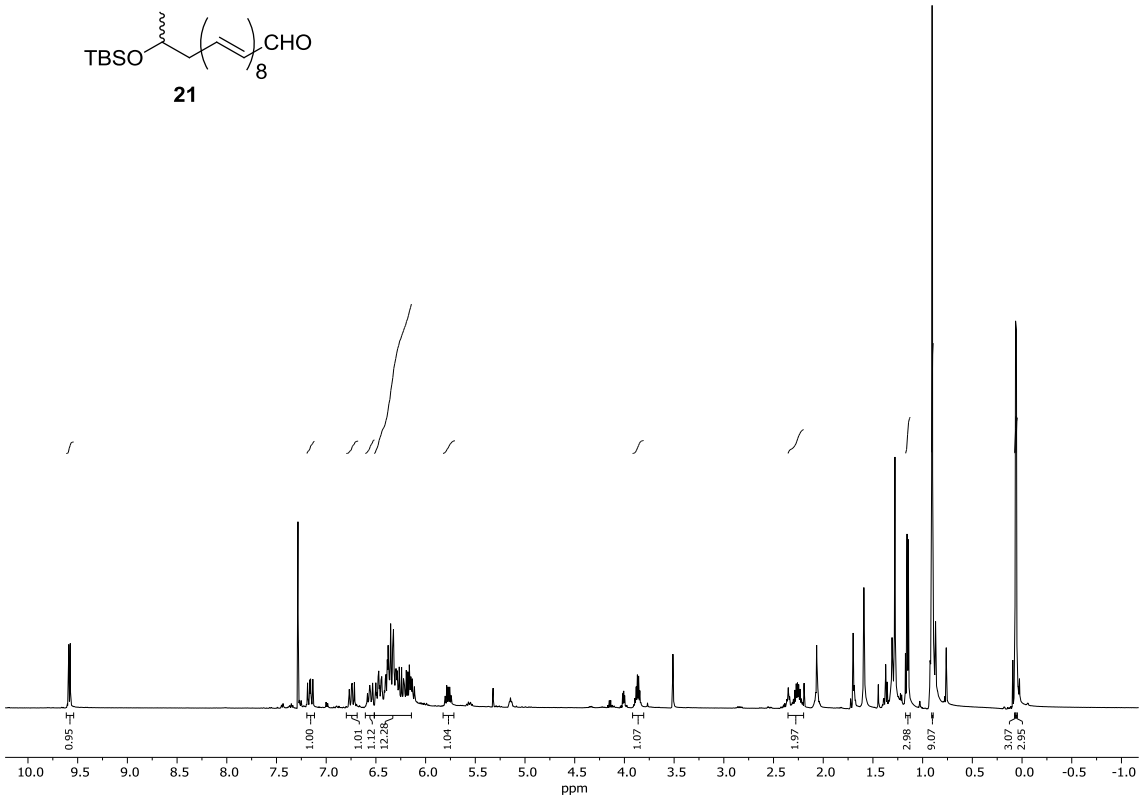

^{13}C NMR **21** (126 MHz, $CDCl_3$)

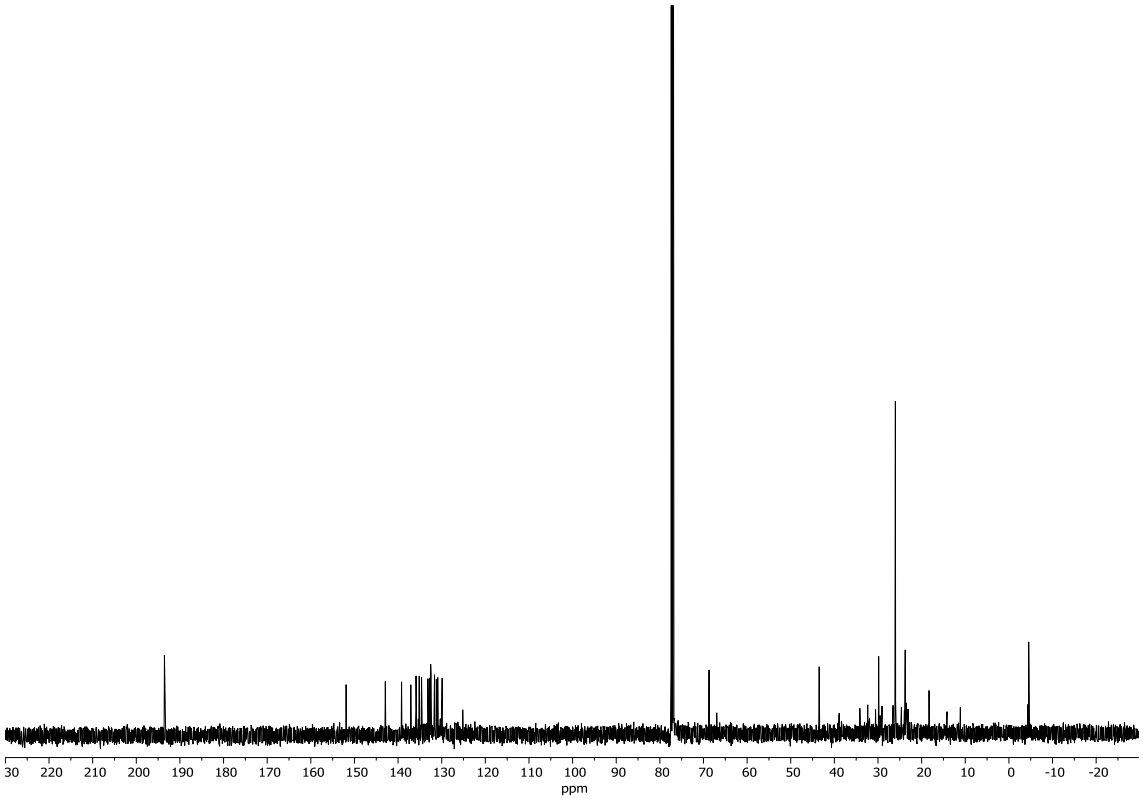

^{1}H NMR **22** (500 MHz, $CDCl_3$)

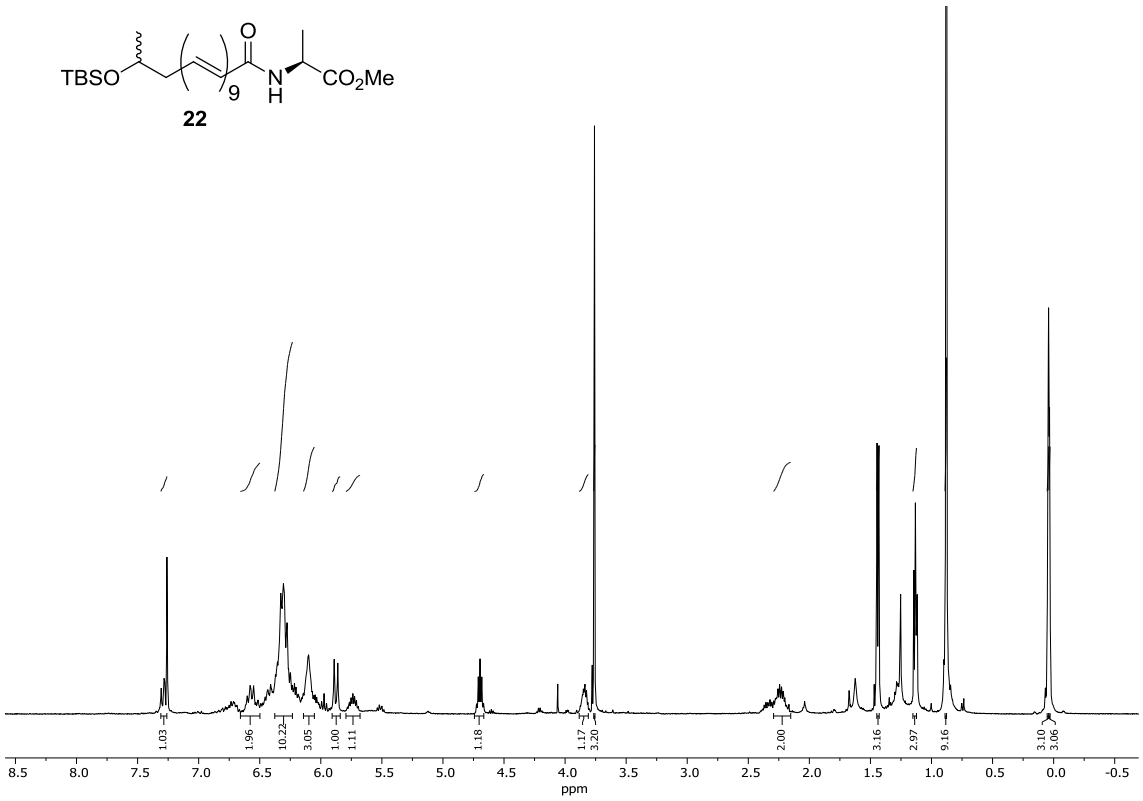

^{13}C NMR **22** (126 MHz, $CDCl_3$)

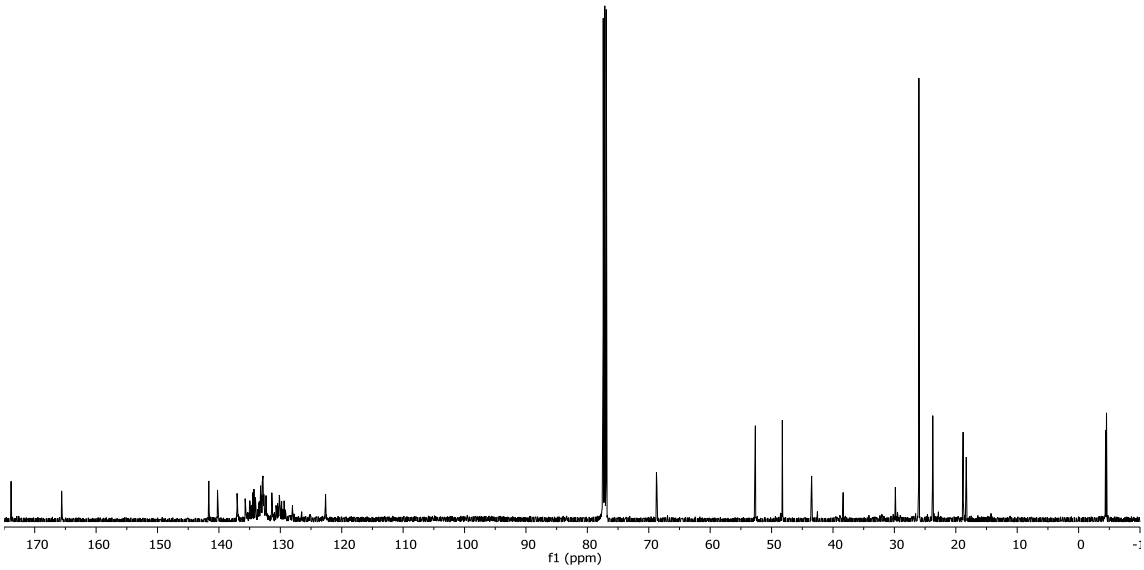
170
160
150
140
130
120
110
100
90
80
70
60
50
40
30
20
10
0
f1 (ppm)

^{1}H NMR **pP9** (500 MHz, Methanol-d_4)

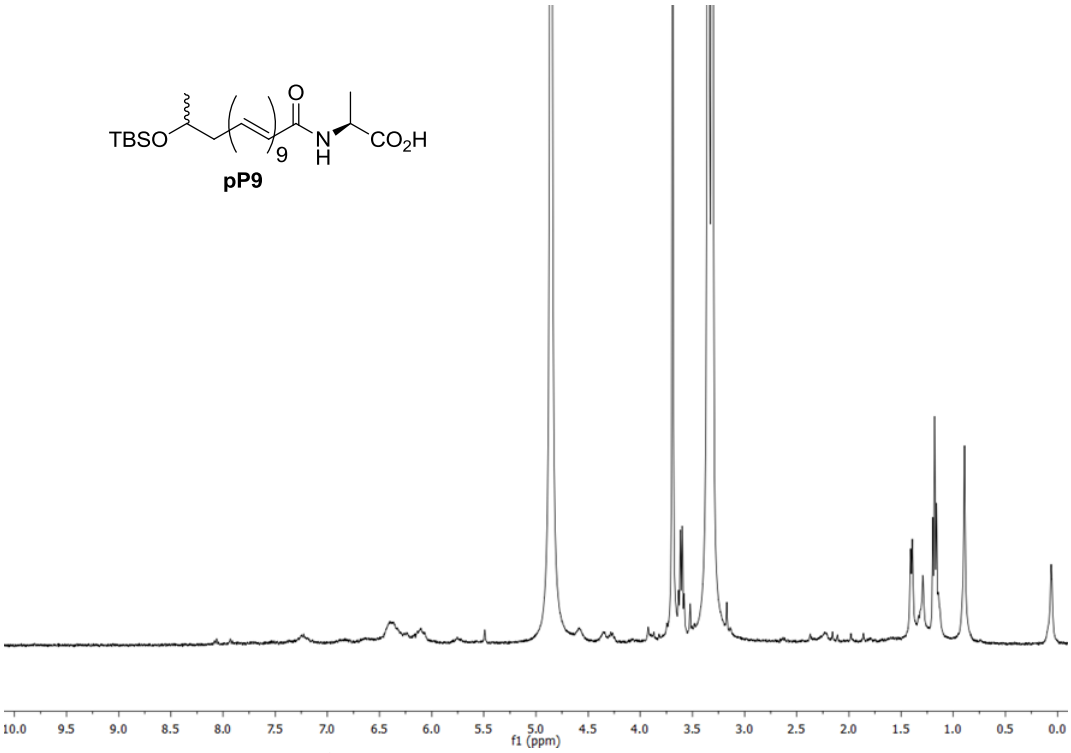

^{1}H NMR **pP9** (500 MHz, DMSO-d_6)

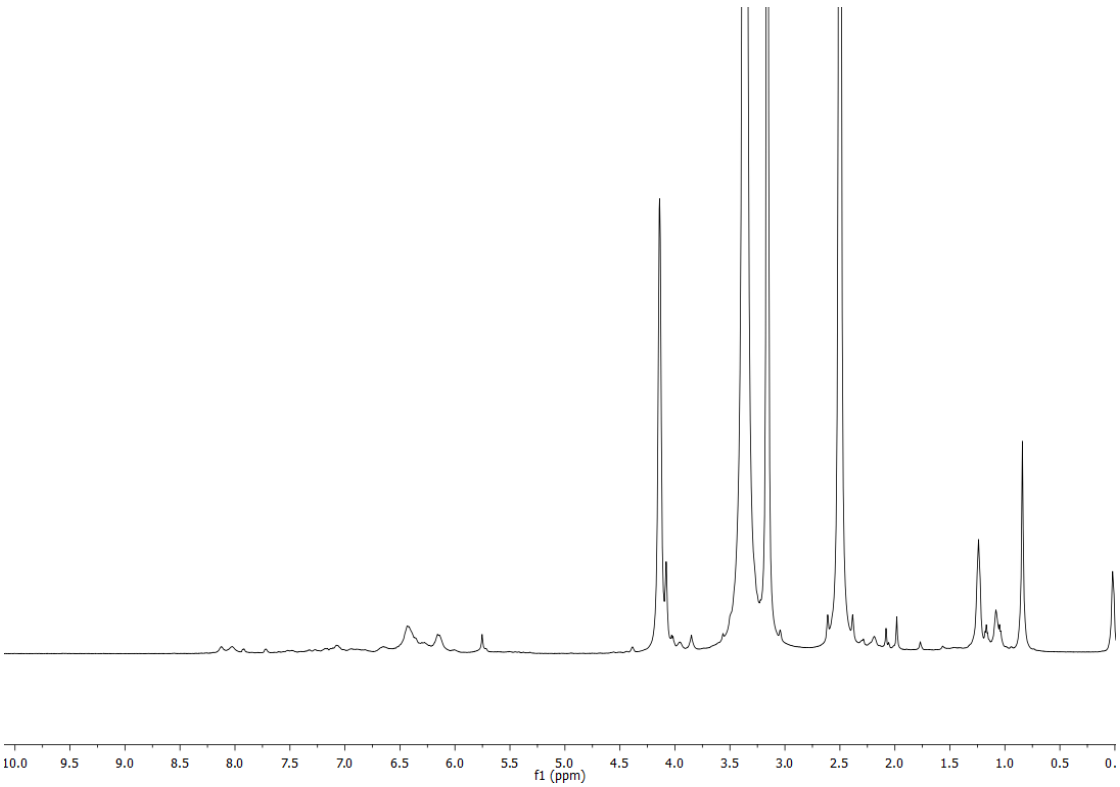

^{1}H NMR **pP9** (500 MHz, DMSO-d_6 + 0.1% TFA-*d*)

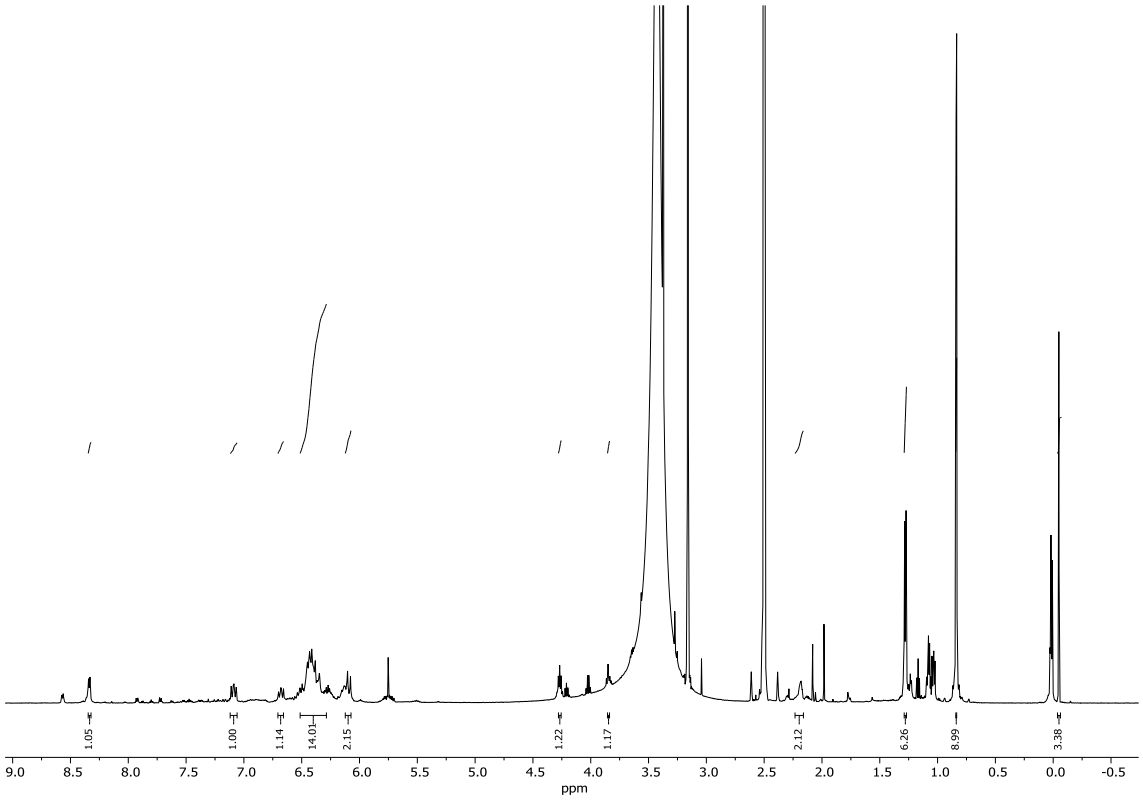

Solubility test of compound **pP9** in different deuterated solvents

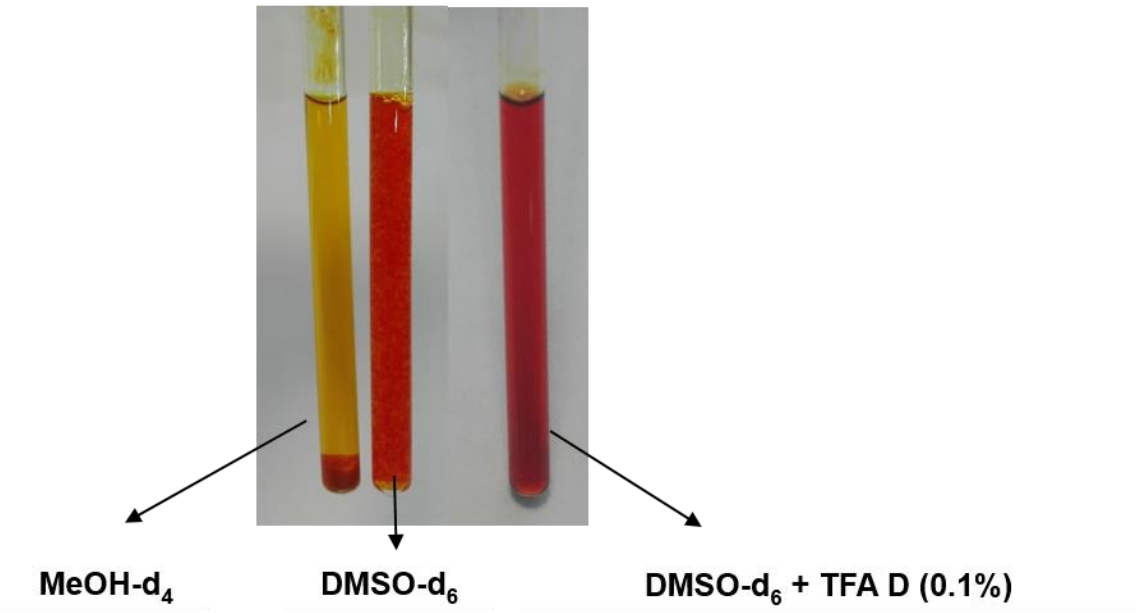

^{1}H NMR **P9** (400 MHz, Methanol-d_4)

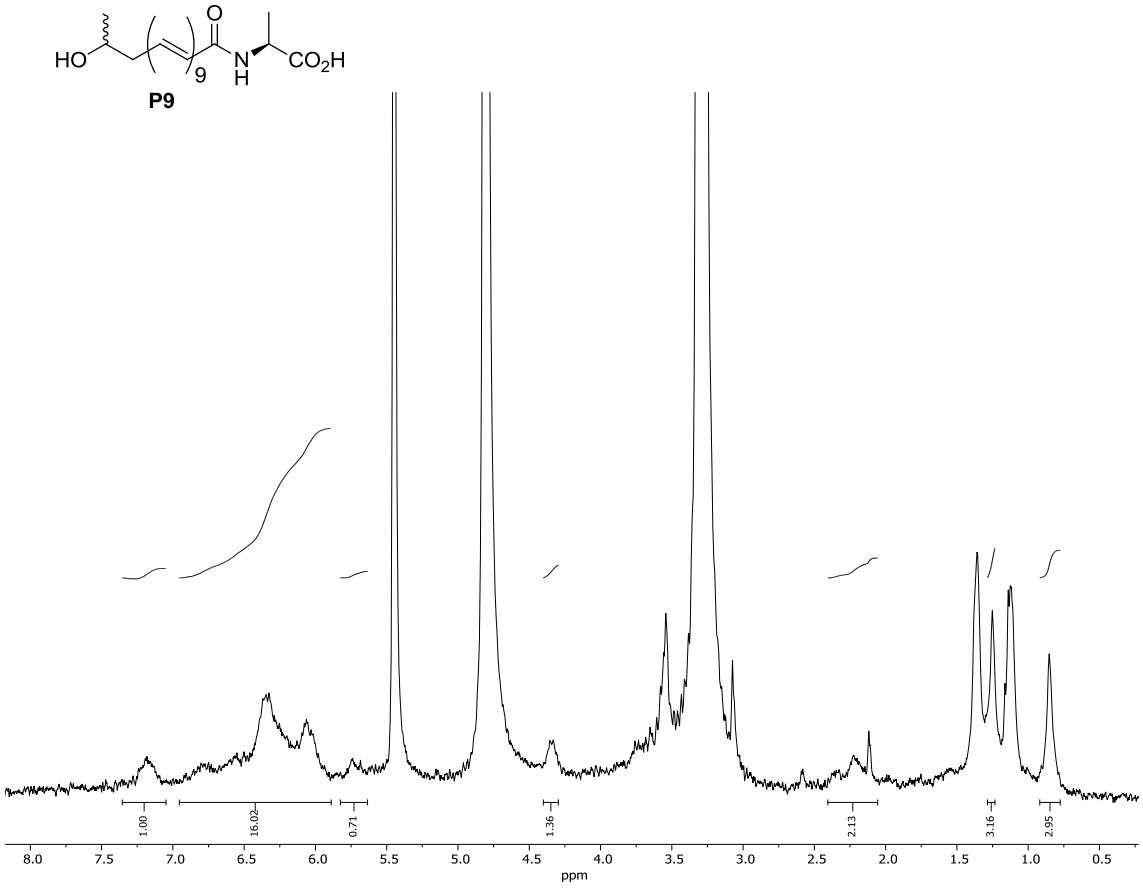

APPENDIX C

SUPPLEMENTARY FIGURE: CHAPTER 4

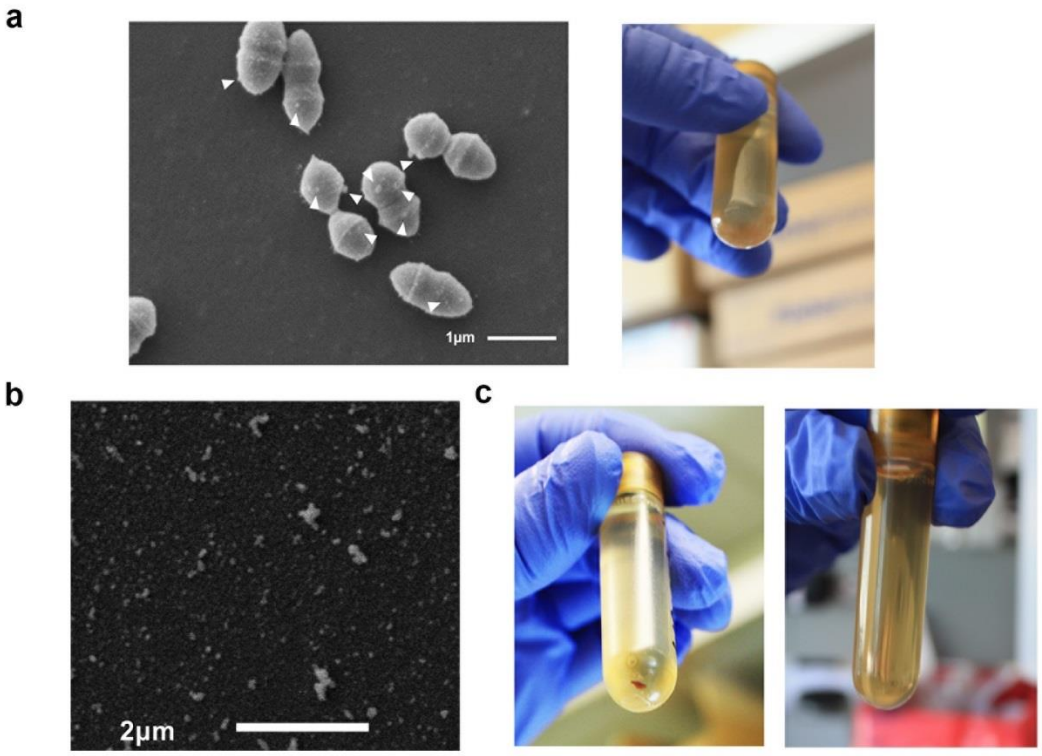

Supplementary Fig. 4.1. Membrane vesicles (MVs) are produced by non-hemolytic GBS and *L. lactis*.

(**a**) Scanning electron micrograph (SEM, left) shows that non-hemolytic (NH) GBS strain GBSΔ*covR*Δ*cylE* produces MVs that emerge from the bacterial surface. No pigmentation is observed in the MV pellet following ultracentrifugation (right). (**b**) SEM of GBS MVs without bacteria show small, spherical structures. (**c**) MV pellets from *L. lactis* p*cylX-K* are pigmented following centrifugation, while pellets from *L. lactis* pDC123 do not have pigmentation.

APPENDIX D

SUPPLEMENTARY FIGURES AND TABLES: CHAPTER 5

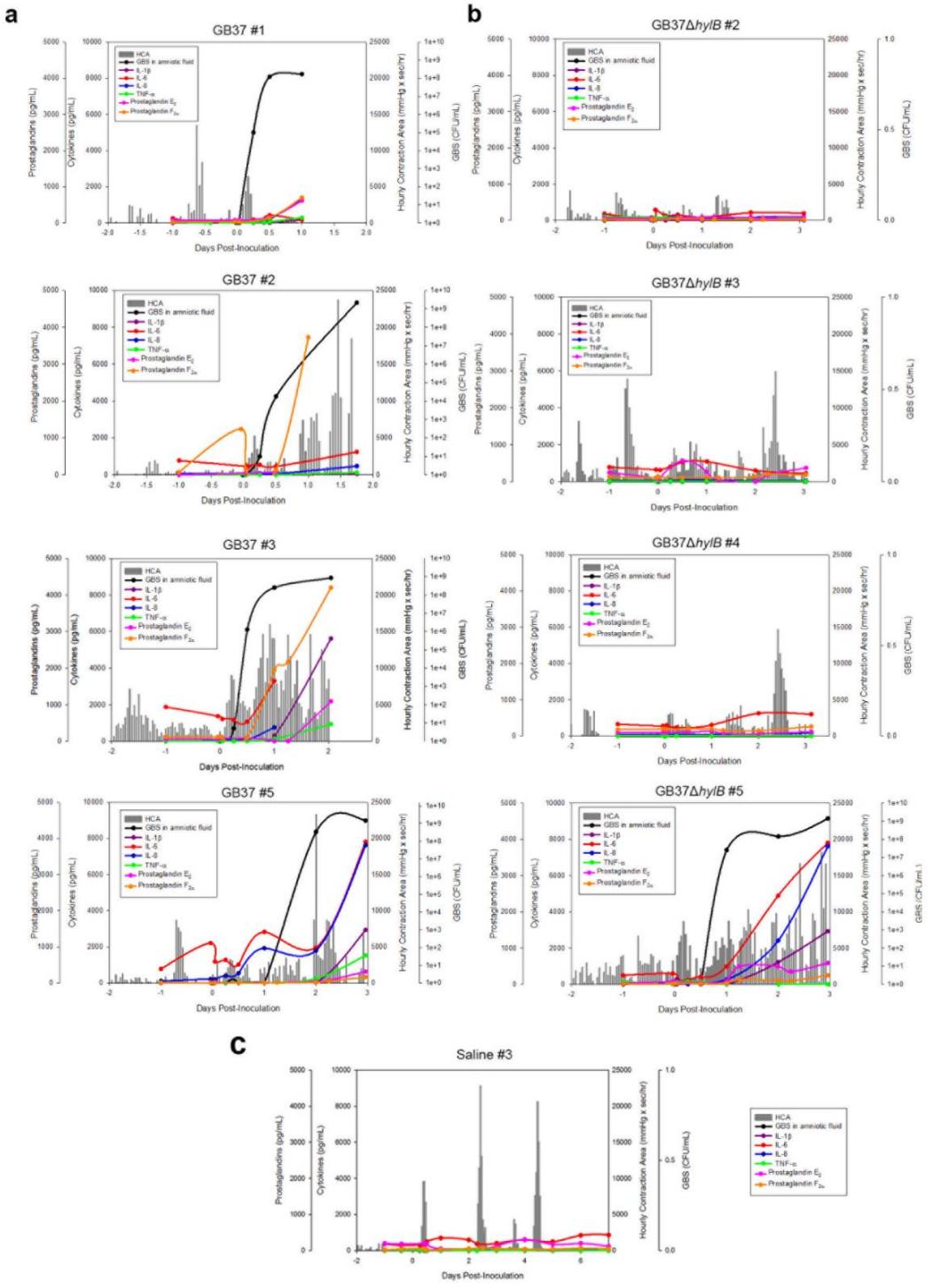

Supplementary Fig. 5.1. Uterine contractions, AF cytokines, prostaglandins, and bacterial CFU from choriodecidual inoculations of GB37, GB37Δ*hylB*, or saline in chronically catheterized pregnant NHP.

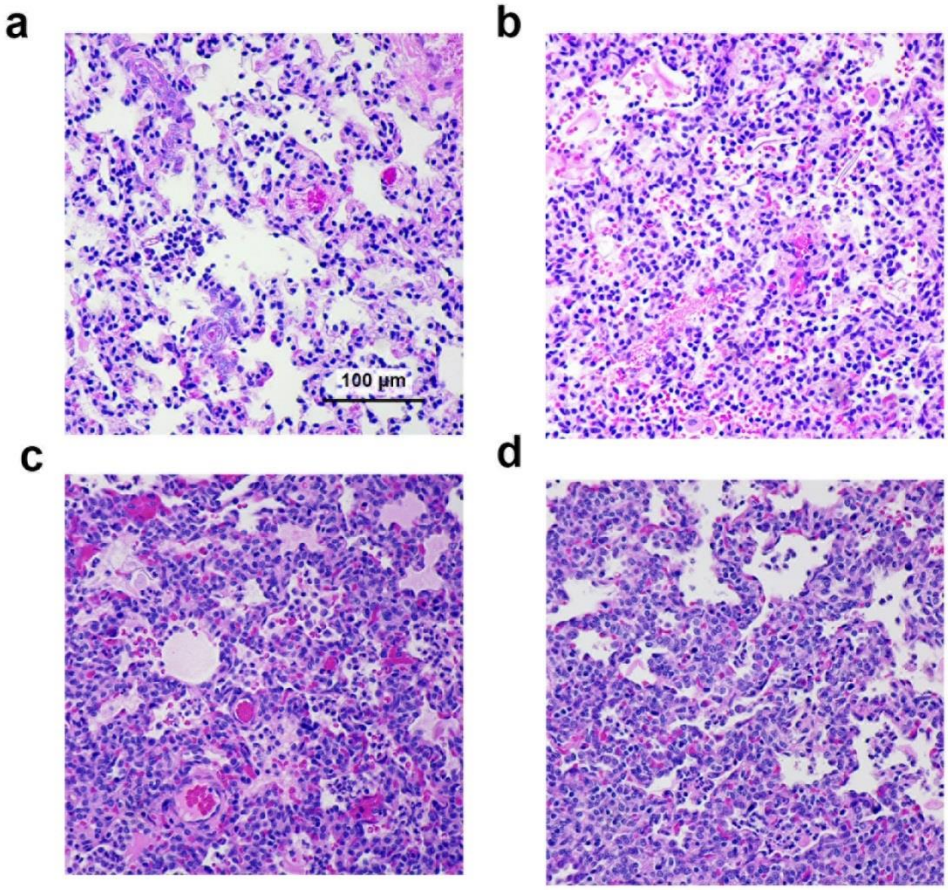

Supplementary Fig. 5.2. H&E staining of NHP fetal lung sections

Representative H&E stained sections from NHP in each group are shown, including Saline #3 (**a**), GB37Δ*hylB* # 2 (**b**), and GB37 #1 (**c**), and GB37 #2 (**d**).

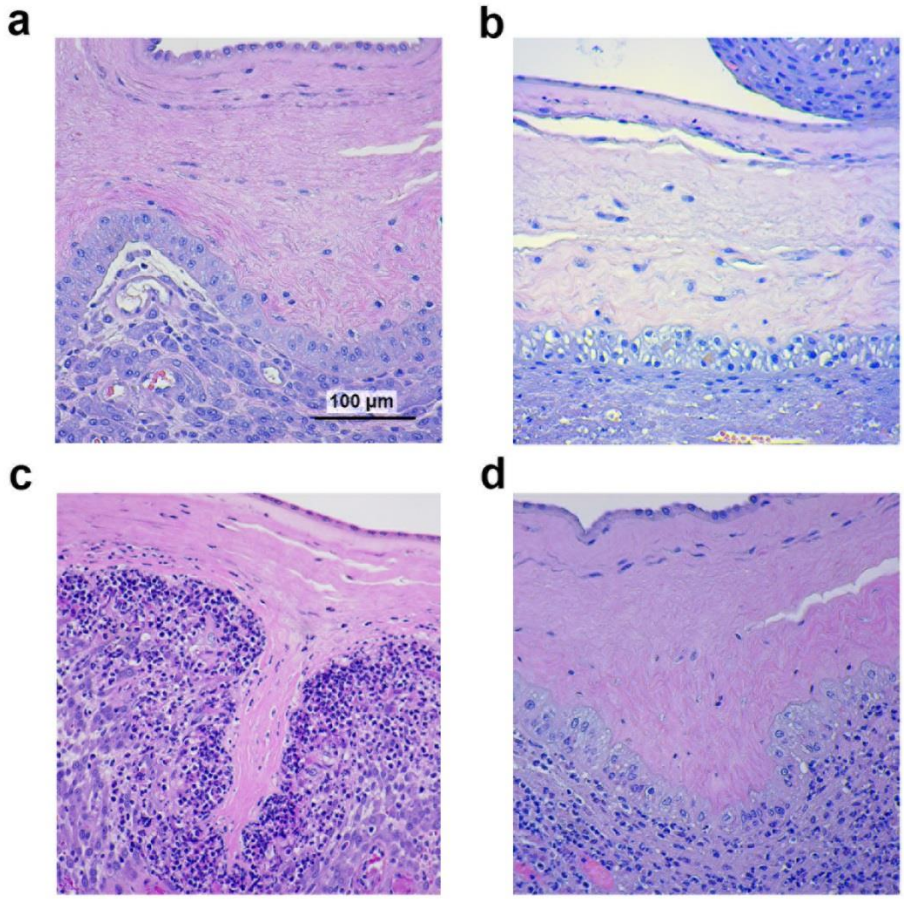

Supplementary Fig. 5.3. H&E staining of NHP placental sections

Representative H&E stained sections from NHP in each group are shown, including Saline #3 (**a**), GB37Δ*hylB* # 2 (**b**), and GB37 #1 (**c**), and GB37 #2 (**d**).

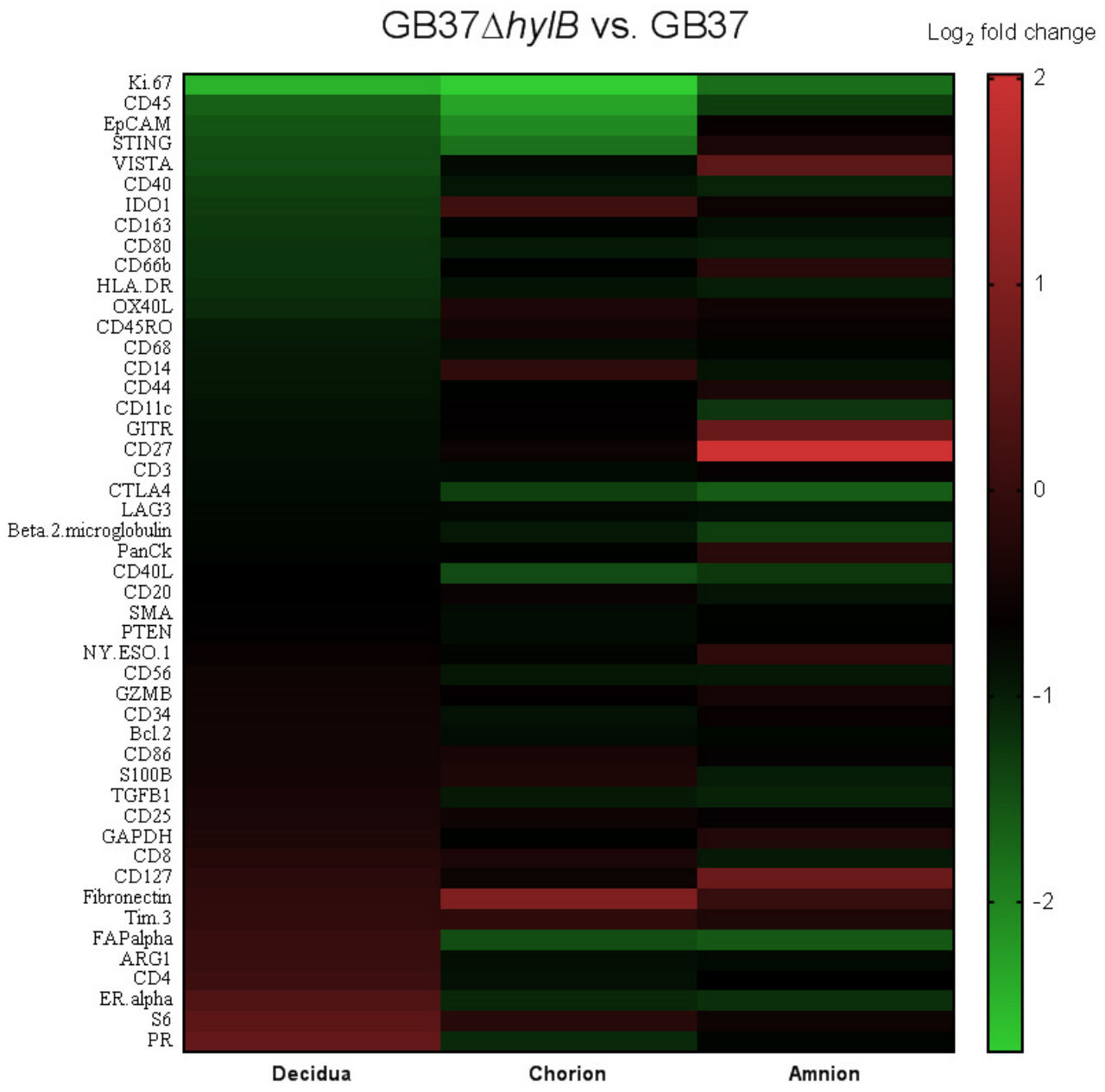

Supplementary Fig. 5.4. DSP analyte fold change: GB37Δ*hylB* vs. GB37

Analyte abundance in distinct placental regions from GB37Δ*hylB*-inoculated NHP and saline-treated NHP were obtained by Digital Spatial Profiling (Nanostring Technologies). Fold changes

in analyte abundance (GB37Δ*hylB* over GB37) were log2 transformed and analyzed by a linear mixed model in R version 3.6.2. Significance tests were controlled for false discovery rate.

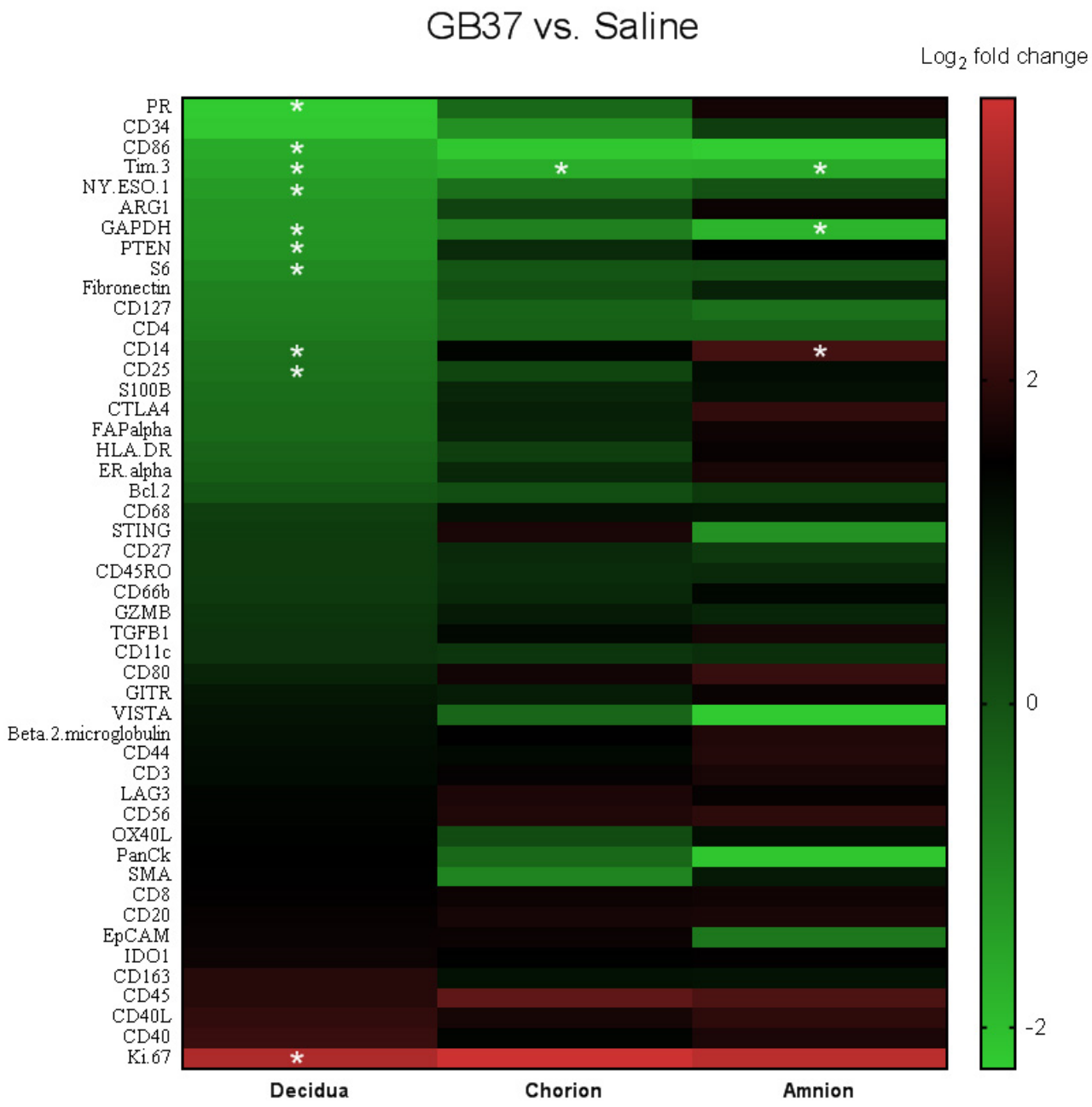

Supplementary Fig. 5.5. DSP analyte fold change: GB37 vs. saline.

Analyte abundance in distinct placental regions from GB37-inoculated NHP and saline-treated NHP were obtained by Digital Spatial Profiling (Nanostring Technologies). Fold changes in analyte abundance (GB37 over saline) were log2 transformed and analyzed by a linear mixed

model in R version 3.6.2. Significance tests were controlled for false discovery rate. White asterisk indicates $p < 0.05$.

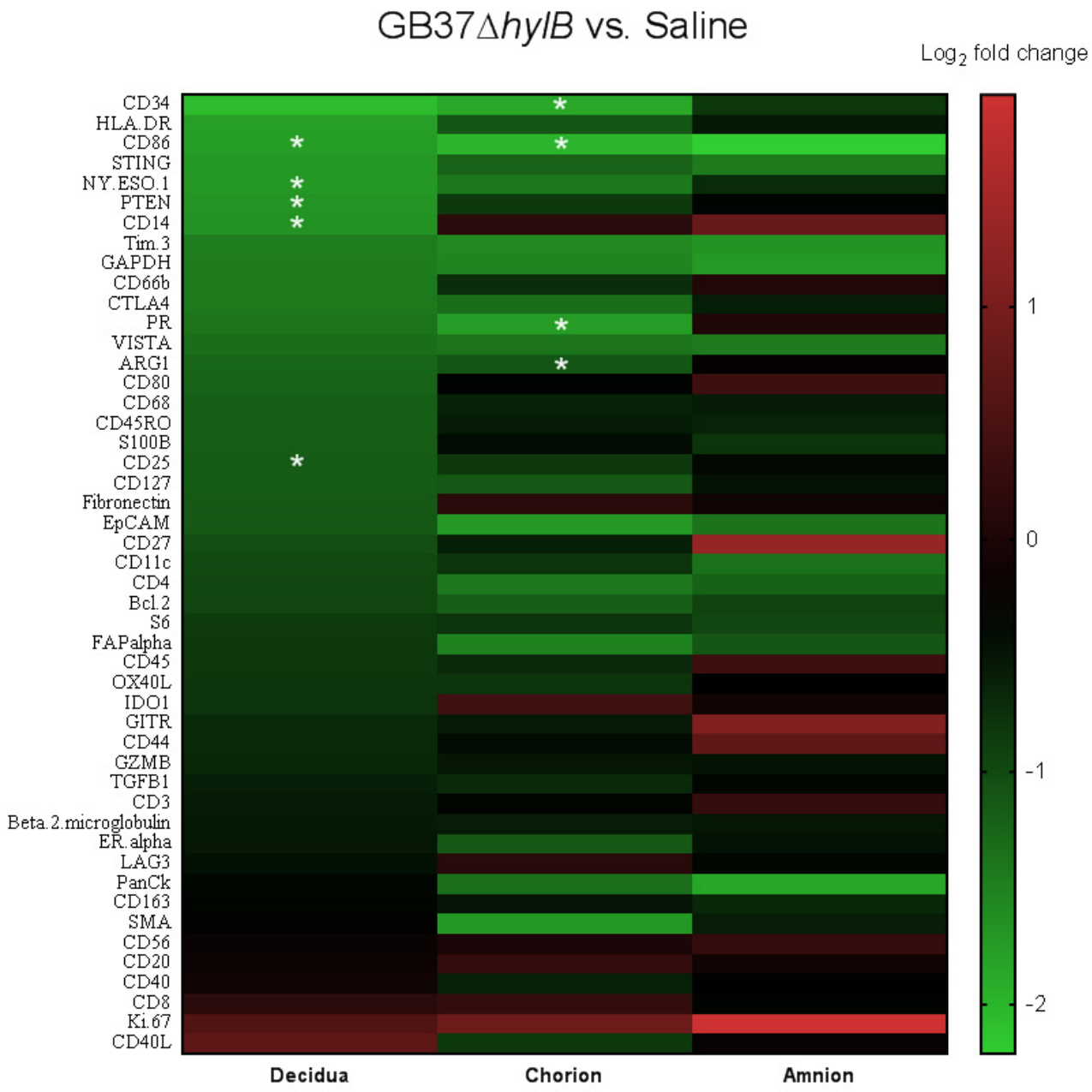

Supplementary Fig. 5.6. DSP analyte fold change: GB37Δ*hylB* vs. saline.

Analyte abundance in distinct placental regions from GB37Δ*hylB*-inoculated NHP and saline-treated NHP were obtained by Digital Spatial Profiling (Nanostring Technologies). Fold changes in analyte abundance (GB37Δ*hylB* over saline) were log2 transformed and analyzed by a linear

mixed model in R version 3.6.2. Significance tests were controlled for false discovery rate. White asterisk indicates $p < 0.05$.

Supplementary Table 5.1. Extracellular flow cytometry panel used on maternal and fetal blood, uterine segments, chorionic villi, and choriodecidual membranes

Extracellular flow cytometry panels					
Panel 1	**Marker**	**Clone**	**Color**	**Manufacturer (cat #)**	**Dilution**
T cells	CD3	SP34	AF700	BD (357917)	1:7
	CD4	L200	FITC	BD (550628)	1:7
	CD8	SK1	APC-Cy7	BioLegend (344714)	1:10
Panel 2	**Marker**	**Clone**	**Color**	**Manufacturer (cat #)**	**Dilution**
B cells, DCs	CD45	D085-1283	AF700	BD (561288)	1:10
	CD20	L27	PE	BD (346595)	1:5
	CD209	D CN46	PerCP/Cy5.5	BD (558263)	1:5
	HLA-DR	L243	FITC	BD (347363)	1:5
Panel 3	**Marker**	**Clone**	**Color**	**Manufacturer (cat #)**	**Dilution**
macrophages, neutrophils	CD45	D085-1283	AF700	BD (561288)	1:10
	CD14	M5E2	BV421	BD (565283)	1:5
	CD11c	S-HCL-3	PE	BD (347637)	1:5
	CD66abce	Tet2	FITC	Miltenyi Biotec (130-093-132)	1:5
Panel 4	**Marker**	**Clone**	**Color**	**Manufacturer (cat #)**	**Dilution**
NK cells, mast cells	CD45	D085-1283	AF700	BD (561288)	1:10
	CD49d	9F10	BV421	BD (565277)	1:20
	NKG2a	REA110	PE	Miltenyi Biotec (130-098-814)	1:10

Supplementary Table 5.2. Intracellular flow cytometry panel used on maternal and fetal blood, uterine segments, chorionic villi, and choriodecidual membranes

Intracellular flow cytometry panels					
Panel 1	**Marker**	**Clone**	**Color**	**Manufacturer (cat #)**	**Dilution**
T cells	IL-4	MP4-25D2	APC	BD (554486)	1:20
	IL-17	eBio64DEC17	PerCP/Cy5.5	Invitrogen (45-7179-42)	1:10
	IFN-g	B27	PE/Cy7	BD (557643)	1:20
	Ki67	B56	BV421	BD (562899)	1:20
	FoxP3	206D	PE	BioLegend (320108)	1:10
Panel 2	**Marker**	**Clone**	**Color**	**Manufacturer (cat #)**	**Dilution**
B cells, DCs	IL-4	MP4-25D2	APC	BD (554486)	1:20
	Ki67	B56	BV421	BD (562899)	1:20
Panel 3	**Marker**	**Clone**	**Color**	**Manufacturer (cat #)**	**Dilution**
macrophages, neutrophils	Granzyme B	GB12	APC	Invitrogen (MHGB05)	1:20
Panel 4	**Marker**	**Clone**	**Color**	**Manufacturer (cat #)**	**Dilution**
NK cells, mast cells	Granzyme B	GB12	APC	Invitrogen (MHGB05)	1:20

VITA

Blair Armistead was born and raised in Morgantown, West Virginia. She graduated from Morgantown High School, received her Bachelor of Science degree in Biology from the University of Richmond (Richmond, VA) and her Master of Public Health degree from Virginia Commonwealth University School of Medicine (Richmond, VA). She looks forward to a career in which she can promote equity through scientific innovation, particularly as it relates to infectious disease and women's health.